



NASA N+3 Subsonic Fixed Wing Silent Efficient Low-Emissions Commercial Transport (SELECT) Vehicle Study

Revision A

*Sam Bruner, Scott Baber, Chris Harris, Nicholas Caldwell, Peter Keding, Kyle Rahrig, and Luck Pho
Northrop Grumman Corporation, El Segundo, California*

*Richard Wlezian
Tufts University, Medford, Massachusetts*

NASA STI Program . . . in Profile

Since its founding, NASA has been dedicated to the advancement of aeronautics and space science. The NASA Scientific and Technical Information (STI) program plays a key part in helping NASA maintain this important role.

The NASA STI Program operates under the auspices of the Agency Chief Information Officer. It collects, organizes, provides for archiving, and disseminates NASA's STI. The NASA STI program provides access to the NASA Aeronautics and Space Database and its public interface, the NASA Technical Reports Server, thus providing one of the largest collections of aeronautical and space science STI in the world. Results are published in both non-NASA channels and by NASA in the NASA STI Report Series, which includes the following report types:

- **TECHNICAL PUBLICATION.** Reports of completed research or a major significant phase of research that present the results of NASA programs and include extensive data or theoretical analysis. Includes compilations of significant scientific and technical data and information deemed to be of continuing reference value. NASA counterpart of peer-reviewed formal professional papers but has less stringent limitations on manuscript length and extent of graphic presentations.
- **TECHNICAL MEMORANDUM.** Scientific and technical findings that are preliminary or of specialized interest, e.g., quick release reports, working papers, and bibliographies that contain minimal annotation. Does not contain extensive analysis.
- **CONTRACTOR REPORT.** Scientific and technical findings by NASA-sponsored contractors and grantees.

- **CONFERENCE PUBLICATION.** Collected papers from scientific and technical conferences, symposia, seminars, or other meetings sponsored or cosponsored by NASA.
- **SPECIAL PUBLICATION.** Scientific, technical, or historical information from NASA programs, projects, and missions, often concerned with subjects having substantial public interest.
- **TECHNICAL TRANSLATION.** English-language translations of foreign scientific and technical material pertinent to NASA's mission.

Specialized services also include creating custom thesauri, building customized databases, organizing and publishing research results.

For more information about the NASA STI program, see the following:

- Access the NASA STI program home page at <http://www.sti.nasa.gov>
- E-mail your question via the Internet to help@sti.nasa.gov
- Fax your question to the NASA STI Help Desk at 443-757-5803
- Telephone the NASA STI Help Desk at 443-757-5802
- Write to:
NASA Center for AeroSpace Information (CASI)
7115 Standard Drive
Hanover, MD 21076-1320



NASA N+3 Subsonic Fixed Wing Silent Efficient Low-Emissions Commercial Transport (SELECT) Vehicle Study

Revision A

*Sam Bruner, Scott Baber, Chris Harris, Nicholas Caldwell, Peter Keding, Kyle Rahrig, and Luck Pho
Northrop Grumman Corporation, El Segundo, California*

*Richard Wlezian
Tufts University, Medford, Massachusetts*

Prepared under Contract NNC08CA86C

National Aeronautics and
Space Administration

Glenn Research Center
Cleveland, Ohio 44135

Acknowledgments

The authors would like to thank Doug Perkins, our NASA Contracting Office Technical Representative (COTR), and Brian Allan, NASA Langley, for their support and guidance during the execution of our study. Their feedback was particularly helpful in keeping us on target during the preparation of this final report. We would like to thank Arnie McCullers, NASA Langley, for his dedication in timely response to our questions on FLOPS, even when dealing with his own medical issues. This work was funded by the Subsonic Fixed Wing project, of the Fundamental Aeronautics Program, under NASA contract NNC08CA86C. Contributors: The following individuals composed the core technical team that performed this study over the 18-month period from October 2008 through March of 2010. The contractor and subcontractors were generous in providing numerous other individuals who were integral to the support of very specialized aspects of this effort. Northrop Grumman: Scott Collins provided programmatic support and guidance and technical review. Dr. Sam Bruner was the Principal Investigator and Program Manager. Chris Harris was the Systems Analysis IPT Lead, and supported technology selection and planning, propulsion integration, the scenario evaluation, and the requirements study. Nicholas Caldwell supported propulsion integration, technology modeling, and vehicle trades/optimization, and led the editing of the final report. Peter Keding supported technology modeling, aerodynamics and performance evaluation, and vehicle trades/optimization. Scott Baber supported configuration design and vehicle trades/optimization. Luck Pho supported aerodynamic design and performance. Kyle Rahrig performed acoustic modeling and analysis. Rolls-Royce Liberty Works: David Eames led the RRLW propulsion support and advanced engine architecture design, and propulsion technologies study. Tufts University: Dr. Rich Wlezien performed the future scenario research and analysis, and led the technology maturation planning effort. Spirit Aerosystems: Dr. Judy Gallman led the technology evaluation of acoustic airframe treatment technologies, and the design of an advanced acoustic inlet liner. Sensis: Dave Miller led the effort to determine N+3 requirements, as well as perform N+3 simulations in the NAS.

This work was sponsored by the Fundamental Aeronautics Program
at the NASA Glenn Research Center.

Level of Review: This material has been technically reviewed by NASA technical management.

Available from

NASA Center for Aerospace Information
7115 Standard Drive
Hanover, MD 21076-1320

National Technical Information Service
5301 Shawnee Road
Alexandria, VA 22312

Available electronically at <http://gltrs.grc.nasa.gov>

Table of Contents

1	EXECUTIVE SUMMARY	1
2	TECHNICAL APPROACH.....	4
3	AIR VEHICLE DESIGN TOOLS AND PROCESSES	7
3.1	Flight Optimization System (FLOPS)	7
3.1.1	Calibration Process	7
3.1.2	Reference Vehicle	10
3.2	Optimization Method.....	11
3.3	Airspace Concepts Evaluation System (ACES)	12
3.4	Conceptual Mass Properties (CONMAP).....	12
3.5	Numerical Propulsion System Simulation (NPSS).....	13
3.6	Acoustic Liner Design Process	13
3.7	Model for Investigating the Detectability of Acoustic Signatures (MIDAS).....	13
3.8	System Effectiveness Rankings	14
4	FUTURE SCENARIO AND REQUIREMENTS DEVELOPMENT	16
4.1	2035 Scenario.....	16
4.1.1	Scenario Development and Key Drivers.....	16
4.1.2	Scenario Synthesis and Impact to Vehicle Optimization.....	23
4.2	Initial Requirements Development	24
4.2.1	Methodology	25
4.2.2	Traffic Growth Implications on Metroplex Operations and Field Length Requirement.....	27
4.2.3	Cruise Speed Sensitivity	33
4.2.4	Passenger Loading and Range Capabilities	34
4.2.5	Mission Requirements	36
5	ADVANCED VEHICLE CONCEPTS.....	38
5.1	Engine Architecture Concepts	38
5.1.1	Reference Engine	38
5.1.2	Three-Shaft Turbofan.....	38
5.1.3	Geared Turbofan	39
5.1.4	Open Rotor.....	39
5.1.5	Engine Comparison and Downselection.....	40
5.2	Airframe Concepts	41
5.2.1	Tube-and-Wing.....	42
5.2.2	Tube-and-Wing With Embedded Turbofans	43
5.2.3	Tube-and-Wing With Canard	43
5.2.4	Hybrid Wing-Body	44
5.2.5	Hybrid Wing-Body With Embedded Turbofans.....	45
5.2.6	Channel Wing	45
5.2.7	Joined Wing	46
5.2.8	Low Aspect Ratio Spanloader	46
5.2.9	Configuration Quantitative Assessment and Downselect.....	47
5.3	New Technology.....	47
5.3.1	Development of Technology Matrix.....	48
5.3.2	Quality Function Deployment Process	48
5.3.3	Down-Selection of Candidate Technologies	51

6	AIR VEHICLE DESIGN STUDY.....	65
6.1	Sizing and Performance Analysis	66
	6.1.1 Objective Function Effect on Aspect Ratio Sizing.....	66
	6.1.2 Advanced Liner Design	66
	6.1.3 Analysis of Engine Mounting Configurations	67
	6.1.4 Laminar Flow Integration	70
	6.1.5 M_{DD} and Sweep Analysis.....	71
	6.1.6 Landing and Takeoff Operations	72
6.2	Analysis of Aircraft Emissions	73
	6.2.1 CAEP/6 NO _x Requirement.....	73
	6.2.2 Simulated LTO Cycle	74
	6.2.3 Emissions Results	74
6.3	Analysis of Aircraft Acoustics.....	75
	6.3.1 FAR Stage 4 Noise Requirement.....	75
	6.3.2 Effective Perceived Noise Level (EPNL) Calculation.....	75
	6.3.3 Acoustics Results	75
6.4	System Effectiveness Rating Results.....	77
	6.4.1 Technology Assessments	77
	6.4.2 Technology Suites.....	79
	6.4.3 Configuration Results	80
6.5	Preferred Configuration	82
	6.5.1 Airframe Configuration	82
	6.5.2 Preferred Technology Package	83
	6.5.3 Weight Breakdown	83
	6.5.4 Propulsion System	85
	6.5.5 Configuration Comparisons	85
	6.5.6 Performance Summary.....	86
7	TECHNOLOGY MATURATION	89
7.1	Physical Landing Gear Fairings.....	89
7.2	Virtual Landing Gear Fairings	90
7.3	Swept-Wing Laminar Flow Slat Integration.....	91
7.4	Swept-Wing Laminar Flow Control of Crossflow Transition	92
7.5	3D Stitched/Woven Composites	93
7.6	Advanced Structural and Subsystems Metal Alloys.....	94
7.7	SMA Variable Geometry Nozzles	95
7.8	M5 Organic Fiber Composites.....	96
7.9	Carbon Nanotube Electrical Cables	97
7.10	Computational Inlet Optimization	98
7.11	Large Integrated Structures.....	99
7.12	Aeroservoelastic Structures	100
7.13	Lightweight Fan Structure and Cowl.....	101
7.14	Intercooled Compressor Stage	102
7.15	Cooled Cooling Air.....	103
7.16	Endothermic Fuel Cracking	104
7.17	Lean-Burn Staged Combustion Liner	105
8	CONCLUSIONS AND RECOMMENDATIONS	106

Appendices

Appendix A	Airframe Selections.....	108
A.1	Airframe Technology Selections	109
A.2	Aerodynamic Technology Selections	109
A.3	Noise Technology Selections.....	110
A.4	Propulsion Technology Selections.....	111
Appendix B	Technology Dispositions.....	113
B.1	Constant Volume Combustors/Wave Rotors	114
B.2	Turboelectric Distributed Fans	114
B.3	Turboshaft-Powered Direct-Drive Distributed Fans.....	114
B.4	Nonturbine Distributed Fans.....	115
B.5	Hybrid All-Electric Propulsion	115
B.6	Inlet Flow Control (Microvortex Generators, Jets, etc.)	116
B.7	Wing Morphing (Piezoelectrics, Shape Memory Alloys, etc.).....	116
B.8	All Electric (No Accessory Gear Box)	117
B.9	Structural Materials Laser Surface Treatment	117
B.10	Lightweight Foamed Composites	117
B.11	Unsteady Circulation Control	118
B.12	Water Injection.....	118
B.13	Variable Pitch Fan Blades.....	118
B.14	Fuel Cell Auxiliary Power Unit	118
B.15	TO/C-Assist Propulsion Unit.....	119
B.16	Microvortex Generators and Riblets.....	119
B.17	Conformal Polymer Solar Cell Power Augmentation	120
B.18	Moveable Winglets	120
B.19	Combined/Compound Cycles	120
B.20	Curved, Scarfed Inlet Ducts.....	121
B.21	Steady Fluidic Separation Control	121
B.22	Synthetic Jet Separation Control.....	121
B.23	Nanotube Liner	122
B.24	Plane Jet Combustion.....	122
B.25	Electric Subsystems	122
B.26	Third Engine Stream	123
B.27	Alternative Hydrocarbon Biofuels.....	123
B.28	Embedded/Conformal Inlets	123
B.29	Low-Noise Fan Blades.....	124
B.30	Fan Blade Flow Control.....	124
B.31	Conformal Load-Bearing Antenna Structures	125
B.32	Upper Surface Exhaust Nozzle and Flap	125
B.33	Lower Surface Exhaust Nozzle and Flap.....	126
B.34	Fluidic Thrust Vectoring for Upper Surface Exhaust Nozzle and Flap.....	126
B.35	Single DOF Liner.....	127
B.36	Active Drag Reduction	127
B.37	Multi-DOF Liner.....	127
B.38	Oil-less Engine.....	128
B.39	Low Tip Speed Counter-Rotating Ducted Fan	128
B.40	Wheel Caps	128
B.41	Wheel Gap Filler.....	129

B.42	Acoustic Excitation.....	129
B.43	Brush-type Trailing Edges.....	129
B.44	Trailing Edge Serrations.....	130
B.45	Chevrons.....	130
B.46	Combined Steam Cycle.....	130
B.47	Linear Acoustic Liner.....	131
B.48	Four-Shaft Turbine.....	131
B.49	Active Noise Cancellation.....	132
B.50	Landing Gear Assembly Plasma Fairings.....	132
B.51	Slat Cove Fillers.....	133
B.52	Continuous Mold-Line Linkages.....	133
B.53	Flap Tip Fences.....	133
B.54	Ejectors.....	134
B.55	Thrust Vectoring Open Rotor.....	134
B.56	Slat Tip Fences.....	135
B.57	Cryogenic Motors.....	135
B.58	Porous Plug Designs.....	135
B.59	Porous Ceramic Materials.....	136
B.60	Porous Flap Side Edges.....	136
B.61	Slat Trailing Edge Serrations.....	137
B.62	Porous Slat Pressure Surfaces.....	137
B.63	Micro-Tab Features.....	137
B.64	Fiber Metal Laminates.....	138
B.65	Metallic Digital Direct Manufacturing.....	139
B.66	Open-Celled and Stamped Composite Structures.....	139
B.67	Post-Buckled Composite Structures.....	140
B.68	Direct Manufacturing/Laser Sintering of Polymeric Materials.....	140
B.69	Slat Gap Liners.....	140
B.70	Streamlined Slat Tracks.....	141
B.71	Thrust Vectoring Nozzles.....	141
B.72	Metal Foam Liner.....	142
Appendix C	Preferred Vehicle Aerodynamics.....	143
Appendix D	Vehicle OASPL Maps.....	146
D.1	Reference Vehicle – OASPL.....	148
D.2	Advanced Tube-and-Wing, Scaled CFM56-3B1, No Technologies – OASPL...	149
D.3	Hybrid Wing-Body, Scaled CFM56-3B1, No Technologies – OASPL.....	150
D.4	Preferred Configuration – OASPL.....	151
Appendix E	QFD Spreadsheet.....	152
References	159

List of Tables

Table 1-1. NASA Generational Aircraft Goals.....	1
Table 1-2. Mission Requirements.....	1
Table 1-3. N+3 Goals Achievement.....	3
Table 3-1. CONMAP and FLOPS Weight Calibration for the Boeing 737-800.....	9
Table 3-2. 737-800 Performance Calibration Points.....	10
Table 3-3. Reference Vehicle Characteristics.....	11
Table 4-1. Specific Scenarios Used to Develop the N+3 U.S. Airspace Overall Scenario [Ref. 10, 11, 12, 13].....	17
Table 4-2. U.S. Air Traffic Growth Rates by Future Scenario.....	28
Table 4-3. N+3 Mission Requirements.....	37
Table 6-1. Baseline and Advanced Inlet Liner Overall Sound Pressure Levels Reduction.....	66
Table 6-2. Baseline and Advanced Fan Duct Liner Overall Sound Pressure Level Reduction....	67
Table 6-3. Impact of Liner Length On Overall Sound Pressure Level Reduction.....	67
Table 6-4. Maximum Lift Coefficient Comparison With and Without Laminar Flow Penalties.	71
Table 6-5. ICAO LTO Reference Cycle.....	74
Table 6-6. FAR Stage 4 EPNL Comparison.....	76
Table 6-7. ATW Technology SER Assessment, Without Noise.....	78
Table 6-8. HWB Technology SER Assessment, Without Noise.....	79
Table 6-9. Major Technology Suites for Hybrid Wing-Body Configurations.....	79
Table 6-10. Major Technology Suites for Tube-and-Wing Configurations.....	80
Table 6-11. Contributions to System Effectiveness Rating Calculations.....	81
Table 6-12. N+3 Goals Achievement.....	82
Table 6-13. N+3 Technology Suite.....	83
Table 6-14. Weight Statement.....	84
Table 6-15. Mission Weight Breakdown.....	85
Table 6-16. Tube-and-Wing Vehicle Comparison.....	85
Table 6-17. Fuel Burn by Mission Segment for Preferred Configuration.....	86
Table 6-18. FAR Stage 4 EPNL Comparison.....	87
Table C-1. Preferred Vehicle High Speed Drag Polar at 45,000 feet Altitude.....	144
Table C-2. Preferred Vehicle Reynold’s Number Drag Coefficient Corrections.....	144

List of Figures

Figure 1-1. N+3 Preferred Configuration 3-View and Mission Performance	2
Figure 2-1. Technical Approach	4
Figure 2-2. Assumed Technology Maturation and Implementation Timeframe	5
Figure 3-1. FLOPS Calibration Process With the 737-800	8
Figure 3-2. Boeing 737-800 Performance Calibration Points (Shown in Red)	10
Figure 3-3. Reference Vehicle	11
Figure 3-4. Optimization Methodology	11
Figure 3-5. ACES Simulation Components and Data Flow Diagram	12
Figure 3-6. Acoustic Liner Conceptual Design Examples.....	13
Figure 3-7. MIDAS Flow.....	14
Figure 4-1. Future Scenario Categorization Quadrants	17
Figure 4-2. Simplified Future Resource Trends for Various Scenario Quadrants.....	18
Figure 4-3. Projected Global Energy Needs Through 2030 [Ref. 15]	19
Figure 4-4. Production Estimates of Current and Future Crude Oil Sources [Ref. 15].....	19
Figure 4-5. ExxonMobil 2006 Projections of Fossil Fuel Growth [Ref. 17].....	20
Figure 4-6. ExxonMobil 2006 Projections of Near-Term CO ₂ Emissions [Ref. 17].....	21
Figure 4-7. Projections of Energy Sources for NiMBY Scenario [Ref. 13]	21
Figure 4-8. Historical Global Crude Oil Availability and Production [Ref. 20]	22
Figure 4-9. Impact of Impulse-Response Input of Various Greenhouse Gases on Atmospheric Temperature [Ref. 21].....	23
Figure 4-10. Synthesized Scenario Impact on N+3 Goals.....	24
Figure 4-11. Simulation and Modeling Approach for This Analysis	25
Figure 4-12. Comparison of Daily Flights per Airframe	27
Figure 4-13. Commercial Aircraft Fuel Efficiency Historical Data Indicating Piston-Prop Performance [Ref. 26].....	27
Figure 4-14. (a) Historical Passenger Enplanements Since 1952; (b) Future Traffic Predictions Comparison Ranges [Ref.].....	28
Figure 4-15. Impact of N+3 Surrogate on Baseline JPDO 1.8 Times Traffic NAS Total Delay, Compared to Baseline Fleet Mix	29
Figure 4-16. (a) OEP Airport Distribution; (b) Effect of Metroplex Operations on Traffic Reductions on OEP Airports.....	29
Figure 4-17. (a) U.S. Population Distribution; (b) Airfield Distribution by Longest Field Length for Untowered Runways, Including >4,000 feet and >5,000 feet Bins, Along With Towered Runway	30
Figure 4-18. Histogram of U.S. Airports (Towered and Untowered) as a Percentage of Towered Airports by Max Field Length	31
Figure 4-19. Comparison of Baseline and N+3 Metroplex Hourly Operations at ATL for Three Times Traffic Levels.....	31
Figure 4-20. U.S.-Wide Delay Instances Distribution for January-July 2009 Period (OPSNET) 32	
Figure 4-21. (a) Baseline 1.8 Times Traffic Delay Distributions; (b) Metroplex Operations Delay With >5,000 foot Airfields.....	32
Figure 4-22. (a) Baseline Three Times Traffic Delay Distributions; (b) Metroplex Operations Delay With >5,000 foot Airfields	33
Figure 4-23. Cruise Speed Distribution Shift for an N+2 NAS Simulation Compared to Baseline 737 Distribution	33
Figure 4-24. Aircraft Delay Distribution for a Cruise Speed Decrease of 12 Knots Compared to 737 for an N+3 Vehicle Study	34

Figure 4-25. Effect of Varying Cruise Mach Number on Number of Airframes Required to Complete 8,000 Flights	34
Figure 4-26. Flight Count Projections for Various Future Daily Passenger Traffic Growth Levels	35
Figure 4-27. Number of Flights per Airframe Type (Line) Superimposed on Range Capability Statistical Bars for U.S. Aircraft	36
Figure 4-28. Cumulative Histogram of Flight Counts by Stage Length in the Current CONUS NAS.....	36
Figure 5-1. Engine Downselection Process	38
Figure 5-2. CFM56-3B1 Turbofan	38
Figure 5-3. Three-Shaft Turbofan Mechanical Profile Diagram	39
Figure 5-4. Geared Turbofan Mechanical Profile Diagram.....	39
Figure 5-5. Open Rotor Mechanical Profile Diagram	40
Figure 5-6. Geared Turbofan and Three-Shaft Turbofan SLS SFC Hook Comparison at Comparable Technology Level.....	41
Figure 5-7. Engine Architecture SLS SFC Hook Comparison, Advanced Technology Level.....	41
Figure 5-8. Airframe Configuration Downselection Process	42
Figure 5-9. Tube and Wing Configuration	42
Figure 5-10. Wing-Root Embedded Turbofans With Canard.....	43
Figure 5-11. Tube and Wing Configuration With Canard.....	43
Figure 5-12. HWB With Podded Propulsors	44
Figure 5-13. HWB With Embedded Propulsors Configuration.....	44
Figure 5-14. HWB With Embedded Propulsors Configuration.....	45
Figure 5-15. Channel Wing Configuration With Canard.....	45
Figure 5-16. Joined Wing Configuration	46
Figure 5-17. LARS Configuration	46
Figure 5-18. Configuration Quantitative Assessment.....	47
Figure 5-19. Configuration Quantitative Assessment Discounting Field Length.....	47
Figure 5-20. Technology Assessment Process Flow	48
Figure 5-21. Format of Master QFD Worksheet and Database	49
Figure 5-22. Applied TRL Risk Index Factor.....	49
Figure 5-23. Technology Effectiveness Ratings for Overall Scenario	50
Figure 5-24. Top Ten Technologies for Each Scenario Based on QFD Analysis	50
Figure 5-25. Laminar Flow Regions Visualization for High Aspect Ratio Wing	52
Figure 5-26. Landing Gear Fairing	52
Figure 5-27. Aft Velocity Profile for Ideal BLI and Podded Propulsion Configurations.....	55
Figure 5-28. Surface Weight Reduction Through Aeroservoelastic Structures as a Function of Aspect Ratio.....	57
Figure 5-29. 3-D Woven/Stitched Composite Structural Concept [Ref. 80].....	58
Figure 5-30. NASA ARC Inverted Flow Model With 20-Lobe Mixer [Ref. 83].....	59
Figure 5-31. Inverted Flow Nozzle Noise Reduction	60
Figure 6-1. Aircraft Vehicle Design Study Overview	65
Figure 6-2. Baseline and Advanced Fan Duct Liner Sound Pressure Level Reduction	67
Figure 6-3. Wing Laminar Flow Extent for (a) Aft Fuselage Mounting, (b) Under-Wing Mounting.....	68
Figure 6-4. Effect of Three-Shaft Turbofan Mounting Location on Tube and Wing Mission Fuel Burn With and Without Laminar Flow	69
Figure 6-5. Effect of Open Rotor Mounting Location on Tube and Wing Mission Fuel Burn With and Without Laminar Flow	69

Figure 6-6. HWB With Laminar Flow Fuel Burn, Laminar Flow Penalty Mitigation Effects.....	71
Figure 6-7. Initial Sizing Tube-and-Wing M_{DD} Sensitivity Study.....	72
Figure 6-8. Initial Sizing HWB M_{DD} Sensitivity Study.....	72
Figure 6-9. CAEP/6 LTO NO _x Requirements.....	73
Figure 6-10. FAR Part 36 Stage 4 Cumulative EPNL Noise Requirements	75
Figure 6-11. ATW Individual Technology Assessment	77
Figure 6-12. HWB Individual Technology Assessment.....	78
Figure 6-13. System Effectiveness Rating Comparison Between Candidate Configurations	80
Figure 6-14. Effect of Configuration Δ EPNL on System Effectiveness Rating.....	82
Figure 6-15. Preferred N+3 Configuration	82
Figure 6-16. Preferred Configuration Planform and Technology Contributions to Mission Fuel Burn Reduction	86
Figure 6-17. Preferred Configuration Platform and Technology Contributions to Community Noise Reduction.....	87
Figure 6-18. CAEP/6 LTO NO _x Emissions Requirement and N+3 Achievements	88
Figure 7-1. TMP for Virtual Landing Gear Fairings	90
Figure 7-2. TMP for Swept-Wing Laminar Flow Slat Integration	91
Figure 7-3. TMP for Swept-Wing Laminar Flow Control.....	92
Figure 7-4. TMP for Stitched/Woven Composite Structures	93
Figure 7-5. TMP for Advanced Structural and Subsystem Alloys	94
Figure 7-6. TMP for SMA Variable Geometry Nozzles.....	95
Figure 7-7. TMP for M5 Organic Fiber Composites	96
Figure 7-8. TMP for Carbon Nanotube Electrical Cables	97
Figure 7-9. TMP for Computational Inlet Optimization.....	98
Figure 7-10. TMP for Large Integrated Structures	99
Figure 7-11. TMP for Aeroservoelastic Structures.....	100
Figure 7-12. TMP for Lightweight Fan Structure and Cowl	101
Figure 7-13. TMP for Intercooled Compressor Stage	102
Figure 7-14. TMP for Cooled Cooling Air	103
Figure 7-15. TMP for Endothermic Fuel Cracking	104
Figure 7-16. TMP for Staged Combustion	105
Figure B-1. Sound Power vs. Blowing Rate (% Inlet Flow Rate) for (a) Inlet Duct and (b) Aft Duct [Ref. 139].....	125
Figure B-2. Upper Surface Exhaust Nozzle and Flap Lift Comparison	126
Figure B-3. Tilt Rotor Aerodynamics.....	135
Figure B-4. Noise Attenuation With And Without Microtab Features.....	138
Figure C-1. Preferred Vehicle Low-Speed Drag Polar for Takeoff at 0 feet Altitude.....	144
Figure C-2. Preferred Vehicle Low-Speed Drag Polar for Landing at 0 feet Altitude.....	145
Figure C-3. Preferred Vehicle High-Speed Drag Polar for Landing at 45,000 feet Altitude	145
Figure D-1. OASPL Example Source Plot	147
Figure D-2. Noise Source Levels Reference Vehicle at 250 feet Altitude [Descent-Landing]..	148
Figure D-3. Noise Source Levels Reference Vehicle at 250 feet Altitude [Takeoff-Climb]	148
Figure D-4. Noise Source Levels ATW, Scaled CFM56-3B1, No Advanced Technologies at 250 feet Altitude [Descent-Landing]	149
Figure D-5. Noise Source Levels ATW, Scaled CFM56-3B1, No Advanced Technologies at 250 feet Altitude [Takeoff-Climb].....	149
Figure D-6. Noise Source Levels HWB, Scaled CFM56-3B1, No Advanced Technologies at 250 feet Altitude [Descent-Landing]	150

Figure D-7. Noise Source Levels HWB, Scaled CFM56-3B1, No Advanced Technologies at 250 feet Altitude [Takeoff-Climb].....	150
Figure D-8. Noise Source Levels Preferred Configuration at 250 feet Altitude [Descent-Landing]	151
Figure D-9. Noise Source Levels Preferred Configuration at 250 feet Altitude [Takeoff-Climb].....	151
Figure E-1. QFD Worksheet.....	153

1 EXECUTIVE SUMMARY

Northrop Grumman has developed an advanced aircraft concept whose mission capabilities enable it to fill a broad, primary need within the future scenario envisioned for the 2030-2035 timeframe. This effort was conducted under NASA Contract NNC08CA86C. No single vehicle type is adequate to meet all needs simultaneously. Multi-objective studies identified vehicle concepts with the best potential for meeting the combined goals. Trade studies provided insight into individual goals, in particular as they related to the future scenario for the 2030-35 and beyond timeframe. It is possible that future capacity challenges at major airports can be addressed by increased use of exiting runways and reliever airports, without the need for public investment in capital infrastructure and without the need for short take-off and landing (STOL) capable aircraft.

The primary vehicle requirements that drove technology selection, configuration selection, and optimization were derived from the published NASA N+3 goals shown in Table 1-1. These goals were further refined based on an overarching future scenario study that captured likely future economic and operational factors.

Table 1-1. NASA Generational Aircraft Goals

Corners of the Trade Space	N+1 (2005 Entry Into Service) Generation Conventional Tube and Wing (Relative to B737/CFM56)	N+2 (2020 Initial Operating Capability) Generation Unconventional Hybrid Wing Body (Relative to B777/GE90)	N+3 (2030 - 2035 Service Entry) Advanced Aircraft Concepts (Relative to User -Defined Reference)
Noise (Cum Below Stage 4)	-32 dB	-42 dB	-71 dB
LTO NOx Emissions (Below CAEP 6)	-60%	-75%	Better than -75%
Performance: Aircraft Fuel Burn	-33%	-40%	Better Than -70%
Performance: Field Length	-33%	-50%	Exploit Metroplex Concepts

A study of the current vehicle fleet mix was used to determine the most broadly applicable airframe in use today based on stage-lengths served, and then extrapolate that based on the future scenarios. Simulations of the future vehicle in the National Airspace System (NAS) with the implementation of NextGen Air Traffic Management (ATM) capabilities were used to assess the impact of vehicle sizing and metroplex operations on projected traffic levels. The ability to adopt metroplex-type operations was assessed by a study of runways at existing airports, combined with NAS simulations. It was found that the use of reliever airports with at least one runway of 5,000 ft length within 70 nautical miles of major population centers would enable metroplex operations while keeping pace with projected traffic levels. A single set of design requirements emerged from these studies, as summarized in Table 1-2.

Table 1-2. Mission Requirements

Mission Requirements	
Range (with reserves):	1600 nm
Passengers:	120
Balanced Field Length (Sea Level/Standard Day):	5000 ft
Landing Distance (Sea Level/Standard Day):	5000 ft
Minimum Cruise Mach:	0.75

Several other critical design concepts emerged. First, it became evident that cruise Mach number can be reduced to save fuel burn without significant impact on throughput or delay in the overall air transportation system. A byproduct of cruising slower is that the airplane will fly higher to achieve the desired cruise lift coefficient for best efficiency. Second, short takeoff and landing (STOL) and extremely

short takeoff and landing (ESTOL) capability is not required to meet the 5000 foot runway requirement. Relaxing the design space on cruise Mach number and maximum lift coefficient provided more latitude for achieving desired improvements in fuel burn. Finally, a wing span limitation of 150 feet was imposed to accommodate space restrictions at metroplex airports.

Two important tasks were undertaken before beginning aircraft design studies. The Flight Optimization System (FLOPS) vehicle sizing program developed by NASA was to be the engine for all optimization studies. First, FLOPS was calibrated using a 737-800 with CFM56-7B27 engines to match published weight and performance data to within an accepted tolerance. Next, a reference vehicle was derived as a baseline against which performance and noise metrics could be measured. This reference vehicle was derived from a 737-500, resized to match the requirements of Table 1-2 (new wing size, new thrust level, etc.), but with the same level of technology as the 737. This reference vehicle would be the “yardstick” for measuring improvement in subsequent designs.

A wide design space of airframe configurations was initially considered. Technologies were then systematically applied in a conceptual design process. Low-order models and a mix of empirical and analytic estimation methods were used to describe component-level benefits over the vehicle flight envelope. Weighting factors for the N+3 goals were developed as part of the future scenario analysis, and these weighting factors were incorporated into a System Effectiveness Rating (SER). The aircraft with the highest SER emerged as the preferred concept vehicle. The preferred concept, summarized in Figure 1-1, reflects a NextGen-capable platform that best meets the potential future traffic demands and satisfies the N+3 goals and the mission requirements listed in Table 1-3.

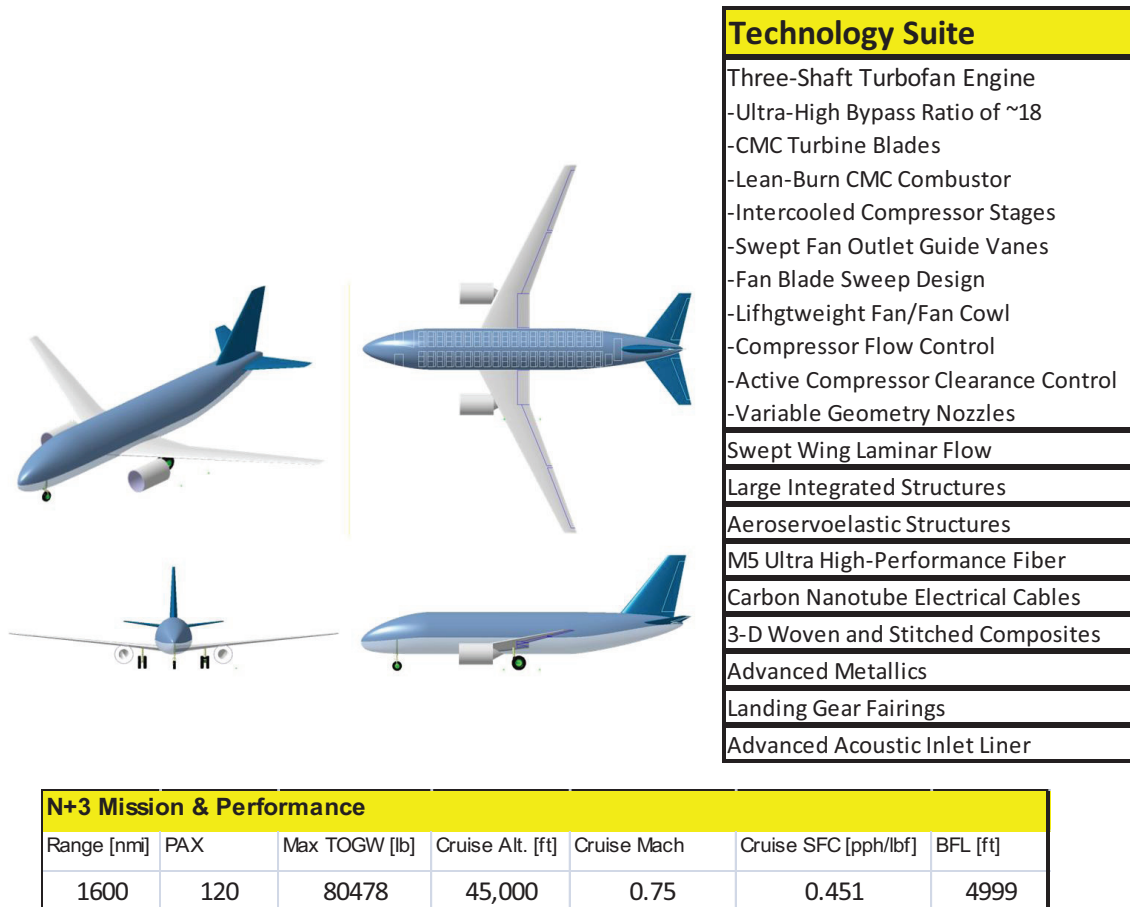


Figure 1-1. N+3 Preferred Configuration 3-View and Mission Performance

Table 1-3. N+3 Goals Achievement

Metric	Requirement		Actual		Achievement	Overall Scenario Weighting Factor
Noise	-71 EPNdB relative to Stage 4	200.3 EPNdB	201.7 EPNdB	69.6 EPNdB below Stage 4	20.00%	
Fuel Burn	70% below reference vehicle	7514 lbf	9145 lbf	63.49% below reference vehicle	33.33%	
Emissions	75% below CAEP/6	25.7 g/kN	9.69 g/kN	90.59% below CAEP/6	33.33%	
Balanced Field Length	exploit metroplex	5,000 ft	4,999 ft	exploited metroplex	13.33%	

Several key technologies influence the outcome of the design. Advanced technology engines contribute to improved fuel efficiency, noise, and nitrous oxide (NOx) emissions. Advanced materials reduce the empty weight of the aircraft and enable high aspect ratio, highly efficient, wings. Swept-wing laminar flow reduces drag and further improves cruise efficiency. Several technologies that initially looked promising did not prove their worth after further study. Hybrid wing-body configurations did not have the volumetric packing factor to be viable in this class of vehicle. Open rotor engine architectures provide significant opportunity to improve SFC, but the extra weight associated with the gear box and propulsor rotors offset much of that benefit in this class of vehicle. The lack of maturity in noise prediction methods for open-rotor configurations, and the associated uncertainty with community noise estimates, also contributed to this technology being set aside. However, the studies did imply that hybrid wing-bodies and open rotors might show benefits in application to extremely large long-range aircraft. A different set of mission requirements might have resulted in a different preferred technology set applied to a different configuration.

A key product of this study was the development of technology maturation plans (TMPs). These TMPs will assist NASA in planning its future investment in a manner that supports enabling critical technology items at Technology Readiness Level (TRL) 6 by the 2025 timeframe. This is essential to support an entry into service (EIS) date of 2030-2035. Technologies and architectures that strongly influence attaining critical mission performance metrics must be at a solid TRL 6 or better in order to minimize commercial risk. TMPs for the selected technologies are available in Section 7. Technologies that were considered but not included for further consideration are listed in Appendix B, including the reasoning for their dismissal from the preferred technology set. In many cases, sufficient TRL in the required timeframe was a determining factor. In others cases, incompatibility with competing technologies played the greatest role in the exclusion of certain technologies from the final package.

This study shows that significant advances in efficiency, community noise, and NOx emissions are attainable with focused technology advances in propulsion systems, aerodynamic technology, material systems, and other technologies. Furthermore, the system-level achievements are shown to be consistent with the broad needs identified in the scenario studies for the 2030-2035 timeframe. Wise investment by NASA in these enabling technologies will benefit not only the flying public, but the environment as well.

2 TECHNICAL APPROACH

Successfully identifying our preferred air vehicle concept for the program's objectives began with defining the anticipated future operating scenario. Through evaluating operations in the context of vehicle performance, passenger count, turnaround time, requirements were determined and then flowed to the design team. This was accomplished by investigating currently available data used in prior NASA studies, by performing new simulations of the NAS using an approximate model of an N+3 vehicle, and by assessing the available infrastructure and how it is impacted by NextGen ATM implementation, which is assumed to be fully completed by the EIS date. Figure 2-1 shows a summarized description of the technical approach used in this program.

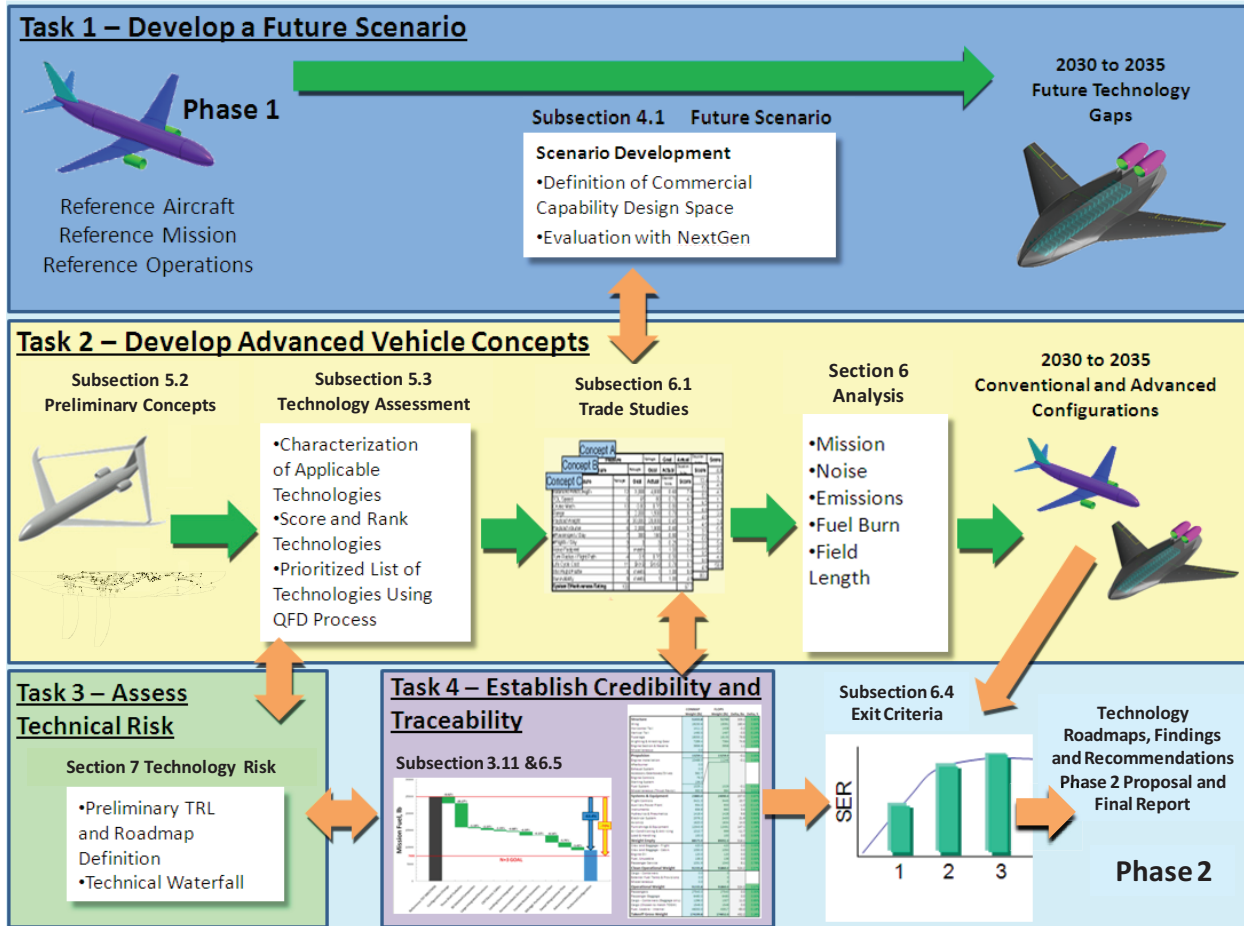


Figure 2-1. Technical Approach

Requirements and weighting factors for the N+3 goals were also derived from examining a set of scenarios for the N+3 timeframe. The scenarios project the future world political, social, and economic states with a focus on the United States. A set of fifteen published reports was used to compile and analyze the drivers most relevant to aviation, including energy resource supply and demand, political turmoil or order, and social protest to environmental factors. These drivers were grouped by common macroeconomic effects and were then used to develop an overall scenario that could bound estimates on future traffic levels, and quantify the relative importance of the N+3 goals.

Modeling tools to predict performance and weight were calibrated using a Boeing 737-800. Comparisons of other NGC tools were used to further validate and assess the accuracy of system weights, acoustic predictions, and aerodynamic performance.

In order to specifically measure the N+3 metrics with respect to a state-of-the-art commercial transport, a reference vehicle was required. The Boeing 737-500 with CFM56-3B1 engines was resized to meet the N+3 mission requirements, while holding a constant level of technology. The resulting reference vehicle had a larger wing area and slightly more thrust than the 737-500. This reference vehicle served as a baseline from which the N+3 fuel burn goal was defined. Similarly, this vehicle was used as a valuable reference for weight, emissions, and acoustic results.

The next task was to develop a super-set of configurations and technologies that best applied to the vehicle mission and requirements defined by the NAS analyses and scenario study. For the technology application, a quality function deployment (QFD) method was used to identify a preliminary set of technologies best suited to the future mission requirements. A technology database, with input from all disciplines, allowed the ranking of a large number of candidate technologies to quickly and effectively identify the best suites for a particular configuration. Each technology was also assessed for compatibility with other technologies, to improve the quality of the identified sets in terms of vehicle-level impact. Risk level was also factored into the ranking process to apply an up-front, first-order risk reduction to the ranking. Technologies that were deemed too immature for the N+3 timeframe were discarded. Figure 2-2 shows the technological development and implementation process that was assumed as a driver behind technology selection. Total development time from concept to EIS must allow key technologies that fundamentally influence aircraft size and configuration to be significantly mature to manage commercial risk. With EIS in 2030-2035, a technology would require substantial maturity, TRL 6, by 2025. This point defines the minimum level of acceptable commercial risk prior to initiating the design and development phase of the aircraft. After this point, technology maturation continues, and risk is further reduced. Subsequent trade studies and analysis would later narrow this technology list further before arriving at a preferred technology set.

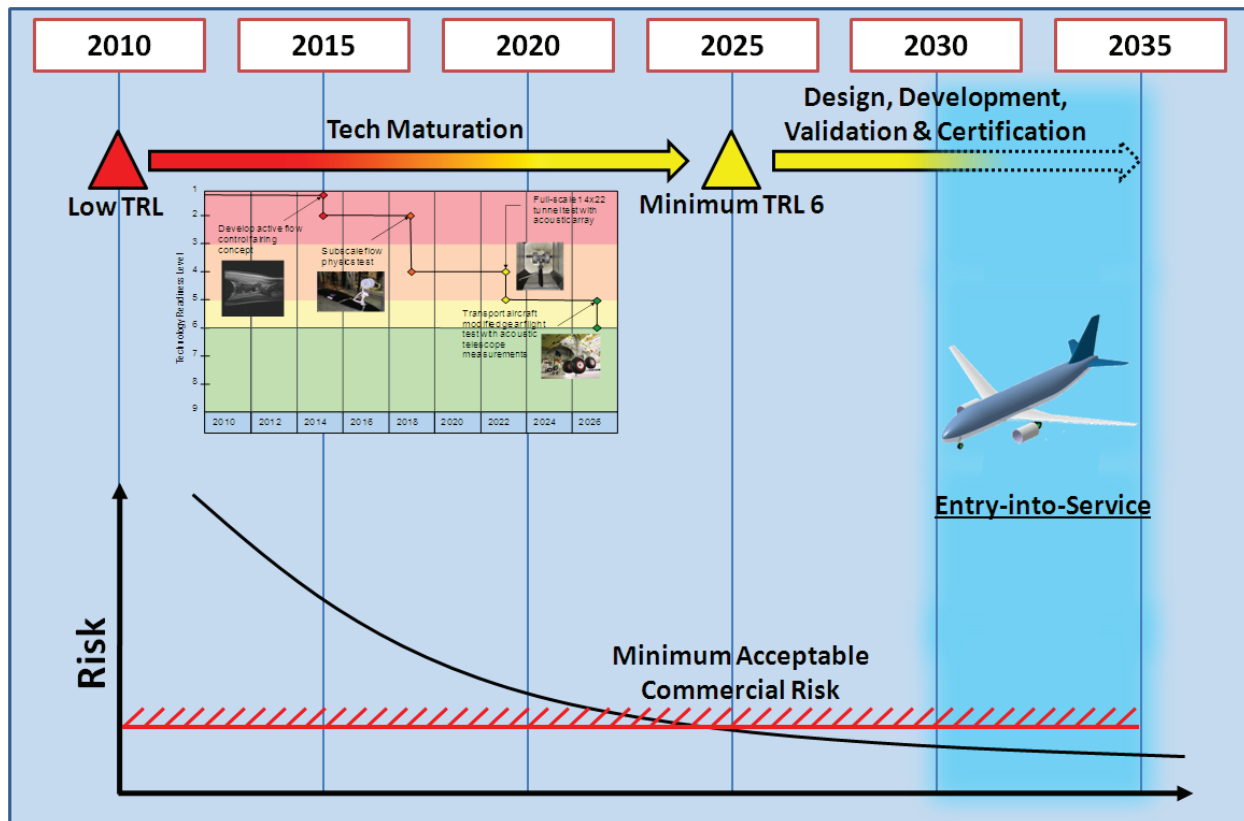


Figure 2-2. Assumed Technology Maturation and Implementation Timeframe

During the conceptual design and examination of the airframe configurations, aerodynamic models were implemented using a mix of empirical and analytical data. Technology packages were assembled to maximize the effectiveness of each airframe against the N+3 goals. A reduced set of candidate technologies was eventually identified that best met all of the N+3 goals on the basis of the technology effectiveness rating (TER), an all-encompassing parameter that is a function of the N+3 goals. These technologies were then modeled using various low-order techniques to simulate their performance and weight impacts across the vehicle flight envelope. Trades were performed with and without the technology packages, since many of the technology applications (for example, laminar flow) required trades to other configuration design parameters. Models for the configurations deemed applicable were refined further in a CAD environment that allowed more technical fidelity. Advanced engine models were developed for the appropriate thrust class for these vehicles, resulting in models for both a high bypass ratio three-shaft turbofan and an open rotor engine architectures. Both engine concepts were investigated in various installations, including aft-mounted, embedded, and under-wing and over-wing installations. These concepts were evaluated in FLOPS for their ability to meet mission requirements. Technology suites and airframe configurations were objectively evaluated on the SER basis to form a preferred package.

In a final iteration with the NAS simulations, the selected N+3 concept (Figure 1-1), was modeled and re-evaluated in a sample Hartsfield-Jackson Atlanta International Airport (ATL) metroplex to identify the benefits of the system on a local level. The impacts of operating the vehicle at a reduced cruise speed compared to the reference vehicle, as well as the impacts of the fuel efficiency and mission performance, were evaluated on a system level to assess more realistic operational effects.

Technology maturation plans for the preferred technology package were devised for the development of the technologies to maturity in a timeframe to support a 2030-2035 EIS. These roadmaps project the developmental requirements associated with maturing each technology to TRL 6 by the year 2025. It is estimated that this lead time will be required to implement these technologies into the design and development phase of the N+3 generation of commercial transport aircraft.

3 AIR VEHICLE DESIGN TOOLS AND PROCESSES

3.1 Flight Optimization System (FLOPS)

FLOPS is a tool developed by NASA Langley Research Center that allows for the preliminary design and analysis of flight vehicles [Ref. 1]. FLOPS combines nine separate modules that allow for the multidisciplinary design of an air vehicle. These modules include weights, aerodynamics, engine cycle, propulsion data scaling and interpolation, mission performance, takeoff and landing, noise footprint, and cost analysis, all controlled by an outer program control loop.

The weights module uses empirical equations to predict the system and mission segment weights, and outputs a high-level weight summary. The module contains detailed inputs for a wide range of aircraft components and subsystems that allow for the calibration of their respective weights. These parameters can be further modified to reflect weight changes caused by the application of various technologies to the vehicle. Once properly calibrated using Northrop Grumman's CONMAP (Section 3.4), a proprietary parametric weight estimation program, the FLOPS weights module outputs the weight summary. Center of gravity and balancing were also performed using the CONMAP program discussed in Section 3.4.

The aerodynamics module stems from the Empirical Drag Estimation Technique (EDET), an algorithm based on user input which calculates drag polars for high-speed performance. The module contains input parameters used to calibrate the high-speed drag polars to achieve expected aerodynamic performance based on in-house databases and experience. Low-speed drag polars were input into this module for takeoff and landing, with corresponding reference values for geometric scaling as the aircraft is resized by FLOPS.

Engine data tables provided, among other things, the thrust and fuel flow information required by FLOPS. The propulsion data scaling and interpolation module fills in any missing data in the engine tables, and uses both linear and nonlinear scaling to adjust them to the required sea level static thrust. While engine scaling is conducted automatically in this module, the user must ensure that the scaling does not exceed the limits imposed by the engine model.

The mission performance module uses outputs from the weights, aerodynamics, and propulsion modules to compute performance, optimum climb profiles, optimum or user-specified cruise segments, and user-specified descent schedules. Other performance parameters may be specified or calculated in this module, including acceleration, turn, refueling, payload release, hold segments, and reserve fuel calculations.

The takeoff and landing module computes balanced and landing field lengths, approach speed, second segment climb gradient, and missed approach climb gradient. The module generates detailed takeoff, climb, landing, and descent profiles that were subsequently used in calculating the aircraft noise characteristics.

The final module contained in FLOPS pertinent to this study is the program control module. FLOPS can perform a point design based on a full set of geometric inputs, conduct a parametric study across an array of design variables, or optimize a geometry based on an input objective function. This optimization may use one of several algorithms, including Broyden-Fletcher-Goldfarb-Shanno and Steepest Descent. The optimization routine in FLOPS was not used during later portions of this study due to its inability to converge over broad design spaces. The point design and parametric analyses were later used in conjunction with an internally-developed optimization tool to be discussed later in Section 3.2.

3.1.1 Calibration Process

In order to calibrate the FLOPS tool, an analysis was performed on the Boeing 737-800, for which weight and performance data was readily available. This process is detailed in Figure 3-1, and will be described in the following sections. As the design study matured and new vehicles began to deviate from

the initial design point, this process was repeated to ensure that the calibration remained valid. In this manner, confidence in the tool was maintained throughout the duration of the study.

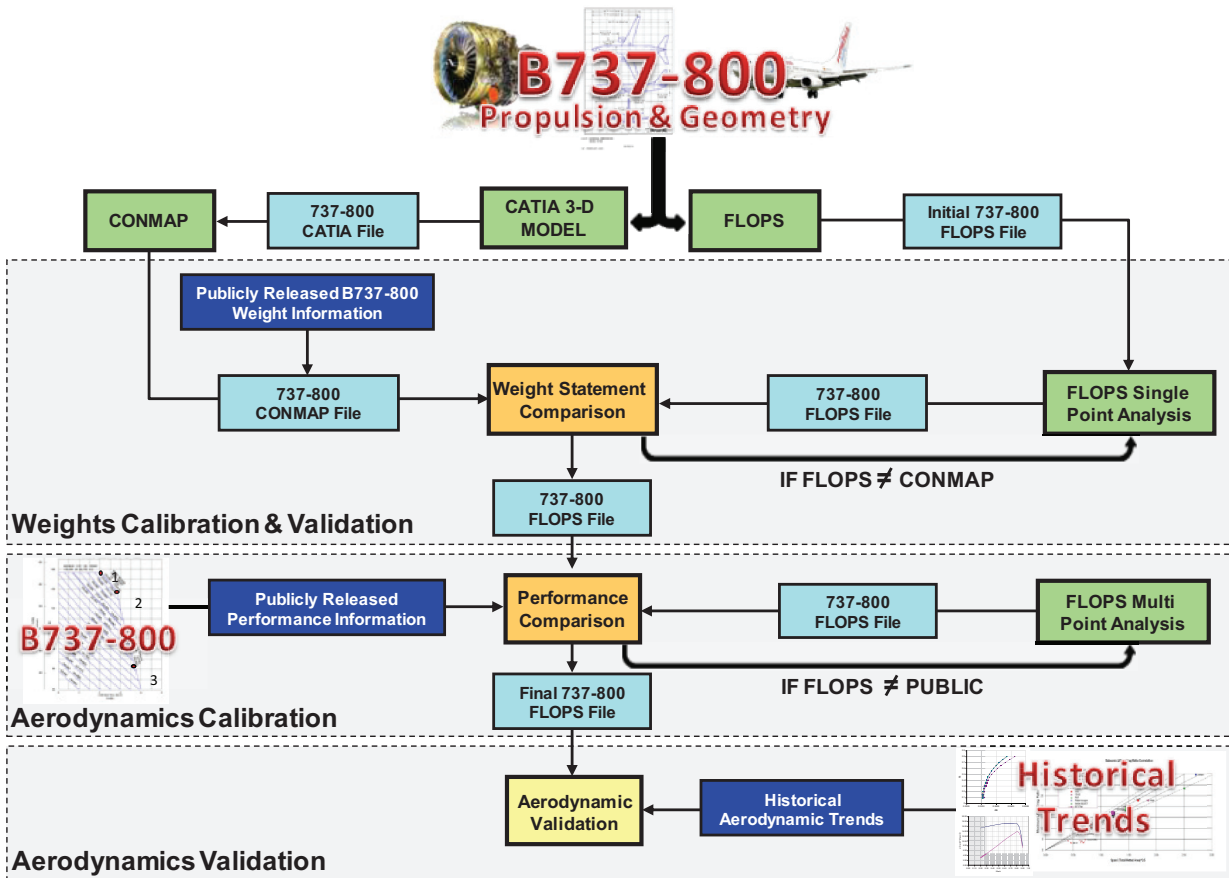


Figure 3-1. FLOPS Calibration Process With the 737-800

3.1.1.1 Configuration Weight Calibration and Validation – The Boeing 737-800 was modeled in CATIA and FLOPS using information from the Boeing 737 Airport Planning Guide [Ref. 2]. Engine tables were obtained for the CFM56-7B27, the engine installed on the 737-800. Upon being modeled in CATIA, the 737-800 CATIA file was analyzed in CONMAP, producing a system- and component-level weight statement. This CONMAP statement was compared against publicly-released weight information for this aircraft to verify its accuracy. In parallel to the CONMAP analysis, the configuration was modeled and analyzed in FLOPS, generating a similar weight statement. The weight statements from both tools were compared and segment level adjustments made in FLOPS to calibrate the component weights predicted by FLOPS to the higher-fidelity predictions of CONMAP to within a specified tolerance. As a result, the subsystem weights, overall vehicle empty weights, operating weights, zero fuel weights, and gross weights output by FLOPS were within one percent of those output by CONMAP. The weight statement comparison between CONMAP and the calibrated FLOPS tool is shown in Table 3-1. It must be noted that in the FLOPS analysis, the weights of the accessory gearbox, engine controls, and starting system are all included in the engine installation weight, and not individually broken down.

Table 3-1. CONMAP and FLOPS Weight Calibration for the Boeing 737-800

	CONMAP	FLOPS	Delta	
	Weight (lb)	Weight (lb)	[lbs]	[%]
Structure	51433.8	51743	309.2	0.60%
Wing	19230.6	19391	160.4	0.83%
Horizontal Tail	1411.2	1408	-3.2	-0.23%
Vertical Tail	1490.5	1487	-3.5	-0.23%
Fuselage	18055.2	18135	79.8	0.44%
Alighting & Arresting Gear	7289.4	7364	74.6	1.02%
Engine Section & Nacelle	3956.9	3958	1.1	0.03%
Miscellaneous	0.0			
Propulsion	13259.1	13259.0	-0.1	0.00%
Engine Installation	10468.0	11246	-0.1	0.00%
Afterburner	0.0			
Exhaust System	0.0			
Accessory Gearboxes/Drives	562.7			
Engine Controls	79.3			
Starting System	136.0			
Fuel System	1029.1	1029	-0.1	-0.01%
Miscellaneous (Thrust Reverser)	983.9	984	0.1	0.01%
Systems & Equipment	23883.0	24090.0	207.0	0.87%
Flight Controls	3421.3	3445	23.7	0.69%
Auxiliary Power Plant	934.0	933	-1.0	-0.11%
Instruments	656.6	660	3.4	0.52%
Hydraulics & Pneumatics	1418.4	1428	9.6	0.68%
Electrical System	2378.2	2400	21.8	0.92%
Avionics	1620.0	1634	14.0	0.86%
Furnishings & Equipment	12343.9	12491	147.1	1.19%
Air Conditioning & Anti-Icing	1010.7	999	-11.7	-1.15%
Load & Handling	100.0	100	0.0	0.00%
Weight Empty	88575.9	89092.0	516.1	0.58%
Crew and Baggage - Flight	420.0	420	0.0	0.00%
Crew and Baggage - Cabin	1050.0	1050	0.0	0.00%
Engine Oil	120.0	120	0.0	0.00%
Fuel, Unusable	138.0	138	0.0	0.00%
Passenger Service	1031.9	1040	8.1	0.78%
Clean Operational Weight	91335.8	91860.0	524.2	0.57%
Cargo - Containers	0.0	0		
External Fuel Tanks & Provisions	0.0	0		
Miscellaneous	0.0	0		
Operational Weight	91335.8	91860.0	524.2	0.57%
Passengers	27540.0	27540	0.0	0.00%
Passenger Baggage	6480.0	6480	0.0	0.00%
Cargo - Containers (Baggage only)	1296.0	1307	11.0	0.85%
Cargo (Chosen to match TOGW)	1548.0	1548	0.0	0.00%
Fuel, Usable - Internal	46000.0	45917	-83.0	-0.18%
Takeoff Gross Weight	174199.8	174652.0	452.2	0.26%

Validation of the FLOPS calibrations against CONMAP was needed to verify the calibration of the tools. The newly calibrated weight statement compared well to publically released weight data for the vehicle [Ref. 2]. Maximum ramp weights, takeoff and landing weights, zero fuel weights, empty weights, structural weights, and payload weights were within an acceptable tolerance, thus validating the weight calibration for additional tube-and-wing. A similar process was used to calibrate these tools for hybrid wing-body vehicles using a Northrop Grumman internal database of all-wing aircraft.

3.1.1.2 Tube-and-Wing Aerodynamic Calibration – After calibrating and validating the vehicle weights, calibration of the FLOPS aerodynamics module followed. Takeoff and landing maximum lift coefficients and low-speed drag polars were set to historically accurate values for comparable tube-and-wing vehicles. The low-speed drag polars were input into FLOPS such that they would be geometrically scaled. High-speed drag polars were calculated internally in FLOPS through the aerodynamics module, but were calibrated to match publically released performance characteristics for multiple payloads and ranges as shown in Figure 3-2 and Table 3-2 [Ref. 2]. Aerodynamic outputs from FLOPS were validated against historical trends for tube-and-wing aircraft of similar gross weight and passenger count.

3.1.1.3 Hybrid Wing-Body Aerodynamic Calibration – The hybrid wing-body aerodynamic characteristics were calibrated against a proprietary database of Northrop Grumman all-wing vehicles. Low-speed drag polars and lift coefficients for takeoff and landing were input into FLOPS such that they would be geometrically scaled as the configuration was resized. High-speed drag polars were calculated internally in FLOPS, but were calibrated to the polars of similar all-wing vehicles. The drag divergence Mach number, maximum lift-to-drag ratio, and cruise lift coefficient were among other aerodynamic parameters calibrated in the FLOPS aerodynamic module against this internal database.

3.1.2 Reference Vehicle

For comparison and traceability during this study, a reference vehicle was configured as shown in Figure 3-3. This reference vehicle was derived from the Boeing 737-500 with the CFM56-3B1 engine. However, the aircraft was resized to meet the same requirements as the N+3 vehicle in terms of field length, passenger count, and range. The 737-500 and CFM56-3B1 engine were modeled in FLOPS and were resized to meet the N+3 mission. In the resizing of the aircraft, technology level was held constant in addition to nondimensional characteristics including aspect ratio, taper ratio, and thickness-to-chord ratio. Engine cycle was held constant, and the engine was scaled in size and weight as necessary. The wing area and thrust increased over the 737-500, primarily driven by the 5,000-foot field length requirement. The resulting vehicle

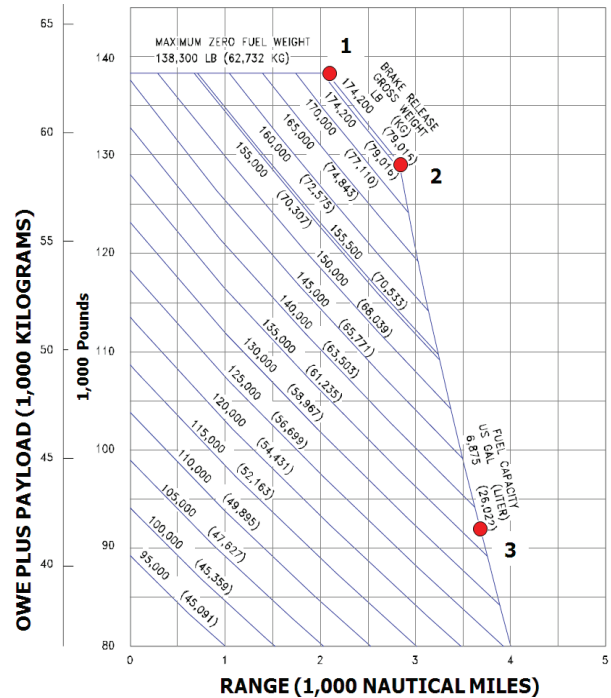


Figure 3-2. Boeing 737-800 Performance Calibration Points (Shown in Red)

Table 3-2. 737-800 Performance Calibration Points

	Unit	1	2	3
Condition	--	Max Payload	Max Fuel	Zero Payload
OWE	lbs	91,300	91,300	91,300
Payload	lbs	47,000	36,700	0
ZFW	lbs	138,300	128,000	91,300
Fuel	lbs	35,700	46,000	46,000
TOGW	lbs	174,000	174,000	137,300
Range	n.mi.	2,075	2,850	3,700

served as a reference from which the N+3 achievements were measured. Its characteristics are summarized in Table 3-3 and are compared against the 737-500 from which it was derived.

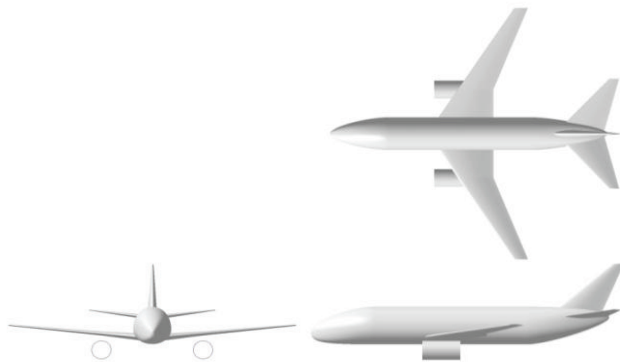
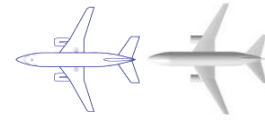


Figure 3-3. Reference Vehicle

Table 3-3. Reference Vehicle Characteristics



	Units	737-500	Reference Vehicle
# Passengers	[]	123	120
Range	[nm]	2,400	1,600
Ramp Gross Weight	[lb]	133,500	120,170
Empty Weight	[lb]	68,860	67,350
Fuel Weight	[lb]	42,186	25,048
Wing Reference Area	[ft ²]	1,135	1,280
Wing Sweep	[deg]	25	25
Wing Span	[ft]	94.9	100.4
Wing AR	[]	7.9	7.9
T/W Ratio	[]	0.3	0.34
Max Wing Loading	[psf]	117	94
Balanced Field Length	[ft]	8,630	4,497
Landing Field Length	[ft]	4,450	4,996

3.2 Optimization Method

Because the FLOPS' optimizer has well-documented problems with converging over broad design ranges [Ref. 3, 4], an internally developed tool was used to optimize parametric FLOPS solutions on a user-specified objective function. For example, an objective function could be defined to minimize fuel weight only, or a weighted combination of empty weight and fuel weight. The optimization tool uses FLOPS' parametric analysis mode to generate an array of vehicles with varying wing area, aspect ratio, sweep and thrust within specified boundaries. A parsing algorithm then sorts the resulting configurations, eliminating those that do not meet imposed requirements. For example, configurations that did not meet the balanced field length constraint were eliminated, as were designs with wingspans greater than 150 ft. The distilled configuration list is then output to an Excel file where the objective function is applied to each configuration to further sort the remaining vehicles and refine the boundaries of the next parametric analysis iteration. This process is repeated for several iterations, until the vehicle design tool converges within a user-specified tolerance on an optimum configuration. The objective function was chosen to minimize a combination of empty weight and fuel weight. Though fuel burn remains a primary target of the N+3 program, the decision was made to maintain some recognition that empty weight must be constrained. Without this constraint, FLOPS would create impractical configurations, most notably very large aspect ratio aircraft. Once an optimum configuration is reached for the given inputs (i.e., airframe configuration, engine, and technology application), it is then analyzed in FLOPS' point-design mode to generate a detailed mission profile, including takeoff and landing trajectories, weight breakdown, and segment fuel reports. Figure 3-4 shows the multitude of solutions developed by the FLOPS parametric solver for four consecutive iterations.

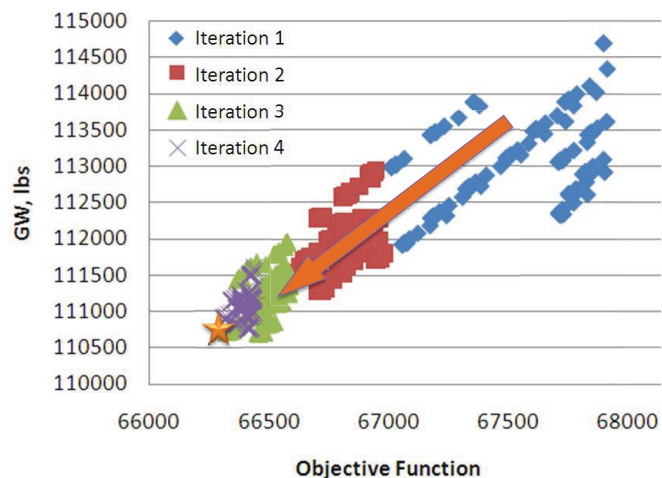


Figure 3-4. Optimization Methodology

3.3 Airspace Concepts Evaluation System (ACES)

ACES is a tool that simulates nationwide air traffic management, flight, and airspace operations center functions [Ref. 5]. ACES simulates the air traffic system by using software that simulates hundreds of airports with Terminal Radar Approach Control (TRACONs), flight centers and sectors, thousands of flights gate-to-gate, and numerous airspace operations centers, as well as the interaction between these agents. ACES is able to simulate a realistic operating environment through complex multi-day flight schedules and flight plans, four dimensional (4-D) gridded winds, and adjustable operation conditions. Aircraft trajectories are realistically simulated through a four degree-of-freedom model that is based on laws of physics, aerodynamics, pilot-based control laws, and elliptic Earth trajectory propagation. ACES creates dynamic visualizations of the airspace and delays, and is equipped with extensive data recording and analysis tools.

The tool allows the system-wide impacts of new aviation concepts to be analyzed, and can visualize how the NAS will handle future flight demands. ACES is able to analyze the effects of introducing N+3 vehicles into current and future air traffic environments. It can also assess the exploitation of metroplex operations by integrating NextGen-enabled satellite airfields. The tool is used in this study to complete trades on cruise Mach number, range, and runway length for N+3 vehicle configurations and the resulting effects on the complex air space and operations environment. A diagram of the components and process used by ACES is shown in Figure 3-5.

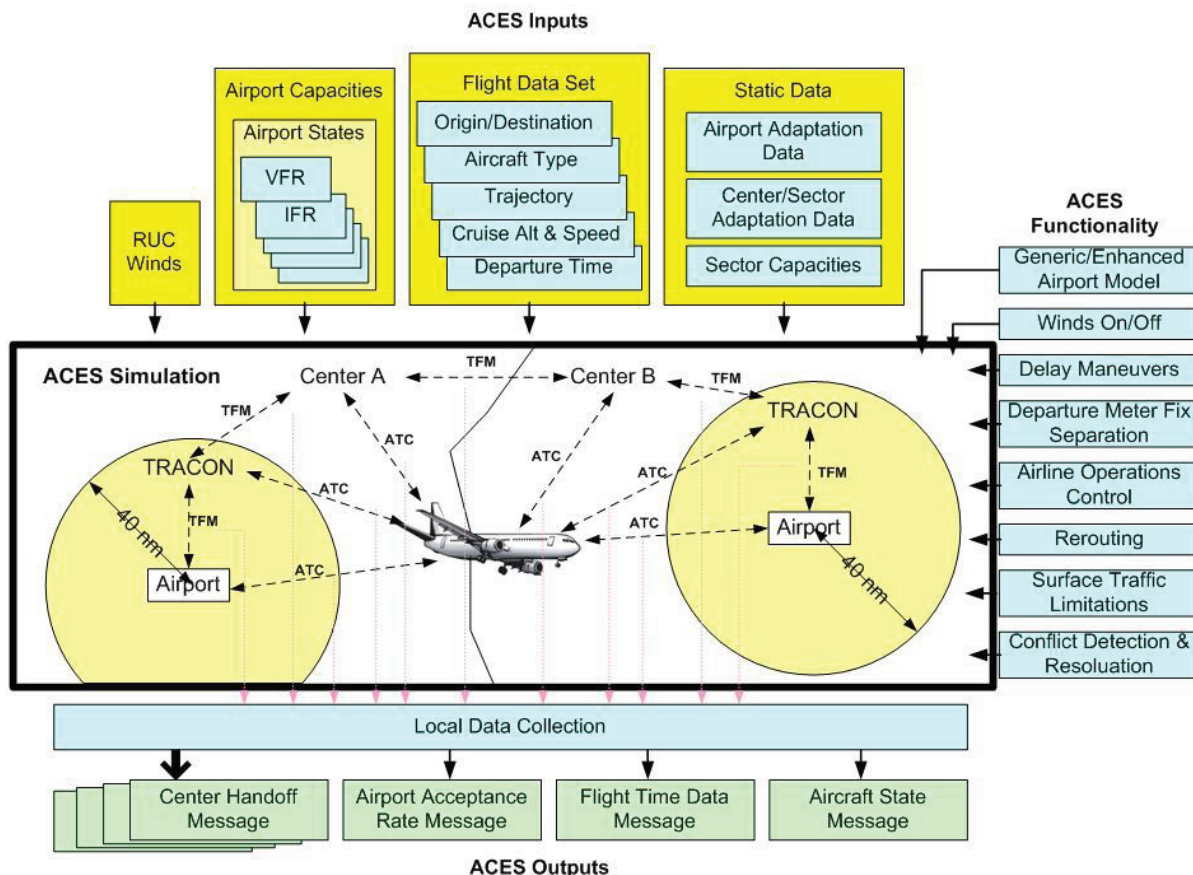


Figure 3-5. ACES Simulation Components and Data Flow Diagram

3.4 Conceptual Mass Properties (CONMAP)

CONMAP is a parametric feature-based weight estimation program developed using the Northrop Grumman aircraft database. This proprietary program provides high-level weight and longitudinal center of gravity estimates based on vehicle geometry, system definitions, and vehicle functions, as well as

allowing for the incorporation of special features not within the database. For initial calibration of the FLOPS tool, a CONMAP tool was used for calculating the mission segments: vehicle empty weight, operational empty weight, and basic mission takeoff weight. Factors within the FLOPS tool were adjusted for calibration on the initial starting points. Furthermore, CONMAP was used to calculate the center of gravity for wing placement on the preferred configuration.

3.5 Numerical Propulsion System Simulation (NPSS)

NPSS is a simulation tool licensed by Wolverine Ventures, Inc. that was originally developed at NASA Glenn Research Center for the analysis and design of complex systems, such as aircraft engines [Ref. 6]. As an object-oriented engineering tool, NPSS is easily integrated into multidisciplinary optimization tools and adaptable to many diverse applications and software. Existing software architecture allows for the simple modeling of aircraft engine components, including compressors, turbines, mixers, ducting, and combustors. Its flexibility allows for user-specified degrees of fidelity in the models of individual engine components. For example, if three dimensional (3-D) computational fluid dynamics (CFD) is available to predict the flow through a particular compressor, this software or its results can be interfaced with NPSS to serve as a performance model. At the same time, a simple polytropic efficiency can be used to calculate the turbine flow. This software has become an industry standard in engine development, and is the primary tool that was used to develop the N+3 advanced engine architectures.

3.6 Acoustic Liner Design Process

Design and analyses were performed of various inlet liners for N+3 vehicle propulsion systems as part of the noise reduction effort (Figure 3-6). Acoustic impedance models were utilized, validated through normal incidence and grazing flow impedance testing conducted at the Spirit Aerosystems flow duct experimental facility [Ref. 7]. Based on bypass fan propulsive sources predictions, these models calculated the impedance impact for various liner designs. Trade studies were performed to design a liner best capable of realizing the greatest insertion loss, thus reducing community noise at multiple flight conditions. These trade studies yielded an optimum conceptual acoustic liner based upon technologies projected to achieve sufficient TRL in the 2025 timeframe for the given propulsion system inlet nacelle, as reflected in the noise analyses of the N+3 vehicles. A summary of the major findings of this study can be found in Section 6.1.2.

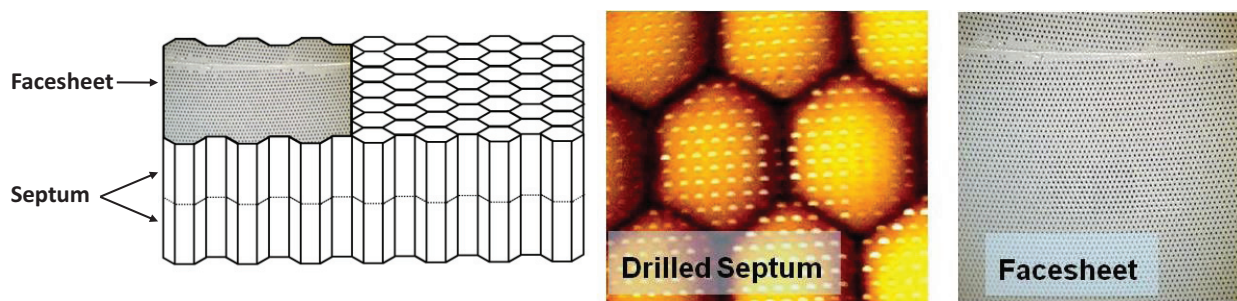


Figure 3-6. Acoustic Liner Conceptual Design Examples

3.7 Model for Investigating the Detectability of Acoustic Signatures (MIDAS)

MIDAS is a Northrop Grumman proprietary atmospheric acoustic detection analysis tool combining significant aspects of aircraft noise source generation, atmospheric propagation, and ground-based or airborne detection systems. It is a comprehensive model that allows for the assessment of acoustic signatures and the establishment of design requirements and constraints. Given a flight profile, a series of algorithms are coordinated to generate a desired acoustic metric (e.g., dBA, DNL, PNL, EPNL, etc.). Noise source algorithms include exhaust mixing, broadband shock cell, combustion, turbomachinery,

trailing edge, discrete frequency rotor, propeller, and models to predict shielding and refraction, acoustic radiation and duct propagation, and acoustic attenuation and reflection. MIDAS generates noise source models, normalized far-field directivity maps, and integrated noise metrics for cumulative noise assessment as defined in FAA FAR Part 36. Some of the noise source generation modules have been adapted from NASA’s Aircraft Noise Prediction Program (ANOPP) program.

The Advanced Sound Propagation in the Atmosphere program (ASOPRAT) is a hybrid ray trace/full-wave model prediction program that represents the state-of-the-art in long-range atmospheric sound propagation, and includes modules for atmospheric absorption, ground reflection, and multipath propagation [Ref. 8]. The software contains discrete frequency and one-third-octave band capability. Thorough testing and validation of the code was performed using data from a joint acoustic propagation experiment conducted at the White Sands Missile Range [Ref. 9].

A diagram of the process used by MIDAS to compute the required noise information is shown in Figure 3-7. Because of the level of detail involved in computing trajectory information at 0.5 second intervals required by MIDAS, acoustic calculations were reserved for the configurations with the most potential for noise reduction, and configurations which best represented the progression of noise reduction from the reference aircraft to the preferred configuration.

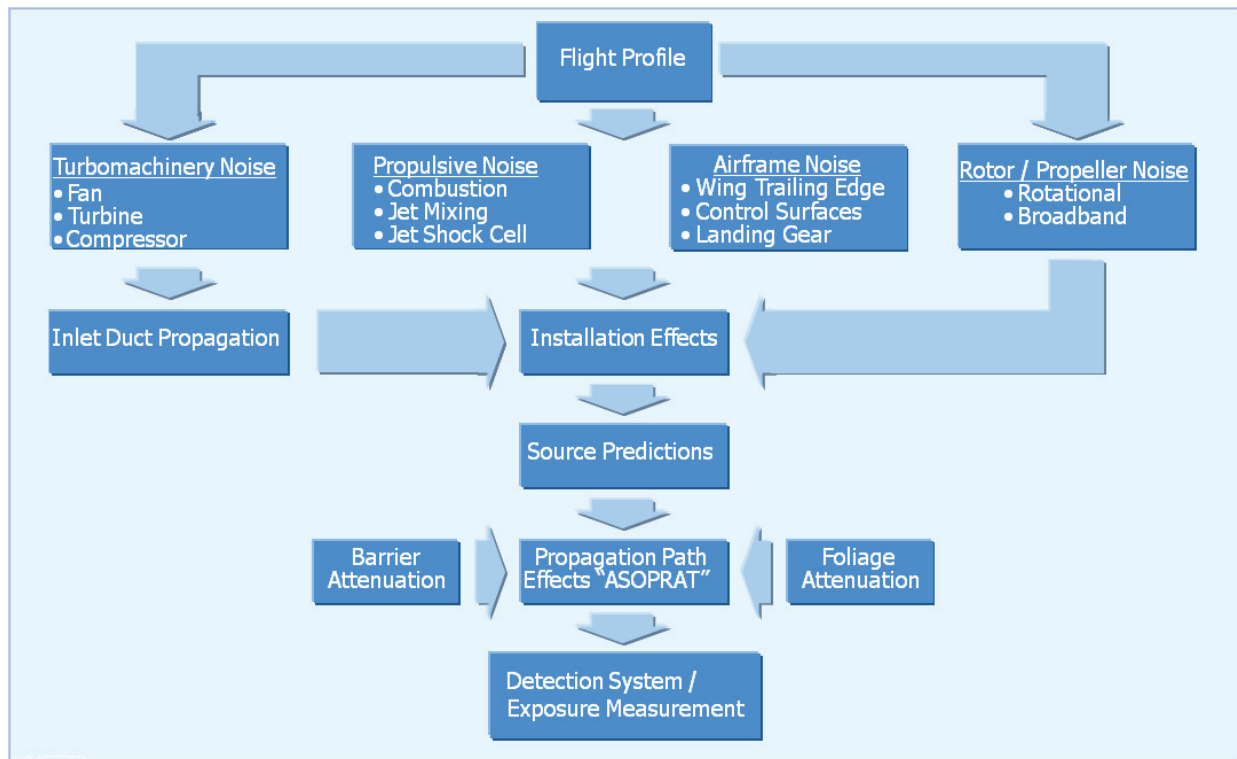


Figure 3-7. MIDAS Flow

3.8 System Effectiveness Rankings

In order to ascertain the preferred configuration, system effectiveness ratings (SERs) needed to be defined, taking into consideration the 2030-2035 future scenario and the N+3 goals for each success metric. This section will define the SER considered for each of the N+3 metrics, as well as the overall SER for each configuration, based on the overall future scenario described in Section 4.1.2.

SER definitions were necessary to quantify the relative successes and shortcomings of various configurations relative to each of the N+3 metrics. For the performance goal of achieving a 70% fuel burn reduction over the reference vehicle and mission, a relationship was defined between the achieved fuel burn, the reference vehicle fuel requirement, and the associated SER:

$$SER_{fuel} = \frac{MF_{ref} - MF}{0.70MF_{ref}} \quad \text{Eqn. 1}$$

where MF_{ref} is the required mission fuel for the reference vehicle (25,048 lbs), and MF is that of the vehicle under consideration. SER_{fuel} reaches one when the fuel burn for the configuration under consideration reaches 30% of that of the reference configuration. If the fuel burn exceeds that of the N+3 goal, no extra credit is given, and the SER for this metric remains unity. However, penalties are assessed through negative values of SER if the fuel burn exceeds that of the reference configuration.

Similarly, the emissions SER is defined by the following equation:

$$SER_{NOx} = \frac{NOx_{CAEP/6} - NOx}{0.75NOx_{CAEP/6}} \quad \text{Eqn. 2}$$

where $NOx_{CAEP/6}$ is the maximum permissible NOx production based on engine OPR and rated SLS thrust, in grams per kN of SLS thrust at maximum power, as described in Section 6.2.1. Again, no extra credit is given for configurations which surpass the N+3 target of 75% reduction in NOx production compared to the CAEP/6 regulation.

In order to quantify the SER for the balanced field length metric, the decision was made to use a simple step function which would give full credit to configurations which met the balanced field length requirement, and no extra credit to those that surpassed the target:

$$SER_{BFL} = \text{floor}\left(\frac{5000 + \varepsilon}{BFL}\right) \quad \text{Eqn. 3}$$

where ε is an arbitrarily small positive number.

The final metric for which a system effectiveness rating definition is required is noise, and this SER was defined with respect to the Stage 4 noise requirement:

$$SER_{EPNL} = \frac{EPNL_{Stage4} - EPNL}{71} \quad \text{Eqn. 4}$$

With definitions in place for effectiveness ratings for each of the N+3 metrics, the mapping between the goals and the future scenario can be completed to define an overall system effectiveness rating. This definition is based on the relative importance of each of the N+3 goals in the framework of the overall future scenario. Using the weighting parameters derived in Section 4.1, the total system effectiveness rating for each configuration can be defined:

$$SER = 0.200SER_{EPNL} + 0.333SER_{fuel} + 0.333SER_{NOx} + 0.133SER_{BFL} \quad \text{Eqn. 5}$$

As defined, the total system effectiveness rating is most heavily weighted by fuel burn and emissions, and least affected by the balanced field length requirement, unless this takeoff capability is not met.

4 FUTURE SCENARIO AND REQUIREMENTS DEVELOPMENT

A future scenario analysis was performed in order to determine the overarching mission requirements for the N+3 vehicle. This analysis took into account mission type, vehicle size class, and the importance of the N+3 goals themselves in the 2030-2035 timeframe. The economic, political, and social environments, as well as available natural resource supply and demand, were investigated to estimate the scope of most-probable global scenarios in the timeframe of EIS. The fifteen scenarios identified in were reviewed and grouped into four categories based on their similar views of the probable future [Ref. 10,11,12,13]. An important guiding tenet was that no specific scenario would be adopted for primary use in the N+3 vehicle studies. This was done to produce a vehicle which, in the context of the N+3 goals, can also fulfill the needs of the future scenario regardless of the actual outcome. This approach should lead to a robust system that fills a broad, primary need in the NAS at the lowest possible risk for technology development funding.

4.1 2035 Scenario

The scenarios described in this section were developed by conducting research on existing studies, performing literature searches on major open issues, and holding technical interchange meetings to review findings and interpret the impact each scenario would have on the N+3 metrics. Three primary scenarios were developed across all of the research findings, in addition to a fourth scenario that was set aside due to its dire implications. Beyond illuminating the key aspects of the future of commercial transports, the primary outcome was the development of weighting factors intended to discern the value of concepts and technologies with respect to the N+3 goals. This drove the technology selection and initial ranking process to create suites applicable to a given airframe concept. A brief overview of the resources used to conduct this investigation is provided, along with descriptions of the three scenario groupings. Finally, the impact of the scenarios in terms of the N+3 goals is provided, and a quantitative estimation of an overall hedged scenario is presented. These scenario weighting factors were then applied to shape the vehicle requirements definition and technology selection process.

4.1.1 Scenario Development and Key Drivers

A total of fifteen existing scenarios were assessed to determine if any categorization existed for likely outcomes in the N+3 timeframe. These reports stem from several different organizations, chosen to encompass various interests in the products of scenario planning. Table 4-1 summarizes and organizes these resources by organization and scenario designations.

The scenarios were then grouped according to key resource demand drivers and the general trends exhibited, based on individual central themes. The scenarios investigated had many secondary drivers in common, and while they were developed across a span of a decade, there were enough similarities across the groupings to warrant categorization. As shown in Figure 4-1, the four categories relating to future resource demands are: (a) reducing demand, (b) balancing supply/demand, (c) increasing resources, and (d) collapse in demand.

**Table 4-1. Specific Scenarios Used to Develop the N+3
U.S. Airspace Overall Scenario [Ref. 10, 11, 12, 13]**

Organization	Report/Scenario Title
A) JPDO Futures Working Group	“Futures Working Group Final Report (Draft)”, 2004 1. <i>Is it hot in here or what?</i> 2. <i>Storm Clouds</i> 3. <i>Markets Rule</i> 4. <i>Asia’s Century</i> 5. <i>Terror Uncontained</i>
B) National Research Council (NRC)	“Maintaining U.S. Leadership in Aeronautics: Scenario-Based Strategic Planning for NASA’s Aeronautics Enterprise”, 1997 1. <i>Pushing the Envelope</i> 2. <i>Grounded</i> 3. <i>Regional Tensions</i> 4. <i>Trading Places</i> 5. <i>Environmentally Challenged</i>
C) World Business Council for Sustainable Development (WBCSD)	“Exploring Sustainable Development”, 1997 1. <i>FROG! First Raise Our Growth</i> 2. <i>Jazz – Dynamic Reciprocity</i> 3. <i>GEOpolity – Sustainable Guidance to Market</i>
D) Shell	“Shell Energy Scenarios to 2050”, 2008 1. <i>Scramble!</i> 2. <i>Blueprints</i>

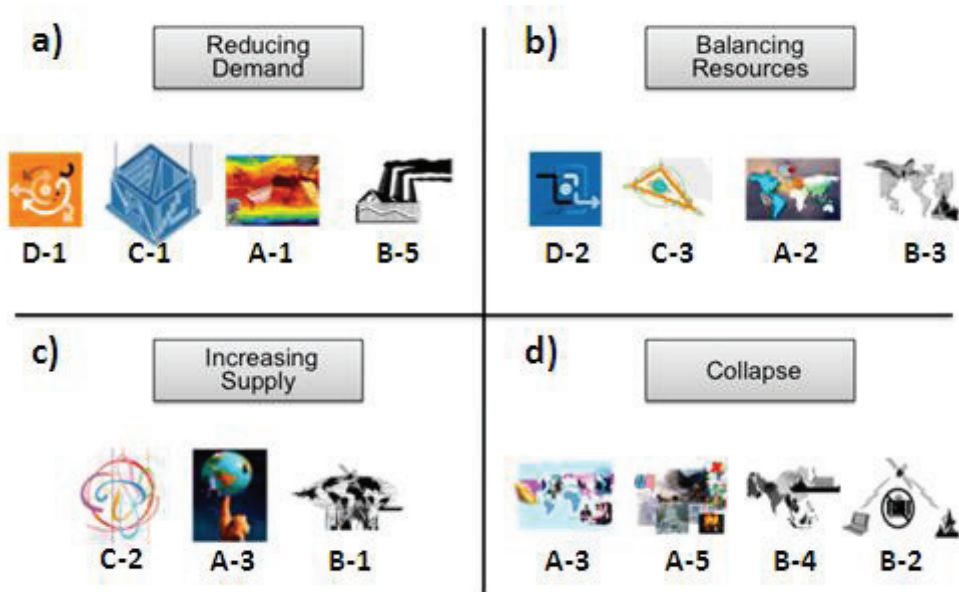


Figure 4-1. Future Scenario Categorization Quadrants

This grouping provided a foundation with which to evaluate vehicle performance against a smaller subset of key market drivers and external constraints, including environmental factors such as noise, pollution, and global CO₂ levels. The resource demand projections in Figure 4-2 reveal the nature of the

four scenario sets. Since the collapse scenario had little effect on vehicle trade studies (i.e., no technology set could achieve a meaningful solution), it was not considered further.

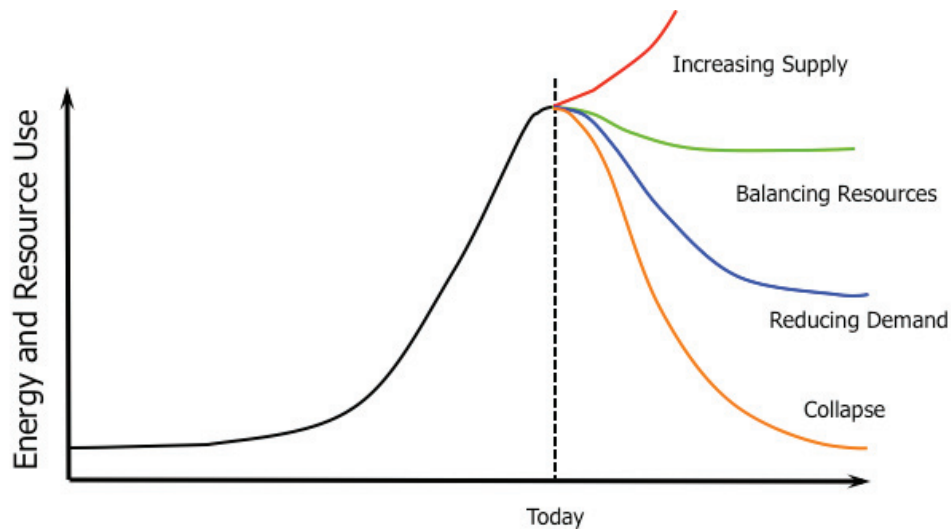


Figure 4-2. Simplified Future Resource Trends for Various Scenario Quadrants

Estimating the future of energy and resource usage involves the synthesis of many factors affecting macroeconomic productivity. Political instability and opposition to collaboration will affect trade balances, tariffs, resource markets, currency markets, and budget allocations. Extreme forms of political change include the U.S. being excluded or self-isolated from major developing and emerging markets. World markets, independent of political interdiction, have a profound effect on traffic demands and the availability of resources at any given time, as shown by recent oil price fluctuations. The coupling of other highly-fluctuating energy resources, for example natural gas, have an unknown effect on oil availability and prices, especially while new methods for natural gas extraction and processing are being developed and used. Furthermore, military acts and conflicts can produce short- and long-term effects, ranging from minor regional resource shortages to essentially indefinite global effects. Technological advances in areas other than aviation toward sustainable or renewable energy sources could greatly contribute to resource availability. Since any of these drivers could have a large impact, and their certainty of occurrence is very difficult to predict, it is important to not delve into the possibility of any one particular scenario, but to investigate the macroeconomic impacts across the range of possibilities. A robust vehicle design, then, is one that will perform as well as possible in terms of the N+3 goals, under any of the likely outcomes. Consideration was then given to the macroeconomic effects of primary concern to commercial air vehicle traffic in the NAS and with regard to the N+3 goals:

- Availability of crude oil (impact on N+3 fuel burn reduction goal)
- Sensitivity of communities and populations to aircraft noise and emissions (impact on N+3 noise, LTO NO_x goal)
- Airfield resources required to sustain or improve NAS system performance (impact on N+3 field length capability).

4.1.1.1 Resource Availability – Over the past decade, the U.S. has experienced unprecedented influences on its aviation market, including terrorism, projections of doubling or tripling air travel demands, significant swings in energy costs, growing environmental issues, ATM saturation, a global financial crisis, “buy American” sentiments, and the continuing development of a national plan for air transport. These variables become even more important when recognizing that the aerospace sector has provided substantial benefits to the national economy. Aerospace technology is consistently the fourth strongest export item when ranked by total export dollars (\$76B in 2007), and represents 6-8% of total exports [Ref. 14]. In 2008, civilian aircraft engines were the fifth largest export growth category (up \$2.5B from 2007).

The future of air transportation is likely to be dominated by national strategies and objectives in energy, the environment, the economy, and defense. Oil and other sources of energy obviously play important roles in the world – and in aviation in particular. Figure 4-3 shows the International Energy Agency (IEA) assessment of historical energy consumption and projections out to 2030. World energy demand expands by 45% between now and 2030, an average rate of increase of 1.6% per year. Today’s world oil consumption is just under 80 million barrels per day (Mbpd), and consumption is projected to grow through 2030.

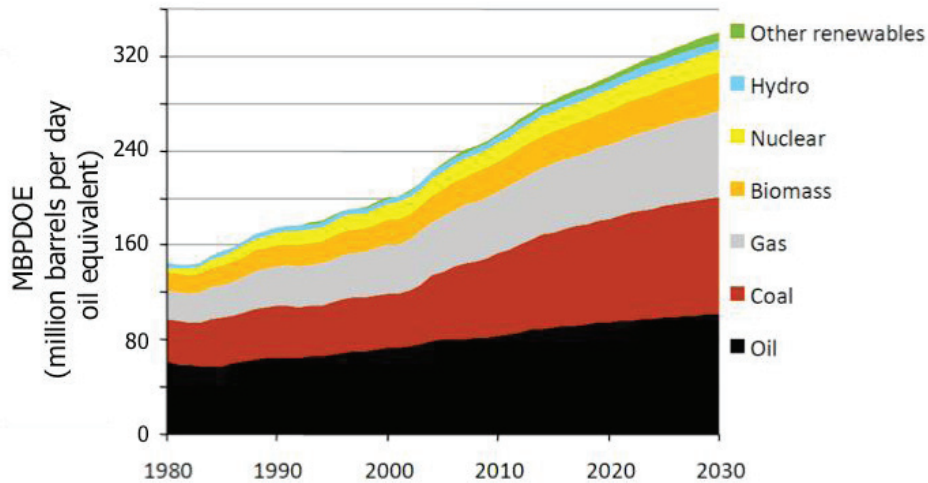


Figure 4-3. Projected Global Energy Needs Through 2030 [Ref. 15]

In considering sources of oil (Figure 4-4), unconventional sources are a growing fraction of the supply. After 2010, by far the greatest sources of oil are those which have yet to be developed [Ref. 15]. A total of 64 Mbpd of gross capacity needs to be installed between 2007 and 2030, a number that is six times the current capacity of Saudi Arabia, in order to meet demand growth and offset the decline of existing oil fields. The primary message of the IEA is that the continued growth of energy consumption is not sustainable.

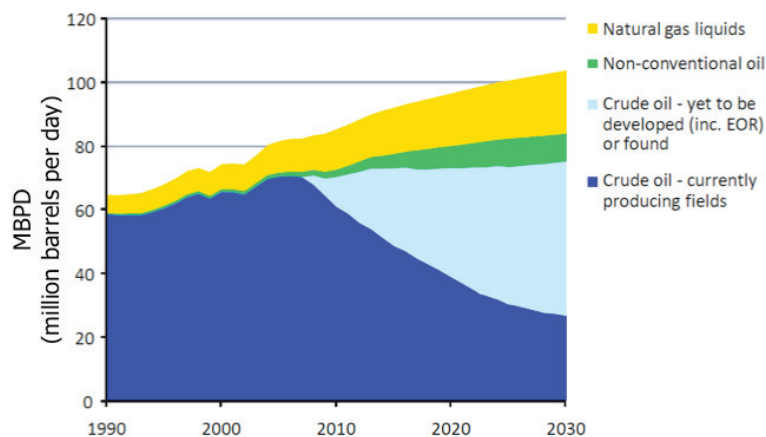


Figure 4-4. Production Estimates of Current and Future Crude Oil Sources [Ref. 15]

The U.S. is the largest consumer of oil, at over 20 Mbpd [Ref. 16]. This is more than twice the second largest consumer, China. U.S. oil production peaked in the 1970s and 1980s, and declining production with increased demand is addressed by oil imports. Today, roughly half of the oil consumed in the U.S. is imported from overseas, and this fraction continues to grow. Such dependencies make the U.S. and the aviation industry susceptible to shortages and attendant fuel price increases regardless of world supply levels. Entities that control the oil supply can greatly influence the capability of the U.S. airspace to meet growing traffic demand.

4.1.1.2 Scenario Descriptions – After carefully studying the fifteen scenarios, they were grouped based on which of the four future energy projections (Figure 4-2) each scenario supported. The scenarios generally aligned with these four projections. As shown in Table 4-1, only the National Research Council (NRC) and Joint Planning and Development Office (JPDO) considered the Collapse scenario. Neither of the studies outside of the air transport sector considered this to be a reasonable outcome. Given that collapse implies an almost complete breakdown of air transport, this scenario was discarded from further consideration in this study. There would appear to be no reasonable mix of technologies that are relevant to this projection.

Another simplification was based on the similarities between the 1997 NRC scenario study and the 2004 JPDO Futures Working Group scenarios. Effectively, since the JPDO scenarios represent a more recent, refined view of the NRC scenarios, the latter was dropped from further consideration. The following sections detail the three final scenarios, present supporting data from other studies, and discuss their implications in brief.

1. Scenario 1: Bright Bold Tomorrow (BBT)

In the framework of this scenario, new approaches to energy initiated in the early 21st century now pervade the transportation system. As a result, reasonably-priced carbon-based biofuels from algae farms are now widely available. The world economy has more than recovered from the downturn of the first decade, and renewed prosperity places high demand on global travel. New investment in airport infrastructure has saturated the hub-and-spoke system, and widespread point-to-point transportation is now available. Smaller, single-pilot aircraft dominate the transportation system, and the only realistic solution is to leverage smaller local airports and closer spacing for aircraft using larger airports.

Buyers want to be able to purchase whatever they want, wherever they are and whenever it is convenient for them. Companies that were not able to respond quickly to rapidly changing demand have disappeared. This frenetic pace has helped to feed a strong economy in the U.S. and the rule of markets has spread increasingly to Asia and Europe. The environment, already deteriorating in many places by the turn of the century, is now approaching crisis levels in Asia.

In a 2006 publication, ExxonMobil paints a rosy future of business-as-usual which supports a scenario of ever-expanding air transport [Ref. 17]. By 2050 they see daily worldwide oil production at 110 million barrels per day oil equivalent (MBpdOE), which is well beyond production predicted in all the other scenarios (Figure 4-5). Their projection is, on average, a 1.5% yearly growth rate for all fossil fuels, as well as similar growth in other sources of energy.

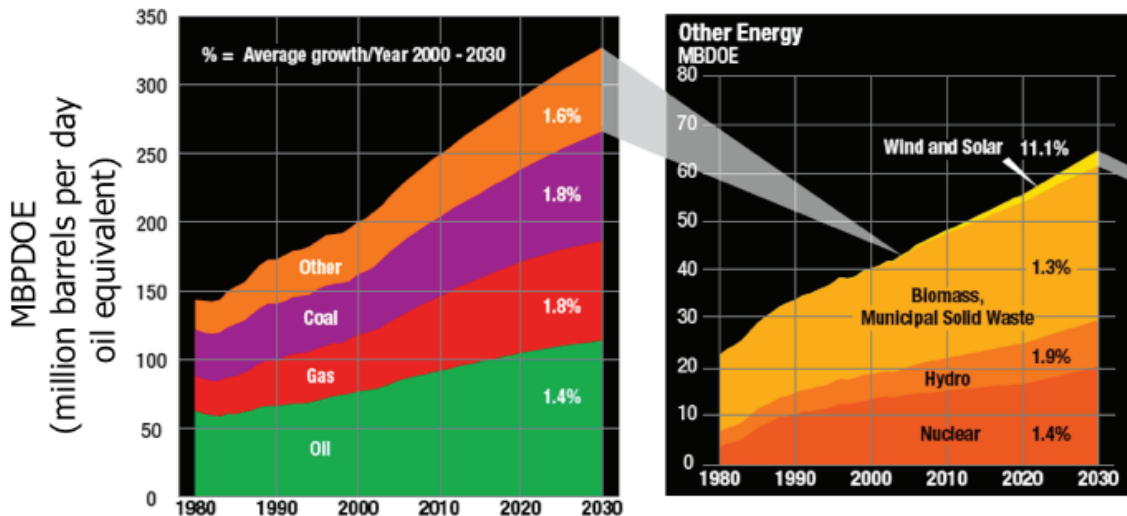


Figure 4-5. ExxonMobil 2006 Projections of Fossil Fuel Growth [Ref. 17]

Attendant with their projections of energy growth are worldwide emissions of CO2 that increase dramatically with application of 1990-era technology, almost doubling over a 50-year period from 1980

to 2030 (Figure 4-6). They project three solution paths which are consistent with the growth scenario: focus on CO₂ sequestration technologies, reduce the energy intensity of the world's economies, and invest in bringing alternative sources of energy online at a more rapid pace. To counter the growth in global CO₂ projected to continue through 2030, an aggressive application of existing technologies, preceded by an aggressive development of new technologies, must be pursued. For the technology set to be available by the N+3 timeframe, the development of multiple technology paths that will hedge against technical, physical, and political hurdles must begin as soon as possible to reduce development costs, and ensure successful deployment. A byproduct of this technology application is the implementation of new technologies that reduce (across all fuel-consuming industries) the specific energy required per dollar of gross domestic product. New manufacturing incentives and the focus on nonenergy-intensive production techniques would raise standards of living while consuming hydrocarbon fuels at a reduced rate. This would presumably keep fuel prices low and spawn increased growth in air transport, driving air traffic levels to the upper end of projections.

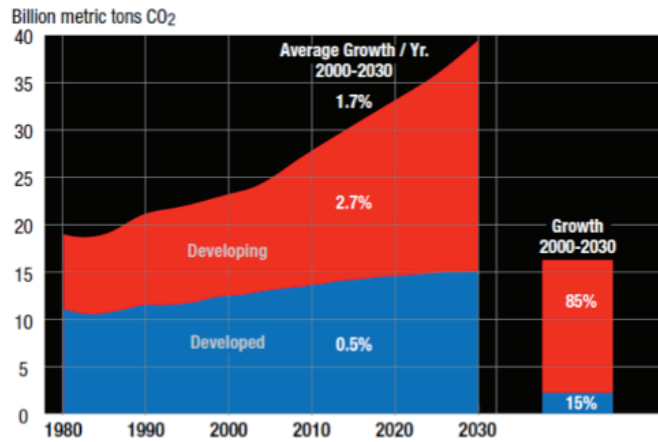


Figure 4-6. ExxonMobil 2006 Projections of Near-Term CO₂ Emissions [Ref. 17]

2. Scenario 2: Not In My Backyard (NiMBY)

A combination of new energy sources and new approaches to energy conservation has brought supply and demand into a long-term balance. The energy projections for NiMBY (Figure 4-7) are more sanguine than those in the previous scenario due to early attention to the peak-oil challenges. By reducing consumption early on, peak oil is stretched across three decades through 2040, allowing time for alternative sources to come online. Air transportation is growing slowly, but remains a strong component of the overall transportation mix. The push to greater efficiency and energy conservation has reinvigorated the cities, leading to much higher population densities. Land for airports is at a premium, and the luxury of large buffer zones between residential areas and airports is not viable. Local populations are becoming increasingly intolerant to noise and airport emissions such as NO_x, soot, particulates, and hydrocarbon emissions. Strict rules evolve first in the European Union and California, and the bar for noise and local emissions regulation is set very high.

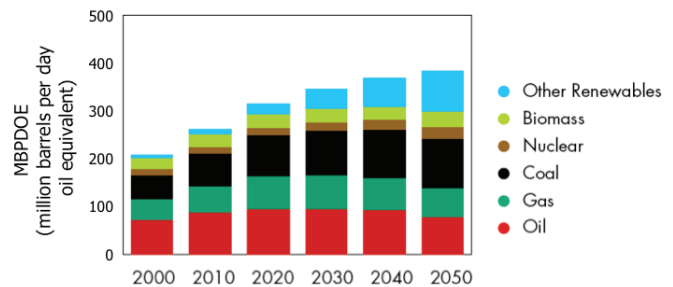


Figure 4-7. Projections of Energy Sources for NiMBY Scenario [Ref. 13]

Diverse players form alliances to solve social and environmental problems in the most pragmatic way possible. This is a world of social and technological innovations, experimentation, rapid adaptation, voluntary interconnectedness, and a powerful and ever changing global market. Many stakeholders are involved, encouraged to step onto the economic stage by advances in information technology. That stage is characterized by a global free market, sound legal systems, and a respect for property rights. The public is made aware of transgressions and quickly acts against companies or countries that violate standards. As a result, effective, market-driven, demand-side efficiency measures emerge more quickly, and CO₂ management practices spread. Carbon trading markets become more efficient, and CO₂ prices strengthen early. Energy efficiency improvements and the emergence of mass-market electric vehicles are

accelerated. The rate of growth of atmospheric CO₂ is constrained, leading to a more sustainable environmental pathway.

In the NiMBY scenario, it is recognized that air travel serves the entire population and must be sustained for our standard of living to persist. It is clear that air travel is vital to all elements of the population [Ref. 18]. The most difficult challenge in this scenario will be limiting the impact of air travel near major airports or airports in densely populated areas to acceptable limits. Given the need for air transportation, the development of environmentally-conscious communities, and the adaptation of more energy-conscious lifestyles, the key question becomes one of airport location. In its report to the United States Congress, the FAA/Partnership for Air Transportation Noise and Emissions Reduction (PARTNER) coalition states [Ref. 19]:

“In 2025, significant health and welfare impacts of aviation community noise and local air quality emissions will be reduced in absolute terms, notwithstanding the anticipated growth in aviation. Uncertainties regarding both the contribution of aviation to climate change, and the impacts of aviation particulate matter and hazardous air pollutants, will be reduced to levels that enable appropriate action.”

Local impact is the dominant factor in expansion of air transport. Five million people live within 55dB DNL areas, and noise is the single biggest local objection to airport expansion [Ref. 19]. Emissions of nitrogen oxides, carbon monoxide, unburned hydrocarbons, and particulate matter from a variety of airport sources contribute to local air quality deterioration. Aviation operations below 3,000 feet contribute 0.4% to the total national NO_x inventory. For unburned hydrocarbons and particulate matter, airport emissions have the potential to be a public health issue rather than simply a local nuisance. In this scenario, the aviation community is driven to take action by a proliferation of local rules and legal barriers to growth.

3. Scenario 3: King Carbon

The confluence of peak oil and global warming concerns results in the imposition of strict “carbon taxes” to limit the burning of fossil fuels (Figure 4-8). Years of complacency and a business-as-usual approach has led to the realization that something must be done quickly. Insufficient investment in alternative fuels and sequestration technologies leaves little time to invest in alternative fuel infrastructure. Ground transport and electricity generation at least have some alternatives; however, air transport must address skyrocketing fuel costs with new approaches to conservation and efficiency. Global alliances cutting across developed and undeveloped countries set global standards for carbon-based fuel consumption.

Long-held fears of global warming effects surface around the globe, though there still remains rampant disagreement on the causes. In spite of the very real and present effects of global warming, the world continued for years to respond with a slow and often low-magnitude reaction. The environment has deteriorated to the point that an international organization has been formed, charged with aggressively addressing global environmental conditions, and with commensurate authority to coerce cooperation from nations. By 2050, there is evidence that the darkest predictions about global warming are actually nearer to the truth than the more optimistic ones.

The impact on energy resources becomes increasingly acute and unpredictably swift. Despite increasing rhetoric, action to address climate change and encourage energy efficiency is pushed into the future, leading to largely sequential attention to supply, demand and climate stresses. Demand-side policy

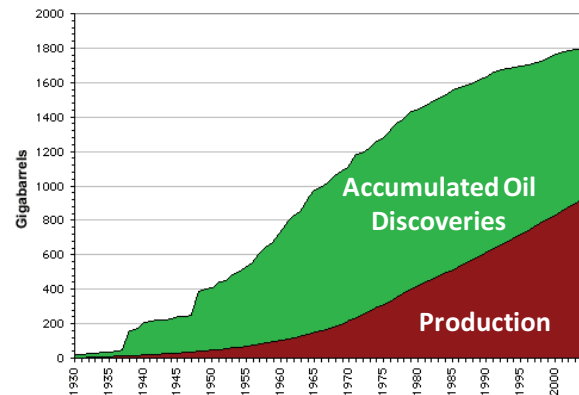


Figure 4-8. Historical Global Crude Oil Availability and Production [Ref. 20]

is not pursued meaningfully until supply limitations are acute. Likewise, environmental policy is not seriously addressed until major climate events stimulate political responses. Events drive late, but severe, responses to emerging pressures that result in energy price spikes and volatility.

The overriding impact of carbon-based fuels in this scenario are the compounding impacts of dependence and the consequences of dependence. On one hand is the projection of peak oil, with no way to back down gracefully from the consumption peak unless aggressive preliminary action is taken. On the other hand are concerns about carbon dioxide emissions and their impact on global climate. Alone, either is a serious issue. Together, they increase the probability of this scenario becoming reality. The fundamental issue is that although oil discovery rates peaked in 1964, demand has continued to grow [Ref. 20]. Figure 4-8 compares accumulated oil discoveries with production through about 2004, with cumulative production beginning to approach cumulative discoveries. Alternative sources of oil exist, but the cost of making them a viable option begins to approach the value of the commodity.

The second part of the impact of carbon-based fuels beyond market factors is the influence of CO₂ production on global climate. In a recent paper by Marais et al [Ref. 21], the long-term impact of a step change in atmospheric emissions was examined (Figure 4-9). In this study, a number of emission constituents were assumed to be injected into the atmosphere over a short period of time. The impulse response in terms of unit global average temperature change and relative effect on GDP were estimated. On the left can be seen the temperature response, which can be divided into two groups. The majority of emission constituents have an initially large impact, but that impact decays to a negligible level within fifty years. This includes NO_x, water vapor and cirrus clouds, and various sulfur compounds. After fifty years, the total emission footprint is dominated by CO₂, and the decay rate of this constituent is very small. On the right, the cumulative impact on gross domestic product (GDP) is computed, and the transient of carbon emissions can last beyond 300 years.

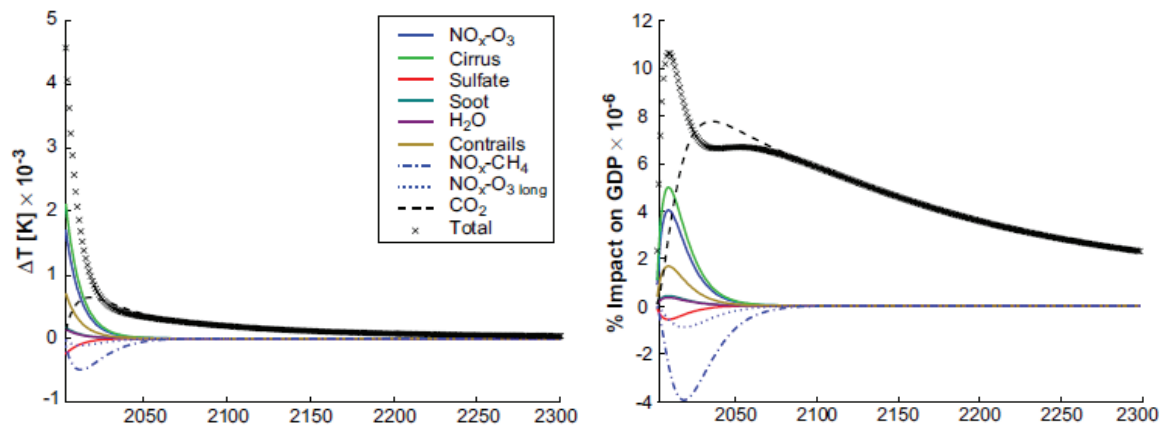


Figure 4-9. Impact of Impulse-Response Input of Various Greenhouse Gases on Atmospheric Temperature [Ref. 21]

4.1.2 Scenario Synthesis and Impact to Vehicle Optimization

The primary use of these detailed scenario descriptions was to illuminate the impact the future may hold on commercial air vehicles, NAS traffic, and the N+3 goals, while ignoring the drivers which could stem from a number of sources not considered, including the development of personal air vehicles, undiscovered power sources, etc. For instance, if personal air vehicles become pervasive before the N+3 timeframe, then the major impact would be a reduction in NAS traffic. Likely, the impact would be small, since ranges and speeds would be very limited, but nevertheless, the effect of this particular example is well within the limits of the traffic growth levels predicted by the three scenario models. The scenarios strive to propose a manageable worst-case future set that covers the most dire decreases in air traffic demand due to huge price increases, as well as the most challenging economic growth levels that drive huge demand increases.

These three scenarios broadly address the spectrum of alternative futures and map directly to future fossil fuel projections. NiMBY is tied to airport site location near populated areas, and thus affects NOx emissions and community noise. King Carbon is primarily a fuel-constrained scenario, and is fundamentally tied to fuel burn and global emissions. The Bright, Bold Tomorrow scenario projects a large expansion in air travel demand, and is thus most closely tied to the field length goal, with little or no linkage to noise, LTO emissions, or fuel burn. In an attempt to make this mapping a quantitative, traceable effect, the impact of these scenarios to each of the N+3 goals was assigned on a percentage basis, with 100% allocated among the four goals. Figure 4-10 indicates these distributions as weighting factors for each of the three scenarios, which have specific implications that will influence the selection of vehicle technologies and mission requirements.

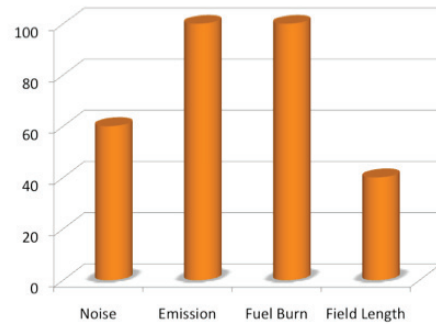


Figure 4-10. Synthesized Scenario Impact on N+3 Goals

NiMBY requires that a viable aircraft meet local emissions requirements that may vary between airports, and strict noise requirements as housing approaches airport boundaries. The focus of these vehicles would be low-noise, low-emissions operations. It would be critical that airlines bring fleets of new-technology aircraft online in a timely fashion to meet the new local requirements.

King Carbon is predicated on the high cost of fuel, driven by shortages and taxes. A viable solution would have a diverse fuel mix, including synthetic and bio-derived fuels, as well as lighter, more efficient aircraft. Airspace solutions must be integrated with vehicles, as efficient flight paths would be mandated. As with NiMBY, airlines must be able to bring fleets of new-technology aircraft online in a timely manner to meet the new efficiency requirements.

The Bright, Bold Tomorrow scenario follows a more business-as-usual trend, with the ability to use a wide range of airports. This scenario implies complex airspace management concerns, and emissions issues driven by a rapidly growing air travel industry.

In support of the goal of this study, which is to define a single vehicle system that best achieves the N+3 metrics in the context of the 2030-2035 scenario, a hedged approach yielded a set of relative goal weightings. These factors were applied to initial technology selections through the technology effectiveness metric, TER, and the vehicle optimization metric, SER, to provide a vehicle and technology package best suited to a broad set of likely requirements. Figure 4-10 shows the values used to initiate the technology QFD process to select applicable best-suited technology suites, as well as begin to define vehicle requirements based on the traffic demand levels predicted by each scenario. This relative weighting of the scenarios reflects an average of the three scenarios previously described, and can be seen to more closely resemble the King Carbon scenario than the others. This is due to the relative importance of the emissions and fuel burn metric across all scenarios.

4.2 Initial Requirements Development

Of the requirements necessary to initiate a design optimization, including field length capability, vehicle range, cruise speed, and passenger count (payload), it was necessary to address the takeoff and landing field length capability before the others. This is a consequence of the metroplex concept being a tradable N+3 goal in the study. Since the field length requirement is dependent on (1) the traffic levels projected by the future scenario and (2) future runway resources enabled by NextGen, a study of these two aspects of the NAS were performed first to provide the basis for investigating field length. The goal was to estimate performance of the NAS in terms of the ultimate mission of delivering the future traffic demand levels predicted in the scenario study. The question of adopting metroplex operations (and to what extent) was assessed by comparing changes in aircraft delay at various traffic levels in two different

cases. One used today’s baseline airport infrastructure, while a second incorporated metroplex resources enabled by NextGen. These simulations were performed with an N+3 surrogate vehicle to estimate the likely vehicle characteristics for that timeframe.

Assessment of the cruise speed requirement was made using simulations that decreased cruise speed and showed the effects on delay. Passenger sizing was determined by investigating the flight distributions currently in the NAS, and reconciling field length requirements with the average mission type (range) of these vehicles to make use of the metroplex concept. This was found to be necessary to serve the challenging traffic demand levels predicted for the N+3 timeframe. The simulation approach and assumptions used to construct these tradeoffs is described prior to discussing results.

4.2.1 Methodology

The methodology used to analyze the advanced N+3 vehicle in the NextGen-enabled infrastructure had the goal of providing a system-wide assessment of passenger throughput and delay using the Airspace Concept Evaluation System (ACES), described in Section 3.3. Figure 4-11 shows the process that was used to assess system-wide performance. AvDemand [Ref. 28] was used to create future schedules using estimates of future passenger demand [Ref. 22]. A description of AvDemand use in creating flight schedules for the N+3 timeframe is described in Subsection 4.2.1.1. A tail-tracking algorithm was then used to link together the flights in the AvDemand-created schedules into airframe-based itineraries. The Base of Aircraft Data (BADA) contains specific aircraft performance data used by the ACES high-fidelity trajectory generator. Finally, the airspace and airport capacities were designed to include NextGen assumptions.

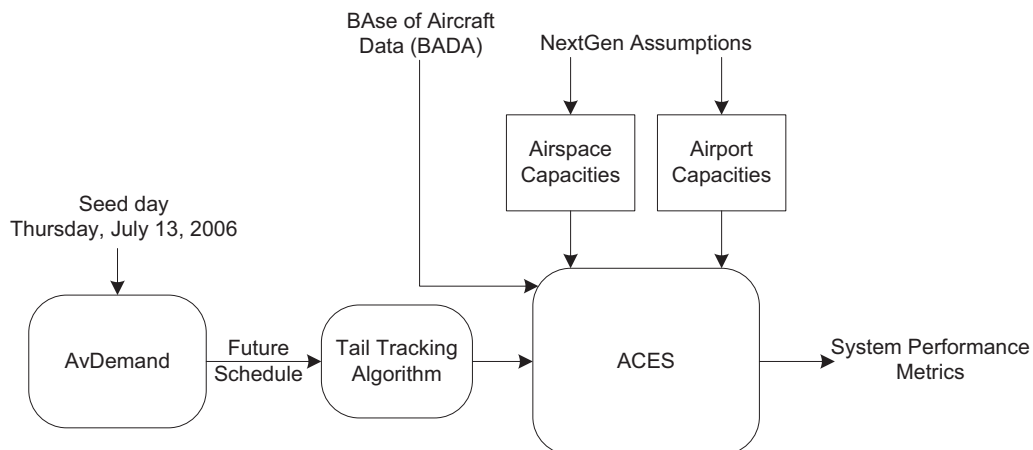


Figure 4-11. Simulation and Modeling Approach for This Analysis

A representative vehicle was chosen for analysis of N+3 vehicle performance and its impact on the National Airspace System. The targeted markets consisted of origination and destination (O/D) pairs serviced by the Boeing 737 and other similar aircraft. The Boeing 737 was selected based on similarities in aircraft size and target market. Separate future schedules were created and simulated for the reference vehicle, similar vehicles, and the advanced N+3 vehicle and the results compared. The differences were used to assess the impact of the advanced vehicle configurations on the NextGen-enabled NAS. Performance metrics included fuel efficiency, thrust, cruise speed, and cruise altitude performance profiles. System-wide comparisons included passenger throughput and delay.

A bypass alternative was used to assess the effect of balanced field length (BFL) on passenger throughput and delay. The bypass alternative seeks to balance the demand to capacity by using policy-based incentives and regulatory measures to shift demand to regional, underutilized facilities [Ref. 23]. Use of these existing metroplex assets was assumed via NextGen improvements such as Virtual Towers which would be implemented in the non-towered airports and allow reasonable hourly departure and arrival rates, estimated for this study at 40/hr.

4.2.1.1 Baseline and N+3 Demand Set Generation – To generate the future demand sets, a representative “seed” day was chosen from which to extrapolate traffic patterns. Thursday, July 13, 2006, was chosen because summer is a busy season for air travel and Thursdays are a busy day of the week. Also, July 13 is not associated with a holiday weekend and can therefore be reasonably assumed to be representative of a busy travel day in the summer of 2006. AvDemand was used to grow the seed-day schedule using the expected passenger growth rates that are published annually in the FAA’s Terminal Area Forecast [Ref. 24]. These growth rates extend 15 to 20 years into the future and are based on factors such as expected growth rates for population and income.

Expected passenger counts are converted into scheduled flights between city-pairs by using what is known as a Frataring algorithm. When additional flights are needed to handle extra enplanements in the future, AvDemand duplicates an existing flight in the seed day, slightly offsetting its departure and arrival times from those of the original flight. This process replaces individual flights in the seed day with multiple flights in the future demand set. The added flights are only offset from each other by a minute or so in order to replicate the operators existing business model. For instance, there are often many flights between certain city pairs early in the morning and late in the afternoon, but not in the middle of the day, as that is when airlines believe passengers want to fly. AvDemand preserves this business model; however, it also means that the forecasted demand sets probably contain slightly more delay than might actually be realized in the future, as the operators might change schedules to avoid congested peaks of arrivals or departures. Due to this approach, future demand sets distributions are similar to today’s, where traffic is concentrated at 30-40 major hubs.

4.2.1.2 Airframe Substitutions – The seed day aircraft distribution was determined through AvDemand and used to develop the baseline and N+3 advanced vehicle usage rates. AvDemand’s passenger-weighted demand generation was used, which first converts flights to passengers and then redistributes passengers using a Gaussian distribution. The demand that is created is based on the fleet mix (percentage of market share for heavy, medium, large, and small) and aircraft type. The aircraft usage rates were adjusted to represent a hypothetical share by N+3 aircraft in the future flight schedules around the 2040 timeframe. The changes took into account: (1) the expected production rate of the N+3 aircraft (~4,000 available then), and (2) the retirement of present-day aircraft types. The JPDO fleet forecast was used for guidance during the development of the schedules. Examples of aircraft in the 2006 schedule assumed to be phased out in varying degrees are the MD-87, DC-9 and its variants, as well as variants of the B737.

4.2.1.3 Tail Tracking – A tail tracking algorithm was used to connect multiple flights in the N+3 and baseline demand sets. Tail tracking the demand sets was required to ensure adherence to aircraft turnaround times and to account for propagated delay in the system. By accounting for propagated delay, a tail-connected itinerary gives a more realistic estimate of delay when run through a simulation like ACES. In the current NAS, propagated delay accounts for about 30% of all delay [Ref. 25].

In a demand set that is not tail-tracked, every aircraft is at the airport and ready to take off at its scheduled departure time; it is only delayed because of congestion at the departure airport, destination, or in the airspace it must fly through to reach its destination. In reality, however, aircraft travel on itineraries between multiple city pairs and flights often take off late because the aircraft was delayed at some bottleneck earlier in the day. For example, an aircraft that departs an hour late from one airport will arrive an hour or so late at its destination. Depending on how much slack is in an airline’s schedule, this aircraft will likely depart late to its next destination, and so on throughout the day.

The tail tracking algorithm generates schedules with a median of five flights per day. Figure 4-12 shows a comparison between the tail tracking algorithm used to generate the N+3 and reference demand sets and the actual schedule for Continental Airlines derived from Bureau of Transportation data.

4.2.1.4 NextGen Assumptions for N+3 Analysis – The airport and sector capacities used to simulate the N+3 vehicle in NextGen were provided by the JPDO, and assume NextGen to be fully implemented by 2025, with only small capacity increases after that year. These capacities include all known new and planned runway construction, as well as all JPDO operational improvements. Airport

capacities under NextGen have been modeled in detail by the JPDO, with NextGen operational improvements increasing average capacity for the top 35 airports by approximately 45%, although there is considerable variation around that average for the individual airports. Similarly, en route sector capacities increased by a factor of 1.7 when all NextGen en route operational improvements were modeled [Ref. 29].

4.2.2 Traffic Growth Implications on Metroplex Operations and Field Length Requirement

The scenario task revealed the importance of determining vehicle requirements that affect the airspace efficiency so that large potential increases in air travel can be accomplished. The availability of oil and economic markets will mainly drive the fuel and operational efficiencies needed to maintain a viable fleet. Figure 4-13 shows steady and substantial progress in increasing fleet efficiency over the past fifty years. The primary contributor is engine efficiency, driven by increasing bypass ratio. The inclusion of the last of the piston-engine propeller transports shows that the past fifty years have been spent returning to the fuel efficiencies of the propeller era. One must ask whether a lower Mach short haul transport aircraft is ultimately a better answer. The answer depends on the future traffic levels predicted, and whether or not the metroplex operations model is needed to meet this traffic demand, beyond the improvement assumed by NextGen with today's infrastructure alone. Incorporating metroplex resource alone enabled by NextGen will increase throughput by fuller resource utilization.

More than half the gains in fuel efficiency over the past fifty years have been related to propulsion systems. The remaining gains have come from higher structural efficiencies and reductions in aerodynamic drag, areas which still hold promise for even further gains. Most of the drive has been to make turbofans more efficient, and drive toward larger bypass ratios, but these are still far less fuel efficient than equivalent turboprops or piston-props. Attendant cruise speeds are much lower for these aircraft though, so the efficiency benefits must be weighed against the designated mission for this vehicle: to best meet the future NAS operational efficiency requirements.

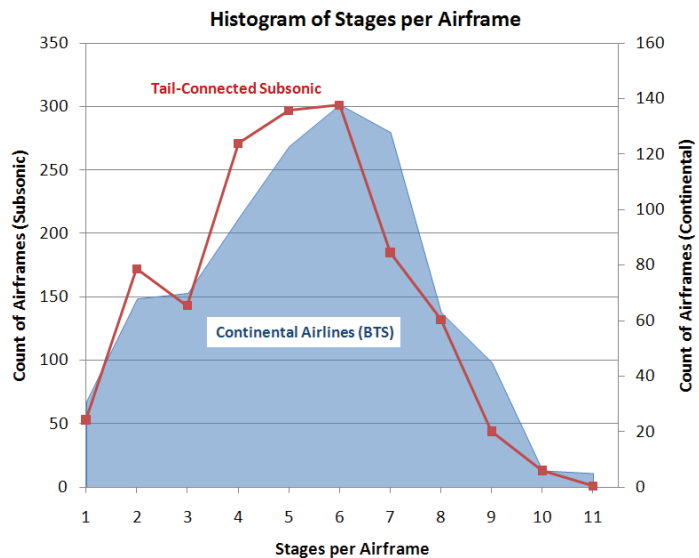


Figure 4-12. Comparison of Daily Flights per Airframe

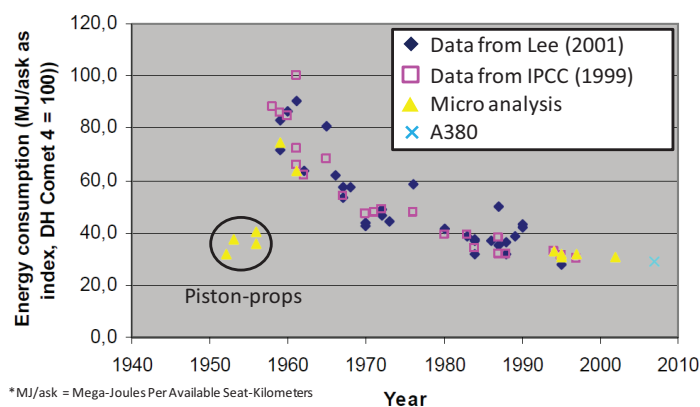


Figure 4-13. Commercial Aircraft Fuel Efficiency Historical Data Indicating Piston-Prop Performance [Ref. 26]

4.2.2.1 Scenario-Based Traffic (Enplanement) Predictions – Based on the collection of

scenario predictions noted above, air traffic growth levels were predicted for each of the scenarios. Table 4-2 indicates the traffic growth levels associated with each of the three individual scenarios relative to a 2008 air traffic baseline. These values are based on our own interpretation of the possible range of economic drivers on traffic growth. However, reports over the last decade have issued predictions across this range from 2-3 times growth levels, for even earlier time periods [Ref. 27].

Table 4-2. U.S. Air Traffic Growth Rates by Future Scenario

Scenario	%/yr	2035
NIMBY	2%	1.6x
KC	-2%	0.6x
BBT	4%	2.7x

To compare this to historical data, the enplanements in the U.S. since the jet era begin are shown in Figure 4-14, plotting a quadratic extrapolation of the historical data against both the JPDO projection of approximately 1.8 times increase for 2040, with the BBT scenario projection of 4% per year growth. Clearly, the historical projection is increasing at nearly quadratic rates and, as long as technology and infrastructure maintain current proportions, would likely continue this growth rate at a minimum. The BBT air traffic growth of approximately 2.7 times by 2040 provides the most challenging environment with which to provide adequate infrastructure capacity and compatible air vehicle requirements, and is in line with the range of other recent predictions shown in Figure 4-14(b) [Ref. 27].

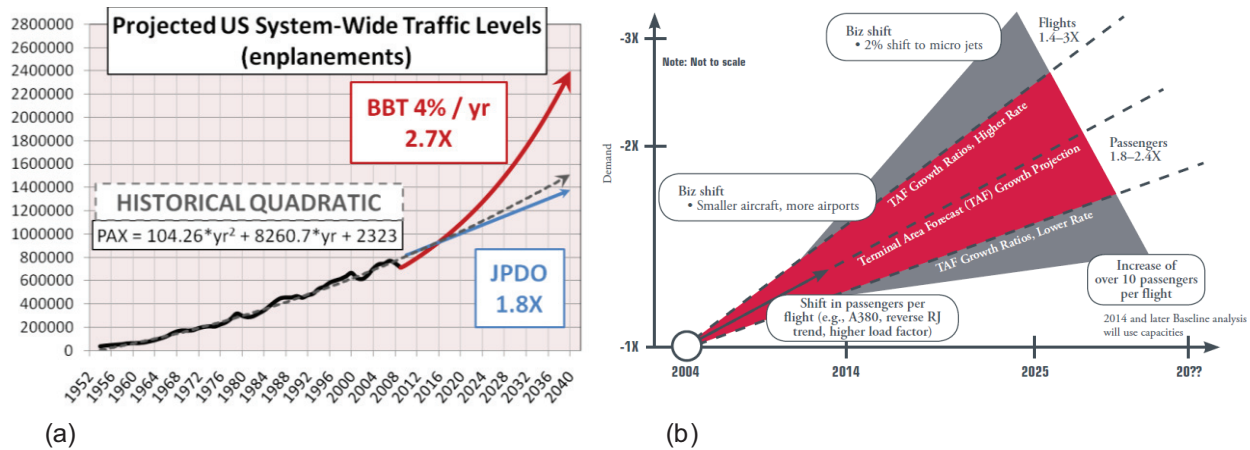


Figure 4-14. (a) Historical Passenger Enplanements Since 1952; (b) Future Traffic Predictions Comparison Ranges [Ref. 27]

This high level of growth of the BBT scenario of 2.7 times 2008 levels is that adopted for the upper bound of the NAS simulations performed in this study is in line with the philosophy that an N+3 vehicle should be able to meet the most strict requirements as predicted by the future scenarios, and as demanded by the N+3 performance metrics. The baseline 1.8 times JPDO demand levels were also investigated for comparison.

4.2.2.2 NextGen Infrastructure Assessment – The impact of the requirement to meet high future

demand levels on metroplex needs was assessed by investigating the effects of traffic levels on future delay levels. A baseline comparison without implementing metroplex assets, but including NextGen improvements was made. NextGen represents a transformation of the air traffic control system from its present highly manual, analog, ground-centric state into one in which digital technology, information sharing, and automation are ubiquitous. This transformation affects the gamut of aviation activity, from air transport service business-models through airspace rulemaking [Ref. 28]. The relevant impact on this study is the increase in sector air capacities in FAA’s Monitor Alert Perimeter (MAP) of 1.7 times, and visual flight rules (VFR) departure and arrival capacity increases of about 45%.

The effect of these increases alone due to NextGen implementation are shown in Figure 4-15, compared to a fleet with an assumed N+3 “like” surrogate vehicle. This was done to estimate the sensitivity without an actual N+3 preferred configuration at this point in the design process. It was modeled based on variations from an N+2 vehicle model and included a shorter range capability to take

advantage of metroplex operations by using airports within 70 nm of an Operational Evolution Partnership (OEP) hub, and with runways at least 100 feet wide and 5,000 feet long. The N+3 surrogate aircraft were inserted to replace 737 type aircraft, with a stage length of 800 nm or less, an initial range requirement estimate. A production rate of 400/yr was assumed to begin in 2030 and continue for 10 years, for approximately 4,000 vehicles inserted into the NAS fleet mix.

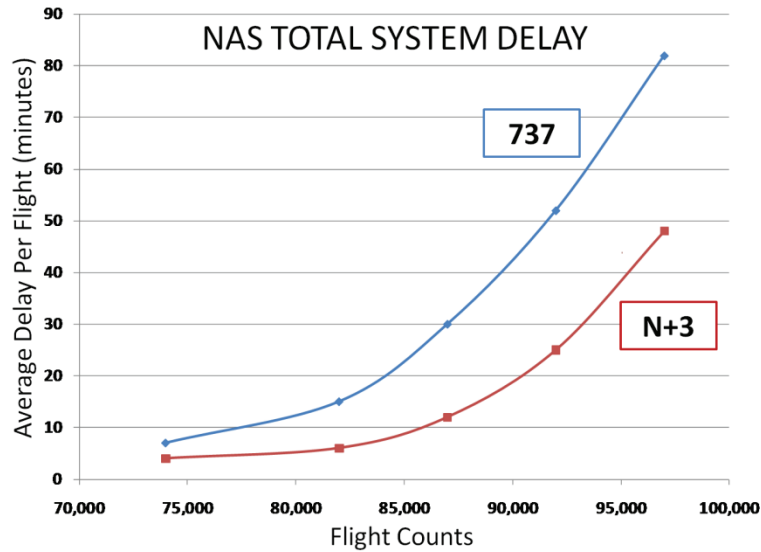


Figure 4-15. Impact of N+3 Surrogate on Baseline JPDO 1.8 Times Traffic NAS Total Delay, Compared to Baseline Fleet Mix

At the higher levels of daily flight counts, there is a clear advantage to enabling the metroplex operations, and it must be adapted to some extent to hope to reach the predicted demand levels. These operations, for the 5,000 foot field length capability, can offload a significant amount of traffic from the OEP airports, as shown in Figure 4-16(b). Focus is made in this study on the metroplex operations at the OEP airports since these are the major economic centers through which the vast majority of air traffic flows, and traffic delays at these airports are highly correlated with delays elsewhere in the system [Ref. 29].

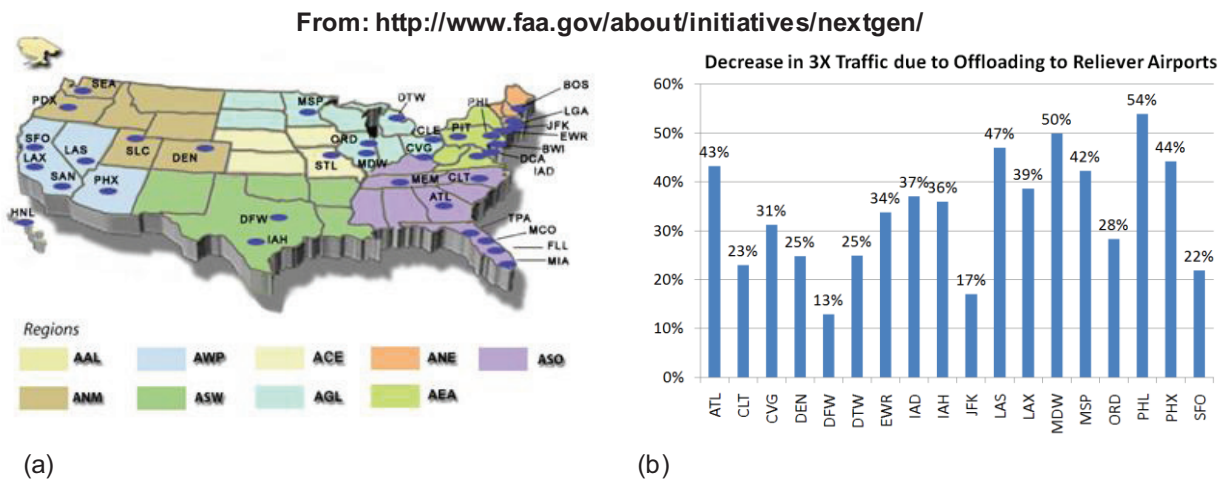


Figure 4-16. (a) OEP Airport Distribution; (b) Effect of Metroplex Operations on Traffic Reductions on OEP Airports

The current baseline operations model, which assumes typical airport assets, but includes operational NextGen improvements, does not offer an acceptable delay level, or conversely, traffic throughput for a fixed delay. So various levels of metroplex infrastructure adaptation levels were investigated to determine the pareto frontier for NextGen enabled towered or non-towered fields. This was done as a tradeoff, not as

a hard driver of field length, so that most of the additional capacity could be added to mitigate the local impact to smaller airports that would likely oppose additional aircraft noise, operations traffic, and exhaust emissions. With this motivation, the distribution of NextGen enabled resources was investigated, using both towered and non-towered airfields assuming virtual tower capabilities. The geographic distribution of the limited set (only fields with 4,000 feet or longer runways) shown in Figure 4-17(b) indicates the close correlation of towered fields with population centers in Figure 4-17(a). The two sets of non-towered runways, one comprised of 4000 feet to 5000 feet runways, the other 5,000 feet or greater runways, show very different qualities in their distribution and relationship to the population. The non-towered 5,000 feet and above airfields have a more even correlation with the population, whereas the 4000 feet bin airfields show more density east of the continental divide and on the eastern seaboard, relative to the western half of the U.S. The N+3 vehicle should leverage airfields across the U.S., and driving to a 4,000 feet BFL would be less useful for many of the major west coast markets. For a developing point-to-point system, that would be well covered geographically by the 5,000 foot runway and greater airfields.

From: U.S. Census Bureau

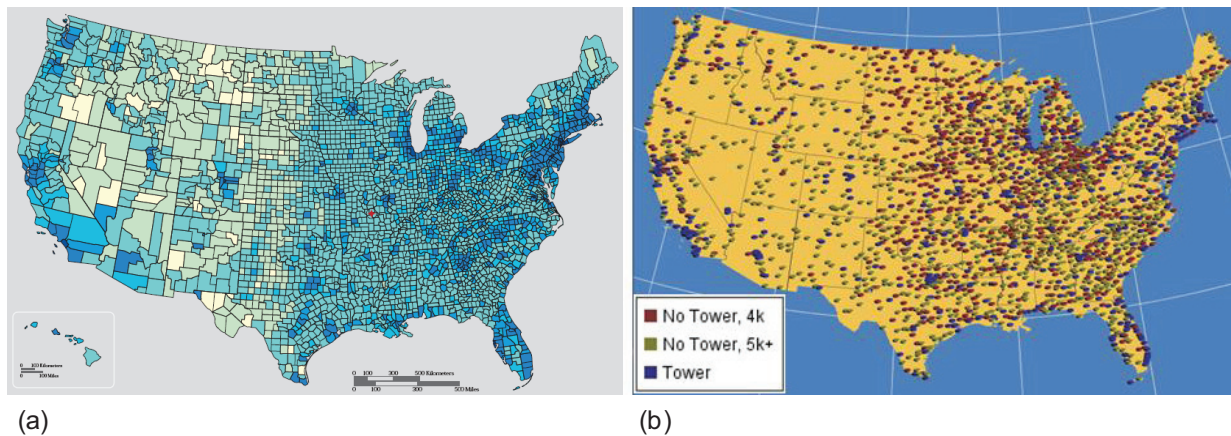


Figure 4-17. (a) U.S. Population Distribution; (b) Airfield Distribution by Longest Field Length for Non-towered Runways, Including >4,000 feet and >5,000 feet Bins, Along With Towered Runway

4.2.2.3 Field Length Requirement – A cumulative histogram of the airfield resource by longest runway length shows this dataset in a quantitative fashion. Assuming that all airfields can be equipped with a virtual tower, Figure 4-18 shows the relative addition of airfields as a percentage of the number of currently towered U.S. airfields. At 6,000 foot fields or greater, there is already 186% (979 fields) of the 525 towered fields available. At 5,000 feet or greater, 329% (1728 fields) of the towered fields is available. Considering the 35 OEP airports carry most of the traffic, and most greatly affect demand, driving the field length requirement to use 5,000 foot runways adds a vast set of infrastructure. Considering only the satellite airports within 90 nm of the 35 OEP airports, the number of with 5,000 foot runways is 709. Decreasing to a 70 nm radius, the number drops to 491, but compared to the number of OEP centers, this is a large capacity boost to accommodate increased demand. Simulations were then performed with the 70 nm, 5,000 foot runways in the metroplex areas surrounding the OEP airports, to estimate the benefit to meeting traffic demands. The baseline scenario is without additional metroplex runways and without the N+3 surrogate, while the offload 3 times scenario indicates the metroplex operations simulation with the N+3 surrogate vehicle. The JPDO reference future traffic scenario, a 1.8 times increase in traffic, was simulated for comparison.

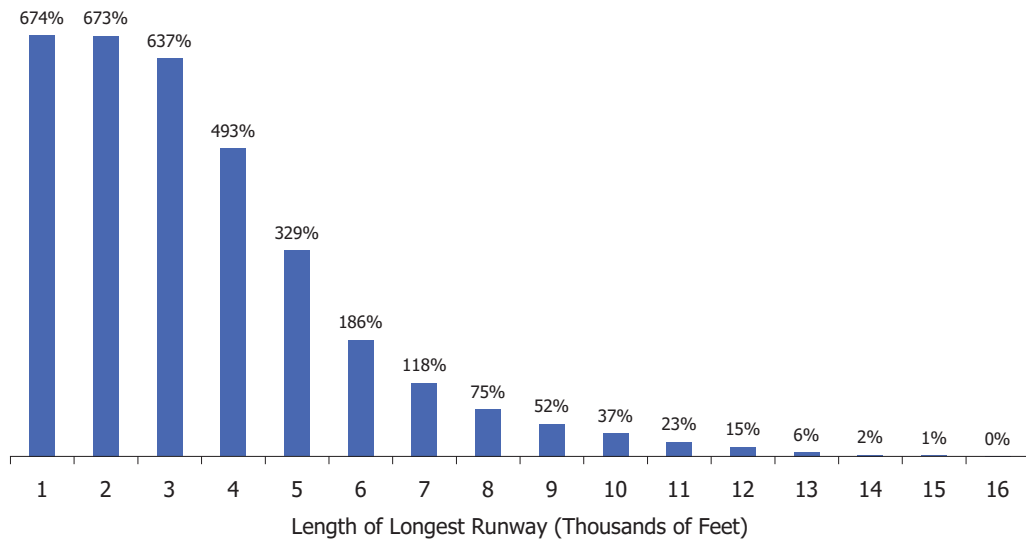


Figure 4-18. Histogram of U.S. Airports (Towered and Non-towered) as a Percentage of Towered Airports by Max Field Length, Assuming Implementation of Virtual Towers

Investigating the three times traffic simulation in the metropolitan Atlanta area, it was observed that the addition of the metroplex fields and a vehicle that can take advantage of the infrastructure can reduce the traffic levels at the OEP airports significantly. The offloading levels were determined by constraining throughput at the OEP fields to 90% of capacity, while allowing up to 40/flights per hour at the metroplex offload fields. This throughput was enough to allow the three times traffic levels, but at increased delay. Figure 4-19 shows the capacity effect of introducing the N+3 surrogate vehicle in the NAS, looking only at the Atlanta metroplex. It was possible to maintain a sustainable traffic throughput at ATL while distributing traffic to the available 5,000 foot and greater metroplex resources. Atlanta is a good example market (although results were similar elsewhere) since its delay is one of the largest in the U.S. (see Figure 4-20 which relies on FAA OPSNET delay data), and it is currently the world’s largest airport by passenger volume. This was the main objective of the future traffic simulations: to determine which resources to include to enable projected demand. However, the levels of delay in these scenarios need further consideration.

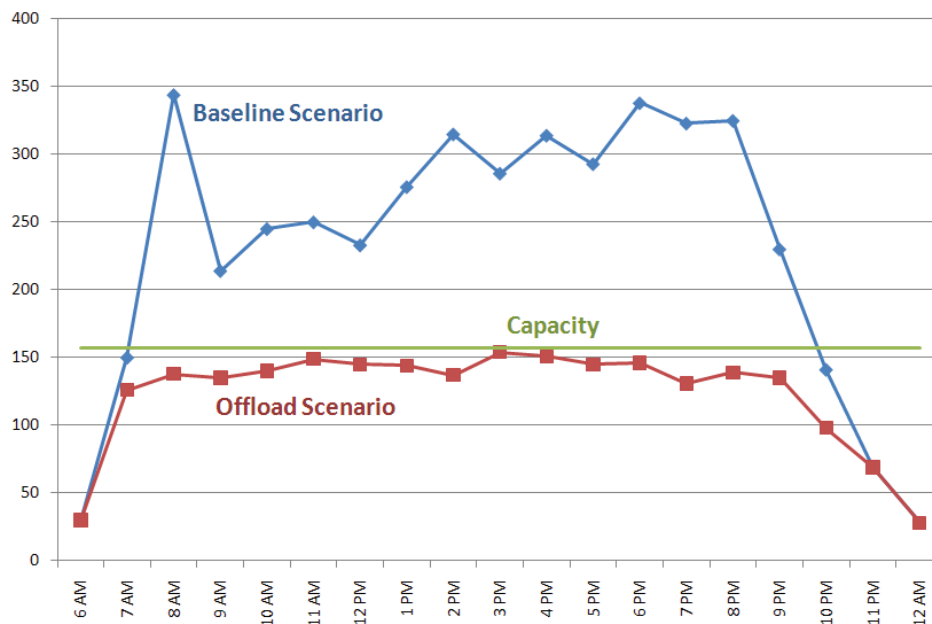


Figure 4-19. Comparison of Baseline and N+3 Metroplex Hourly Operations at ATL for Three Times Traffic Levels

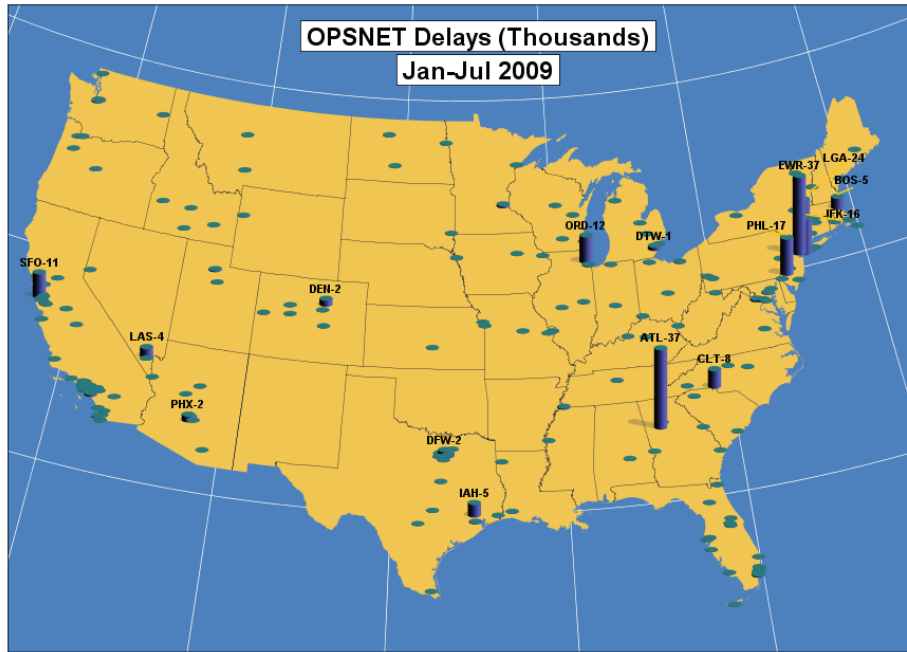


Figure 4-20. U.S.-Wide Delay Instances Distribution for January-July 2009 Period (OPSNET)

The result for reducing severe delay was significant for the 1.8 times traffic levels (JPDO) simulation in the metroplex operations model, especially at ATL, LAS, PHX, and EWR. Many other airports saw substantial decreases in delay as well. The relative levels of delay across the NAS (shown as vertical bars indicating the minutes of delay on average) are compared for the 1.8 times prediction in Figure 4-21. The left figure shows the baseline scenario, without the metroplex operations, and without the N+3 surrogate, while the right figure shows the results with the N+3 surrogate in place with the metroplex operational model.

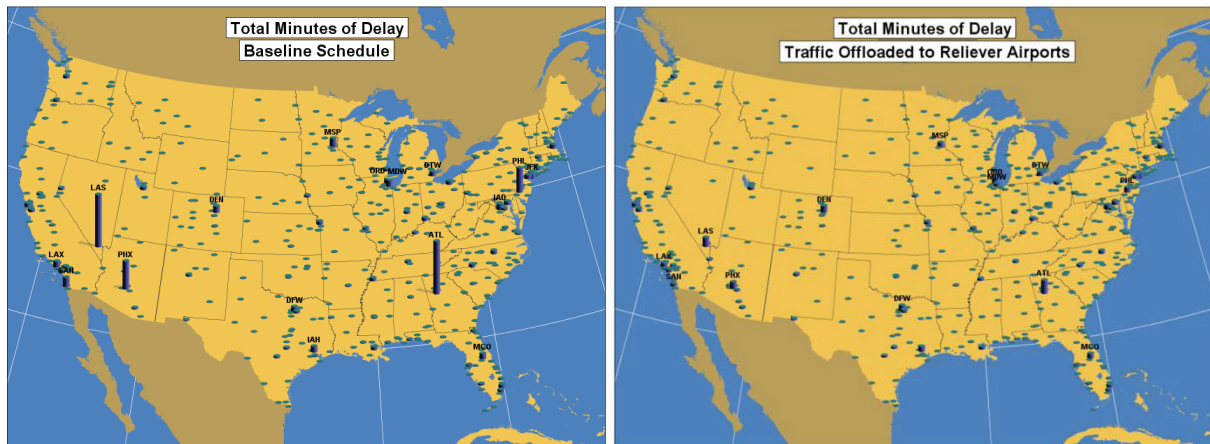


Figure 4-21. (a) Baseline 1.8 Times Traffic Delay Distributions; (b) Metroplex Operations Delay With >5,000 foot Airfields

NAS delay for the three times traffic level scenario is shown in Figure 4-22, which reduces average delays greatly across the board with the addition of the 5,000 foot runways. Compared to the 1.8 times scenario, the three times simulation results show a large number of areas with substantial delay while maintaining more fields much nearer to their capacities full-time as seen in Figure 4-20. This is very near the threshold of requiring a lower field length to include additional resources, but since the tradeoff between enabling a larger number of the smaller metroplex airfields, and imposing new aircraft noise and emissions seems unclear, it was decided to use 5,000 feet as the driving requirement for field length. This

is a direct cause of the high traffic demand levels predicted in the 2030 timeframe, in the range of 1.8-3 times 2008 levels. Potentially for a later EIS date, it would be necessary to drive to a 4,000 feet, or perhaps a 3,000 feet field length requirement.

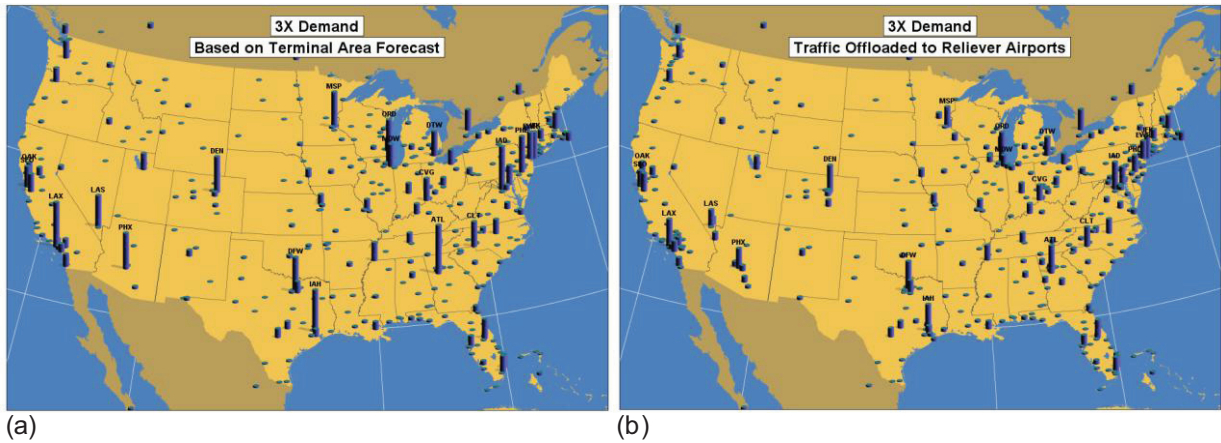


Figure 4-22. (a) Baseline Three Times Traffic Delay Distributions; (b) Metroplex Operations Delay With >5,000 foot Airfields

4.2.3 Cruise Speed Sensitivity

In a related NAS simulation study, the effect of varying the cruise speed to accommodate a 737 replacement N+2 aircraft was considered using that previously composed dataset [Ref. 30]. This study was leveraged to produce a first-order sensitivity of delay resulting from cruise speed changes for a 737-like aircraft. The simulation decreased the mean cruise speed slightly by approximately 12 knots in the manner indicated in Figure 4-23, which shows the speed distribution of the flight simulation set of approximately 10,000 flights in and out of the NYC metroplex. The mean cruise speed for the 737 was 448 knots, while the N+2 vehicle cruised at approximately 436 knots, mostly by shifting the fastest flights into the lower speed bins, resulting in a more pronounced peak in the set distribution about the mean flight speed.

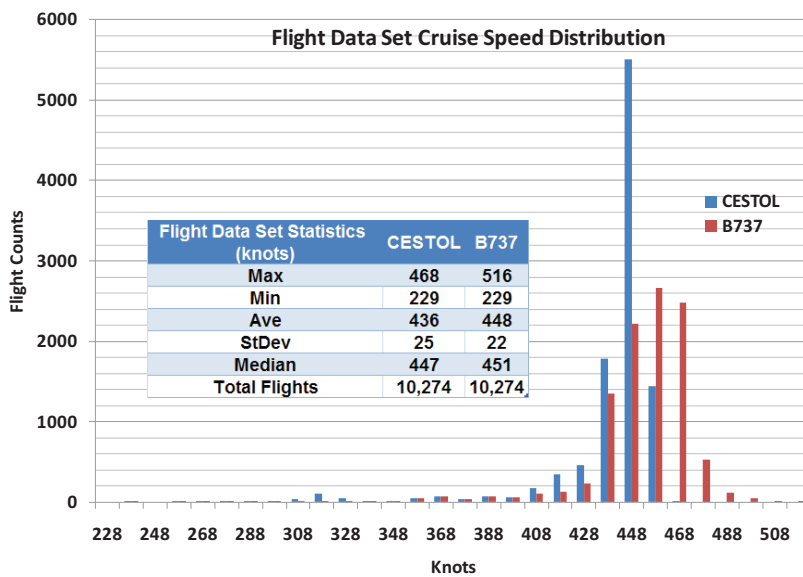


Figure 4-23. Cruise Speed Distribution Shift for an N+2 NAS Simulation Compared to Baseline 737 Distribution

The outcome of the speed reduction was an expected effect on delay, acting to increase mean delay over the baseline case by about 9.2 minutes on average. That corresponds to an increase of 7.6 minutes of delay per airframe for every 10 knots decrease in cruise speed. The delay increase distribution is shown in

Figure 4-24. This delay level is on par with the average delay for the JPDO 2040 demand set at the 1.8 times traffic level. This is clearly an unacceptable increase in delay, approximately doubling the projected future delay levels, which would in turn reduce traffic throughput.

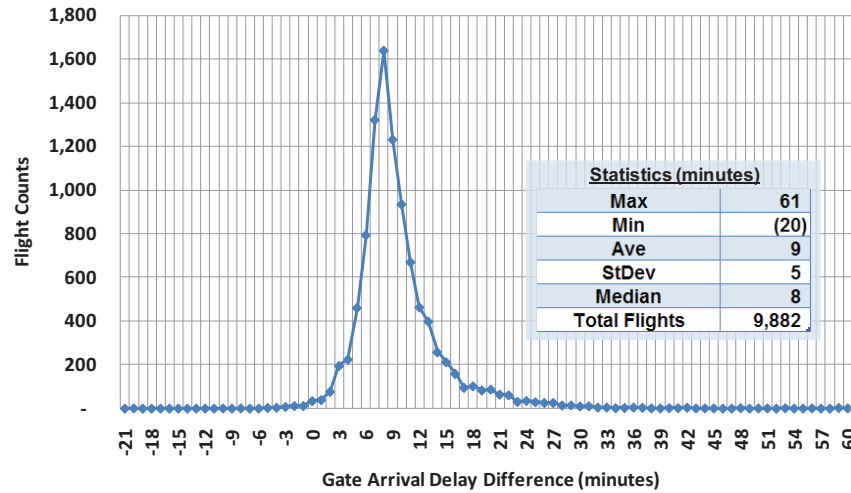


Figure 4-24. Aircraft Delay Distribution for a Cruise Speed Decrease of 12 Knots Compared to 737 for an N+3 Vehicle Study

A second implication is that increased delay then requires more airframes to complete the same number of flights per day. Referring to Figure 4-12, it is clear that operating efficiency is dependent on the number of segments completed per airframe per day, and that also leads to a larger fleet requirement. For the N+3 analysis, the effect of cruise speed on the number of required airframes was analyzed for a range of Mach numbers from 0.60 to 0.85. For a flight replacement strategy consisting of replacing 4,000 airframes with ranges of less than 1600 nm, without any shift to the metroplex concept at the JPDO 1.8 times levels, the effect of cruise speed on the number of airframes required is shown in Figure 4-25. These flights have airborne cruise times on average of only 25 minutes shorter for the Mach 0.85 flights compared to the 0.60 flights.

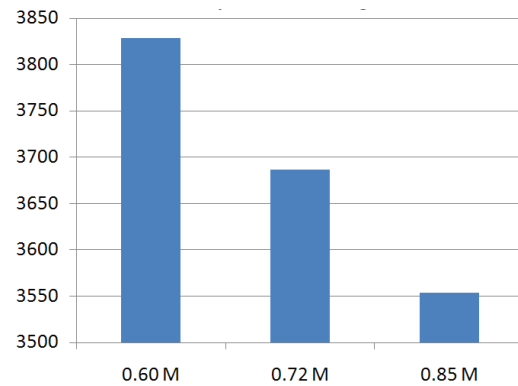


Figure 4-25. Effect of Varying Cruise Mach Number on Number of Airframes Required to Complete 8,000 Flights

This is another advantage of sizing a vehicle to leverage the metroplex concept – that the sensitivity to the cruise speed is lower than compared to a large, long-haul transport, and so the effects of slight decreases in cruise speed can be mitigated. However, the effect on the number of airframes required, from an economic standpoint, is not small even for these relatively short flights investigated. For a Mach 0.60 mission, there is about an 8% increase over the 0.85 Mach cruise, which is a significant economic driver also to keep cruise speed high. The cruise speed requirement was set at Mach 0.75 or higher in order to maintain traffic levels and the current delay averages, and to minimize the economic impacts of cruising at potentially slower speeds to improve vehicle-level efficiencies. This lower bound represents a slight decrease from the 737 average speed of about Mach 0.77 for the same mission mix seen in the baseline JPDO demand set. The vehicle optimization trades will be allowed to approach this lower bound, but not venture lower to preserve the ability of the platform to meet the top level objective of delivering projected future traffic levels.

4.2.4 Passenger Loading and Range Capabilities

To best size the payload (PAX count) and range capabilities of the N+3 type vehicle, a study of the current vehicle fleet mix was used to determine the most broadly applicable airframe entry into the future

landscape for use with the metroplex concept. The current fleet mix was investigated since the extrapolation of usage for future flight levels is very similar, and detailed demand studies were not performed to investigate additional point-to-point routes enabled by the N+3 type vehicle between metroplex satellite airport pairs. The Terminal Area Forecast (TAF) was used to determine and then further extrapolate the future fleet mix as indicated in Figure 4-26. Although there is some variation between the growth rates of individual vehicle classes, the most prominent airframes persist to the future demand scenarios, being the sub-30, 60-90, and 120-150 passenger classes. The philosophy for the vehicle insertion into the commercial fleet was to assume a production rate of 400/yr, and perform the NAS simulations in 2040 when 4,000 vehicles have been inserted. Based on this level, and to take advantage of metroplex operations without an insurmountable requirement for a high-lift system to make the 5,000 foot field length requirement (and also to achieve high loading rates), the primary need and best tradeoff appeared to be at the 120-150 passenger level.

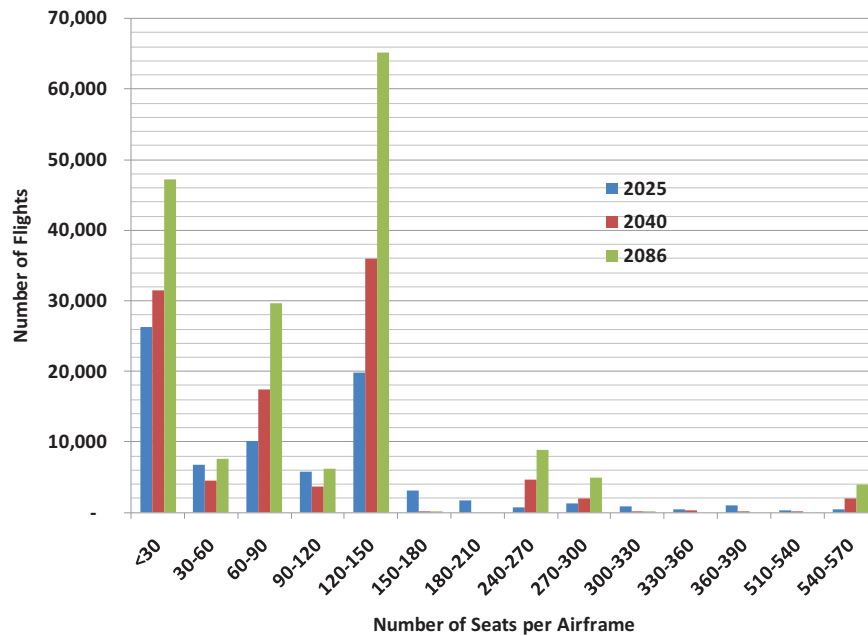


Figure 4-26. Flight Count Projections for Various Future Daily Passenger Traffic Growth Levels

To refine the passenger level further, the distribution of most often flown vehicles currently in use was investigated with respect to range capability to determine if there was a clear need to fly many shorter routes typical of smaller RJ type vehicles, or whether there was a need to deliver a larger passenger count on a longer cruise typical of some B757 or A320 aircraft. Figure 4-27 shows the number of flights for each airframe currently in use in the CONUS, as well as the typical range capability usage. The majority of the airframes with the most use rarely exceed 1,600 nm more than 25% of the time. The correlation with Figure 4-26 is clear, in that it serves the best need of the current and extrapolated demand distribution to bias toward a smaller vehicle in the 120-150 seat class, and so a nominal value of 120 passengers was adopted for the vehicle requirement.

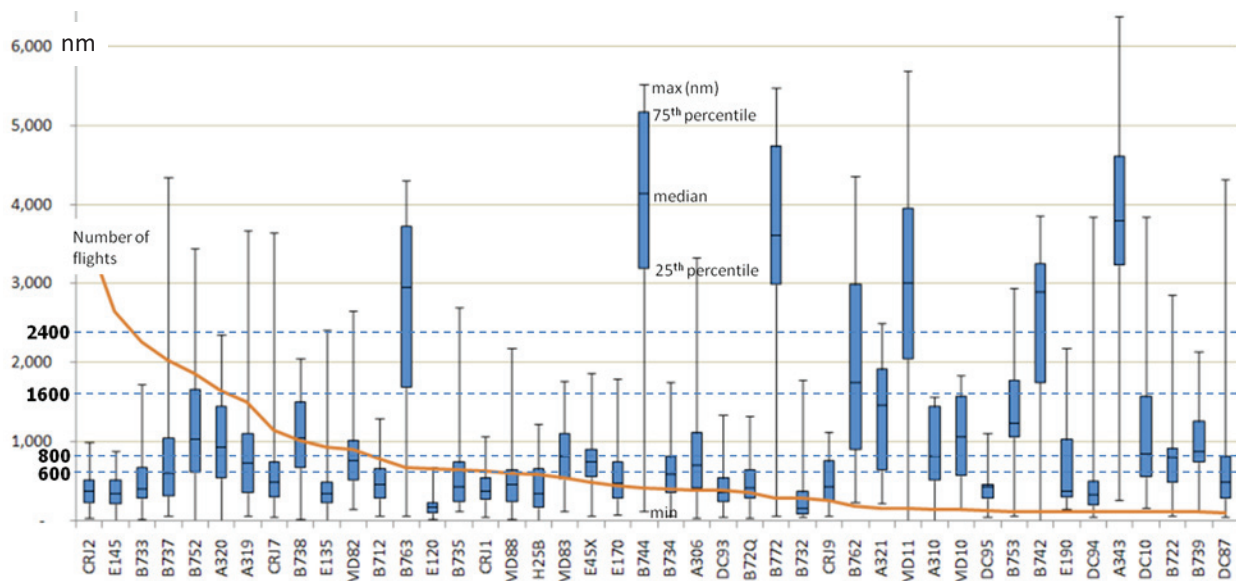


Figure 4-27. Number of Flights per Airframe Type (Line) Superimposed on Range Capability Statistical Bars for U.S. Aircraft

To preserve similar operating characteristics throughout the range of most-used aircraft the N+3 vehicle could potentially replace, the vehicle range capability of 1,600 nm was also adopted. Of the current flight segment distribution for CONUS flights, this clearly positions the airframe to perform the vast majority of operations as seen in Figure 4-28. This ensures that the broadest need segment will be served by the advanced technology platform, while also bolstering compatibility with metroplex operations in order to meet traffic levels.

4.2.5 Mission Requirements

The goal of this requirements study was to determine the proper vehicle capabilities to meet the broad, primary need of the future scenario. Future traffic projections were developed over a range determined by JPDO estimates as well as the most challenging estimates of the scenario analysis, from 1.8 times levels to approximately 3 times levels.

Simulations of delay and traffic performance with NextGen implementation alone, compared to a fleet containing an N+3 vehicle that enabled the metroplex, were performed. For both the 1.8 times and 3 times levels, the N+3 metroplex concept greatly reduced delay compared to the baseline simulation with NextGen only. A study into existing runways revealed that the ability to use non-towered airports can dramatically increase the number of available runways for use in the 2030-2035 timeframe, and thus makes the metroplex concept viable. Using non-towered airports with 5,000 feet or greater runways can add enough alternative fields to keep pace with projected traffic growth, although delay will suffer at the higher traffic projections. Furthermore, a bypass alternative study at ATL showed that the integration of the N+3 vehicle into the NAS while taking advantage of these airports can reduce delay times 16% for low traffic days and up to 44% in cases of high demand. For this reason, and the preceding discussions, it was decided to implement a mission requirement of a 5,000 ft field length for the aircraft. A maximum wingspan of 150 ft was adopted to accommodate the space constraints associated with metroplex

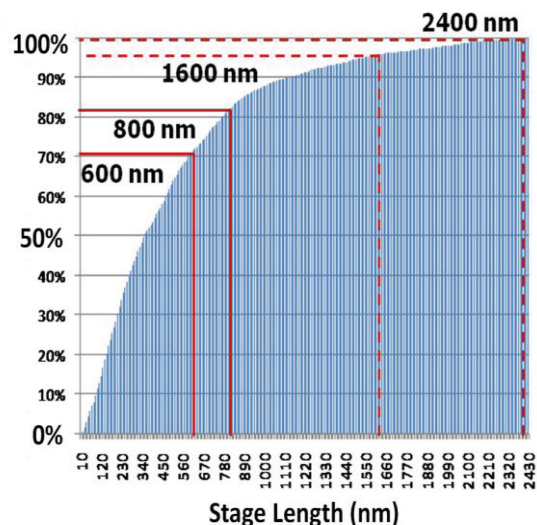


Figure 4-28. Cumulative Histogram of Flight Counts by Stage Length in the Current CONUS NAS

runways. To mitigate the impact on operational efficiency, it was decided to allow a small decrease in cruise Mach number down to 0.75. This will help ensure the N+3 vehicle does not exacerbate delay any further within the traffic ranges predicted. An important assumption was made that these traffic levels will not greatly alter the future distribution of average fleet capabilities, in terms of number of operations at the various stage lengths and passenger loadings. Thus, the passenger and range capabilities were set to meet the vast majority of operations in the projected fleet mix, which is similar to the current picture. A summary of the requirements determined in this study is given in Table 4-3.

Table 4-3. N+3 Mission Requirements

Mission Requirements	
Range (with reserves):	1600 nm
Passengers:	120
Balanced Field Length (Sea Level/Standard Day):	5000 ft
Landing Distance (Sea Level/Standard Day):	5000 ft
Minimum Cruise Mach:	0.75

5 ADVANCED VEHICLE CONCEPTS

5.1 Engine Architecture Concepts

Three advanced engine configurations projected into the 2030-2035 EIS timeframe were developed, the major features of which will also be described here. At an interim point in the sizing of the aircraft, re-sized engines were generated based on updated thrust requirements. These re-sized engines also incorporated advanced propulsion technologies to be described in the sections below. Selection of engine architectures for initial development were driven by the outputs of the technology QFD study (Figure 5-1).

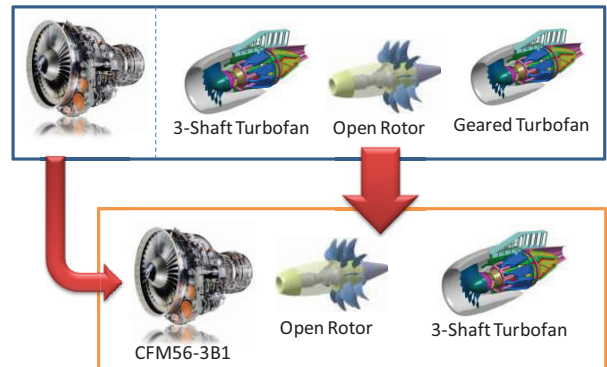


Figure 5-1. Engine Downselection Process

5.1.1 Reference Engine

The CFM56-3B1 turbofan used on the 737-500 was used as a scalable reference engine (Figure 5-2). It was necessary to acquire engine data for the CFM International CFM56-3B1 turbofan in order to quantify the mission fuel consumed by the reference vehicle, and hence to develop the N+3 fuel burn target. This dual-shaft turbofan uses a 60 inch diameter fan consisting of 38 titanium blades with a maximum speed of 5,490 RPM. The axial low-pressure (LP) and high-pressure (HP) compressors contain three and nine stages, respectively, comprising an overall pressure ratio of 27.5 at maximum climb. The fully annular combustor leads into a single-stage HP turbine followed by a four-stage LP turbine. The fan duct achieves a bypass ratio of 6.0, leading to a maximum takeoff thrust of 20,000 lbf, a cruise thrust of 4,650 lbf, and a cruise specific fuel consumption of 0.67 pph/lbf.



Figure 5-2. CFM56-3B1 Turbofan

5.1.2 Three-Shaft Turbofan

The 2030 EIS three-shaft advanced technology turbofan uses separate shafts for the fan module, intermediate pressure (IP) compressor, and a combination axial/centrifugal HP compressor. Three-shaft turbofans are a proven technology and are in broad application in the Rolls-Royce Trent engines [Ref. 31]. A mechanical profile diagram of the engine is shown in Figure 5-3. At takeoff, this engine achieves a bypass ratio near 18, with a fan pressure ratio of 1.34 and an overall pressure ratio (OPR) of 50. At SLS conditions, the engine achieves a specific fuel consumption of 0.226 pph/lbf. The high flow rate fan module consists of 22 composite fan blades combined with 54 swept stator vanes. In terms of installation effects, the engine model assumes a constant core nozzle C_v of 0.995, no customer bleed, fan stream suppression generated by the core nozzle which drives it to a base C_d of 0.995, and a constant power extraction of 100 hp. An inlet recovery of 99.7% is also assumed.

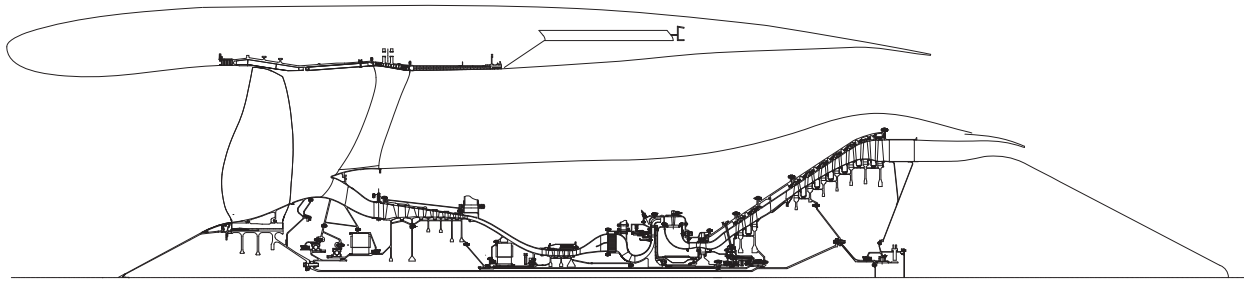


Figure 5-3. Three-Shaft Turbofan Mechanical Profile Diagram

Technologies embedded inside the engine include active tip clearance control in the HPC and high pressure turbine (HPT), high overall pressure ratio (OPR) materials and seals, and active flow control in the integrated power system (IPC). Additional advanced high temperature materials are employed, fuel-cooled cooling air is used to reduce ceramic matrix composite turbine blade temperatures, and high-strength shaft materials provide additional structural integrity. The engine also uses high temperature sumps, electric fuel and oil pumps, and an embedded starter/generator. Lean combustor technology enables low NOx production. Finally, shape memory alloys enable a variable geometry (two-position) nozzle for reduced takeoff jet velocity and noise. At a TRL of 6, this engine technology is expected to be fully mature by the N+3 timeframe. Fuel consumption characteristics of the engine will be discussed in Section 5.1.5.

5.1.3 Geared Turbofan

An engine architecture receiving widespread attention is the geared turbofan [Ref. 32]. Pratt & Whitney is anticipating the certification of its PW1000G geared turbofan in 2011, preferring the noise reduction capability of this configuration over the fuel consumption benefits of the open rotor [Ref. 33]. Similar in design to the three-shaft turbofan, the geared turbofan incorporates an additional design consideration in the gearbox which breaks the direct shaft connection between the LPC/LPT and the fan module. This allows for both the fan module and the LPT to be operating in their optimum speed range, instead of one being constrained by the other. Originally estimated at a TRL of 5, recent flight testing of the PW1000G on the 747SP and the A340 has led to an increased TRL of this propulsion system, now estimated to be in the range of 6-7 [Ref. 34]. While the engine performance far surpasses that of the CFM56-3B1, its fuel consumption is nearly identical to that of the three-shaft turbofan. At SLS conditions, the engine achieves a specific fuel consumption of 0.229 pph/lbf. In terms of installation effects, a constant core nozzle C_v of 0.995 is assumed, along with no customer bleed, fan stream suppression generated by the core nozzle which drives it to a base C_d of 0.995, and a constant power extraction of 100 hp. An inlet recovery of 99.7% is modeled.

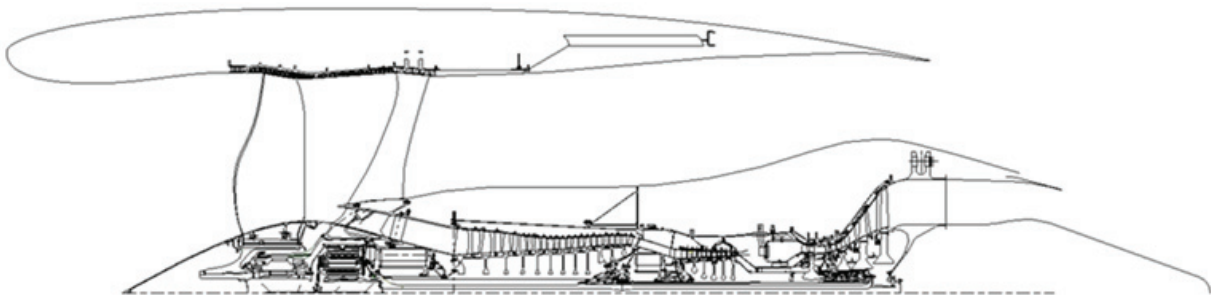


Figure 5-4. Geared Turbofan Mechanical Profile Diagram

5.1.4 Open Rotor

The open rotor engine concept has been revived in recent years by most major engine producers due to increasing fuel costs [Ref. 35]. Previous research conducted by General Electric on the GE36 Unducted

Fan and Pratt and Whitney/Allison on the 578-DX similarly followed high-fuel price trends in the 1970s [Ref. 36]. Though the open rotor exhibits the high fuel efficiency inherent in turboprop engines, its thrust-to-weight ratio is significantly less than that of the three-shaft turbofan (Figure 5-5). The open rotor achieves a takeoff SLS thrust-to-weight ratio of 2.32 with respect to the dry engine system, whereas the three-shaft turbofan reaches up to 6.15. During cruise, the difference is not quite as significant, with the open rotor and three-shaft turbofan achieving thrust-to-weight ratios of 0.47 and 0.87, respectively. These weight differences are due to the massive nature of the propeller system. When comparing to the three shaft turbofan, the weights of each common module are quite similar. It is the addition of the gearbox and propeller pitch change mechanism that penalizes weight so significantly. First, the gearbox outputs enormous torques due to the slow rotational speed of the propellers. This torque level requires the size of the gearbox to be significant as a percentage of engine weight. In addition to the gearbox, the pitch change mechanism is another reason for the open rotor weight penalty. Each individual propeller blade requires independent and redundant pitch control mechanisms. These mechanisms must overcome the centrifugal loading from 7 foot propeller blades while precisely controlling attack angles to tenths of a degree. Significant acoustic penalties also accompany this configuration due to its external counter-rotating propellers. While some aeroacoustic prediction capabilities have been developed for counter-rotating propellers by Whitfield et al [Ref. 37,38] and Hanson [Ref. 39], validation of these tools with experimental data has been limited. High-fidelity numerical models have not yet been developed in the public domain.

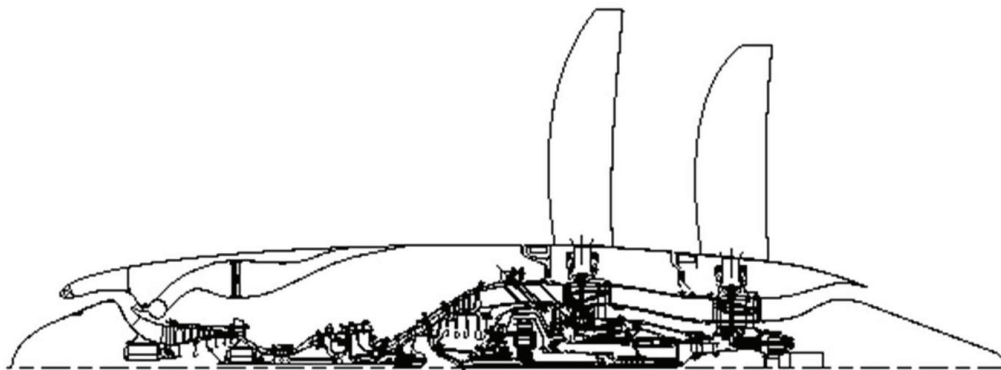


Figure 5-5. Open Rotor Mechanical Profile Diagram

The 2030 EIS open rotor engine uses an IP compressor and a combination axial/centrifugal HP compressor. Hot-side flow is used in conjunction with a gearbox to drive the counter-rotating propeller system. At SLS takeoff the engine achieves an OPR of 35 and a specific fuel consumption of 0.157 pph/lbf. The model for the engine core assumes a constant nozzle C_v of 0.995, no customer bleed, and a constant power extraction of 100 hp. Ideal inlet recovery is also assumed.

Technologies embedded inside the engine include active tip clearance control in the HPC and HPT, high OPR materials and seals, and active flow control in the IPC. Advanced high-temperature materials are employed, fuel-cooled cooling air is used to reduce turbine blade temperatures, and high-strength shaft materials provide additional structural integrity. The engine also uses high-temperature sumps, electric fuel and oil pumps, and an embedded starter/generator. Lean combustor technology enables low NO_x production. Currently estimated at a TRL of 5, this technology is expected to be fully mature by the N+3 timeframe.

5.1.5 Engine Comparison and Downselection

Figure 5-6 shows a comparison between the specific fuel consumption of the geared turbofan and the three-shaft turbofan when sized for the same takeoff thrust. It can be seen that the performance of the engines is nearly identical. At idle, the three-shaft turbofan has a slightly improved fuel consumption compared to that of the geared turbofan. Similarly, Figure 5-7 compares the specific fuel consumption of the advanced engine architectures compared to the reference CFM56 engine. It can be seen that the

advanced technology engines exhibit significantly reduced fuel burn compared to the baseline engine (44% and 60% reduction for the three-shaft turbofan and open rotor, respectively, during this portion of the mission). While this comparison is a huge selling point for the open rotor architecture, it does not articulate either the difference in weight or noise between the two engines. Again, the geared turbofan showed the same characteristics as the three-shaft turbofan and, as a result, is not displayed on this graph. The geared turbofan was set aside for the remainder of the study, not because of any deficiency in the technology, but rather to limit the number of possible combinations of configuration and propulsion system. It is expected that any results stemming from the study of the three-shaft engine will be applicable to any aircraft using a high-bypass ratio turbofan architecture, including a geared turbofan.

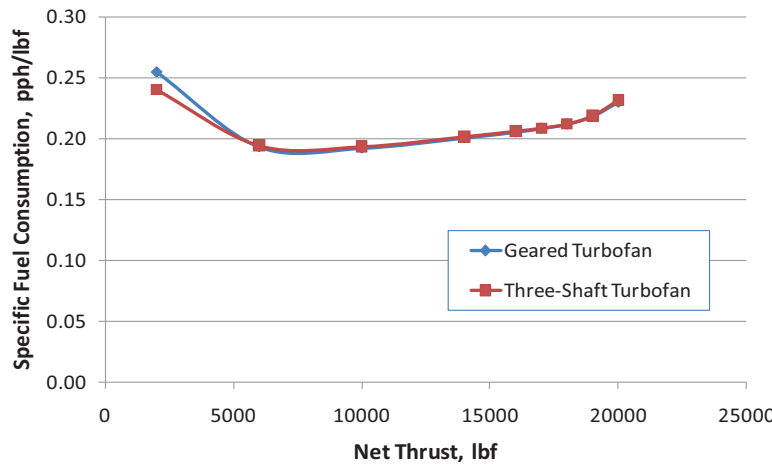


Figure 5-6. Geared Turbofan and Three-Shaft Turbofan SLS SFC Hook Comparison at Comparable Technology Level

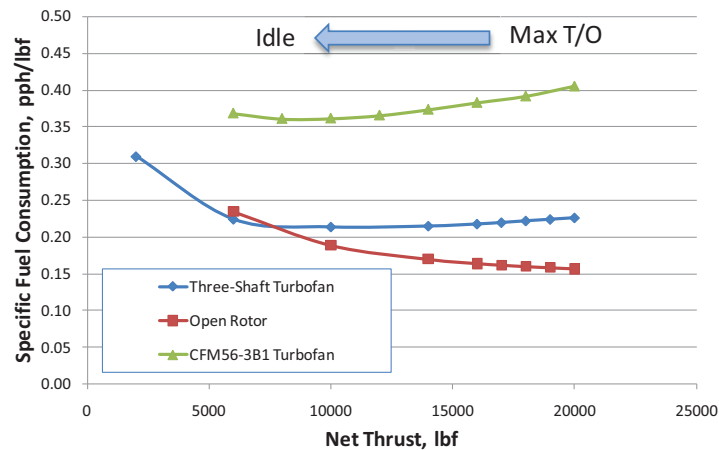


Figure 5-7. Engine Architecture SLS SFC Hook Comparison, Advanced Technology Level

5.2 Airframe Concepts

The airframe concept downselection process is shown in Figure 5-8. Beginning with a wide initial design space, various analyses were made to reduce the number of possible configurations for detailed study. The aircraft comprising the initial design space will be described below, followed by a description of the processes which narrowed the field of candidate configurations.

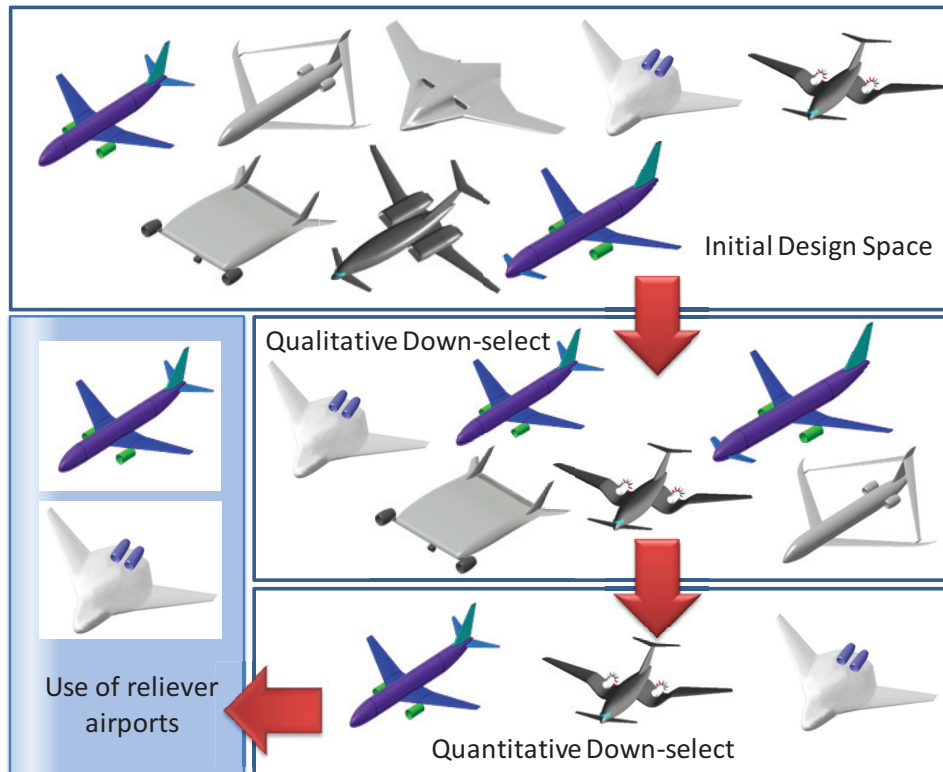


Figure 5-8 .Airframe Configuration Downselection Process

5.2.1 Tube-and-Wing

The tube-and-wing vehicle configuration is the classic design configuration for modern transport aircraft. This configuration offers good packaging for passengers, cargo, and propulsion systems while maintaining relatively low drag characteristics (Figure 5-9). The engine placement on the undersides of each wing permits low-cost, straightforward integration and easy maintenance access to the propulsion system. The large main wing is balanced in pitch by the smaller rear horizontal tail, which can be placed at any height along the vertical tail. When the engines are placed in an aft-mounted configuration, a T-tail empennage is required to minimize the interference of the engine exhaust with the control surfaces. A study of this alternate configuration is presented in Section 6.1.1. However, T-tails result in heavier vertical tails out of structural necessity [Ref. 40]. The inverse proportionality of aspect ratio to induced drag suggests that this is a primary design driver of low fuel consumption aircraft. However, the additional wing weight that accompanies larger wings must be taking into consideration. The cylindrical geometry of the fuselage required for passenger seating forces a fineness ratio in the range (greater than three) associated with low fuselage friction drag [Ref. 41]. While not a revolutionary configuration, advanced technologies that may be mature by the 2030-2035 EIS timeframe may unlock advanced versions of this configuration by allowing for higher aspect ratio wings and reduced drag through the implementation of surface features on the fuselage or laminar flow wing design. Such configurations will be referred to as advanced tube-and-wings (ATWs). Among the disadvantages of this configuration is the drag associated with the wetted area of podded engines and aft empennage [Ref. 42].



Figure 5-9. Tube and Wing Configuration

5.2.2 *Tube-and-Wing With Embedded Turbofans*

The tube-and-wing configuration with an embedded propulsion system offers the same advantages as the tube-and-wing configuration with potential for noise reduction benefits due to the acoustic shielding inherent in embedded engines (Figure 5-10). Furthermore, there is a potential reduction in aircraft wetted area due to the removal of the engine pods, depending on the extent of engine integration. An example of this type of configuration in the commercial industry is the de Havilland Comet 4 [Ref. 43]. Powered by four Rolls-Royce Avon Mk 524 turbojets, each wing contained two engines embedded near the root. However, this configuration experienced undesirable levels of fuel consumption. The implementation of the buried inlet introduces losses in pressure recovery, resulting in a reduction in the propulsive efficiency capabilities of the engine. Additionally, placing the engine near the wing root can lead to the ingestion of boundary layer flow off of the fuselage, further hindering the pressure recovery potential of the inlet. Since the propulsive efficiency of the engine is inversely proportional to specific fuel consumption, both inlet pressure recovery losses and boundary layer prohibit the engine from achieving its full potential. The flow over the wing in the vicinity of the engine inlets can become disturbed and lead to a reduction in lift capacity, counteracting the wetted area reduction achieved by removing the engine pods [Ref. 42]. Additionally, modern commercial transport speeds and their respective wing sweeps would result in high spillage drag with wing-embedded propulsion systems [Ref. 44]. While additional technologies could be included to reduce inlet pressure distortion and alleviate flow disturbances over the wing, these technologies would add weight to the system, on top of fuel weight that must compensate for reduced engine efficiency. In addition, active systems may require substantial amounts of engine bleed. Perhaps the most compelling argument against this type of aircraft configuration is the incompatibility of this design with the use of a very high bypass turbofan. In order to embed a large-diameter engine inside the wing, the volume must be available at the wing root. However, because of the large diameters associated with fans, this becomes impractical. Furthermore, the open rotor engine architecture is not feasible with this type of aircraft design. Due to the penalties significantly outweighing the benefits, tube-and-wing embedded propulsion configurations were not considered for further analysis.

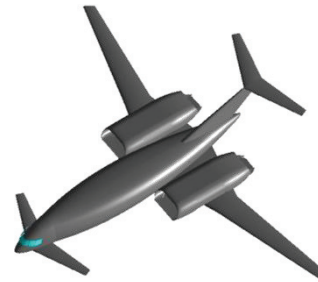


Figure 5-10. Wing-Root Embedded Turbofans With Canard

5.2.3 *Tube-and-Wing With Canard*

The addition of a lifting canard onto a conventional tube-and-wing configuration with or without aft tail geometries provides an alternative method to achieve stability and control. Its implementation in the absence of an aft horizontal tail results in a more unconventional geometry to control (Figure 5-11). Work by McGeer and Kroo has shown that this type of configuration will generally result in a higher total drag than the conventional layout [Ref. 45]. Canard designs studied by Keith and Selberg showed that the wing loading on the canards required to trim the aircraft was excessive, leading to extreme levels of induced drag [Ref. 46]. Vertical placement of the canard has been shown to be a main design driver behind this type of configuration. When the canard is combined with an aft horizontal tail, minimum control surface deflections can be used which minimizes trim drag [Ref. 47]. However, additional weight penalties will be realized, in addition to the increased skin friction and induced drag arising from the presence of another lifting surface [Ref. 48].



Figure 5-11. Tube and Wing Configuration With Canard

5.2.4 Hybrid Wing-Body

The hybrid wing-body is a revolutionary alternative to the tube-and-wing configuration considered in this concept design study (Figure 5-12). Reports have shown that the hybrid wing-body (HWB) configuration can have significantly decreased root bending stresses compared to traditional tube-and-wing configurations [Ref. 49].

This reduction in bending loads, combined with the vehicle operating at a significantly lower wing loading, allows for increased structural efficiency. Additionally, decreased wing loading would contribute to a decrease in takeoff and landing field length. HWB vehicles also permit the elimination of tail sections. Eliminating these surfaces would decrease vehicle drag through a reduction in skin friction and form drag, increasing lift-to-drag and reducing fuel burn [Ref. 50]. The centerbody of the HWB allows for engine noise reduction by acting as a noise shield. In a study by Papamoschou et al [Ref. 51], a cumulative effective perceived noise level (EPNL) reduction of 7.4 EPNdB was possible through the use of centerbody noise shielding with an aft shield length of five jet diameters. The study suggests that increased exhaust mixing would increase the effectiveness of noise shielding. In addition, boarding operations become faster and more efficient due to the seating layout of the vehicle, decreasing turnaround time during ground operations.

Though this configuration offers structural benefits, it presents a structural challenge in creating a pressure vessel for the cabin without adding significant empty weight. The configuration deviates from the traditional cylinder vessel to a pentagon-shaped design, which is more challenging to design with a low weight and ability to support adequate loads during cabin pressurization [Ref. 49]. Past studies have concluded that hybrid wing-bodies might be best used for large cargo or passenger missions, as opposed to shorter mission lengths and passenger counts due to the internal volume of the vehicle increasing faster than the external surface area. For large vehicles and passenger counts, this could lead to decreased drag; however, scaling the vehicle for a smaller passenger count results in the internal volume decreasing faster than the external surface area which would lead to an increase in drag [Ref. 50].

The minimum centerbody height is determined by the size of the passengers, regardless of the mission. Centerbody volume is subsequently set by passenger count. This is shown graphically in Figure 5-13. Wing spar and engine location then drive the length of the fuselage, driving the fuselage thickness-to-chord ratio. As a result, the minimum allowable size for the hybrid wing-body is dictated by passenger count, regardless of the mission. Based on the passenger count defined in the mission requirements, the minimum fuselage length was 70 feet, further constraining the root chord of the outboard wings.

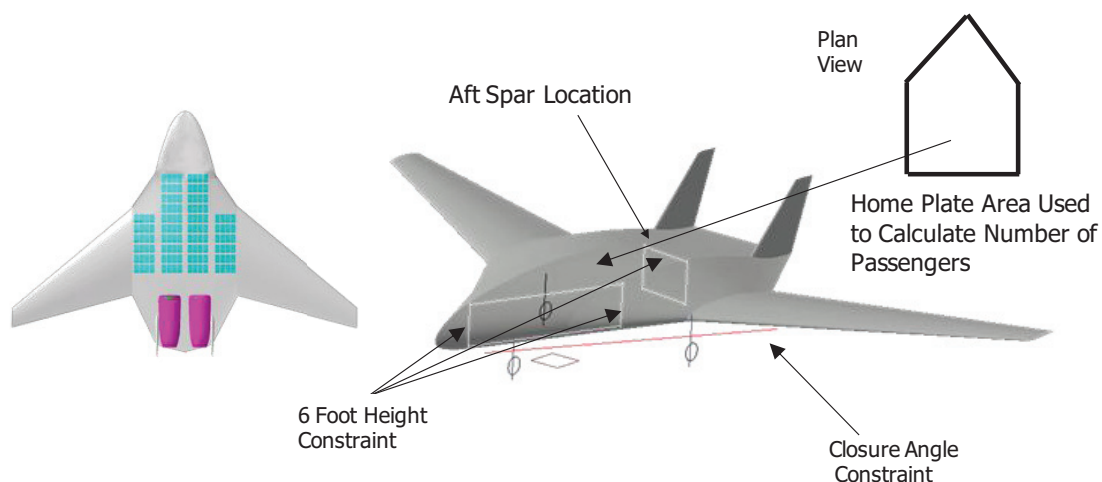


Figure 5-13. HWB With Embedded Propulsors Configuration

5.2.5 Hybrid Wing-Body With Embedded Turbofans

The HWB configuration with an embedded propulsion system offers the same advantages as the HWB configuration with the additional benefit of further engine noise reduction (Figure 5-14). This noise reduction would be a result of engine noise shielding due to the burying of the engines into the body. Integrating the propulsion systems would reduce wetted area due to the removal of the nacelles, assuming volume is available in the centerbody, and would allow augmentation of the vehicle aerodynamics through the use of the propulsion system [Ref. 50]. Furthermore, reductions in ram drag can be realized due to the ingestion of boundary layer flow into the inlets.



Figure 5-14. HWB With Embedded Propulsors Configuration

The introduction of buried inlets introduces pressure recovery penalties that can translate into losses in propulsive efficiency. Specifically, embedding the propulsion system increases inlet distortion, worsening the efficiency of the system compared to a podded engine configuration. This decrease in propulsive efficiency would result in increased fuel burn [Ref. 52]. Embedded engines would also occupy internal volume in the fuselage which would otherwise be available for passengers and cargo. With a fixed passenger count, adding internal volume to support an embedded propulsion system would lead to an increase in wetted area, empty weight, and drag. In addition, embedding the propulsion system would add complexity to engine maintenance and decrease vehicle structural volume [Ref. 50]. Due to the penalties relative to the N+3 mission goals significantly outweighing the benefits, HWB embedded propulsion configurations were not considered for further analysis.

5.2.6 Channel Wing

An adaptation of the tube-and-wing concept, the channel wing consists of a fuselage and aft tail with modified wing geometry (Figure 5-15). Instead of a flat wing planform, a circular channel is built into the wing in which the engines are mounted. The vehicle can use the same variety of aft tail geometries common on tube-and-wing configurations, and employ a canard if deemed necessary. The implementation of the engine channels allows for the increase in velocity over the upper surface of the channel to augment the circulation and lift of the wing [Ref. 53]. While stall angles have been shown to be extended out to 45 degrees using a channel wing, the high lift associated with these extreme angles of attack have been inaccessible due to tail scrape angle limitations. Hence, channel wing geometries are typically accompanied by circulation control to achieve lift coefficients in the range of 8.5 to 9.0 [Ref. 54]. Channel diameter will be constrained by propeller size, and may lead to a reduced thrust potential of the open rotor because half of the propeller disk is effectively ducted. An experimental study by Blick and Homer showed that this penalty could be as much as 10% [Ref. 55]. As the basic geometry remains in the shape of a tube-and-wing, the same benefits can be sought in this configuration by maximizing aspect ratio to minimize induced drag and seeking laminar flow over the flat portions of the wing. However, it must be taken into consideration that smaller portions of the wing are available for laminar flow purposes. The channel wing configuration has increased risk associated with it over more conventional designs due to the limited amount of channel wing research. Compared to more conventional platforms, the channel in the wing also presents a structural challenge that must be addressed. Furthermore, a flat wing of the same projected platform will mathematically produce less profile drag for a lower structural weight.



Figure 5-15. Channel Wing Configuration With Canard

5.2.7 *Joined Wing*

The joined wing configuration consists of a typical cylindrical fuselage with a swept front wing and a vertical tail. Instead of a horizontal stabilizer, a second forward-swept wing, whose root is typically placed at some spanwise position along the length of the vertical tail, joins the trailing edge of the front wing, as shown in Figure 5-16. It has been shown that a joined wing can weigh 22%-35% less than an aerodynamically equivalent cantilevered wing and tail [Ref. 56,57]. This has been attributed to the rear wing behaving as a strut for the front wing. Wolkovitch showed in his work that using trailing edge control surfaces should be sufficient for all stability and control requirements [Ref. 58].

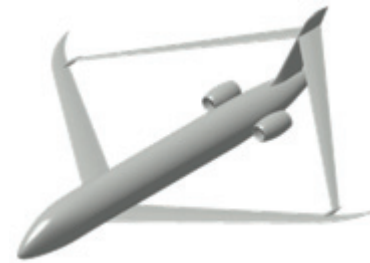


Figure 5-16. Joined Wing Configuration

In addition, the joined wing configuration distributes the wing area over a larger portion of the vehicle, decreasing wave drag and improving transonic aerodynamic properties [Ref. 56]. However, as a result of using a second intersecting wing, excess wetted area would exist and interference drag would increase from surface intersections. In addition, joined wing vehicles are more difficult to trim at maximum lift coefficients for equivalent tube-and-wing configurations [Ref. 59]. As seen in Figure 5-16, like the tube-and-wing, the joined wing configuration would offer no engine shielding from the main wing, diminishing its ability to contribute to the N+3 acoustic goal.

5.2.8 *Low Aspect Ratio Spanloader*

Low-aspect ratio spanloader (LARS) configurations offer improved boarding operations due to the seating configurations and entrances offered by a spacious passenger cabin layout (Figure 5-17). With the ability to load and unload passengers more quickly, reduced time associated with ground operations can be realized by this vehicle design. This would improve the time utilization of the vehicle when introduced into NAS operations. This configuration also offers a viable platform for distributed propulsion and boundary layer-ingesting inlets. However, similar to the issue encountered with hybrid wing-body aircraft, using a non-cylindrical fuselage introduces difficulties in pressure vessel design. For a rectangular fuselage with the same order of magnitude in perimeter as a round fuselage, the associated bending stresses can be an order of magnitude higher [Ref. 60]. Low-aspect ratio experimental aircraft have shown that these configurations can be built extremely light, reducing their required lift and, in turn, the associated induced drag [Ref. 61]. However, the low aspect ratio nature of the vehicle will counteract these induced drag benefits. Furthermore, it is expected that these studies would not translate well into a full-sized commercial transport, as the size of the vehicle will be driven by the size of the passenger cabin.



Figure 5-17. LARS Configuration

Though LARS was selected as a candidate platform for studies of distributed propulsion, it was determined that many of the enabling technologies behind this form of propulsion system would not be ready for production given the N+3 timeframe. However, because the configuration held promise in terms of ground operations, it was carried through the qualitative down-select process to be examined in more depth.

5.2.9 Configuration Quantitative Assessment and Downselect

In order to downselect the advanced body configurations (Sections 5.2.3, 5.2.6-5.2.3), the vehicles were quantitatively assessed with respect to five parameters determined to be representative of the mission goals: aerodynamic drag, mission fuel, empty weight, vehicle noise, and field length. For each of these metrics, the airframe configurations were assigned scores based off of their estimated performance with respect to one another. These scores were subsequently converted into a figure of merit that shows the relative benefits and disadvantages of the configurations, shown in Figure 5-18. For example, because of the large wetted area and drag associated with the LARS configuration, it received a low score in the aerodynamic drag category. Due to the potential weight savings associated with the joined wing configuration, a high score was assigned to its empty weight category. The hybrid wing-body and the channel wing were determined to have the best potential to shield engine noise. With this scoring system, and with these metrics, this initial quantitative assessment between airframe configurations yielded the hybrid wing-body, channel wing, and tube-and-wing vehicles as the three most promising airframes to be carried forward. LARS configuration was determined to be the least promising of the airframe configurations, followed by the joined wing and the canard configurations.

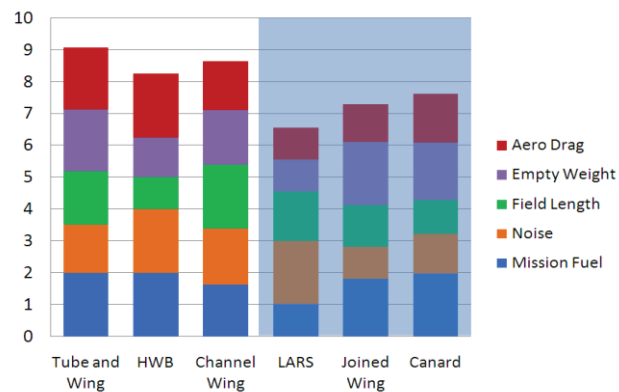


Figure 5-18. Configuration Quantitative Assessment

Less weight was placed on extreme short takeoff and landing capability as a result of the analysis of field length requirements. Unusually high lift coefficients were not needed to achieve metroplex operations. Traditional high lift systems proved to be sufficient. Relaxing the field length constraint in the vehicle qualitative assessment yielded the tube-and-wing and hybrid wing-body as the two preferred configurations out of the six vehicles, as seen in Figure 5-19. In addition to these quantitative results, the added complexity and risk associated with the channel wing led to the dismissal of the configuration from further consideration. The result of the quantitative assessment showed that the conventional nature of the tube-and-wing configuration may be the most suitable platform upon which to build and mature future technologies. Furthermore, for the N+3 EIS timeframe, it may be the best balance of risk and solution for the mission objectives. A summary of the configuration downselection process is illustrated in Figure 5-8.

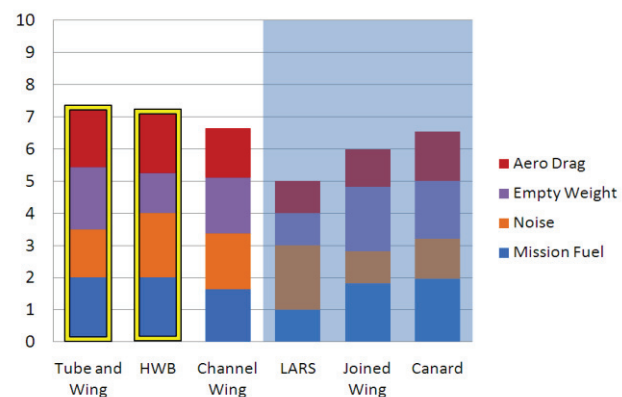


Figure 5-19. Configuration Quantitative Assessment Discounting Field Length

5.3 New Technology

The assessment of candidate technologies for aircraft entering service in the N+3 timeframe required careful consideration of the relative benefits and penalties associated with each technology, as well as their potential for maturation in a timeframe consistent with their incorporation into a new aircraft. In order to perform this analysis, an extensive matrix of candidate technologies was developed, as described in Section 5.3.1. This list of technologies was then qualitatively ranked according to a QFD process,

described in Section 5.3.2. Technologies consistent with the N+3 timeframe were selected from among the top candidates. The remainder of this section details the reasoning behind the selection of certain technologies for continued study. It will further describe the models that were used to depict the benefits and penalties of those technologies that were chosen for further examination. A diagram of the process is shown in Figure 5-20.

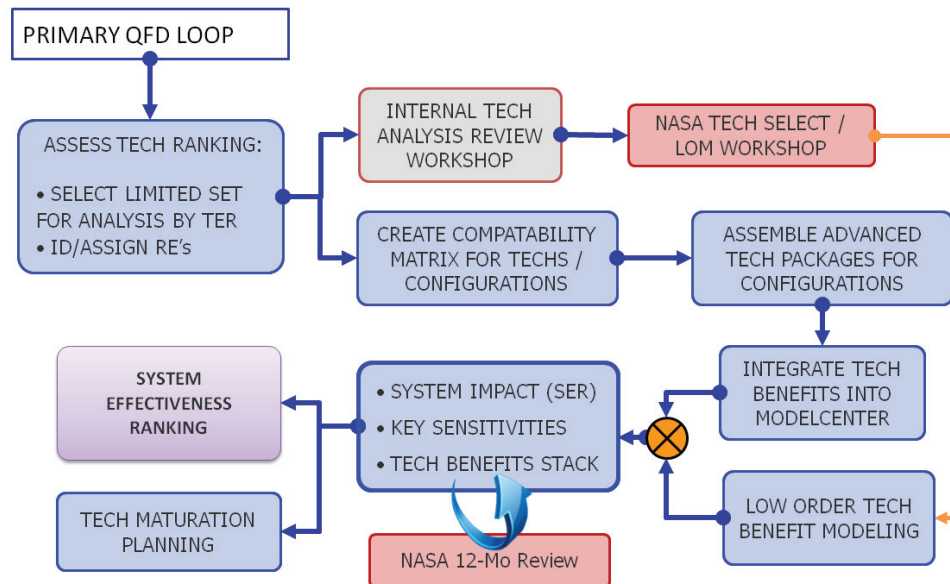


Figure 5-20. Technology Assessment Process Flow

5.3.1 Development of Technology Matrix

In the generation of the original technology matrix, input was gathered from subject matter experts (SMEs) on the Northrop Grumman team. Each group submitted technology concepts within its area of expertise, e.g., an extensive list of candidate propulsion and noise technologies was developed in collaboration with Rolls-Royce Liberty Works. Appendix A lists the candidate technologies broken into four major subheadings: airframe, aerodynamics, noise, and propulsion.

5.3.2 Quality Function Deployment Process

In order to rank the candidate technologies in preparation for the final downselection, a QFD method was used. QFD made it possible to translate qualitative assessments of the relative benefits and penalties of individual technologies into a common quantitative foundation. SMEs familiar with the technologies were called upon to rate each technology with respect to the N+3 objectives. These scores were used to develop technology effectiveness ratings (TERs), or scenario-weighted rankings of each technology. Five potential scores were used to define the impact of each technology with respect to the N+3 goals. For each goal, the SME could assign a value of 1, 3, 5, 7, or 9, where a value of 3 represented a technology having no impact on a specific N+3 goal, a value of 1 corresponded to a detrimental impact, and 5, 7, and 9 were relative levels of positive benefits. When weighted for each scenario, the summation of these scores comprised the TER for the technology. Input was also gathered from SMEs concerning TRLs for all candidate technologies. A snapshot of the master QFD worksheet at an interim point in the information gathering process is shown in Figure 5-21. A full listing of the QFD worksheet is given in Appendix D.

SELECT Goals:		Fuel Burn		Take-off & Landing Field Length		NOx Emissions		Noise		SER Total	TRL	Interaction Quotient							
Scale Factor (Priority)	1.00	1.00	1.00	1.00	1.00	1.00	1.00	1.00	1.00	0.25	1.00								
Normalized Scale Factor Units:	25	25	25	25	25	25	25	25											
Qualitative	3	3	3	3	3	3	3	3											
Quantitative	3	3	3	3	3	3	3	3											
Threshold Fz (Threshold Value On Gaussian Curve):	0.3	0.3	0.3	0.3	0.3	0.3	0.3	0.3											
Max Score	This is the maximum score																		
Baseline	Baseline																		
FB	9	25.00	9	25.00	9	25.00	9	25.00	9	25.00	100.0	9	10	5	9	2			
F3	3	7.50	3	7.50	3	7.50	3	7.50	3	7.50	30.0	1	100	0	1	0			
FL	3	3	3	3	3	3	3	3	3	3									
FNx	3	3	3	3	3	3	3	3	3	3									
LDN	3	3	3	3	3	3	3	3	3	3									
LDN	3	3	3	3	3	3	3	3	3	3									
Total	9	25.00	9	25.00	9	25.00	9	25.00	9	25.00	100.0	9	10	5	9	2			
TRL	1	100	0	1	0	1	0	1	0	1	0	1	100	0	1	0			
Interact																			
IQ																			
IQ																			
Score																			
ID	Designation:	Description:	Physical Principles:	FB Input	F3 SER	FL Input	FL SER	FNx Input	FNx SER	LDN Input	LDN SER	SER	TRL	TRL Risk	Interact	IQ	IQ	Score	Comments / Assumptions
92	Prop Concept #4.24	TO/C-Assist Propulsion Unit	Detachable takeoff/climb autonomous propulsion units propel vehicle to cruise altitude, then return to airport increasing cruise efficiency.	5	14.64	9	25.00	5	14.64	5	14.64	68.9	1	100.0	2.3.4				Assume lower flight velocity for low-power 'engine' matching. Decreased cruise weight. High bypass allow for large mass flow @ sea level, and improved SFC with small weight and penalty despite nacelle drag.
39	Noise Concept #3.11	Ultra-High (10+) Bypass Ratio Turbofans	Trading Velocity for Mass Flow Rate	7	21.87	5	14.64	3	7.50	7	21.87	65.9	6	65.7	3.4				Assumes high lift benefit without cruise penalties typically associated w/ fixed high lift devices
56	Noise Concept #3.28	Wing Morphing (Shape Memory Alloys, Piezoelectrics)	High-Lift Device Integration into the Wing	3	7.50	7	21.87	5	14.64	7	21.87	65.9	2	95.0	1.2.3				Hi lift systems typically add weight and increase cruise drag, but greatly improve takeoff performance.
20	Aero Concept #2.06	Distributed Exhaust Nozzle Flap (DEN Flap)	Distributed Exhaust Nozzles Integrated Into Flap Provide Flow Control/Supercirculation.	1	2.94	9	25.00	5	14.64	7	21.87	64.5			2.3.4				Hi lift systems typically add weight and increase cruise drag, but greatly improve takeoff performance.
21	Aero Concept #2.07	Steady Circulation Control (Offtake Engine Flow Used for Circulation Control via Blown Flap, IBF, Coanda Jet Flap, etc.)	Low-Cm Exhaust Provides Flow Control and Circulation Control Wing (CCW)	1	2.94	9	25.00	5	14.64	7	21.87	64.5			2.3.4				Hi lift systems typically add weight and increase cruise drag, but greatly improve takeoff performance.
22	Aero Concept #2.08	Unsteady Circulation Control (Offtake Engine Flow Used for Circulation Control via Blown Flap, IBF, Coanda Jet Flap, etc.)	Pulsed Effectors Provide Similar Benefits as Steady CCW	1	2.94	9	25.00	5	14.64	7	21.87	64.5			2.3.4				Weight Penalty, moderately better SFC, moderate to high reduction in NOx.
35	Noise Concept #3.07	Geared Turbofan	Allows Very High-Bypass Cycles	5	14.64	1	2.94	9	25.00	7	21.87	64.5	5	75.0	1.3.4				Multiple options available. Could be combined

Figure 5-21. Format of Master QFD Worksheet and Database

In order to properly accommodate for low-TRL technology risk in the technology effectiveness ratings, a TRL Risk Factor was applied. The curve, shown in Figure 5-22, emphasizes how technologies currently rated below TRL 3 are penalized through this risk factor, while those greater than TRL 3 are given advantage due to their higher likelihood to mature in the N+3 timeframe.

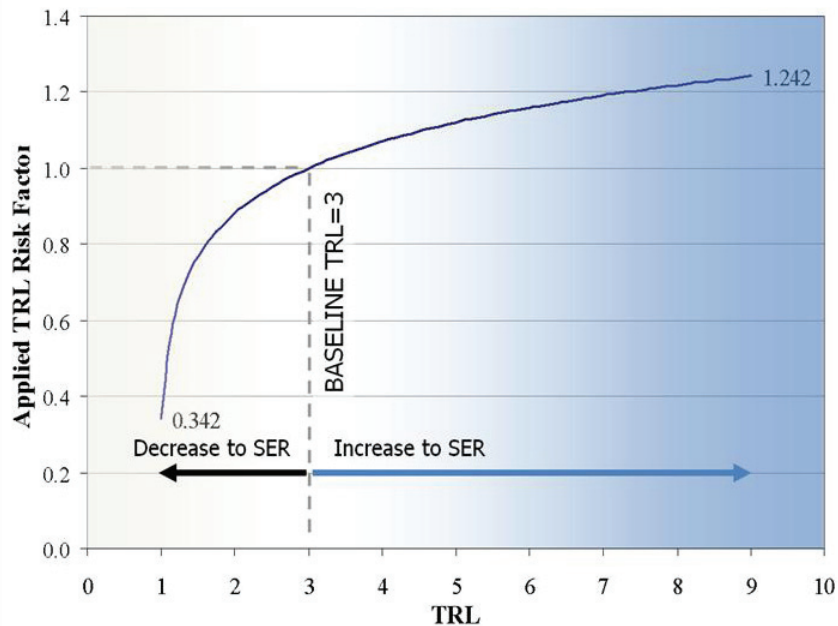


Figure 5-22. Applied TRL Risk Index Factor

The final weighting parameter considered in the TER framework is the relative importance of each of the N+3 metrics in the overall scenario defined in Section 4.1.2. Since fuel burn and emissions were the metrics of most concern to the projected future scenario, technologies that most impacted these metrics positively were given additional weighting in the TER system. Although not considered in the overall TER for each technology, interactions between technologies were assessed in a separate interaction quotient, to illuminate mutually beneficial and exclusive technology packages. For the overall scenario, Figure 5-23 shows a compiled TER worksheet which was used in the technology down-selection process, taking into consideration the risk index factor. The top ten technologies for each scenario are shown in Figure 5-24.

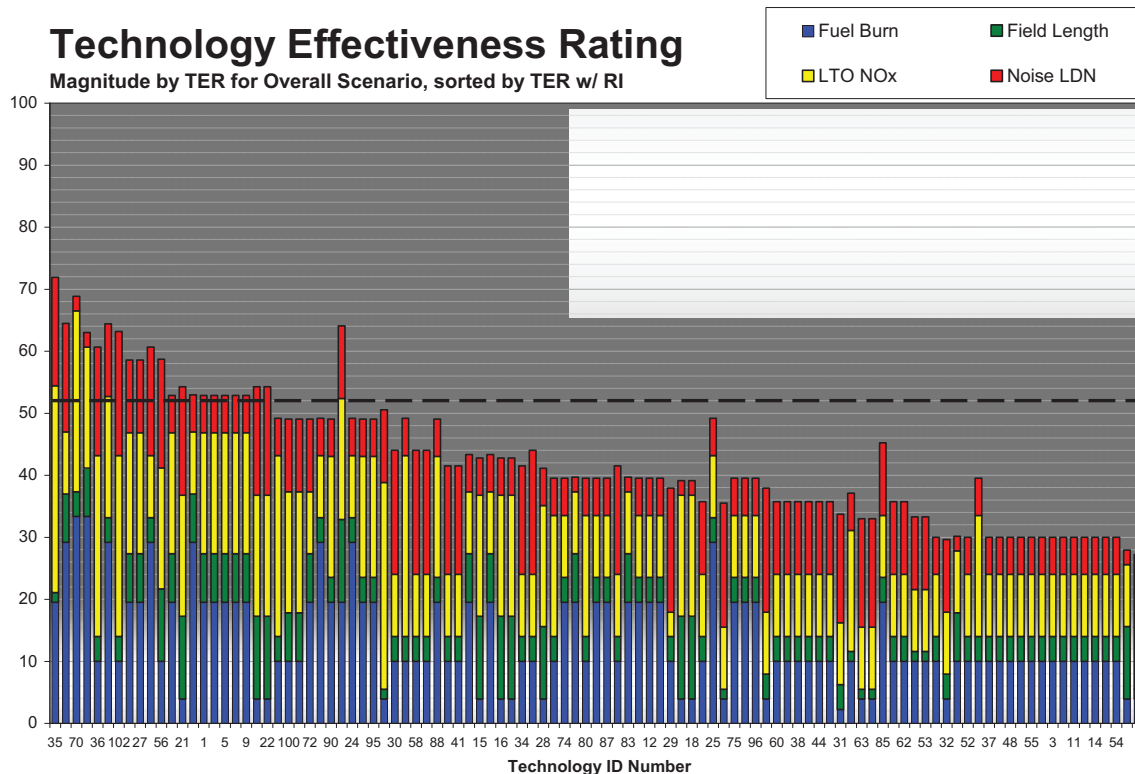


Figure 5-23. Technology Effectiveness Ratings for Overall Scenario

Rank	DESCRIPTION	TER Rating*	Rank	DESCRIPTION	TER Rating*
1	Geared Turbine	85.3	1	Ultra-High Bypass Ratio Turbofan	67.8
2	Variable Geometry Nozzles	79.0	2	Steady Circulation Control	65.1
3	Non-Turbine Distributed Fans	77.8	3	Wing Morphing	63.3
4	Steady Circulation Control	69.6	4	Geared Turbine	63.1
5	Wing Morphing	67.4	5	Distributed Exhaust Nozzle (DEN) Flap	62.5
6	Distributed Exhaust Nozzle (DEN) Flap	66.9	6	Unsteady Circulation Control	62.5
7	Unsteady Circulation Control	66.9	7	Open Rotor	61.9
8	Ultra-High Bypass Ratio Turbofan	64.8	8	Modeling for Engine Inlet Optimization	58.6
9	Hybrid All-Electric Propulsion	63.2	9	Inlet Flow Control	58.6
10	Noise Shielding	62.6	10	Variable Geometry Nozzles	58.1

Rank	DESCRIPTION	TER Rating*	Rank	DESCRIPTION	TER Rating*
1	CVC / Wave Rotor	91.9	1	Geared Turbine	74.8
2	Open Rotor	88.9	2	Ultra-High Bypass Ratio Turbofan	67.9
3	Geared Turbine	76.0	3	CVC / Wave Rotor	66.2
4	Turbo-Electric Distributed Fans	74.3	4	Open Rotor	65.5
5	Ultra-High Bypass Ratio Turbofan	70.9	5	Variable Geometry Nozzles	63.1
6	Swept-Wing Laminar Flow	68.9	6	Turbo-Electric Distributed Fans	61.9
7	All Electric Engines (no AGB)	67.4	7	Non-Turbine Distributed Fans	60.7
8	Microvortex Generators / Riblets	67.4	8	Modeling for Engine Inlet Optimization	58.6
9	Turboshaft-Powered Direct Drive Distributed Fans	64.7	9	Inlet Flow Control	58.6
10	Deployable Vortex Generators	60.9	10	Turboshaft-Powered Direct Drive Distributed Fans	58.3

Figure 5-24. Top Ten Technologies for Each Scenario Based on QFD Analysis

5.3.3 *Down-Selection of Candidate Technologies*

While the QFD process succeeded in sorting the candidate technologies best suited for the overall future scenario, it was necessary to reduce the number of technologies to a manageable number for more detailed investigation. Those technologies receiving the highest TER rating were considered first, and divided into the disciplines of aerodynamics, propulsion, structures, and noise. Decisions were made to limit the number of technologies among the disciplines to more equally distribute the candidate technologies. In this section, technologies selected for further consideration will be discussed, and modeling within the framework of the design tools will be described in detail. Technologies were modeled in such a way that they could be packaged to accurately reflect the additive effects of combining individual technologies. As technologies are packaged together, the net system benefit increases. However, the benefits do not necessarily combine in a linear fashion. For example, if two separate technologies both reduce vehicle empty weight by 50%, adding these technologies would not result in a 100% decrease in empty weight. Coupling these technologies would yield a net reduction less than 100%, but still greater than the 50% reduction seen by each individual technology.

Technologies that were considered but set aside are listed, along with a discussion of the rationale, in Appendix B. Technology maturation plans for the preferred technology package for the final vehicle design, along with current TRL level estimates and required development milestone paths to reach TRL 6 by 2025 are provided in Chapter 7. For those technologies that are already beyond TRL 6, no additional development path was developed, and it is assumed that sufficient investment will occur to make these available for the N+3 EIS.

5.3.3.1 *Natural Swept-Wing Laminar Flow* – Regions of laminar flow greatly reduce profile drag through skin friction drag reduction compared to those of turbulent flow [Ref. 62]. Implementation of laminar flow can lead to a significant reduction in vehicle drag and a subsequent reduction in fuel burn. For a typical transonic commercial aircraft, natural laminar flow over 25% of the upper and lower surfaces would result in an approximately 25% reduction in wing profile drag [Ref. 63]. Natural swept-wing laminar flow is enabled through the use of airfoils conducive to laminar flow, elimination of surface breaks, and a more favorable surface geometry. A laminar flow tool was developed to calculate and visualize the potential regions of laminar flow on a given surface. In-house experimental research has quantified the achievable chord-wise extent of laminar flow regions in the form of maximum transition Reynolds number as a function of wing sweep, and these empirical results have been incorporated into this model. Based on this proprietary research and experimental testing, the maximum transition Reynolds number was found for the given sweep and projected to the 2030 timeframe. The geometry of the surface is input, along with vehicle operating conditions such as altitude and Mach number. The tool then plots the regions of laminar flow on the given surface, along with calculating the percentage of the surface in the laminar flow region, as in Figure 5-25. The tool takes into account turbulent wakes caused from section interference, such as the wing-fuselage interface, engine and nacelle, pylon, wing tips, and control surfaces. No regions of laminar flow can exist aft of section breaks, such as flaps. The drag divergence Mach number of the vehicle was corrected, as the presence of shocks precludes the existence of laminar flow. In addition, the maximum lift coefficient is penalized due to slat removal and airfoil profile change to accommodate laminar flow.

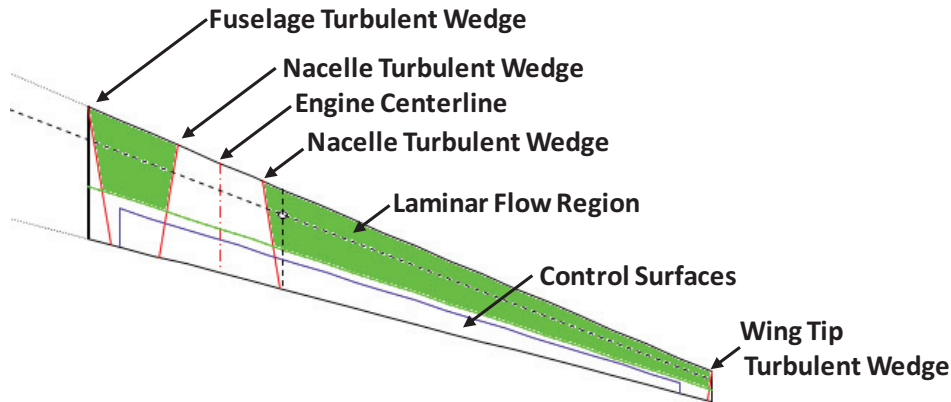


Figure 5-25. Laminar Flow Regions Visualization for High Aspect Ratio Wing

The percentage of laminar flow per surface, the corrected drag divergence Mach number, and the maximum lift coefficient penalties were modeled in the aerodynamics module in FLOPS. The existence of laminar flow in MIDAS was reflected by the removal of slat noise during acoustic calculations.

5.3.3.2 Landing Gear Assembly Component Integration – Landing gear assembly component integration entails the incorporation of smaller landing gear assembly components into more inclusive parts. This may often include placing smaller components inside larger components, reducing landing gear drag by removing sources of small-scale vortex shedding. Consequently, reduced turbulent and vortex shedding leads to a reduction in source (and far-field) noise during approach. Landing gear must be designed to be structurally sound, and the integration of smaller components must be performed in a manner that does not sacrifice the sturdiness of the gear. A large downside to this process is the difficulty in maintenance that would result from reducing access to smaller landing gear components.

According to Guo et al [Ref. 64], a clean landing gear configuration is attenuated, conservatively, by 3 dB of broadband noise compared to a fully dressed landing gear configuration for wind tunnel Mach numbers between 0.18-0.24. Furthermore, referring to Quayle et al [Ref. 65], a faired landing gear sees a drag reduction of approximately 30%. According to in-house SMEs, an integrated assembly would not be quite as aerodynamic as a faired gear, so the estimated drag reduction was estimated to be 25%.



Figure 5-26. Landing Gear Fairing

$$\Delta C_{D_{Gear}} = -0.25C_{D_{Gear}} \quad \text{Eqn. 6}$$

Landing gear component integration was modeled in FLOPS as a drag reduction specific to the landing gear in the aerodynamics module, at no cost to weight for either the main and nose landing gear. In MIDAS, landing gear component integration was modeled as a landing gear part count reduction.

5.3.3.3 Landing Gear Fairings – Landing gear assembly fairings are designed to streamline the landing gear assembly during landing and takeoff of the aircraft (Figure 5-26). Vortex shedding due to the bluff body nature of both the nose and main landing gear is a major contributor to high amplitude airframe noise. Fairings are a passive method by which to present a more aerodynamic surface to the oncoming flow during low altitude operations, at which distances to observers are minimal. Fairings can be applied to any landing gear as long as geometric constraints allow for them. However, they will add extra weight and possibly volume to the system. Furthermore, they must be designed to deploy

simultaneously with the landing gear assembly, adding complexity to the overall system. Reduced drag during landing associated with the addition of fairings is typically undesirable to pilots, as landing gear drag aids in slowing down the aircraft. However, in light of the potential acoustic benefits, this has not been taken into consideration. Failure of a landing gear assembly fairing could cause damage in many ways. The possibility of it detaching from the aircraft during takeoff and landing would pose a threat to neighborhoods surrounding airports. For an aircraft, the landing gear assembly that loses its fairing would generate high noise and drag. Furthermore, the loss of the fairing would result in asymmetric drag loading on the landing gear. At most directivity angles, Dobrzynski et al experimentally found a broadband noise reduction of approximately 2.7 dB [Ref. 66]. A landing gear drag reduction study predicts approximately 30% reduction in landing gear drag due to the addition of fairings [Ref. 65]. Weight penalties are estimates based on landing gear size.

$$\Delta C_{D_{Gear}} = -0.3C_{D_{Gear}} \quad \text{Eqn. 7}$$

$$\Delta W_{Gear} = 0.2W_{Gear} \quad \text{Eqn. 8}$$

Landing gear fairings were modeled in FLOPS as a landing gear drag reduction and a weight increase. The landing gear drag coefficient in FLOPS was corrected to reflect the aerodynamic effects of fairings in a manner similar to the modeling of landing gear component integration. To be conservative, landing gear fairings were modeled in MIDAS as a broadband reduction of 2 dB from the source sound pressure level (SPL) of the landing gear at all directivity angles. Landing gear fairing technology is well-established, at a current TRL of 8, but is not prevalent in modern commercial aircraft. However, the extreme nature of the N+3 acoustic goal is expected to revitalize interest in this technology, and drive it towards designs more widely accepted in the industry.

5.3.3.4 Distributed Exhaust Nozzle (DEN) and Flap – The distributed exhaust nozzle concept involves the transition from a typically round exhaust nozzle to a nozzle with a large array of smaller holes through which the engine exhaust may flow. These smaller holes are generally rectangular or triangular. Because the exhaust area becomes restricted (even if it matches that of a baseline round nozzle), there is a thrust penalty associated with distributed exhaust nozzles. However, the noise reduction potential is significant. Exhausting through small holes instead of a large area creates smaller jets with a higher wave-number peak in the turbulence spectra, shifting the far-field noise to higher frequencies where it can be attenuated by the atmosphere to a greater extent [Ref. 67]. This technology could possibly be retrofitted to an existing exhaust nozzle, but in practical applications it would replace an existing nozzle. It would need to be designed to the same temperature constraints as existing nozzles, though there may be additional pressure requirements because of the flow restrictions imposed by the porous exhaust surface. Creating a nozzle from an array of small holes leads to the potential of clogging or the melting closed off some of the exhaust ports. If this were to happen, the overall thrust would diminish, but there is also a high degree of redundancy in the system with so many holes in the nozzle. If the structure between a series of holes were to rupture, the flow through the nozzle would tend towards this larger opening (possibly causing an even larger rupture), and there would be a source noise increase associated with this larger flow. In Gaeta et al [Ref. 67], a 10% reduction in thrust is reported due to DEN, based on computational results. A 4-8 dB reduction in far field noise is achieved at subsonic jet velocities, with an increase in high frequency noise due to the shifting of the peak frequency. Extrapolating this concept to a flap system, engine exhaust flow is diverted through ducting to the trailing edges of the wings. This flow is then distributed evenly across the wing span, and blown over the trailing edge flap system and resulting in increased circulation and lift.

The DEN flap was modeled in FLOPS as an increase in lift coefficient during takeoff and landing, as well as a thrust penalty across the entire flight envelope. The increase in lift coefficient is a function of the deflection angle of the flap and the percentage of the span that experiences blowing as seen in Eqn. 10. The thrust penalty is also modeled as a function of flap deflection angle, as seen in Eqn. 9.

$$T_{factor} = \cos \delta - 0.15 \quad \text{Eqn. 9}$$

$$\Delta C_L = \frac{\delta}{15} \frac{b_{blown}}{b} \quad \text{Eqn. 10}$$

$$\Delta W_{engine} = 0.18 W_{engine} \quad \text{Eqn. 11}$$

$$\Delta C_{D,0} = .001 \quad \text{Eqn. 12}$$

where δ is the flap deflection, b_{blown} in the percentage of the span over which the nozzle exhausts, and b is the total span.

The engine weight parameter in the FLOPS weights module was corrected to accurately reflect the increase in engine weight as a result of installing DEN flaps. There is a drag penalty associated with the technology that was applied in the aerodynamics module across the entire mission. DEN was modeled in MIDAS as a reduction in sound pressure level for all frequencies associated with jet noise and flap sources. Currently estimated at TRL 2, this technology should mature quickly due to the similarity of its subsystems to those of circulation control technology.

5.3.3.5 Boundary Layer Ingesting Inlet – Boundary layer ingesting (BLI) inlets are a propulsive concept that could lead to an increase in propulsive efficiency. The engines are partially embedded while still having a portion of the propulsion system protruding into the flow near the vehicle surface. This allows for the ingestion of a segment of the boundary layer that has formed along the vehicle [Ref. 68]. Engine exhaust normally produces an increased region of velocity aft of the vehicle, while low-momentum boundary layers produce a decreased region of velocity aft of the vehicle, leading to a nonuniform velocity profile in the wake. Nonuniform velocity profiles aft of the vehicle lead to a decrease in propulsive efficiency [Ref. 107]. Ingestion of this low-momentum flow allows for the production of a more uniform velocity profile aft of the vehicle and a reduction in ram drag, which improves propulsive efficiency, as illustrated in Figure 5-27. However, due to the embedded inlet and inlet placement in the boundary layer, inlet distortion is increased compared to podded engine configurations. Inlet distortion decreases pressure recovery, which consequently decreases propulsive efficiency. To measure the effectiveness of this technology, reduction in drag and increased inlet distortion were modeled in terms of aerodynamic and propulsion, with no consideration given to packaging and integration. Results from Rodriguez were scaled for a two-engine configuration and used for analysis [Ref. 69]. BLI inlets on the hybrid wing-body were approximated to reduce vehicle zero-lift drag 2.2% and pressure recovery 2.9%.

$$\Delta C_{D,0} = -0.022 C_{D,0} \quad \text{Eqn. 14}$$

$$\Delta p_r = -0.029 p_r \quad \text{Eqn. 13}$$

where p_r represents pressure recovery. A percentage decrease in inlet pressure recovery decreases engine thrust by approximately the same percentage. BLI inlets were modeled in FLOPS as a drag reduction in the aerodynamics module. This module in FLOPS contains lift-induced drag and zero-lift drag coefficient parameters. The zero-lift drag coefficient parameter was corrected to reflect the reduction in drag for two engines. Due to the increase in inlet distortion from BLI inlets, a thrust penalty was applied to the entire engine table prior to being input into FLOPS. For commercial applications, BLI inlets are estimated to be at TRL 2. However, the technology is expected to mature quickly due to the groundwork laid by its application in military vehicles.

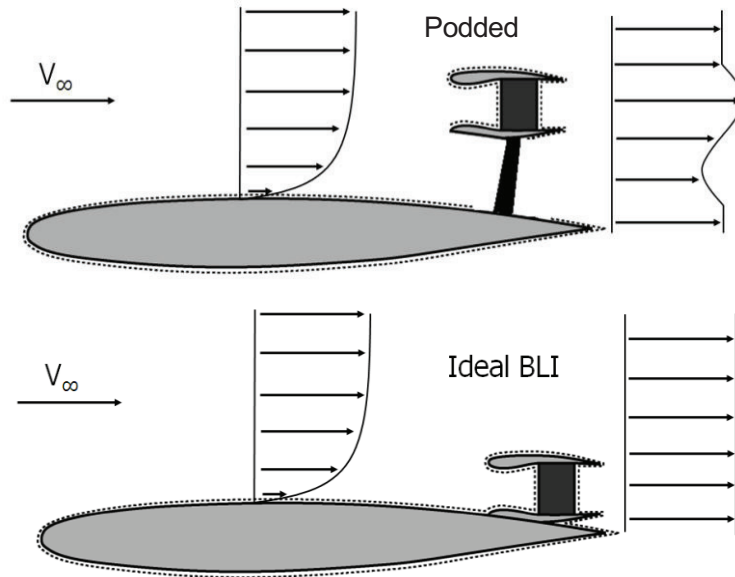


Figure 5-27. Aft Velocity Profile for Ideal BLI and Podded Propulsion Configurations

5.3.3.6 Two Degree-of-Freedom Liner – Two degree-of-freedom (DOF) liners are built upon the current state-of-the-art single DOF acoustic liners for reducing tonal fan noise. Double DOF liners contain two layers of absorbing material and additional perforated sheets separating them from the other layers. Similar to single DOF liners, two DOF liners can have their absorbing sections divided up into smaller cells designed to target specific tonal frequencies. Two DOF liners allow attenuation to target two different tonal frequencies. A tradeoff exists between the absorption capacity of the liner and the drag that is generated by the porous face sheet. Additionally, the weight and volume penalties associated with acoustic liners increase as the degrees of freedom increase. Based on analysis, it was found that a two DOF inlet liner provided superior noise reduction and overall system performance compared to a single DOF liner and multi-DOF liners. Two DOF acoustic liners are currently estimated to be TRL 8, and this technology was determined to be the best solution for inlet fan noise suppression. Analysis and results of the liner design study are described in Section 6.1.2.

5.3.3.7 Deployable Vortex Generators – Deployable vortex generators (VG) are used to increase the lift of an aerodynamic surface while minimizing the drag penalty. They consist of small ramps of various geometries that are typically scaled to the size of the boundary layer. By generating vortices in the flow, the boundary layer stays energized and separation is subsequently delayed [Ref. 70]. In this manner, higher lift capabilities exist and reduced noise is achieved. Vortex generators can be applied to slats, flaps, or wing surfaces, and may be either active or passive. In a passive system, they must be affixed to the aerodynamic surface, penetrate through the aircraft skin, or be built into the airframe itself. An active system will involve a deployment capability of the vortex generators, leading to weight penalties, but no additional drag penalties at cruise conditions. Failure of this technology could involve either the detachment of a vortex generator from the wing surface, or the failure of the deployment mechanism. If a vortex generator were to become detached from the wing surface or the deployment failed, the designed acoustic and aerodynamic benefits would not be achieved, and airframe noise would be increased. If the vortex generator actuator were to fail in the deployed state, drag penalties would be incurred at all flight conditions. It must be noted that the specific application of this technology in this study targets noise associated with slats. Estimated sound pressure level reductions were taken from Kuo and Sarigul-Klijn describing a retractable VG system and its influence on noise [Ref. 71]. Although VGs and microtabs are technically different, they are equivalent from an acoustic and aerodynamic standpoint. In terms of weight estimates, piezo-compliant linear actuators by Flexsys, Inc. exist on the order of 20 grams per actuator (preliminary description can be found in Osborn et al [Ref. 72] with subsequent specifications of the constructed system on the Flexsys website [Ref. 73]), and have been used in the construction of deployable vortex generator models. An efficient VG array will have approximately nine VG's per 2 feet

of wing span, so assuming a conservative 40 grams per actuator to accommodate wiring and installation, a formal relationship between wingspan and weight penalty can be developed:

$$\Delta W_{wing} = \lambda b W_{VG} \quad \text{Eqn. 15}$$

where b is the wingspan over which the vortex generators are applied, λ is their linear density along the wing, and W_{VG} is the weight of a single vortex generator with allowances for installation effects. Deployable vortex generators were modeled in the FLOPS weights module by increasing the wing weight parameter to reflect an increase in weight due to their installation. Vortex generators were modeled in MIDAS as a narrowband reduction in sound pressure levels in the range of 1-3 kHz to target slat noise sources. Furthermore, higher frequency noise penalties were assessed to account for the shifting of noise to these frequencies. Estimated at TRL 5, this technology is fully expected to mature in time for 2030-2035 EIS commercial transport aircraft.

5.3.3.8 M5 Ultrahigh-Performance Fiber – M5 ultrahigh-performance fiber is a high-strength, low-density polymer fiber, prepared from monomers by the addition of an extremely hydrophilic and acidic compound to align the monomers and fuse them through chemical bonds along the length of the fibers [Ref. 74]. The fibers undergo hydrogen bonding, a process absent in previous composites. This bonding between the fibers and graphenic planes allows for a significant increase in strength. In addition, M5 fiber exhibits impressive thermal and flame resistances. M5 could be substituted for many, if not all, composite applications on most current aircraft, such as the Boeing 787, serving as a replacement for the commonly-used carbon fiber-reinforced plastic. M5 can be integrated into the fuselage structure, main wing, both vertical and horizontal tail sections, and nacelle. M5 fiber would allow for larger integrated structures, thus reducing part count and further reducing structural weight. Limitations of application include leading edges of the wing, tails, and nacelles, which historically use metallic materials, as these surfaces often encounter debris. Weight reduction estimates, based on the report by Cunniff et al, suggest that current M5 fiber technology exhibits a strength of 3.96 GPa, a failure strain of 1.4%, and a modulus of 271 GPa [Ref. 74]. Conservative estimates of the properties that can be achieved with M5 fiber in the near future are a strength of 8.5 GPa, a failure strain of 2.5%, and a modulus of 300 GPa. According to Cunniff, the ultimate goals are 9.5 GPa, 2.5%, and 450 GPa, respectively. The density of M5 fiber is 1.7g/cm^3 . For reference purposes, the strength, modulus of elasticity, and density of carbon fiber-reinforced plastic are 3.0 GPa, 220 GPa, and $1.71\text{-}1.72\text{ g/cm}^3$, respectively. The significantly improved structural properties stemming from the use of M5 fiber, in addition to its relatively low density, would result in potentially large weight reductions. The percentage of vehicle structure that could be replaced by M5 fiber is equivalent to that of a state-of-the-art aircraft, whose airframes are approximately 50% composite by weight [Ref. 84].

$$\Delta W_i = -0.22W_i \quad \text{Eqn. 16}$$

where W_i corresponds to component structural weight, with i representing the components to which this structural benefit can be applied: wing, tail, fuselage, and nacelle structures. If this technology is used in combination with advanced metallics, described in Section 5.3.3.13, the relative contribution of this technology to structural weight reduction must be decreased. M5 ultrahigh-performance fiber was not modeled explicitly in MIDAS, as it is strictly an airframe weight reduction technology. Currently estimated at TRL 3, this technology is predicted to mature sufficiently for use in the development of commercial transports entering service in the 2030-2035 timeframe.

5.3.3.9 Integrated Aeroservoelastic Structures – Aeroservoelasticity uses directional stiffness in the aircraft structural design to control aeroelastic deformation in such a fashion as to affect the aerodynamic, control, and structural performance in a beneficial way [Ref. 75]. Performance characteristics are a function of many parameters, including weight, aerodynamics, flight mechanics, dynamics, and structures. All of these categories should influence wing design from an early conceptual stage in the design process. Multidisciplinary design optimization (MDO) methods can be used to design a wing for specific loads, flight conditions and performance, improving design efficiency. MDO and aeroservoelastic structures use structural deformation of lifting surfaces to achieve performance objectives not associated with structural design and find the most favorable design point that satisfies structural, weight, aerodynamic, performance, and control constraints. MDO allows the wing of an aircraft to experience significant weight reduction as a result of the structure being designed to specific conditions and restrictions through gust/flutter/maneuver load control. Since aerodynamics is factored into the conceptual design process, aerodynamic loads are better distributed, resulting in a decrease in drag. Loads on control surfaces can be decreased, resulting in reduced power requirements, and hence actuation system weight [Ref. 76,77]. Based on internal research, and data from Wakayama and Kroo, flight control system, wing, and tail weight reductions were estimated as a function of their respective aspect ratios as shown in Figure 5-28 [Ref. 77]. The aspect ratios of the horizontal tail, vertical tail, and wing were used to compute the respective weight reduction from aeroservoelastic structures. Higher aspect ratio surfaces exhibited greater deflection than lower aspect ratio surfaces, allowing for increased aeroservoelastic tailoring, and thus greater weight reduction.

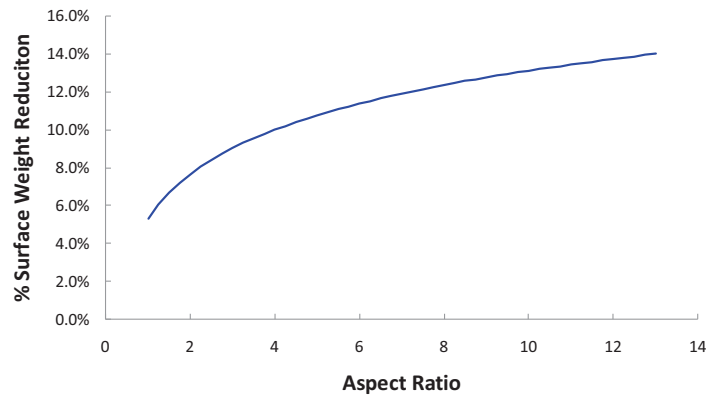


Figure 5-28. Surface Weight Reduction Through Aeroservoelastic Structures as a Function of Aspect Ratio

$$\Delta W_i = -f_i(AR)W_i \quad \text{Eqn. 17}$$

$$\Delta W_{SurfaceControls} = -0.09W_{SurfaceControls} \quad \text{Eqn. 18}$$

where f_i corresponds to the weight reduction multiplication factor as a function of the respective aspect ratio and W_i corresponds to component structural weight, with i representing the components to which this structural and subsystem benefit can be applied: wing, horizontal tail, and vertical. Aeroservoelastic structures were modeled in FLOPS as a weight reduction in these particular parts of the aircraft, but were not modeled explicitly in MIDAS, since the technology is primarily an airframe weight reduction technology. However, aeroservoelastic design could potentially reduce control surface size, thereby affecting control surface noise. Noise from high-lift systems, landing gear, and engines are much more dominant than the noise produced by control surfaces, and so no effort was made to model this effect.

5.3.3.10 Affordable Airframe Large Integrated Structures – Affordable airframe large integrated structures allow for a unitized structure methodology yielding specifically tailored structures for given loads and load paths. This leads to an increase in structural efficiency, reductions in manufacturing processes, time, and cost, as well as a drastic reduction in part count. This technology eliminates structural discontinuities and fastened assemblies, while increasing structural efficiency [Ref. 78]. Large integrated structures use new design capabilities and manufacturing options, coupled with advancements in metallic alloys, composites, and composite joint technology, to achieve a new level of design flexibility in unitized structures [Ref. 79]. Developments in materials reduce cost and weight, while new design methods further reduce structural weight. Affordable large integrated structures would replace current

primary and secondary vehicle structures in order to create more unitized structures, and offer a weight benefit:

$$\Delta W_i = -0.05W_i \quad \text{Eqn. 19}$$

where W_i corresponds to component structural weight, with i representing the components to which this structural and subsystem benefit can be applied: wing, tail, fuselage, and nacelle structures, in addition to the fuel and plumbing subsystem. Affordable large integrated structures were modeled in the FLOPS weights module as an airframe weight reduction. Large integrated structures were not modeled explicitly in MIDAS.

5.3.3.11 3-D Woven/Stitched Composites – 3-D woven/stitched composites facilitate larger, integrated structures by replacing traditionally metallic joints on highly-loaded primary structures. Composite pi-joints, as depicted in the diagram of Figure 5-29, allow for the creation of highly-loaded joints without large and heavy metallic fasteners. This is possible due to the joint providing a large surface area for bonding a substructure to the structure skin. This joint technology allows for complex preforms to be connected and fused with one other, reducing part count and allowing for complex structures to be designed and integrated into the vehicle.

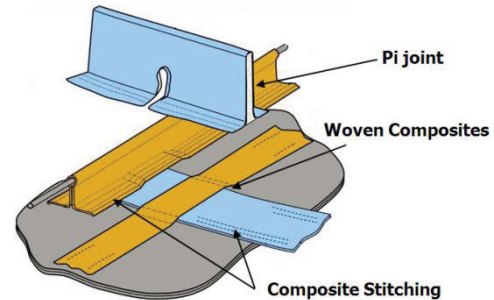


Figure 5-29. 3-D Woven/Stitched Composite Structural Concept [Ref. 80]

Three-D stitching exploits the orthotropic properties of carbon fiber and limits out-of-plane failure modes through stitching. This allows for failure arrest design in the structure. All of the materials in stitched and woven assemblies are dry. This eliminates out-time and autoclave requirements, which are normally found in prepreg systems and limit component size. These composite joints would replace all of the metallic joints in structural applications, including, but not limited to, skin/stiffened fuselage panels and window belts, fuselage circumferential frames, and fuselage keel beam frames. On wing structures, this technology can be utilized in joints on the upper and lower cover panels, stiffeners and spar caps, intercostal clips, and main landing gear attachments. According to Velicki and Thrash, this technology has been integrated into the C-17, including fairings, gear doors, and integral fuselage [Ref. 80]. Based on research and testing performed by Sheahen and Bersuch [Ref. 81] and internal research, weight reduction from replacement of metal joints with 3-D woven and stitched composites was estimated to be 2.62%. This reduction was applied to the wing, tail, fuselage, and nacelle structural weights:

$$\Delta W_i = -0.0262W_i \quad \text{Eqn. 20}$$

where W_i corresponds to component structural weight. Currently estimated to be TRL 3, a roadmap has been established for this technology to be sufficiently mature to drive the design of aircraft entering service in the 2030-2035 timeframe.

5.3.3.12 Inverted Flow Nozzle – In order to invert the bypass and core engine streams, a flow crossover duct is embedded between the engine nozzle and turbine. By properly shaping the velocity profile exiting the engine, a significant degree of noise attenuation can be achieved. Specifically, placing the high-speed, high-temperature primary flow on the outside and forcing the low-speed, cooler fan flow to the inside, generates two mixing interfaces for the core stream [Ref. 82]. Since more mixing is available, noise generation is reduced. Furthermore, noise generated at the internal mixing interface is less likely to propagate. This technology would need to be incorporated into the original design of an engine. The crossover duct would add significant weight to the engine system, at a small performance cost. Failure of the technology would involve either the failure of the structure of the crossover duct, or melting due to the high temperature jet engine environment. In either case, there would be a risk of further damage to the engine, and the creation of a blockage in the aft portion of the engine.

Experimental wind tunnel measurements of a flow inverter nozzle have been conducted at the NASA Ames 40 by 80 foot tunnel, shown in Figure 5-30 [Ref. 83]. The inverter tested was approximately 36 inches long, embedded inside a 123.5 inches JT8D engine. The inverter was 29.1% of the total engine length. Although it added weight, it did not add length, as it was embedded inside the engine.

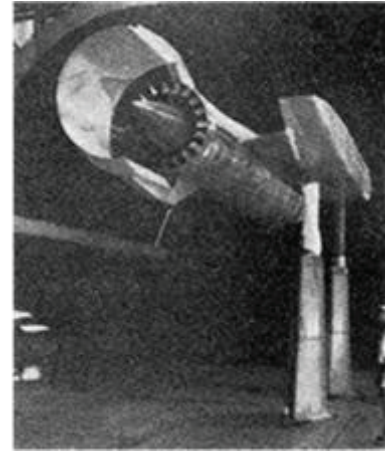


Figure 5-30. NASA ARC Inverted Flow Model With 20-Lobe Mixer [Ref. 83]

A good first-order approximation is to add 29.1% to the weight of the engine. This is to account for the increased volume occupied inside the engine, since the inverter spans the entire engine cross section. This work also showed how the overall sound pressure level (OASPL) in the vicinity of the engine was affected by the flow inverter nozzle, and gave estimates of the associated thrust penalty.

$$\Delta W_{engine} = 0.29 W_{engine} \quad \text{Eqn. 21}$$

$$\Delta T = 0.985 T \quad \text{Eqn. 22}$$

The inverted flow nozzle was modeled in the FLOPS weight module as an increase in engine weight as a result of installing a crossover duct into the propulsion system. The weight module contains a miscellaneous propulsion weight parameter that is a percentage of the engine weight. This parameter was set to a value to accurately simulate the increase in engine weight from this technology. In addition, a thrust penalty was applied to the engine deck prior to being input into FLOPS. The technology was modeled in MIDAS as a sound pressure level reduction over different frequencies for jet noise source, shown in Figure 5-31.

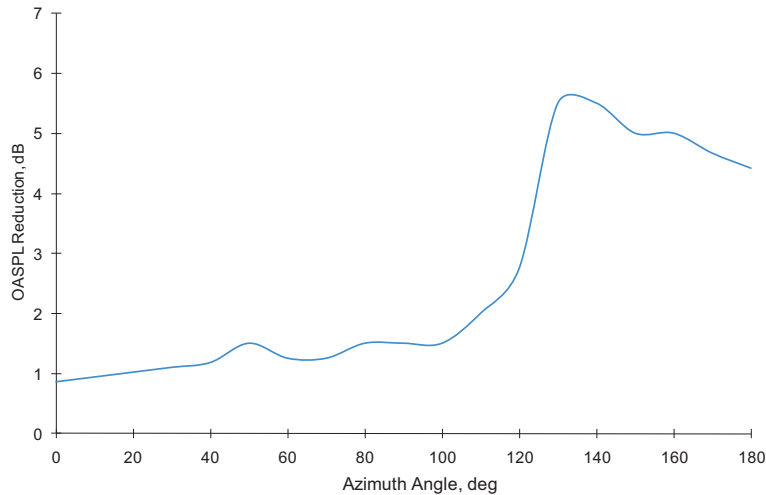


Figure 5-31. Inverted Flow Nozzle Noise Reduction

5.3.3.13 Advanced Metallic Structural and Subsystem Alloys – New alloys are in high demand for structural applications that can withstand elevated temperatures and improve strength-to-weight ratio. Advanced metallic alloys could exhibit improved fatigue and crack growth properties. These alloys would be used for primary and secondary structural components, as well as subsystem components. The increased high-temperature performance of aluminum and titanium alloys also represents significant weight saving potential for engines and engine mounts. It was assumed that 45% of the weight of the N+3 vehicle is metallic weight, similar to the Boeing-787 [Ref. 84]. Internal research has shown that advanced metallic alloys offer up to double-digit weight reductions in terms of the percentage of structural weight, depending on their application:

$$\Delta W_i = -0.1W_i \tag{Eqn. 23}$$

$$\Delta W_{LandingGear} = -0.1W_{LandingGear} \tag{Eqn. 24}$$

where W_i corresponds to component structural weight, with i representing the components to which this structural benefit can be applied: wing, tail, fuselage, and nacelle structures. If this technology is used in combination with M5 ultrahigh-performance fiber, described in Section 5.3.3.8, its maximum relative contribution to structural weight reduction must be decreased in Equations 14 and 15. Advanced metallics were modeled in the FLOPS weights module as an airframe weight reduction. Advanced metallics were not modeled in MIDAS, as it is strictly an airframe weight reduction technology.

5.3.3.14 Carbon Nanotube Electrical Cables – Carbon nanotubes (CNTs) are manufactured, in either sheet or thread form, by injecting fuel and reaction gas into a floating catalyst suspended in a furnace. The CNT sheets and threads, which are woven together to form a braid, are extremely lightweight, strong, and exhibit electrical conductivity comparable to that of copper wire. A CNT sheet can be integrated into a coaxial electrical cable as the replacement for the traditionally copper mesh that lies between the outside and inside insulation. CNT woven fiber can be integrated into the coaxial electrical cable as the replacement for the traditionally copper wire. Internal research and testing has shown significant weight reduction from replacing the copper mesh alone. Replacement of the wire would lead to a further increase in weight reduction.

$$\Delta W_{Electrical} = -0.4W_{Electrical} \tag{Eqn. 25}$$

CNT electrical cables were modeled in FLOPS weights module as a subsystem weight reduction. The electrical subsystem parameter was reduced in the weights module in FLOPS to reflect the weight reduction from CNT electrical cables throughout the vehicle. CNT electrical cables were not modeled in MIDAS, as it is a subsystem weight reduction technology.

5.3.3.15 Modeling for Inlet Optimization – MDO tools and analysis allow for optimum engine configuration and propulsive efficiency, while reducing drag in certain body configurations. While podded engines on tube-and-wing configurations achieve nearly perfect inlet pressure recovery, hybrid wing-body configurations offer potential for further optimization, as their engines are mounted on the lifting surface fuselage. According to Rodriguez, MDO analysis for engine configurations on hybrid wing-bodies can result in decreased zero-lift drag. However, due to engine configuration changes from MDO analysis, inlet distortion may increase. Inlet distortion decreases pressure recovery, and thus propulsive efficiency. To reflect the effect of this technology, system-level drag reduction and increased inlet distortion were modeled. Results from Rodriguez were scaled for a two-engine configuration and used for analysis [Ref. 69].

$$\Delta C_{D,0} = -0.0503C_{D,0} \quad \text{Eqn. 26}$$

$$\Delta p_r = -0.003p_r \quad \text{Eqn. 27}$$

where p_r represents pressure recovery. A percentage decrease in inlet pressure recovery decreases engine thrust by approximately the same percentage. The aerodynamics module in FLOPS contains induced drag and zero-lift drag coefficient parameters. The zero-lift drag coefficient parameter was corrected to reflect the drag reduction for each of the two engines. Due to the predicted increase in inlet distortion, a thrust penalty was applied to the entire model. Inlet optimization was not taken into account for wing-mounted podded engines due to their sufficiently high level of pressure recovery and inlet efficiency. Robust inlet optimization modeling is becoming established as a method by which to maximize pressure recovery, and thus propulsive efficiency.

5.3.3.16 Steady Circulation Control – Circulation control technology extracts engine bleed for jet-blowing over a round trailing edge surface to increase lift. A blown sheet of air remains attached to the round circulation control (CC) surface, acting as a boundary layer control at low blowing flow rates. At higher blowing rates, the blown jet stays attached at the round CC trailing edge, moving the stagnation point of the airfoil and its corresponding streamline to the lower surface of the airfoil [Ref. 85]. Circulation control technology increases the lift of an airfoil without the need for flaps and other mechanical high-lift systems. This high-lift capability enables shorter takeoff and landing distances, as well as steeper climb angles. Drag and downstream wakes may also be affected by the implementation of steady circulation control as opposed to mechanical high-lift devices. Elimination of mechanical high-lift systems reduces the complexity and weight of the wing structure, however this is compensated by the ducting required to disperse the engine bleed flow the wing trailing edge.

$$\Delta C_l = C_{l,\max} \frac{b_{\text{blown}}}{b} \quad \text{Eqn. 28}$$

Steady circulation control was modeled in the FLOPS aerodynamic module as an increase in takeoff and landing maximum lift coefficients. The improvement in lift coefficient is given in Equation 28, where b_{blown} is the span length over which blowing occurs, and b is the total span of the vehicle. To simulate the weight of the engine ducting that would need to be installed, the engine weight parameter in the FLOPS weights module was increased appropriately. The engine data table was penalized for thrust to account for engine bleed. A drag increase was not included, assuming that an acceptable trailing edge geometry (whether active morphing or an innovative integral design) would be implemented.

5.3.3.17 Engine Shielding – This concept advocates either embedding propulsive components of the aircraft into the airframe itself, or locating them above the wings, fuselage, and tails to impede the propagation of acoustic waves. This is a well-proven method for reducing aircraft noise, especially at higher frequencies, that has found its way into the design of many aircraft [Ref. 86]. Fan shielding alone can be accomplished by placing the engine on the top part of the fuselage near the aft section of the aircraft, while extensive shielding is achieved by embedding the entire engine into the airframe. Utilization of shielding methods must be considered extremely early in the design phase of an aircraft.

Based on work from Goodmanson and Gratzner, engine shielding from mounting the nacelles over the wing can affect noise significantly, reducing EPNL by approximately 5 dB [Ref. 87].

The aerodynamic effects of locating the engine in a position to promote shielding were modeled in FLOPS through engine placement. FLOPS allows for the placement of the engines on either the wings or aft fuselage. Configuration changes, including tail geometry, were appropriately designed and modeled in FLOPS per engine mounting configuration. MIDAS contains routines that enable estimates of noise shielding based on the geometry of the aircraft and engine location.

5.3.3.18 Engine Technologies

1. Ceramic Matrix Composite Turbine Blades

Due to their potential for high temperature tolerance, ceramic matrix composite (CMC) turbine blades have become increasingly attractive. Their implementation could ease requirements for turbine blade cooling, and allow combustors to burn at higher temperatures. CMC turbine blades are also estimated to weigh less than their metallic alloy counterparts, contributing to an overall engine weight reduction. According to LaChapelle et al [Ref. 88], the use of CMC could increase the temperature range of these components between 200-400°R. However, driving the combustor to higher temperatures must be balanced against higher emissions levels. At a TRL of 3, it has been projected that this technology will have sufficient time to mature before the N+3 timeframe. CMC turbine blades have been assumed for all advanced engines under examination in this study.

2. Lean Staged Combustor

Staged combustors incorporate multiple distinct combustion zones serviced by independent fuel injection systems. These fuel injectors are separated axially in space, and can be optimized at different positions along the length of the combustor. Depending on the engine power setting, different combinations and power levels of combustor stages can be used. In addition, the burner can be optimized to run lean for multiple flight conditions, giving better control over NO_x production at all flight conditions [Ref. 89]. This is especially significant at the low power settings during which a significant portion of LTO NO_x is formed. This feature also delivers the capability to reduce velocities in the near-injector region, reducing acoustic instabilities and improving lean blowout and ignition characteristics.

While the improvements in LTO NO_x can be dramatic for this technology, this benefit must be weighed against the added complexity of the fuel system and the associated weight and volume penalties that accompany it.

3. Intercooled Compressor Stages

This technology involves using a heat exchanger to reduce the temperature of the compressed flow between compressor stages. Since it requires less work to compress the lower temperature gas that exits the heat exchanger, thermal efficiency gains can be realized. A significant benefit can be achieved with reductions in temperature on the order of 40°R. Theoretically, intercooling could be implemented between every compressor stage to achieve maximum benefit; however, spatial and weight considerations must be made for the heat exchangers. While this technology is currently estimated to be at TRL 3 for aircraft applications, it has in fact been implemented on ground-based engines. For example, the LMS100 ground-based gas turbine engine generates over 100 MW at a thermal efficiency of 46%, in part due to the presence of an intercooler between its LP and HP compressors [Ref. 90]. This technology has been implemented in the engines under investigation in this study, with intercooler placed between the axial and centrifugal stages on the HP spool. Flow losses were under 5%, with upwards of 50% exchanger effectiveness by employing endothermic fuel as the heat sink. It was found that implementing the technology led to a reduced overall engine weight (including intercools) due to the downstream flowpath and component sizing reductions.

4. Swept Fan Outlet Guide Vanes

Introducing sweep into the design of the fan outlet guide vanes has the potential to decrease pressure losses, while simultaneously reducing fan tip noise. This is achieved through delaying the impact of the

turbulent wake of the fan rotor onto the leading edges of the outer guide vanes. According to work by Schulten, reductions in sound pressure level on the order of 8 dB are possible through vane sweep [Ref. 91]. This technology was integrated into the common design of all advanced turbofan engines.

5. Fan Blade Sweep Design

Fan blades are swept in the engine to reduce noise and improve engine efficiency. Fan blades operate in a transonic environment with the root normally subsonic and the tip supersonic, due to rotational velocity. Above relative Mach numbers of 0.8, shock waves begin to form along the tips of the fan blades, increasing both noise and shock losses, reducing fan efficiency. Sweeping the fan blades results in a reduction of the velocity component normal to the shock surface, weakening shocks and the losses associated with their interactions. According to Thomson et al [Ref. 92], forward-swept fan blades may provide greater fan efficiency than backward-swept blades by creating a more favorable boundary layer. However, forward-swept fan blades are more unstable, as the flow would amplify any vibrations that might occur. Conversely, backward-swept blades would dampen vibrations. In addition to poor stability, forward-swept fan blades are subject to higher stresses than backward-swept fan blades. In a report by Neubert et al, sweeping the fan blades reduced tip Mach number from 1.588 to 0.8, yielding a shock-free fan blade and a 1.5% increase in adiabatic fan efficiency [Ref. 93]. Noise levels produced by the fan are estimated to be proportional to fan tip speed to the fifth power, which indicates that swept fan blades could reduce fan noise significantly. This design feature is assumed in the performance of the advanced turbofan engine models.

6. Lightweight Fan Structure and Cowl

Through optimization of the front structure of the engine, front-end integration was improved through the use of a lightweight fan structures and cowl. This configuration features a greatly shortened fan casing which allows for reduction in nacelle length, and thus weight and wetted area, improving aerodynamic performance. Highly integrated components lead to engine performance improvements and significant weight reduction, including mounting the accessory gear box closer to the core. The lightweight fan structure and cowl incorporates a lifted intake and outlet guide vane sweep which further increase engine performance and reduce engine noise, drag, and weight. This technology has been assumed in the front-end of the advanced turbofan engines.

7. Compressor Flow Control

Extracting diffuser bleed flow, and injecting it into the compressor face in order to mitigate flow distortion, may minimize the likelihood of stall or surge. On top of controlling flow distortion, it can also be used to dampen flow instabilities that are associated with stall or rotating surge. However, this type of flow control requires the use of sensors and controllers to measure, detect, and control instabilities. These sensors measure pressure disturbances that occur prior to flow separation, and energize the flow upstream. This prevents flow separation from occurring and can increase compressor efficiency. Compressor flow control could increase the LPC and HPC polytropic efficiencies by 2% and reduce CO₂ emissions by 3-3.5% compared to current state-of-the-art baseline engines [Ref. 94]. As with any control system, this adds weight and complexity to the system, which must be balanced against the potential benefits in engine performance. With a current TRL of 4, compressor flow control was modeled into the IPC of the candidate engine configurations for this study.

8. Active Compressor Clearance Control

The clearance between compressor rotor blade tips and the shroud can vary during flight, due to thermal expansion effects. Active compressor clearance control provides higher compressor efficiencies by minimizing blade tip losses. This is done by actively maintaining small tip clearances [Ref. 94]. Generally taking the form of variable flexible structures, active clearance control can be maintained by electromagnetic actuators. However, this type of control requires the use of complex capacitance sensors and controllers. This technology is needed to measure, record, and calculate the proper actuator inputs to maintain the desired tip clearances. As reported by Weimer, at maximum rotor speed, the blade is only in the vicinity of the sensor for approximately 6 milliseconds, requiring exceptionally high frequency

sensors [Ref. 95]. This experimental work showed about a 1% increase in compressor efficiency imparted by active clearance control. Not only does this control system add weight to the engine system, but spatial considerations must also be made for such a system. For the engines under investigation in this study, it has been implemented in not only the HP compressor, but also in the HP turbine.

9. Variable Geometry Nozzles

Variable geometry nozzles use an SMA-actuator to expand and contract nozzle exit area. This capability allows for the control of engine exit conditions, mainly for affecting jet velocity. This allows for a trade between engine noise and performance at each power setting and throughout the flight profile. This technology is seen on many modern military aircraft to accommodate variable flight conditions and performance requirements. Commercial vehicles would use this technology to optimize cruise fuel efficiency, as well as reduce noise during takeoff and landing. During takeoff and landing, the engine would operate at a designated mass flow rate with a large nozzle exit area and decreased jet velocity, reducing noise. This would adversely affect fuel efficiency, but for a very short period in the flight profile. When the vehicle reaches cutback altitude where noise is not a concern, the nozzles adjust to improve propulsive efficiency for improved fuel burn. The benefit of this technology on propulsive efficiency decreases with increasing bypass ratio. Shape memory alloys could allow up to 20% nozzle area variability, with a possible 10% increase in nozzle weight. Variable nozzle geometry could also reduce CO₂ emissions by up to 8.3% [Ref. 94].

Jet source noise in MIDAS is calculated using exhaust flow properties at discrete points along the aircraft trajectory.

6 AIR VEHICLE DESIGN STUDY

Figure 6-1 details the process followed in the synthesis of the air vehicle design which eventually led to the selection of the preferred vehicle concept. Airframe configurations were integrated with technology packages to form advanced vehicle configurations. These configurations were influenced by trade studies on engine mounting location, M_{DD} and sweep, and laminar flow integration. The resulting configurations were modeled and analyzed in FLOPS and MIDAS to quantify field length, mission fuel requirements, noise characteristics, and emissions performance. A trade study was performed to select an objective function for the optimizer that resulted in feasible wing geometry, while still yielding maximum reduction in fuel burn prior to detailed vehicle analysis. Additional trade studies were performed to analyze landing and takeoff operations, and their respective effects on noise. With input from these trade studies, emissions, field length, mission fuel, and noise were used, in conjunction with the scenario weighting factors described in Section 4.1.2 and mission requirements, to calculate the SER for each vehicle. Vehicle characteristics were compared to both historical trends and other N+3 configurations. SER values were tabulated and sorted, and the vehicle with the highest SER was selected as the preferred N+3 concept.

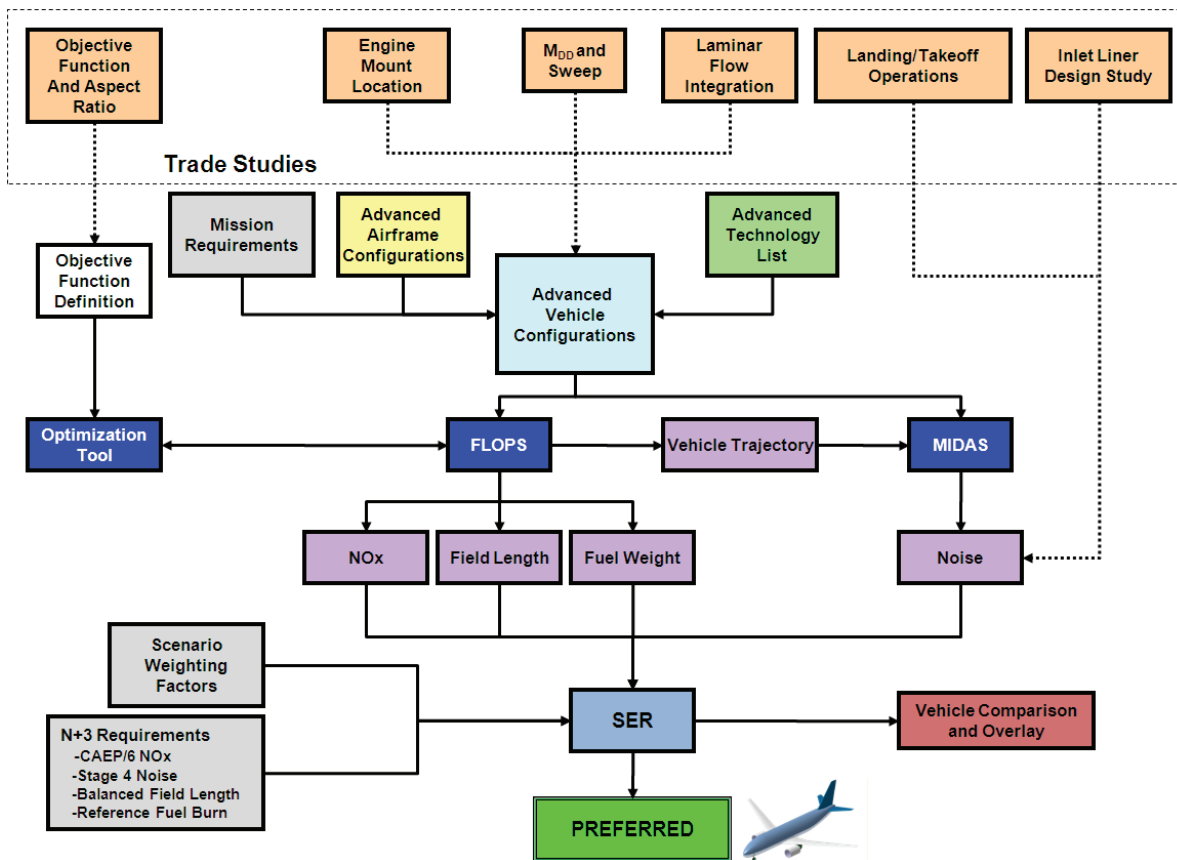


Figure 6-1. Aircraft Vehicle Design Study Overview

6.1 Sizing and Performance Analysis

6.1.1 Objective Function Effect on Aspect Ratio Sizing

As described in Section 3.2, an objective function was needed to drive the design of configurations in the optimization process. Optimizing purely for mission fuel resulted in configurations with unattainably high aspect ratios, whereas optimizing for gross weight resulted in lower weight vehicles. Assuming that empty weight is a surrogate for vehicle cost, the issue becomes one of trading cost for fuel efficiency. An objective function was chosen as a weighted combination of both mission fuel and gross weight. This yielded aspect ratios that drove down induced drag, but still accounted for the empty weight of the vehicle.

6.1.2 Advanced Liner Design

A study was conducted into the potential of advanced inlet and fan duct liners to aid in the reduction of noise towards the N+3 goal levels. Using the methods previously described in Section 3.6, advanced inlet and fan duct liners developed for the International Aero Engines V2533-A5 were compared to current state-of-the-art liners. Knowledge gained from this study was used to estimate the acoustic benefits of implementing these liner designs into the N+3 configurations. Additional studies examined the possible weight penalties that would be associated with various liner types, and the impact on attenuation as a function of liner length.

The baseline inlet liner was designed, and sound pressure reduction computed, using an eigenvalue expansion algorithm for the duct acoustic equation, combined with reference V2533 sound pressure levels at power levels corresponding to 0, 1,000, and 5,000 ft altitudes. The baseline inlet liner design was a 2 DOF liner with a length of 15 inches and a septum inserted to about 1/6 of the core depth. Considerations were given to penalties associated with hard walls and splices associated with the manufacturing process. The advanced inlet liner took into consideration improved manufacturing processes that would eliminate these splices, combined with advanced materials which exhibit better absorptive properties. Due to projected advances in installation capabilities, the advanced liner is also capable of extending farther into the inlet, stretching up to 28 inches long. As a function of frequency, both baseline and advanced liner attenuations remained essentially independent of power setting. Their attenuations of the OASPL relative to a hard-walled inlet are shown in Table 6-1.

Table 6-1. Baseline and Advanced Inlet Liner Overall Sound Pressure Levels Reduction

Power Setting Altitude, ft	Δ OASPL, dB		
	Hard Wall	Baseline	Advanced
0	---	-3.8	-6.9
1000	---	-3.3	-5.7
5000	---	-3.3	-5.8

A similar study explored liner design for fan duct applications, on both the inner and outer annulus of the duct. The baseline and advanced fan duct liners were both designed to a length of 50 inches, while the advanced liner was designed to achieve attenuation over a more broad range of frequencies. For the low altitude power setting, the attenuation of the liner as a function of frequency is shown in Figure 6-2. It can be seen that while the baseline liner achieves a higher peak attenuation, its SPL attenuation exceeds 8 dB only in the approximate range 1400 Hz – 4500 Hz. On the other hand, the advanced liner achieves this level of SPL attenuation over a broader range, 800 Hz – 5500 Hz.

A summary of the OASPL reduction generated by the baseline and advanced fan duct liners relative to the hard wall case are shown in Table 6-2. Again, the reduction has been shown to be largely insensitive to power setting.

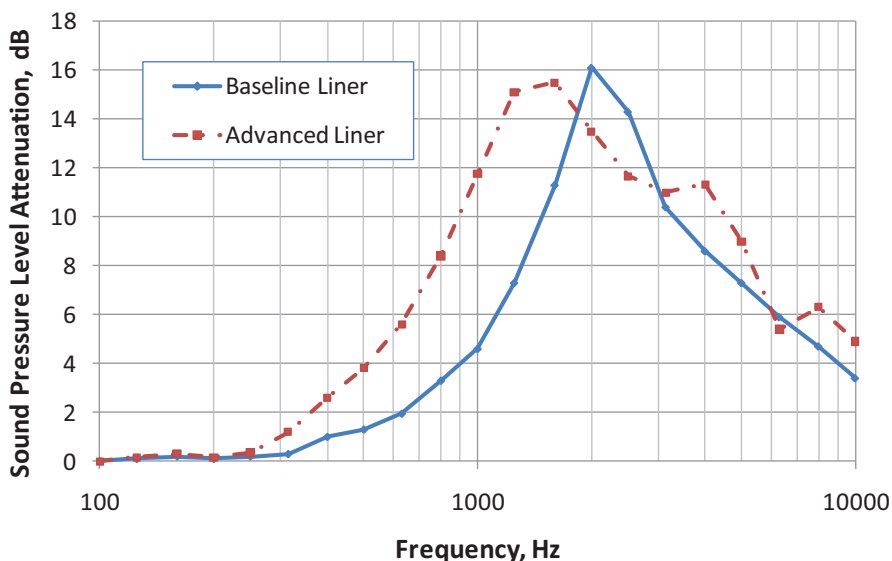


Figure 6-2. Baseline and Advanced Fan Duct Liner Sound Pressure Level Reduction

A brief study of the weight impact of the liners showed that the baseline and advanced inlet liners would increase the weight of the engine by 0.33% and 0.48%, respectively. The increased weight of the advanced inlet liner relative to the baseline liner is due largely to the increased length of the advanced liner. Assessing the weight impact of the fan duct liners, it was found that the baseline and advanced liners total up to 0.28% and 0.49%, respectively. Since the two liners have the same overall length, the weight difference stems from the additional thickness in the core of the advanced liner designed to target lower frequency ranges.

Table 6-2. Baseline and Advanced Fan Duct Liner Overall Sound Pressure Level Reduction

Power Setting Altitude, ft	Δ OASPL, dB		
	Hard Wall	Baseline	Advanced
0	---	-5.2	-6.8
1000	---	-4.3	-5.7
5000	---	-4.3	-5.8

Additional work focused on examining the effect of liner length on OASPL reduction for both the inlet and fan duct liners. The major conclusion drawn from this work was that increasing liner length results in a more dramatic reduction in the overall sound pressure level. However, it is noted that this increased length must be balanced against the increasing weight impact on the engine. Table 6-3 summarizes the OASPL reductions found in both the fan duct and inlet liners as a function of length, compared to the hard wall case.

Table 6-3. Impact of Liner Length On Overall Sound Pressure Level Reduction

Inlet		Fan Duct	
Length, in	Δ OASPL, dB	Length, in	Δ OASPL, dB
15	-5.4	50	-5.6
20	-6.3	60	-6.0
28	-7.6	70	-6.3
30	-7.8	80	-6.7
35	-8.4	90	-7.0
40	-8.9	100	-7.2
45	-9.3		
50	-9.7		

When more in-depth analysis is warranted, advanced studies can examine configurations in which the impedance of the liner varies along the length of the inlet or fan duct to target spatially-varying acoustic sources.

6.1.3 Analysis of Engine Mounting Configurations

6.1.3.1 Engine Mounting Configurations for Tube-and-Wing – The tube-and-wing configuration allows placement of the engines on the wing or the aft fuselage. Wing-mounting the engine is common for traditional aircraft of similar size and range. Appropriate tail geometry and volume

coefficients were chosen for this configuration. To model fuselage-mounting accurately on the tube-and-wing, a T-tail configuration was implemented in order to place the horizontal tail out of the engine exhaust. As a result, the taper ratio of the vertical tail was increased, while the root chord was held constant. This increase in volume and weight was needed to structurally support the raised horizontal tail. Engine placements and tail geometries were input into FLOPS to simulate the different engine mounting configurations. In addition to the resized tail weight, FLOPS internally computed a weight change for the wing and fuselage associated with the different engine mounting configurations.

A trade study was conducted to quantify the performance and weight change associated with each engine mounting configuration. To accurately quantify this effect, a baseline tube-and-wing was used. In addition, both mounting configurations were analyzed with the addition of laminar flow. This would determine if the tail weight penalty associated with aft-mounting the engines could be overcome by its laminar flow benefits.

The three-shaft turbofan was analyzed for four different design and technology combinations. As seen in Figure 6-3(b), wing-mounting affects the potential laminar flow region by creating a turbulent wake aft of the pylon. In this study, the size of the turbulent wedge is conservatively estimated based on nacelle diameter as opposed to pylon size. Aft-mounting the engines would allow for a greater extent of laminar flow on the wing, Figure 6-3(a). Depending on configuration, the removal of the engine could result in approximately an 8-10% increase in laminar flow on the wing.

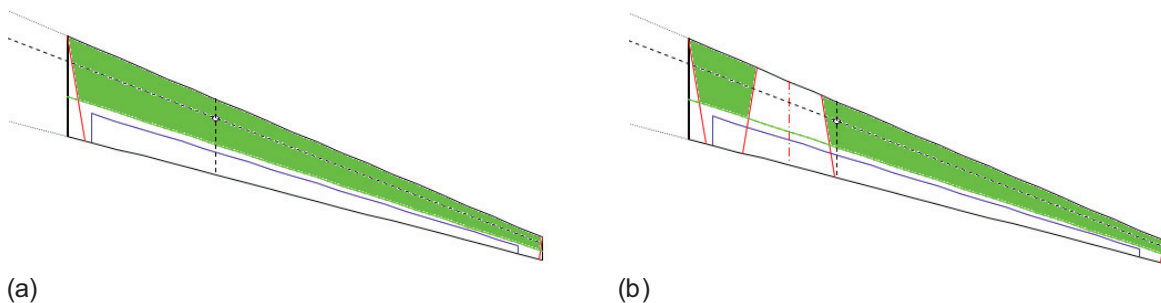


Figure 6-3. Wing Laminar Flow Extent for (a) Aft Fuselage Mounting, (b) Under-Wing Mounting

As illustrated in Figure 6-4, given the tube-and-wing body with the three-shaft turbofan configuration, wing-mounting the engine resulted in the lowest fuel burned between configurations with no laminar flow, with a 50.9% reduction in mission fuel from the reference vehicle. Fuselage-mounting the three-shaft turbofan resulted in a 46.4% reduction in mission fuel from the reference vehicle. This difference in fuel is a direct result of the increased weight and drag associated with fuselage-mounting the engines. As discussed in Section 5.2.1, a T-tail configuration is necessary to move the horizontal tail out of the engine exhaust and subsequently increases the empennage structural weight and wetted area, leading to an increase in drag.

When laminar flow is applied to both mounting configurations, wing-mounting is still preferred, and shows a 53.3% decrease in mission fuel compared to the reference vehicle whereas fuselage mounting shows a 51.4% reduction. As mentioned above, the increased T-tail weight and drag of the fuselage-mounted configuration results in a less fuel-efficient vehicle. Although this is offset somewhat by a greater extent of laminar flow on the wing, the net effect is that the wing-mounted configuration shows a 1.9% fuel burn reduction improvement over the fuselage mounted configuration.

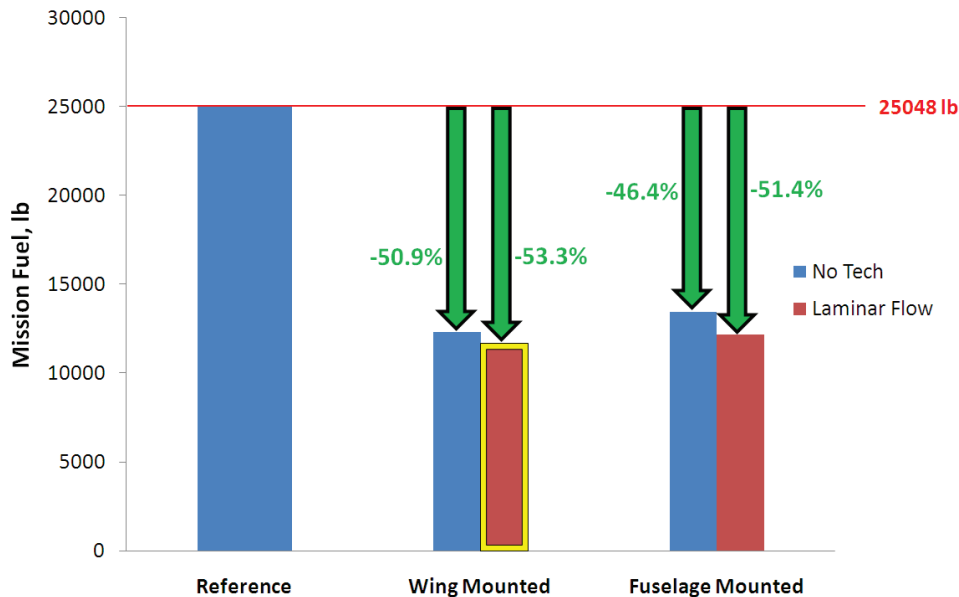


Figure 6-4. Effect of Three-Shaft Turbofan Mounting Location on Tube and Wing Mission Fuel Burn With and Without Laminar Flow

The open rotor was analyzed for three different configurations, as seen in Figure 6-5. However, the laminar flow field differs between the open rotor and three-shaft turbofan configurations. Specifically, laminar flow over the wing was assumed to be absent from the open rotor configuration. This is due to increased vibration in the wing and the disturbance of free stream air caused by the presence of rotors. Aft-mounting the engines, however, would allow for laminar flow on the wing, as seen in Figure 6-3(a).

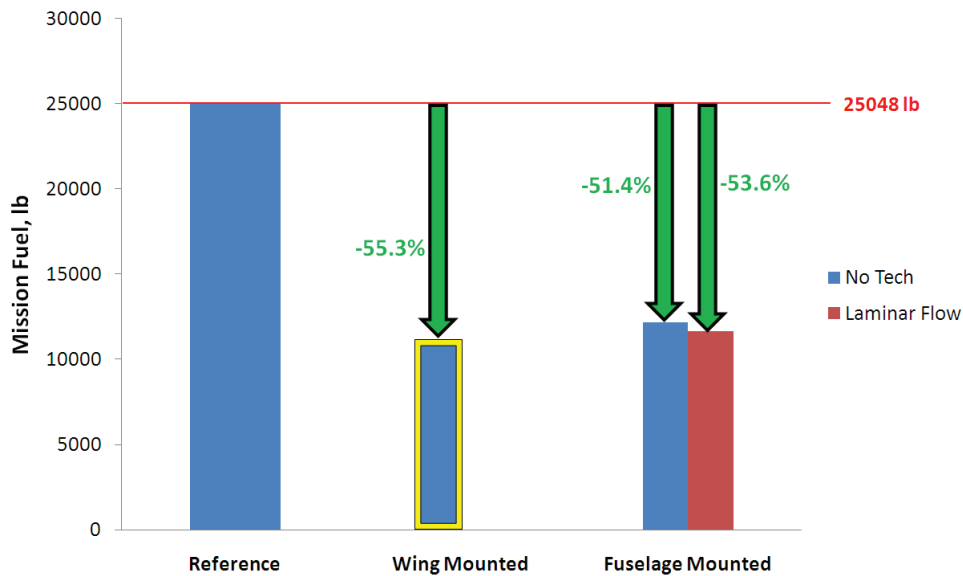


Figure 6-5. Effect of Open Rotor Mounting Location on Tube and Wing Mission Fuel Burn With and Without Laminar Flow

A trade study was performed to quantify the fuel burn and weight change associated with changing the engine mounting location. These mounting configurations were compared to the baseline tube-and-wing without laminar flow technology. In addition, analysis was performed to determine how much, if at all, full laminar flow over the wing offset the added structural weight associated with the aft-mounted configuration.

As illustrated in Figure 6-5, given the tube-and-wing body with an open rotor, wing-mounting the engine results in the lowest fuel burn in the absence of laminar flow, reducing the fuel over the reference

vehicle 55.3%. Fuselage mounting the open rotor configuration in the absence of laminar flow resulted in a 51.4% fuel reduction compared to the reference vehicle. This slightly higher fuel burn reduction is a result of the increase in wetted area, drag, and weight associated with fuselage mounting the engines.

Laminar flow was applied to the fuselage mounted configuration to see if the benefits associated with laminar flow would overcome the penalties associated with fuselage mounting. This configuration led to a 53.6% reduction in fuel burn compared to the reference. Though the fuel burn is further reduced with the addition laminar flow, the wing mounting configuration still resulted in the largest fuel burn reduction. However, wing mounting the open rotor leads to significant complications.

Due to the large rotor diameter, mounting the open rotor under the wing, which is common on tube-and-wing vehicles, would result in a rotor-tip ground clearance problem. Over-wing mounting would eliminate this problem, as engine is mounted on a pylon above the wing, increasing the distance between the ground and rotor tip. Additional benefits of over the wing mounting the engine would include a significant reduction in noise from noise shielding as mentioned earlier in Section 5.3.3.17 [Ref. 87]. However, cabin noise would increase significantly [Ref. 96]. Apart from an increase in cabin noise, mounting the engines above the wing would add complexity to servicing during engine maintenance and replacement. Structural complications would also arise, including unfavorable flutter characteristics [Ref. 97] and the need to mount the engine at a significant location above and aft on the wing in order to minimize detrimental aerodynamic interference [Ref. 98]. Though wing mounting the open rotor resulted in less fuel burn in this study, the complications associated with wing mounting this engine were seen to outweigh the improved fuel burn reduction and this configuration was not further investigated.

6.1.3.2 Engine Mounting Configurations for Hybrid Wing Body – Because under-wing engine mounting is not practical with the hybrid wing-body, only a fuselage-mounted configuration was explored. The centerbody allowed for easy engine placement without having to reconfigure any aspect of the vehicle. There is no tail weight or size increase due to the HWB being a tailless vehicle. Additionally, fuselage-mounting provided improved noise shielding benefits over wing-mounting. Fuselage-mounting was determined to be the preferred configuration for both the open rotor and three-shaft turbofan engines. The centerbody of the HWB was assumed to have no laminar flow, due to the increased leading edge sweep angle and thickness-to-chord ratio. As a result, there were no trade studies performed between laminar flow and engine mounting.

6.1.4 Laminar Flow Integration

It was found that swept-wing laminar flow had a detrimental impact on the fuel burn of the HWB, whereas this technology led to a significant fuel burn improvement for the tube and wing vehicles. This is a result of the loss in takeoff and landing maximum lift coefficients associated with swept-wing laminar flow technology. Integrating laminar flow requires the removal of any upstream surface discontinuities that would otherwise trip the flow and create a zone of turbulence aft of this point. To ensure that this does not happen, the leading edge slat system needed to be removed. As a result of the leading edge slat removal, the lift generated by this high lift device was removed as well, penalizing the landing and takeoff maximum lift coefficients. Maximum lift coefficient is additionally penalized for using an airfoil more conducive to laminar flow. Wing area must be increased, with a subsequent penalty in empty weight, to meet the field length constraint with a reduced maximal lift coefficient. Consequently, the fuel required to carry out the mission will increase. Even with turbulent flow, a hybrid wing-body aircraft achieves a much lower maximum lift coefficient for takeoff and landing than a conventional tube-and-wing aircraft. Therefore, the lift penalties associated with laminar flow are much more significant on a HWB than with the tube-and-wing configuration, as seen in Table 6-4. Mitigating these laminar flow penalties could result in reduced fuel burn for both configurations. Figure 6-6 illustrates that applying laminar flow to the hybrid wing-body with lift coefficient penalties results in a 13.55% increase in fuel burned. If the penalty associated with slat removal is mitigated through the use of wing morphing technology, steady leading edge blowing, or other forms of active or passive control, fuel burn is only increased by 4.32% from the reference configuration. Mitigating both laminar flow maximum lift

coefficient penalties actually results in a 6.8% improvement in the fuel burn of the hybrid wing-body compared to a fully-turbulent wing. Conversely, laminar flow yielded mission fuel reductions when integrated on the tube-and-wing vehicle while accounting for maximum lift coefficient penalties. As such, mitigating the laminar flow lift penalties on the tube-and-wing vehicle would lead to an increased fuel burn reduction.

Table 6-4. Maximum Lift Coefficient Comparison With and Without Laminar Flow Penalties

		Tube and Wing	Hybrid Wing Body
Takeoff	Initial Max CL	2.68	1
	Final Max CL	2.232	0.72
	% CL Reduction	16.72%	28.00%
Landing	Initial Max CL	3.24	1
	Final Max CL	2.736	0.72
	% CL Reduction	15.56%	28.00%

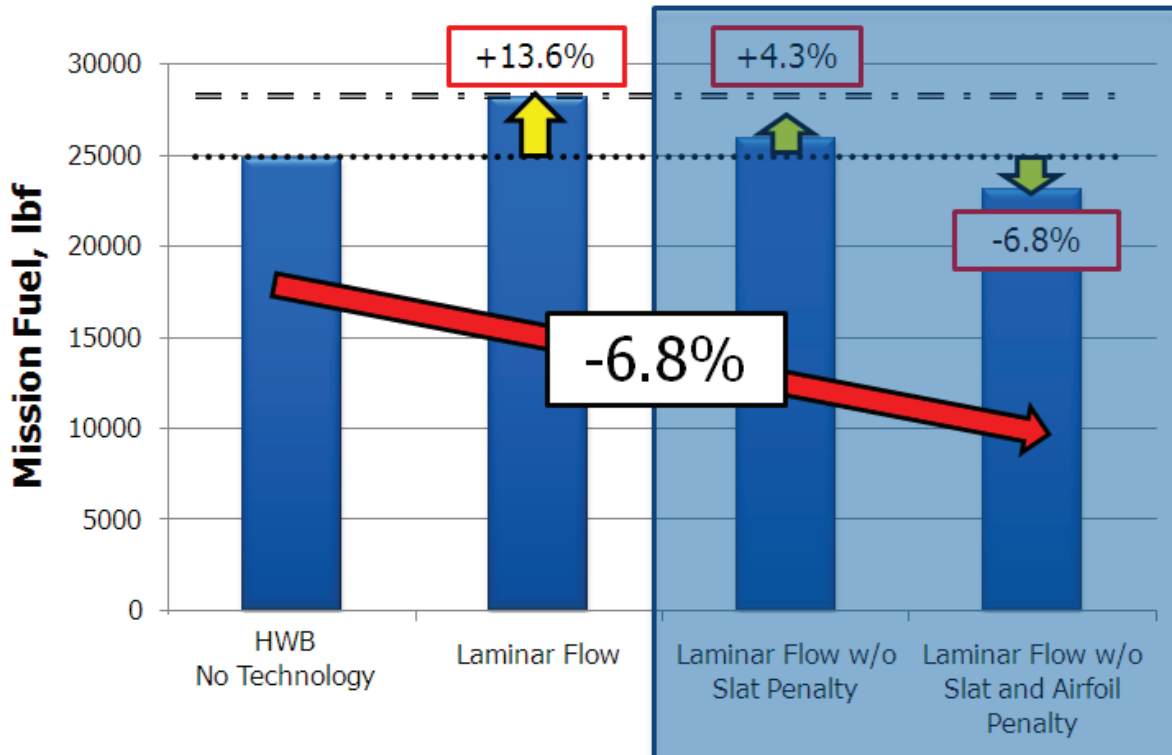


Figure 6-6. HWB With Laminar Flow Fuel Burn, Laminar Flow Penalty Mitigation Effects

6.1.5 M_{DD} and Sweep Analysis

Drag divergence Mach number studies were performed for initial sizing purposes. A range of values for aspect ratio, sweep, lift coefficient, and weight were used to provide M_{DD} sensitivities to wing sweep, thickness-to-chord ratios, and wing technology. Drag divergence Mach number calculations utilized the Korn Equation with 3-D effects and a defined range of parameters [Ref. 99]. Thickness-to-chord ratio was varied between 0.10 and 0.14, sweep was varied between 10 and 45 degrees, and lift coefficient was varied from 0.20 and 0.65. Both conventional and modern airfoils were examined. Conventional airfoils were comparable to the reference vehicle. Modern airfoil technology improves the drag divergence Mach number for constant sweep.

A drag divergence Mach number for the tube and wing configuration was chosen to be 0.85. The selection of a drag divergence Mach number at this value allowed for the minimum cruise Mach number constraint of 0.75, discussed Section 4.2.3, to easily be met. A drag divergence Mach number of 0.85 enables Mach 0.8 cruise capabilities. Through additional configuration and aerodynamic analysis, a thickness-to-chord ratio of 0.12 was decided upon. This ratio was in-line with historical values for tube-and-wing vehicles with similar size and passenger count. Interpolating the carpet plot illustrated in

Figure 6-7 yields a minimum sweep of 19.5 degrees when designing for a drag divergence Mach number of 0.85 and a thickness-to-chord ratio of 0.12. Further sweep definition was attained through refinement of the cruise lift coefficient for values consistent with historical values with similar vehicles.

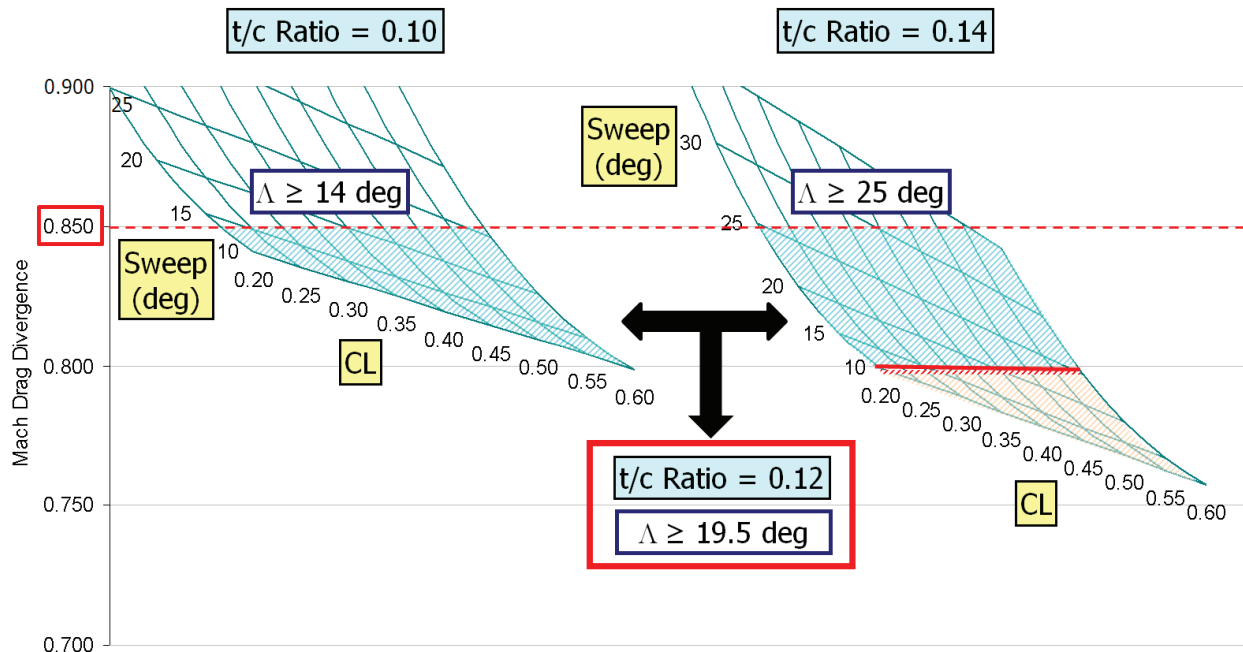


Figure 6-7. Initial Sizing Tube-and-Wing M_{DD} Sensitivity Study

The same drag divergence Mach number was chosen for HWB as the tube and wing configuration at 0.85 which would allow for Mach 0.8 cruise capabilities. Through additional configuration and aerodynamic analysis, a thickness-to-chord ratio of 0.12 was decided upon which is historically similar to NGC all wing vehicles. Figure 6-8 shows that for a M_{DD} of 0.85 and the given range of lift coefficients, the minimum allowable sweep was 25 degrees. A wing sweep was chosen to be 40 degrees which allowed for improved balance and increased stability and control. Figure 6-8 illustrates that a wing sweep of 40 degrees is more than sufficient for a drag divergence Mach number of 0.85.

6.1.6 Landing and Takeoff Operations

Detailed trajectories below 10,000 feet altitude were developed for each final vehicle configuration for takeoff and climb, as well as descent and landing. Detailed engine cycle characteristics were calculated at each 0.5 second increment and were used for predicting noise source levels for acoustic analysis. These trajectories were developed from 4-D linear interpolations of detailed FLOPS outputs.

Takeoff and climb trajectories were calculated assuming a 100% power level for both engines. Part 36 rules permit commercial aircraft to perform an engine cutback that would enable them to meet the minimum single-engine gradient in the event they lost an engine after the cutback. For descent and

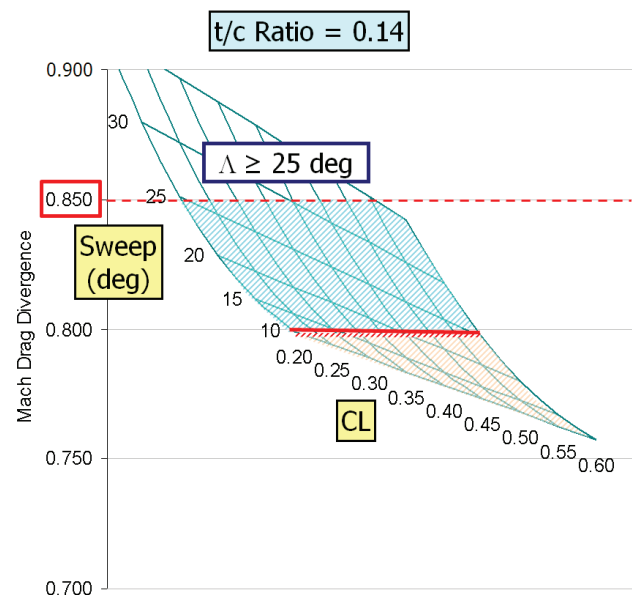


Figure 6-8. Initial Sizing HWB M_{DD} Sensitivity Study

landing, the vehicles initially followed a three degree glide slope in the approach configuration. At the outer marker; landing gear was extended, flaps were set to the landing setting, and thrust was adjusted as required to maintain a three degree descent at Vref + 10 KCAS.

6.2 Analysis of Aircraft Emissions

Nitrous oxide (NOx) emissions were computed for each aircraft and engine combination by examining the production of emissions during a simulated LTO cycle, defined by the International Civil Aviation Organization (ICAO), and described below. It was found that each configuration met the CAEP/6 NOx requirement, and that the advanced engine architectures far surpassed N+3 emissions goals due to their lean combustor technology, high overall pressure ratios, and high bypass capabilities.

6.2.1 CAEP/6 NOx Requirement

The Committee on Aviation Environmental Protection (CAEP) defined their CAEP/6 requirement on aviation emissions to take effect on engines entering service after 31 December 2007. Limiting the production of NOx per kN of SLS thrust, the requirement is a function of both overall pressure ratio and engine rated output at ISA sea-level static conditions.

For engines with OPR < 30, the CAEP/6 requirement is defined by the following equation:

$$D_p / F_\infty = \begin{cases} 16.72 + 1.4080\pi_\infty & , F_\infty > 89.0kN \\ 38.5486 + 1.6823\pi_\infty - 0.2453F_\infty - 0.00308\pi_\infty F_\infty & , 26.7kN < F_\infty < 89.0kN \end{cases} \quad \text{Eqn. 29}$$

Where D_p/F_∞ is the NOx production in grams per kN of thrust, π_∞ is the SLS OPR of the engine, and F_∞ is the SLS rated thrust output. For engines with $30 < \text{OPR} < 82.6$, the following CAEP/6 requirements apply:

$$D_p / F_\infty = \begin{cases} -1.04 + 2.0\pi_\infty & , F_\infty > 89.0kN \\ 46.1600 + 1.4286\pi_\infty - 0.5303F_\infty + 0.00642\pi_\infty F_\infty & , 26.7kN < F_\infty < 89.0kN \end{cases} \quad \text{Eqn. 30}$$

Additional restrictions are in place for $\text{OPR} > 82.6$; however, as none of the configurations considered in this study extend into this range, these restrictions will not be discussed.

Shown graphically in Figure 6-9, the CAEP/6 requirement varies linearly on either side of $\text{OPR} = 30$, with the NOx requirement being less stringent with increasing OPR. In addition, the requirements for the higher thrust class engine are slightly more rigorous than those of the lower thrust-class, lower OPR range.

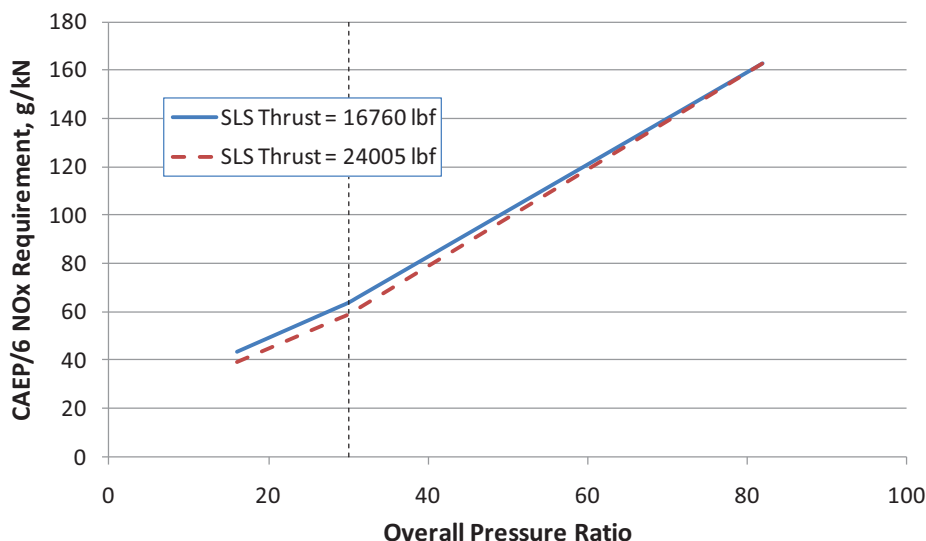


Figure 6-9. CAEP/6 LTO NOx Requirements.

6.2.2 Simulated LTO Cycle

In computing the emissions performance of the configurations in question, the simulated LTO cycle defined by ICAO was used [Ref. 100]. This is a standard sea-level static engine cycle used to consistently quantify the emissions behavior of aircraft engines. Four cycle points are defined in terms of engine power setting, and time duration at each point, to simulate an entire LTO cycle (Table 6-5). The majority of the reference LTO cycle consists of maintaining the engine at a 7% idle condition, while only a small portion of time is used to simulate engine takeoff power. The emissions produced at each of these cycle points are summed for a total NO_x production level, and divided by the rated SLS output of the engine to generate its NO_x production rate.

Table 6-5. ICAO LTO Reference Cycle

	Power Setting Time, min	
Takeoff	100%	0.7
Climb	85%	2.2
Approach	30%	4.0
Idle	7%	26.0

6.2.3 Emissions Results

6.2.3.1 CFM56-3B1 – Emissions indices for the CFM56-3B1 at the LTO cycle points were taken from the ICAO engine emissions certification listed in the ICAO Engine Exhaust Emissions Data Bank [Ref. 101]. This report shows that the turbofan produces 17.7, 15.5, 8.3, and 3.9 g NO_x per kg of fuel burned at the simulated takeoff, climb, approach, and idle conditions, respectively. In addition, the engine certification lists the fuel burn rate at each of these conditions: 0.946, 0.792, 0.290, and 0.114 kg/sec. Using these numbers, combined with the cycle point durations listed in Table 6-5, it is found that the CFM56-3B1 generates 3595 g NO_x during the LTO cycle. Since this engine is rated at 20,000 lbf SLS thrust, its NO_x production is 40.3 g/kN. With this rated thrust, and a SLS OPR of 22.44, the CAEP/6 NO_x requirement for this engine is 48.33 g/kN. It can be seen that this particular engine is already certified below its CAEP/6 NO_x requirement, by 16%. This shows that much progress must be made in combustor technology relative to this design to achieve the N+3 emissions goal.

6.2.3.2 Open Rotor – NO_x emissions index (EI), as a function of engine power setting, was computed for the lean combustor technology common to the open rotor and three-shaft turbofan engine cores based on research and past experience. Through staging of the combustor and the use of direct injection, an overall reduction in the EI at both low and high power settings leads to significant reductions in NO_x production throughout the LTO cycle. In the range of thrust class for which the engine models were developed, fuel flow rate and thrust scale linearly, leading to the conclusion that the NO_x production rate is independent of SLS thrust for each engine configuration. For example, an open rotor exhibiting a SLS thrust of 16760 lbf, with fuel flow rates of 0.331, 0.290, 0.149, and .093 kg/sec at the respective cycle points, leads to a NO_x production of 10.63 g/kN. At SLS conditions, the OPR for this engine is 35.18, giving this particular model a CAEP/6 NO_x emission requirement of 73.72 g/kN. As a result, the engine outperforms the CAEP/6 NO_x requirement by 85.58%, or 10.58% beyond the N+3 emissions goal.

6.2.3.3 Three-Shaft Turbofan – Since the three-shaft turbofan shares a common core with the open rotor architecture, the NO_x emissions indices at the LTO cycle points of interest remain the same as those described in the previous section. However, the fuel flow rates at the cycle points during SLS conditions are different, producing a NO_x emissions level of 9.69 g/kN. At SLS conditions the OPR for this engine is 49.32. With a rated output of 14393 lbf SLS thrust, the engine CAEP/6 NO_x emission requirement is 102.9 g/kN. As a result, the engine outperforms the CAEP/6 NO_x requirement by 90.59%, or 15.59% beyond the N+3 emissions goal. For cases in which the engine is sized to a thrust class below the 89.0 kN inflection point in the CAEP/6 restrictions, the regulation would become less stringent, and the turbofan engine more easily surpass the N+3 emissions goal.

6.3 Analysis of Aircraft Acoustics

6.3.1 FAR Stage 4 Noise Requirement

Limits imposed by the Federal Aviation Regulation (FAR) Part 36, Section 103 on the noise allowable by large transport category airplanes and jet airplanes are described in Appendix B to the rule [Ref. 102]. This regulation, currently broken into Stages 1-4, regulated the noise allowable by aircraft, depending on EIS date. The noise metric used to regulate commercial aircraft is Effective Perceived Noise Level (EPNL). The requirements are defined in terms of three component metrics: community, sideline, and approach exposure levels. Limitations on each of the EPNL components are enforced by the Federal Aviation Administration (FAA), and the values of these restrictions are a function of the number of engines propelling the aircraft and its gross weight. Since all aircraft in the current N+3 study carry two engines, the Stage 4 noise requirements, as a function of gross weight alone, are shown in Figure 6-10. Requirements formally dictate a maximum EPNL for each of the three component metrics, the Stage 3 regulations of which are also plotted in Figure 6-10. To meet Stage 4 requirements, these component metrics must be met individually, as well as having a cumulative margin that exceeds 10 EPNdB below Stage 3. The N+3 goal, however, focuses only on cumulative noise, targeting a 71 EPNdB reduction over the Stage 4 requirement.

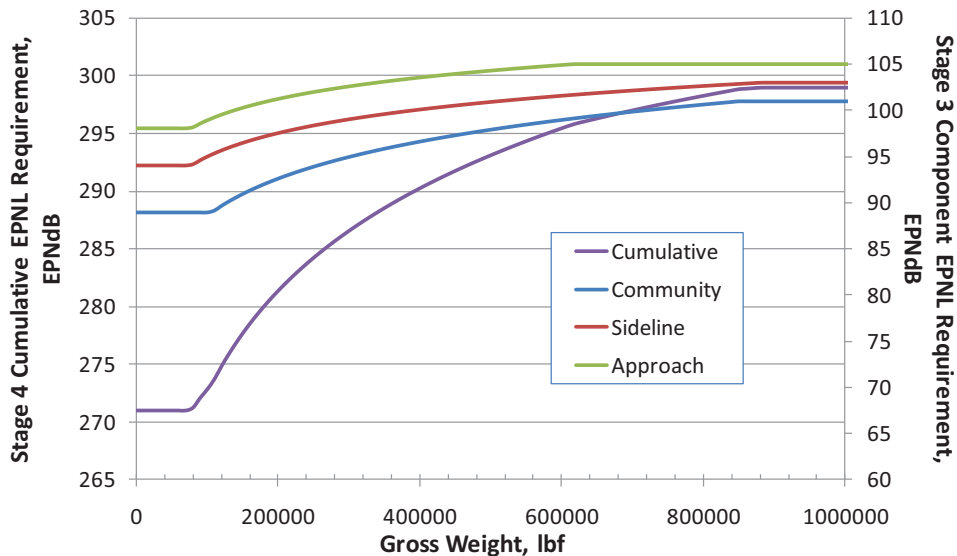


Figure 6-10. FAR Part 36 Stage 4 Cumulative EPNL Noise Requirements

6.3.2 Effective Perceived Noise Level (EPNL) Calculation

As defined by FAR Part 36, Section 101, EPNL is derived from the maximum tone-corrected instantaneous perceived noise levels, documented in Appendix A2 of the standards. Using the tools described in Section 3.7, computations for EPNL are performed for the three conditions described above: community, sideline, and approach. For the approach condition, the measurement is taken during flyover at a point located 1.24 mi up range from the end of the runway. For the community measurement, the flyover noise is monitored at a point 4.04 mi down range from the point of brake release. During the sideline measurement, the noise is recorded at incremental locations 1476 ft on either side of the runway during takeoff. The cumulative EPNL is defined as the linear sum of these three components.

6.3.3 Acoustics Results

The following sections present the acoustic results for the reference, advanced tube-and-wing, and HWB vehicles. Sound pressure level (SPL) calculations of the different acoustic sources per vehicle allowed for the identification of the dominant sources for both takeoff-climb and descent-landing. Open rotor noise sources were unable to be computed given the insufficient and inadequate source models

available to date, so results described in this section correspond to vehicles with either the reference engine or the three-shaft turbofan installed. Jet and fan noise sources were the two most dominant component sources during takeoff and climb trajectories, due to the engines operating at maximum power and these sources being strong functions of thrust. Other acoustic sources (e.g., airframe noise sources) were not analyzed during takeoff and climb, as relative noise contributions from other vehicle components were negligible in comparison to jet and fan noise. Overall sound pressure level maps for the various acoustic sources during takeoff and approach are given in Appendix D. A summary of the acoustic analysis is shown in Table 6-6 and is discussed in further detail in the following subsections.

Table 6-6. FAR Stage 4 EPNL Comparison

Metric (EPNdB)	Reference Vehicle	ATW No Technologies	HWB No Technologies
Community	76.15	61.15	78.59
Sideline	87.15	87.15	101.08
Approach	106.39	103.22	95.27
Cumulative	269.69	251.52	274.94

6.3.3.1 Reference Vehicle – Acoustic analysis of the reference vehicle showed EPNL levels slightly higher than those available from open literature. The community, sideline, and approach EPNL values were 76.15, 87.15, and 106.39 EPNdB, respectively. However, the cumulative EPNL value of 269.69 EPNdB does not account for the inclusion of an inlet acoustic liner, possibly explaining the slightly higher than expected value.

Approach noise is found to be dominated primarily by landing gear noise, with a greater contribution from the main gear. The distinct forward-directed emission pattern of the acoustic signature of the landing gear are shown in Appendix D. The reference vehicle takeoff noise is dominated by both jet and fan noise sources for reasons mentioned in Section 6.3.3.

6.3.3.2 Advanced Tube-and-Wing, Scaled CFM56-3B1, No Technologies – Acoustic analysis was performed for the advanced tube-and-wing configuration with a scaled CFM56-3B1 engine having no advanced technologies applied. Analysis on this vehicle, when compared to the analysis performed on the reference vehicle, allows for noise reduction to be quantified with respect to configuration change and re-sizing. The community, sideline, and approach EPNL for this configuration were 61.15, 87.15, and 103.22 EPNdB respectively. The cumulative EPNL of 251.52 EPNdB does not account for the inclusion of an inlet acoustic liner. The increase in approach EPNL relative to the reference vehicle is a result of the trajectory of the re-sized vehicle. This is a function of the ATW’s geometry and weight. The landing gear noise levels are reduced from those of the reference vehicle as a result of the reduced gross weight of the advanced tube-and-wing. These comparisons can be seen in Appendix D.

The most significant reduction in EPNL came from engine re-sizing. This is evident when comparing the jet and fan noise levels during takeoff and climb. The configuration change and re-sizing from the reference vehicle resulted in an overall reduction of 27.49 EPNdB.

6.3.3.3 Hybrid Wing-Body, Scaled CFM56-3B1, No Technologies – Acoustic analysis was performed for the hybrid wing-body configuration with no advanced technologies and a scaled CFM56-3B1 engine. Analysis on this vehicle, when compared to the analysis performed on the reference vehicle, allows for noise reduction to be quantified with respect to configuration change and re-sizing. The community, sideline, and approach EPNLs were 78.59, 101.08, and 95.27 EPNdB, respectively. The cumulative EPNL of 274.94 EPNdB does not account for the inclusion of an inlet acoustic liner. In addition, due to the exceptionally high fuel burn levels associated with the HWB, it will be shown that any noise benefits achieved through engine shielding would not drastically alter the overall SER for this vehicle relative to the other configurations. For this reason, complex noise shielding effects were not calculated.

Increased gross weight and engine size led to increased far-field noise levels when compared to the ATW vehicle. Noise shielding offers potential noise reduction, but effects would largely be reflected in takeoff and climb noise analysis where engine noise is dominant.

6.4 System Effectiveness Rating Results

6.4.1 Technology Assessments

In order to quantify the benefits of each technology at the system level, their individual effects were quantified with respect to the reference configuration on an SER basis. Using the definitions from Section 3.8, the system effectiveness rating for a reference configuration implementing individual technologies were computed. Because of the complexity of the acoustic calculation, SER_{EPNL} is assumed to be zero for all cases to be discussed below. Figure 6-11 shows the ratings of the individual non-propulsion technologies that were applied to the tube-and-wing vehicle. Sorted by increasing overall SER, the figure shows that M5 ultrahigh-performance fiber had the greatest impact on the overall scenario, followed by advanced metallic structural and subsystem alloys. Though swept-wing laminar flow results in an aircraft that burns less fuel than one using either aeroservoelastic structures or advanced metallics, the higher thrust requirement of the laminar flow aircraft drives a more stringent NO_x requirement. Hence, the weighting of the emissions goal in the overall scenario actually drives the SER of the laminar flow aircraft lower than that of aircraft implementing these structural technologies. SERs pertaining to the Bright, Bold Tomorrow scenario are higher than the others due to the significant weighting of balanced field length, for which all aircraft are given full credit. The aerothermal inverted flow nozzle shows the least benefit, and is ranked below the no technology vehicle, due to the weight it adds to the propulsion system and the negative impact it has on thrust. However, the acoustic benefits of the technology are not reflected in this figure. Table 6-7 shows the SER values computed for each combination of technology and scenario.

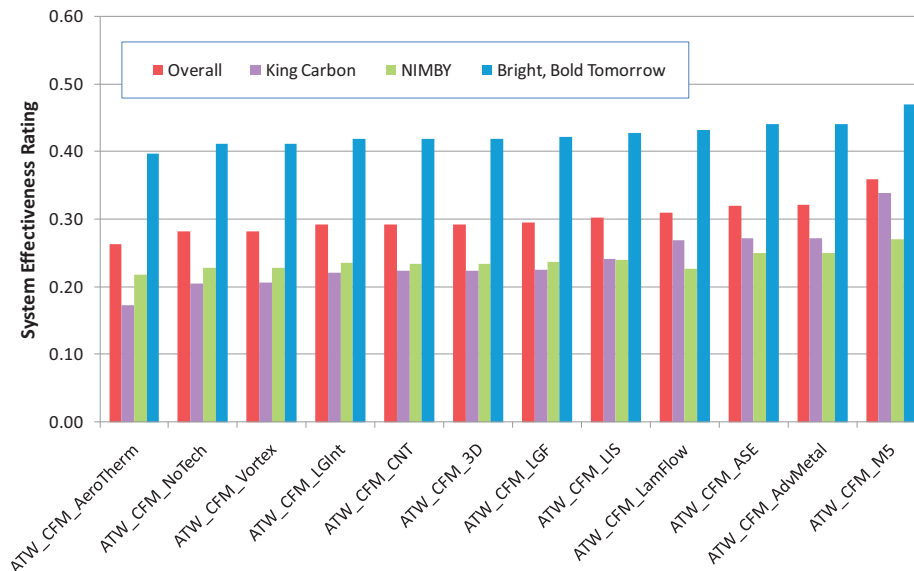


Figure 6-11. ATW Individual Technology Assessment

Table 6-7. ATW Technology SER Assessment, Without Noise

Advanced Tube & Wing				
	Overall	King Carbon	NIMBY	Bright, Bold Tomorrow
Reference	0.0690	0.0724	0.0828	0.0517
ATW_CFM_AeroTherm	0.2624	0.1732	0.2172	0.3968
ATW_CFM_NoTech	0.2812	0.2050	0.2278	0.4109
ATW_CFM_Vortex	0.2820	0.2063	0.2283	0.4115
ATW_CFM_LGInt	0.2919	0.2215	0.2353	0.4189
ATW_CFM_CNT	0.2921	0.2233	0.2339	0.4191
ATW_CFM_3D	0.2926	0.2241	0.2343	0.4195
ATW_CFM_LGF	0.2947	0.2258	0.2373	0.4210
ATW_CFM_LIS	0.3026	0.2408	0.2399	0.4269
ATW_CFM_LamFlow	0.3092	0.2690	0.2267	0.4319
ATW_CFM_ASE	0.3202	0.2711	0.2493	0.4401
ATW_CFM_AdvMetal	0.3207	0.2715	0.2501	0.4405
ATW_CFM_M5	0.3595	0.3381	0.2708	0.4696

Similarly, the non-propulsion-related technology effects have been measured on the SER basis relative to their effect on the HWB configuration. These results are presented in Figure 6-12. The same trends are noticed in these technologies, with the exception that the laminar flow case achieving a high SER assumes that all penalties associated with the integration of laminar flow have been mitigated, through flow control technology (for example, leading edge morphing, steady blowing, etc.). Laminar flow with the integration penalties assumed is ranked lowest among all technologies. In a more broad sense, it can be seen that the SERs calculated for the HWB configurations are notably smaller than the corresponding tube-and-wing cases. This is attributed to the benefits of accessing higher aspect ratio wings in driving toward the N+3 metrics compared to reconfiguring to a hybrid wing-body airframe. Table 6-8 shows the SER values computed for each combination of technology and scenario.

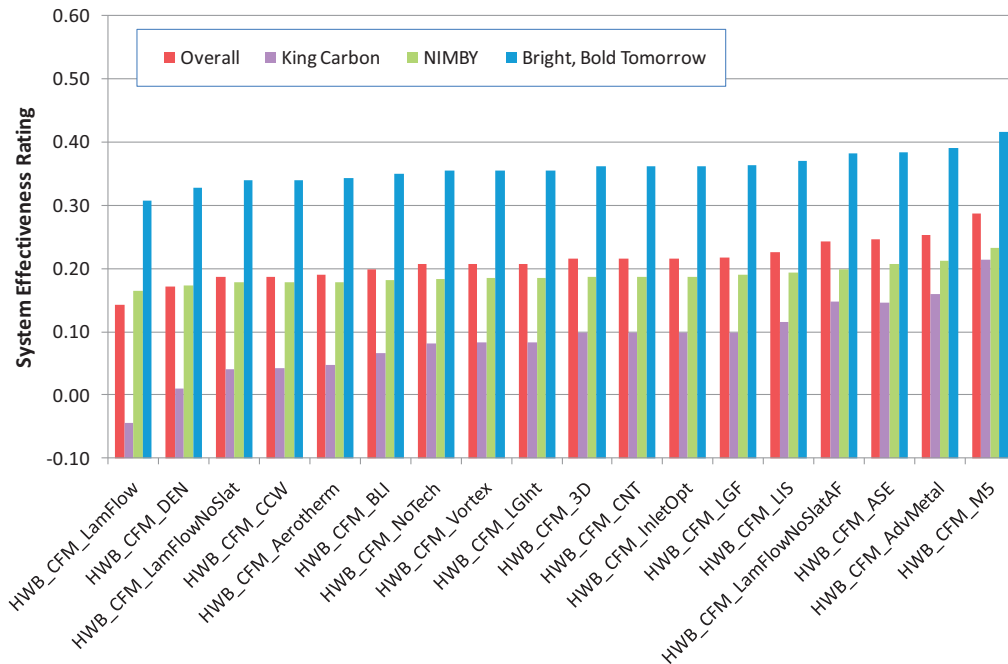


Figure 6-12. HWB Individual Technology Assessment

Table 6-8. HWB Technology SER Assessment, Without Noise

Hybrid Wing-Body				
	Overall	King Carbon	NIMBY	Bright, Bold Tomorrow
Reference	0.0690	0.0724	0.0828	0.0517
HWB_CFM_LamFlow	0.1426	-0.0440	0.1649	0.3069
HWB_CFM_DEN	0.1706	0.0106	0.1733	0.3280
HWB_CFM_LamFlowNoSlat	0.1862	0.0410	0.1779	0.3396
HWB_CFM_CCW	0.1871	0.0427	0.1782	0.3403
HWB_CFM_Aerotherm	0.1899	0.0481	0.1790	0.3424
HWB_CFM_BLI	0.1992	0.0663	0.1818	0.3494
HWB_CFM_NoTech	0.2065	0.0807	0.1840	0.3549
HWB_CFM_Vortex	0.2074	0.0824	0.1843	0.3556
HWB_CFM_LGInt	0.2075	0.0825	0.1843	0.3556
HWB_CFM_3D	0.2153	0.0978	0.1868	0.3615
HWB_CFM_CNT	0.2154	0.0979	0.1867	0.3615
HWB_CFM_InletOpt	0.2154	0.0980	0.1867	0.3616
HWB_CFM_LGF	0.2172	0.0986	0.1901	0.3629
HWB_CFM_LIS	0.2262	0.1149	0.1939	0.3696
HWB_CFM_LamFlowNoSlatAF	0.2427	0.1477	0.1984	0.3821
HWB_CFM_ASE	0.2461	0.1463	0.2075	0.3846
HWB_CFM_AdvMetal	0.2536	0.1591	0.2114	0.3902
HWB_CFM_M5	0.2875	0.2146	0.2323	0.4156

6.4.2 Technology Suites

Based on the results of the technology assessment, technology suites were developed to target noise and performance for each configuration. Each technology suite was developed with both the open rotor and three-shaft turbofan engine architectures. Technologies that were determined through the SER assessment to provide less of a system level benefit were discarded. For example, on a system level, the effect of landing gear component integration was determined to be less than that of landing gear fairings, and as a result, landing gear component integration is not carried through into the technology suites. These packages are shown in Table 6-9 for the hybrid wing-body, and Table 6-10 for the advanced tube-and-wing.

Table 6-9. Major Technology Suites for Hybrid Wing-Body Configurations

Technology	HWB No Tech	HWB Noise Tech	HWB Performance Tech		
Scaled CFM56-3B1	X				
Open Rotor		X			X
Three-Shaft Turbofan			X	X	
Aeroservoelastic Structures				X	X
M5 Ultra-High Performance Fiber				X	X
Affordable Large Integrated Structures				X	X
3-D Woven and Stitched Composites				X	X
Advanced Metallics				X	X
Swept-Wing Laminar Flow					
Carbon Nanotube Electrical Cables				X	X
Landing Gear Fairings		X	X	X	X
Landing Gear Integration	CONFLICTS WITH LANDING GEAR FAIRINGS, LOWER SYSTEM EFFECT				
Aerothermal Concepts		X	X		
Boundary Layer Ingestion		X	X		
Steady Circulation Control					
Inlet Optimization				X	X
Distributed Exhaust Nozzle		X	X		
Vortex Generators		X	X		

Table 6-10. Major Technology Suites for Tube-and-Wing Configurations

Technology	ATW No Tech	ATW Noise Tech		ATW Performance Tech	
Scaled CFM56-3B1	X				
Open Rotor		X			X
Three-Shaft Turbofan			X	X	
Aeroservoelastic Structures				X	X
M5 Ultra-High Performance Fiber				X	X
Affordable Large Integrated Structures				X	X
3-D Woven and Stitched Composites				X	X
Advanced Metallics				X	X
Swept-Wing Laminar Flow				X	X
Carbon Nanotube Electrical Cables				X	X
Landing Gear Fairings		X	X	X	X
Landing Gear Integration	CONFLICTS WITH LANDING GEAR FAIRINGS, LOWER SYSTEM EFFECT				
Aerothermal Concepts		X	X		
Boundary Layer Ingestion	NOT ANALYZED				
Steady Circulation Control					
Inlet Optimization	PR ≈ 1 FOR PODDED INLETS				
Distributed Exhaust Nozzle		X	X		
Vortex Generators		X	X		

6.4.3 Configuration Results

Implementing the technology suites onto the two airframe configurations allowed for both the quantification of the technology benefits and a comparison of the overall system performance of the aircraft configurations. These comparisons are made in Figure 6-13, with corresponding data listed in Table 6-11. It was difficult to accurately determine the effect of an open rotor configuration on the overall aircraft noise, because open rotor noise prediction methods are still immature. Without the benefit of noise prediction for open rotor engines, it was possible only to compare configurations based on assumed EPNL differences between configurations using these engines. While not precise, this methodology did permit relative comparisons. Hence, all data described in this section is subject to the assumption that there are no EPNL differences between configurations when replacing a three-shaft turbofan with an open rotor.

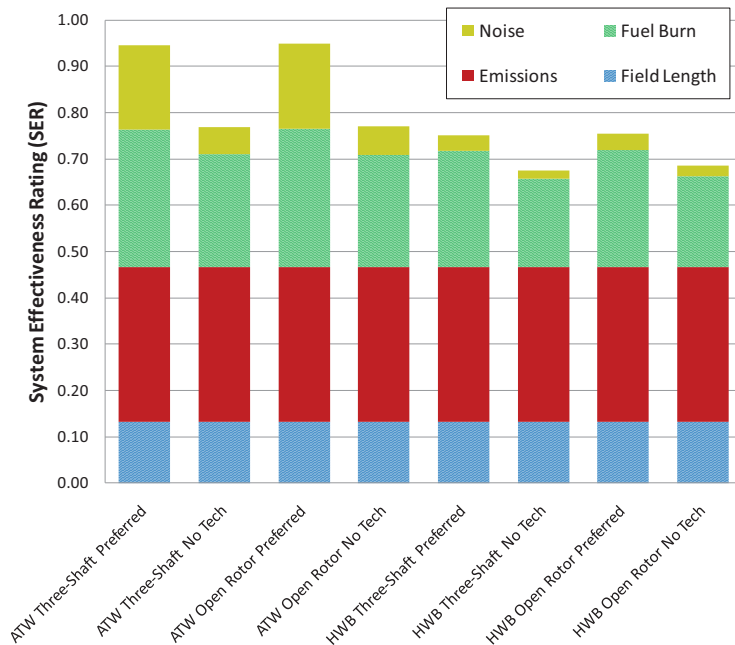


Figure 6-13. System Effectiveness Rating Comparison Between Candidate Configurations

Table 6-11. Contributions to System Effectiveness Rating Calculations

	Requirements and Metrics					
	Fuel, lbf	BFL, ft	Stage 4 Cum	EPNL, EPNdB	CAEP/6 NOx, g/kN	NOx, g/kN
Reference	25048	4999	274.6	269.7	48.3	40.3
ATW 3-Shaft Preferred	9409.7	4896	271.1	201.7	103.2	9.69
ATW 3-Shaft No Tech	12196	4996	272.3	251.5	100.9	9.69
ATW Open Rotor Preferred	9338.7	4999	272.0	201.7	77.6	10.61
ATW Open Rotor No Tech	12331.7	4998	273.4	251.5	73.6	10.61
HWB 3-Shaft Preferred	11818.5	4682	271.6	259.9	101.5	9.69
HWB 3-Shaft No Tech	15002.2	4831	273.1	266.9	97.6	9.69
HWB Open Rotor Preferred	11768	4989	272.6	259.9	73.3	10.61
HWB Open Rotor No Tech	14730	4745	275.1	266.9	69.3	10.61

	SER Components				Scenario Weighted SER	
	Fuel	BFL	EPNL	NOx	SER, w/o Noise	SER w/ Noise
Reference	---	---	---	---	---	---
ATW 3-Shaft Preferred	0.892	1.000	0.906	1.000	0.764	0.960
ATW 3-Shaft No Tech	0.733	1.000	0.292	1.000	0.711	0.769
ATW Open Rotor Preferred	0.896	1.000	0.919	1.000	0.765	0.963
ATW Open Rotor No Tech	0.725	1.000	0.309	1.000	0.708	0.770
HWB 3-Shaft Preferred	0.755	1.000	0.164	1.000	0.718	0.751
HWB 3-Shaft No Tech	0.573	1.000	0.087	1.000	0.658	0.675
HWB Open Rotor Preferred	0.757	1.000	0.179	1.000	0.719	0.755
HWB Open Rotor No Tech	0.588	1.000	0.116	1.000	0.663	0.686

The most prominent result from this analysis is that the hybrid wing-body configurations are less effective on a system level with respect to the mission requirements. For example, with the preferred technology package, the advanced tube-and-wing realized an overall SER of 0.960 when using the three-shaft turbofan, while the HWB with the same engine only achieved an overall SER of 0.751. While both configurations achieved the N+3 goals of field length and NOx emissions, the ATW significantly outperformed the HWB in terms of fuel burn and noise. A comparison between engines showed that configurations using the open rotor marginally outperformed those implementing the three-shaft turbofan. The advanced tube-and-wing configuration with open rotors had an overall SER of 0.963, while the same airframe configuration powered by three-shaft turbofans had an SER of 0.960.

Knowing that the system effectiveness ratings between the two most promising configurations differed by such a small amount, it was possible to calculate the threshold EPNL that would be required for the open rotor configuration to surpass the three-shaft configuration in terms of SER. For a range of EPNL differences between configurations (open rotor relative to three-shaft configurations), the resulting system effectiveness ratings are plotted in Figure 6-14, holding everything else constant. As long as the open rotor configuration is less than 2.65 EPNdB louder than the three-shaft turbofan configuration, the open rotor configuration edges out the three-shaft turbofan. However, for higher EPNL differences between configurations, the three-shaft turbofan is clearly the preferred engine. The general consensus among internal and external acoustics experts is that the open rotor will be significantly louder than the three-shaft engine, and that the actual acoustics of this engine will place it beyond the constraint imposed by the SER. For this reason, the open rotor architecture was not carried forward onto the preferred configuration.

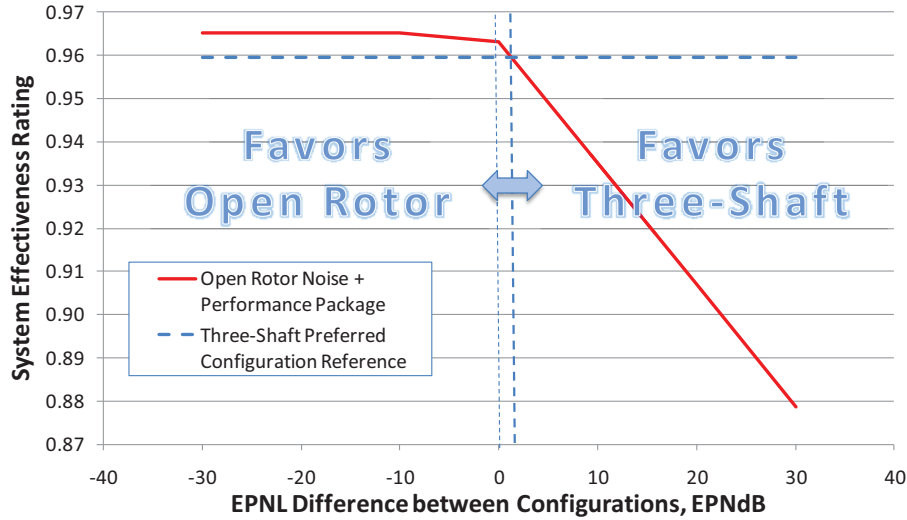


Figure 6-14. Effect of Configuration Δ EPNL on System Effectiveness Rating

6.5 Preferred Configuration

A preferred configuration emerged from the conceptual design study that best meets the goals for the N+3 aircraft. Table 6-12 shows the requirements for the preferred configuration in terms of the N+3 goals, and the achievements that were made towards each of these targets. The final configuration resulted in a fuel burn that was 63.49% below that of the reference vehicle, an EPNL that was 69.6 EPNdB below the FAR Stage 4 requirement for aircraft of its weight class, NO_x production that was 90.59% below the CAEP/6 requirement for aircraft using engines of its OPR and thrust class, and a balanced field length of 4,999 feet, showing the potential of the aircraft to exploit metroplex operations. While not all N+3 goals were met with this configuration, tremendous strides were made towards these objectives while taking into consideration the reality of technology maturation, aircraft entry-into-service schedules, and the N+3 timeframe.

Table 6-12. N+3 Goals Achievement

Metric	Requirement	Actual	Achievement	Overall Scenario Weighting Factor	
Noise	-71 EPNdB relative to Stage 4	200.3 EPNdB	201.7 EPNdB	69.6 EPNdB below Stage 4	20.00%
Fuel Burn	70% below reference vehicle	7514 lbf	9145 lbf	63.49% below reference vehicle	33.33%
Emissions	75% below CAEP/6	25.7 g/kN	9.69 g/kN	90.59% below CAEP/6	33.33%
Balanced Field Length	exploit metroplex	5,000 ft	4,999 ft	exploited metroplex	13.33%

6.5.1 Airframe Configuration

The resulting airframe configuration from the N+3 study was a tube-and-wing configuration optimized for its mission and using advanced propulsion systems, light-weight structural materials, and laminar flow technology (Figure 6-15). Designed for 120 passengers and a 1600 nm mission, this advanced configuration uses high aspect ratio wings (AR = 12.7) made possible by lighter wing and nacelle structures. Additional technologies, including landing gear fairings, were used to mitigate the acoustic footprint of the aircraft during takeoff and landing.

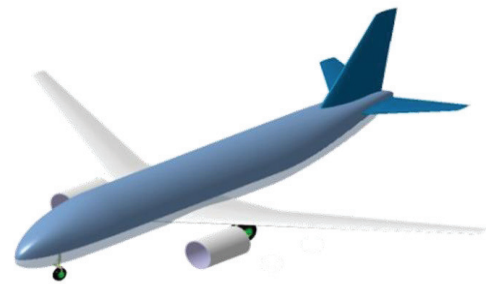


Figure 6-15. Preferred N+3 Configuration

6.5.2 Preferred Technology Package

The preferred configuration is comprised of technologies that enable fuel burn reduction and vehicle noise source mitigation (see Table 6-13). Airframe technologies that reduce empty weight include large integrated structures, aeroservoelastic structures, M5 ultrahigh-performance fiber, carbon nanotube electrical cables, 3-D woven and stitched composites, and advanced metallic alloys. Propulsive technologies include the three-shaft turbofan engine with compressor intercooling, CMC turbine blades, fuel-cooled cooling air, variable nozzle geometry, and lean combustor technology. Engine noise was reduced by both the variable geometry nozzle and advanced inlet acoustic liner, and total airframe noise was mitigated by landing gear fairings and the removal of leading edge slats attendant with swept-wing laminar flow. Laminar flow dramatically reduced fuel burn by reducing skin friction drag associated with turbulent flow regions.

6.5.3 Weight Breakdown

A summary of the weight for this aircraft is shown in Table 6-14. It can be seen that because of the weight savings caused by the use of advanced materials, the structural weight comprises only 23.9% of the takeoff gross weight. Besides the passengers and cargo, the largest contributor to the aircraft weight is systems and equipment, accounting for 24.0% of the total weight. The majority of this is due to furnishings and equipment, suggesting a possible target for future weight reduction. Table 6-15 shows a breakdown of the aircraft mission weight. The maximum ramp weight for this aircraft is only 80,478 lbf, driven down both by the reduced mission fuel requirement brought about by engine and aerodynamic efficiency, and the reduced empty weight derived from significant use of advanced materials throughout the airframe.

Table 6-13. N+3 Technology Suite

Technology Suite
Three-Shaft Turbofan Engine
-Ultra-High Bypass Ratio of ~18
-CMC Turbine Blades
-Lean-Burn CMC Combustor
-Intercooled Compressor Stages
-Swept Fan Outlet Guide Vanes
-Fan Blade Sweep Design
-Lifghtweight Fan/Fan Cowl
-Compressor Flow Control
-Active Compressor Clearance Control
-Variable Geometry Nozzles
Swept Wing Laminar Flow
Large Integrated Structures
Aeroservoelastic Structures
M5 Ultra High-Performance Fiber
Carbon Nanotube Electrical Cables
3-D Woven and Stitched Composites
Advanced Metallics
Landing Gear Fairings
Advanced Acoustic Inlet Liner

Table 6-14. Weight Statement

System/Components	% TOGW	Weight, lbf
Structural	23.9%	19264
Wing	7.9%	6365
Horizontal Tail	0.9%	691
Vertical Tail	0.4%	356
Fuselage	7.9%	6324
Landing Gear	4.4%	3552
Nacelle	2.5%	1976
Propulsion	6.3%	5058
Engines	5.5%	4453
Fuel Tanks & Plumbing	0.8%	605
Systems & Equipment	24.0%	19341
Surface Controls	1.7%	1377
Auxiliary Power	0.8%	626
Instruments	0.7%	587
Hydraulics	4.4%	3581
Electrical	1.1%	865
Avionics	1.5%	1232
Furnishings & Equipment	11.8%	9518
Air Conditioning	1.7%	1357
Anti-icing	0.2%	198
Empty Weight	54.3%	43663
Flight Crew & Misc.	3.1%	2470
Crew & Baggage Flight, 2	0.6%	450
Crew & Baggage Cabin, 4	1.0%	800
Unusable Fuel	0.6%	492
Engine Oil	0.1%	70
Cargo Containers	0.8%	658
Operating Weight	57.3%	46133
Passengers & Cargo	31.3%	25200
Passengers	26.8%	21600
Passenger Baggage	4.5%	3600
Zero Fuel Weight	88.6%	71333
Fuel	11.4%	9145
Mission Fuel	11.4%	9145
Max Ramp Weight	100.0%	80478

Table 6-15. Mission Weight Breakdown

Mission Weight Breakdown	
Empty Weight	43663 lbf
Operating Weight	46133 lbf
Zero-Fuel Weight	71333 lbf
Max Ramp Weight	80478 lbf
Maximum Landing Weight	72430 lbf

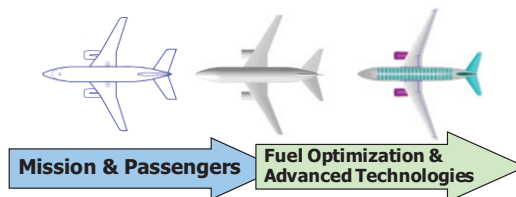
6.5.4 Propulsion System

The three-shaft turbofan engine design was selected as the propulsion system for the preferred aircraft configuration. Generating a maximum sea level static thrust of 14,393 lbf, the engine has a takeoff thrust-to-weight ratio of nearly 6.47 when considering the weight of the engine system, and a takeoff specific fuel consumption of only 0.226 pph/lbf. At cruise the thrust-to-weight ratio is 0.91. The fan itself has a diameter of 59.5 inches, with 22 rotor blades and 54 stator vanes. Having a flange-to-flange length of 94.7 inches, the total engine weight (including electrical and control systems) is 2226.7 lbf. With the nacelle, the overall length and diameter of the propulsion system are 164.7 inches and 76.7 inches, respectively. Heavy use of composites is assumed in the front-end fan module, while the LP compressor and HP compressor rely primarily on titanium alloys and inconel, respectively. The turbine section makes use of ceramic matrix composite blades, while the lean burn combustor is also constructed of CMC material.

6.5.5 Configuration Comparisons

Table 6-16 allows for the comparison between the calibration, reference, and preferred vehicle. Comparison between the 737-500 and the reference vehicle illustrates the resizing for reduction in passenger count and range in addition to meeting the mission goal. Comparison between the reference and preferred vehicle shows the effects of vehicle optimization on mission fuel and integration of advanced technologies including advanced propulsion. The wing reference area is shown to be drastically reduced while achieving a higher aspect ratio of 12.7. The ramp gross weight of the preferred vehicle is reduced by 39,692 pounds, owing to its reduced structural weight and reduced fuel requirements.

Table 6-16. Tube-and-Wing Vehicle Comparison



	Units	737-500	Reference Vehicle	Preferred Configuration
# Passengers	[]	123	120	120
Range	[nm]	2,400	1,600	1,600
Ramp Gross Weight	[lb]	133,500	120,170	80,478
Empty Weight	[lb]	68,860	67,350	43,660
Fuel Weight	[lb]	42,186	25,048	9,144
Wing Reference Area	[ft ²]	1,135	1,280	967.5
Wing Sweep	[deg]	25	25	26
Wing Span	[ft]	94.9	100.4	111.0
Wing AR	[]	7.9	7.9	12.7
T/W Ratio	[]	0.30	0.34	0.36
Max Wing Loading	[psf]	117	94	83.2
Balanced Field Length	[ft]	8,630	4,497	4,999
Landing Field Length	[ft]	4,450	4,996	4,906

6.5.6 Performance Summary

6.5.6.1 Aircraft Mission Fuel Summary – The reference vehicle fueled for a 1600 nm range and a passenger count of 120 burned 25,048 pounds of fuel. NASA N+3 objectives set a 70% reduction in this fuel weight as the target mission fuel, or 7514.4 pounds. The mission fuel burn for the preferred configuration is 9145 lbf, reducing fuel burn 63.49% from the reference vehicle.

A waterfall of mission fuel reduction is shown in Figure 6-16. The fuel burn progression is traced from the reference vehicle to the final preferred configuration. However, as mentioned in Section 5.3.3, technologies can be packaged in different combinations that change their relative benefit. The waterfall illustrated represents the consensus interpretation of the individual benefit of each technology. The three-shaft turbofan engine was the greatest contributor to fuel burn reduction with a 28.18% reduction in mission fuel. Wing resizing, reduced fuselage length, aspect ratio increase, and cruise Mach number reduction led to a fuel burn savings of 8.23%. Among the individual technologies, M5 ultrahigh-performance fiber, swept-wing laminar flow, aeroservoelastic structures, and advanced metallic alloys were the greatest contributors to fuel burn reduction with 8.12%, 5.73%, 4.18%, and 3.40% reductions in mission fuel, respectively. A detailed segment fuel breakdown is shown in Table 6-17.

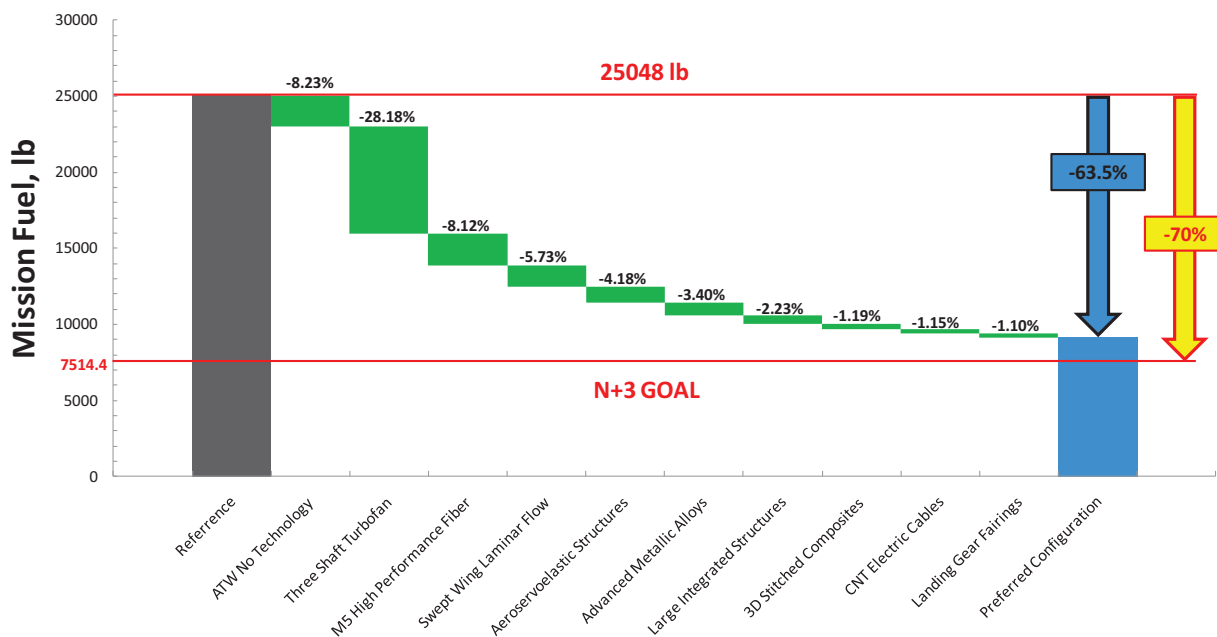


Figure 6-16. Preferred Configuration Planform and Technology Contributions to Mission Fuel Burn Reduction

Table 6-17. Fuel Burn by Mission Segment for Preferred Configuration

Mission Performance	Reference	Preferred	% Reduction
Max Ramp Weight, lbf:	119794	80478	-
Mission Fuel, lbf:	25049	9145	63.49%
Taxi Out, lbf:	188	112	40.43%
Takeoff, lbf:	156	93	40.38%
Climb, lbf:	2476	1496	39.58%
Cruise, lbf:	15343	5077	66.91%
Descent, lbf:	1740	513	70.52%
Approach, lbf:	512	162	68.36%
Reserves, lbf:	4634	1692	63.49%

While not achieving the N+3 goal of 70% fuel burn reduction, tremendous progress was made in this direction. Though many candidate technologies were dismissed in the early stages of the study, their potential contributions to this goal are now evident. Their implementation on the preferred configuration may lead to the successful accomplishment of the N+3 mission fuel burn objective. Future analyses could explore additional key technologies and their integration.

6.5.6.2 Aircraft Acoustic Summary – Analysis on the preferred configuration, when compared to that of the ATW vehicle described in Section 6.3.3.2, allows for the noise reduction associated with slat removal, advanced technologies, the three-shaft turbofan, and advanced inlet liner to be quantified. The acoustic inlet liner was scaled appropriately and applied to the three-shaft turbofan engine, resulting in significant fan noise reduction during takeoff and climb. In addition, the inlet liner reduced engine fan noise during descent and landing, but this effect was less significant during this stage of the flight. The inlet liner reduced the total vehicle EPNL by 6.0 EPNdB. Significant landing gear noise reduction was achieved due to the landing gear fairing integration, reducing total EPNL by approximately 6.2 EPNdB. The removal of leading edge slats further reduces cumulative EPNL by approximately 6.51 EPNdB. Furthermore, due to the reduction in gross weight and, consequently, required engine thrust, additional reductions in noise were achieved through lower exhaust jet velocities.

The community, sideline, and approach EPNL values were 44.64, 67.65, and 89.46 EPNdB, respectively, resulting in a cumulative EPNL of 201.75 EPNdB. The preferred configuration reduces cumulative EPNL by 67.94 EPNdB compared to the reference vehicle. The NASA N+3 acoustic metric, 71 EPNdB below the Stage 4 requirement, is a function of vehicle gross weight. The Stage 4 requirement based on the gross weight of the preferred vehicle is 271.3 EPNdB, making the N+3 acoustic goal 200.3 EPNdB. The preferred configuration generates an EPNL that is 69.55 EPNdB below its respective Stage 4 requirement and is 1.45 EPNdB higher than the N+3 acoustic goal. A waterfall of acoustic reduction is shown in Figure 6-17 which traces the noise reduction from the reference vehicle to the final preferred configuration. In addition, a detailed comparison between the individual and cumulative acoustics metrics is shown in Table 6-18 for the preferred configuration and the vehicles discussed in Section 6.3.3.

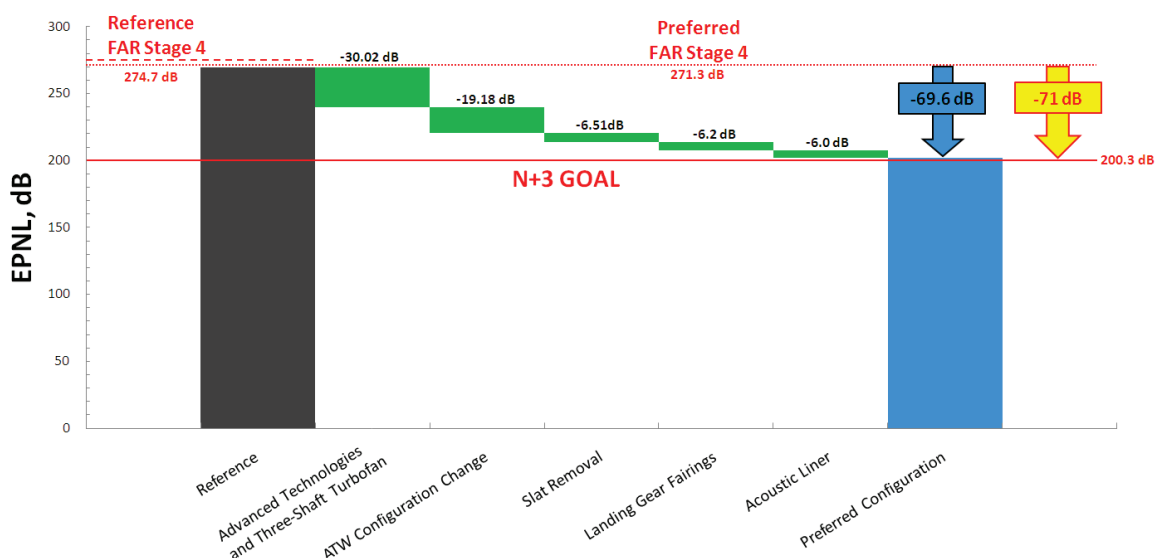


Figure 6-17. Preferred Configuration Platform and Technology Contributions to Community Noise Reduction

Table 6-18. FAR Stage 4 EPNL Comparison

Metric (EPNdB)	Reference Vehicle	ATW No Technologies	HWB No Technologies	Preferred Configuration
Community	76.15	61.15	78.59	44.64
Sideline	87.15	87.15	101.08	67.65
Approach	106.39	103.22	95.27	89.45
Cumulative	269.69	251.52	274.94	201.74

6.5.6.3 Aircraft Emissions Summary – NASA N+3 objectives set a 75% reduction in NO_x production below the CAEP/6 requirements as the target emissions goal. Section 6.2.1 discusses the calculation of the CAEP/6 requirements and vehicle emissions. For the gross thrust and OPR of the preferred vehicle, the CAEP/6 requirement is 102.92 g/kN, making the N+3 emission goal 25.73 g/kN.

The preferred configuration generates NO_x at a rate of 9.69g/kN, which is 90.58% below its respective CAEP/6 requirement and 62.33% below the N+3 emissions goal. This large reduction in emissions production is a result of the staged lean combustor. The CAEP/6 requirement and the N+3 emissions goal are shown in Figure 6-18, along with the reference and preferred vehicles.

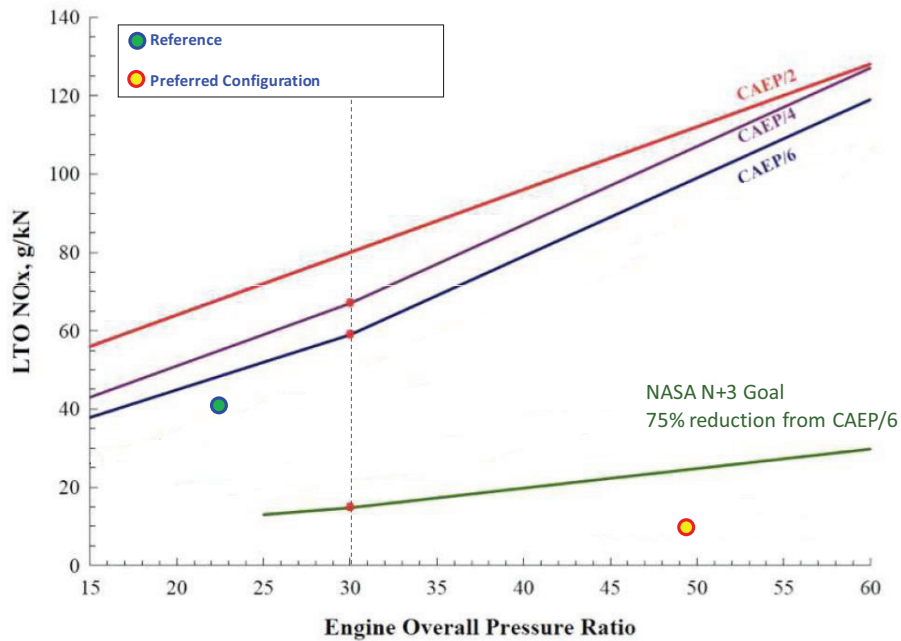


Figure 6-18. CAEP/6 LTO NO_x Emissions Requirement and N+3 Achievements

6.5.6.4 Aircraft Field Length Summary – NASA N+3 goals call for the exploitation of metroplex operations. Based on the analysis described in Section 4.2, it was concluded that aircraft capable of using runway lengths of 5,000 feet would be optimum for operating in the metroplex flight environment. All vehicles were designed to meet the 5,000 foot balanced field length requirement and landing field length. Field length calculations assumed sea level and standard day conditions. The preferred configuration operates with a 4,999 foot balanced field length and a 4,906 foot landing field length, successfully meeting field length requirements.

7 TECHNOLOGY MATURATION

Key enabling technologies were identified in Section 6.5.2 that contributed toward the N+3 goals. In order for these technologies to be ready for EIS in the N+3 timeframe of 2030-2035, these technologies need to achieve TRL 6 by 2025. To ensure that these technologies achieve this TRL goal, top-level technology roadmaps were created that map out the major definitive milestones that must be met. The milestones include analysis, experiments, and scope of experiments planned out in high-level risk waterfalls to capture the critical path to technology insertion. Each of the maturation activities were assigned an appropriate duration to accomplish the task assuming reasonable levels of investment, and with the facilities available in the United States. It is envisioned that minor sideline activities will be performed alongside these major milestones to support the fundamental understanding of the physics involved, and to hedge the investment with other technologies that could offer a similar benefit. However, this study focused on the technologies that were found to offer the most probable success for the timeframe needed, for the mission and vehicle class, and with the most benefit to the configuration. These caveats should be kept in mind for evaluation of the TMPs developed here.

7.1 Physical Landing Gear Fairings

Physical landing gear fairings have been investigated in numerous recent evaluations at TRL levels of 7 or 8, which is beyond the goal level for 2025. These fairings have been implemented mainly around the wheel axes in flight tests of full-scale aircraft intended for high design maturity. Further design efforts to improve these fairings should improve to lower the wake strength and turbulent kinetic energy distributed throughout the wake of landing gear. This activity should be coordinated with both virtual landing gear fairing efforts and component integration efforts.

7.2 Virtual Landing Gear Fairings

Virtual fairings are estimated to be at a current TRL of 2, as low-level development has occurred only in controlled lab settings, on highly simplified models, and without realistic environmental affects (Figure 7-1). Plasma actuators are viewed as a prime candidate for implementation since although they offer relatively low momentum addition compared to other active flow actuators, they may greatly affect the coherent structure of the shed vorticity so that the dipole air-structure interaction noise sources will be reduced. However, at this low TRL, it is viewed as a prime candidate in a series of actuator trials, so that the most effective control scheme can be developed. In combination with physical fairings, robust control may provide sufficient forcing to accrue significant tonal noise reduction in the several main components of gear noise, stemming from the wheels (low-frequency), struts (mid-frequency), and non-integral components (high-frequency). A challenge to this choice for active flow control application will be integrating an actuator that consumes little power, and creates less noise addition than the broadband sources it will attenuate. These, along with proving an essential control scheme to minimize weight and cost, are seen as the primary activities of the TRL 3 activity, in a laboratory bench-test setting.

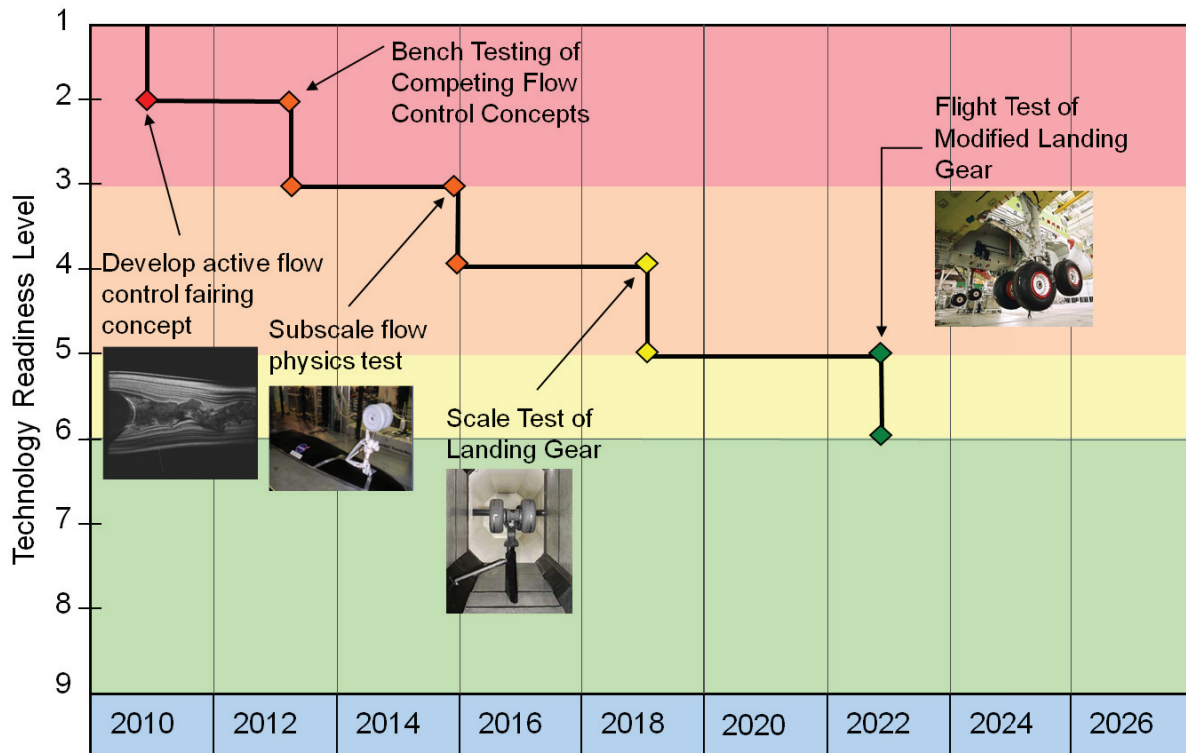


Figure 7-1. TMP for Virtual Landing Gear Fairings

7.3 Swept-Wing Laminar Flow Slat Integration

Elimination of the slat by integrating virtual or seamless leading edge concepts is estimated at a current TRL of 2. This technology item spawned from a more detailed consideration of the laminar flow requirements, not initially assumed in the technology QFD study. Continued development of new approaches through experimental and computational approaches is envisioned, working towards approaches that are both effective at increasing CL on a laminar flow wing, and have a tolerable failure mode that prohibits immediate stall. Both passive and active techniques should be investigated, including virtual aerodynamic flow control, as well as actuated deployable geometry that is amenable to transition concerns on a relatively sharper leading edge typical of laminar airfoil designs (Figure 7-2).

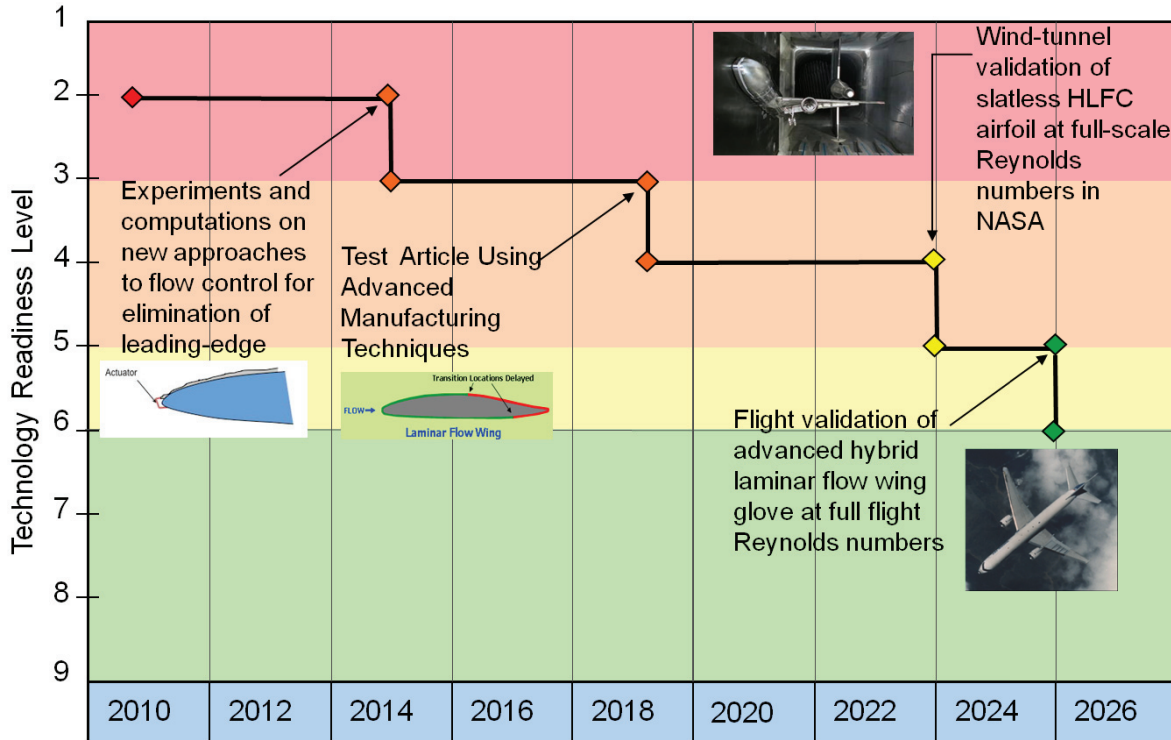


Figure 7-2. TMP for Swept-Wing Laminar Flow Slat Integration

To add value at this level, and progress to TRL 3, a NASA-sponsored development task should include dissemination of a particularly promising wing/airfoil geometry so that university and other researchers can implement CFD and experimental studies across a common platform, and compare physical mechanisms and performance on a more equivalent basis. This task is expected to last several years, defining promising concepts that tradeoff performance with robustness and graceful failure modes. Modeling (CFD and empirical) efforts should be coordinated for inclusion on further system-level assessments. For TRL 4 maturation, several candidates should be scaled up for inclusion on a swept-wing laminar flow section test article, that demonstrates slatless augmented-lift capability in a moderately realistic integration at or approaching the full-scale takeoff and landing Reynolds numbers. A complete test matrix should be pursued that includes not only design conditions, but simulation of random failure modes, and the ability of the control system to augment failure. The outcome of this activity should verify that a realistic standalone integration can prove the estimated benefit and system-level cost (weight, complexity) with a design that attempts to be compatible with laminar flow without extensive documentation of this facet. Compatibility with laminar flow design will be explicitly confirmed in a TRL5 activity at a full-scale Reynolds number after validation and further development of candidate NLF/HLFC designs pursued in separate development activities. Therefore, transition measurements should be made at this point in an adequate ground-based facility, and/or coordinated leading edge

excrescence effects on transition location should be available at the appropriate Reynolds number. Control schemes should be validated and optimized at this level. The TRL 6 maturation activity should be a flight-test validation of a partial-section wing-glove integration. The primary goal is to confirm scaled model behavior and CFD predictions of the slat CLmax benefits, and the effects on laminar flow extent. These full-scale results will provide a crucial update to benefit models, and provide weight and integration effects, both of which should be implemented in system-level effects studies.

7.4 Swept-Wing Laminar Flow Control of Crossflow Transition

Crossflow transition delay is established as a primary hurdle to enabling swept-wing laminar flow. This technology was further defined after initial consideration of laminar flow concepts in the technology QFD study (Figure 7-3).

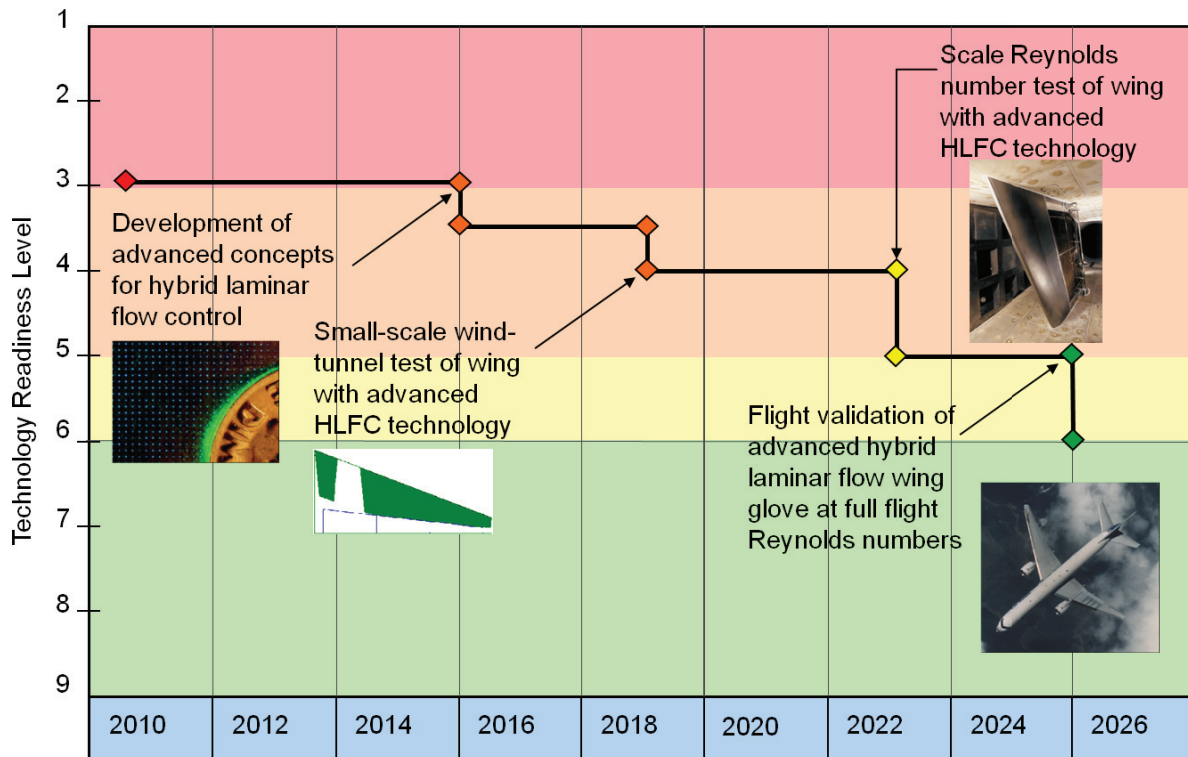


Figure 7-3. TMP for Swept-Wing Laminar Flow Control

HLFC using passive and/or active elements is approximated at a current TRL of 3, due to the dearth of realistic systems that will not greatly impose unacceptable system-level penalties of weight and suction or power levels. Advancement activities at this level to both delay transition while being capable of integrating high-lift techniques are required for downselecting capable candidate concepts designed for minimal vehicle-level system penalties. These activities should conclude in several years after considering several alternatives, and improving the understanding of the delay mechanisms and instability growth rate predictions. The culmination should be a set of designs that may be validated in a TRL 4 subsystem validation that demonstrates control effectiveness at relevant simulated flight conditions. Facilities with low-turbulence qualities may need to be improved to offer sufficient freestream disturbance levels and character at the required Reynolds numbers for sufficiently confident validation. Crossflow transition delay models as a function of the major control parameters are key outputs of this demonstration. For advancement to TRL 5 maturity, a full-scale Reynolds number experiment of a swept wing section with an advanced design should be used to assess crossflow delay effectiveness. Implementation of a high-lift system (surrogate or functional) to verify integration and influence on transition mechanisms would be a highly desirable element at this level. TRL 6 attainment should be a product of a full-scale flight test demonstration, integrating results of key correlations developed in

previous activities, using a wing glove and an integrated high-lift system. This activity may be synergistic with the leading-edge slat elimination activity, in which a precursor system without high-lift integration may be tested as a baseline system for this activity, then leveraged for the further virtual slat integration and test.

7.5 3D Stitched/Woven Composites

Continued fabrication technique development of a stitched/woven composite structure will take this technology to a TRL 4 level in the very near term (Figure 7-4). A set of several candidate structures should be assessed at the NASA COLTS facility, potentially as a common activity with the large integrated structures technology development path. Wing boxes and main fuselage structures should be designed to a specific purpose (vehicle type and class), with competing candidate approaches used to verify the importance and magnitude of industrial knowledge and successful application of previous development guidelines, to reach TRL 5. A TRL 6 activity should be the successful instrumented implementation of successful candidates into a flight platform, with robust instrumentation, or perhaps in concert with novel health management and prognostic systems in place to gain valuable in-flight modeling static and dynamic characteristics for these novel structures that will ensure acceptable commercial acceptance.

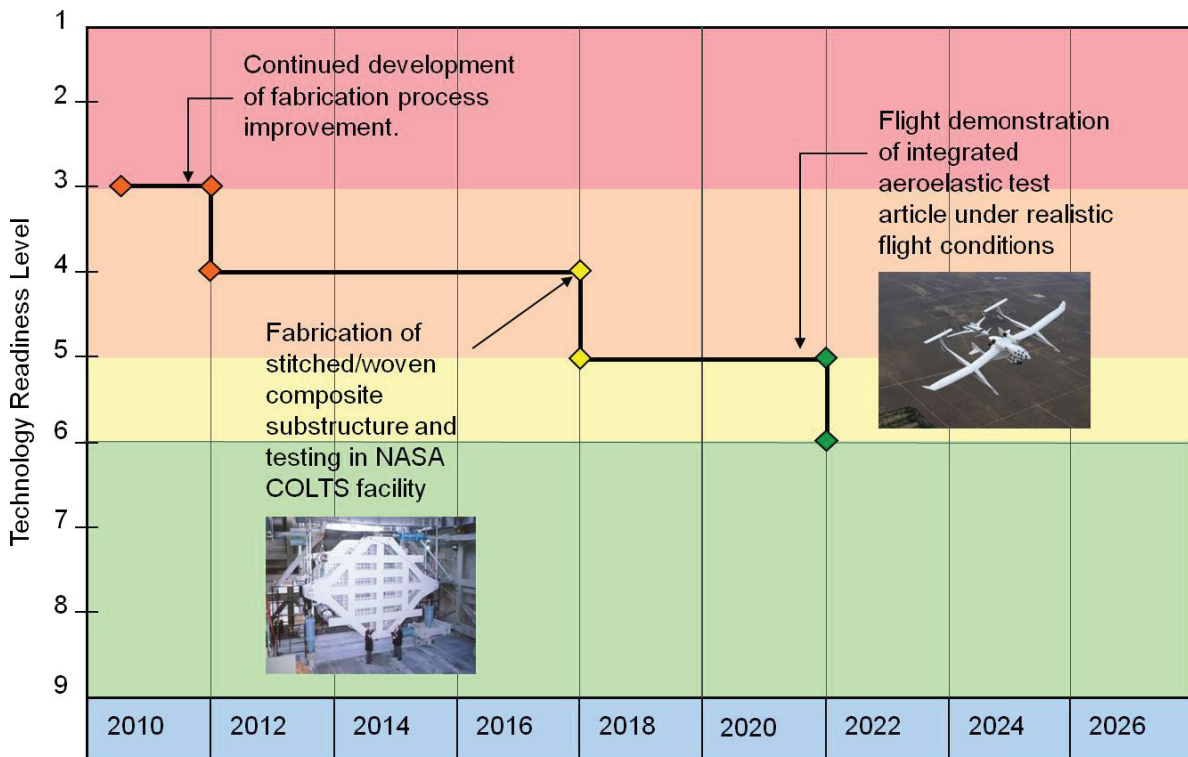


Figure 7-4. TMP for Stitched/Woven Composite Structures

7.6 Advanced Structural and Subsystems Metal Alloys

At a current TRL of approximately 4 (depending on which material class of several), optimizations of alloy chemistries for structural and subsystem components should continue to investigate good candidates for limited sample production throughout the next several years (Figure 7-5). Near-term goals should focus on higher strength in compressive and tensile modes, as well as at elevated temperatures and at room temperatures. High-pressure, dynamic, hydraulic applications should be targeted as well. 2XXX and 6XXX series alloys may offer some of these advances, while titanium-aluminum alloys, typical of structural use, may be investigated for use in subsystem applications such as hydraulics. Advancement to TRL 5 will be performed through advancing the selected chemistries through further thermo-mechanical optimization, and documentation of more thorough mechanical properties. TRL 6 will be reached through demonstrating these samples in limited, realistic loading and thermal environments, simulating the pressures and temperatures reached in intended applications throughout the airframe. Limited properties databases should be developed for comparison purposes to existing commodities.

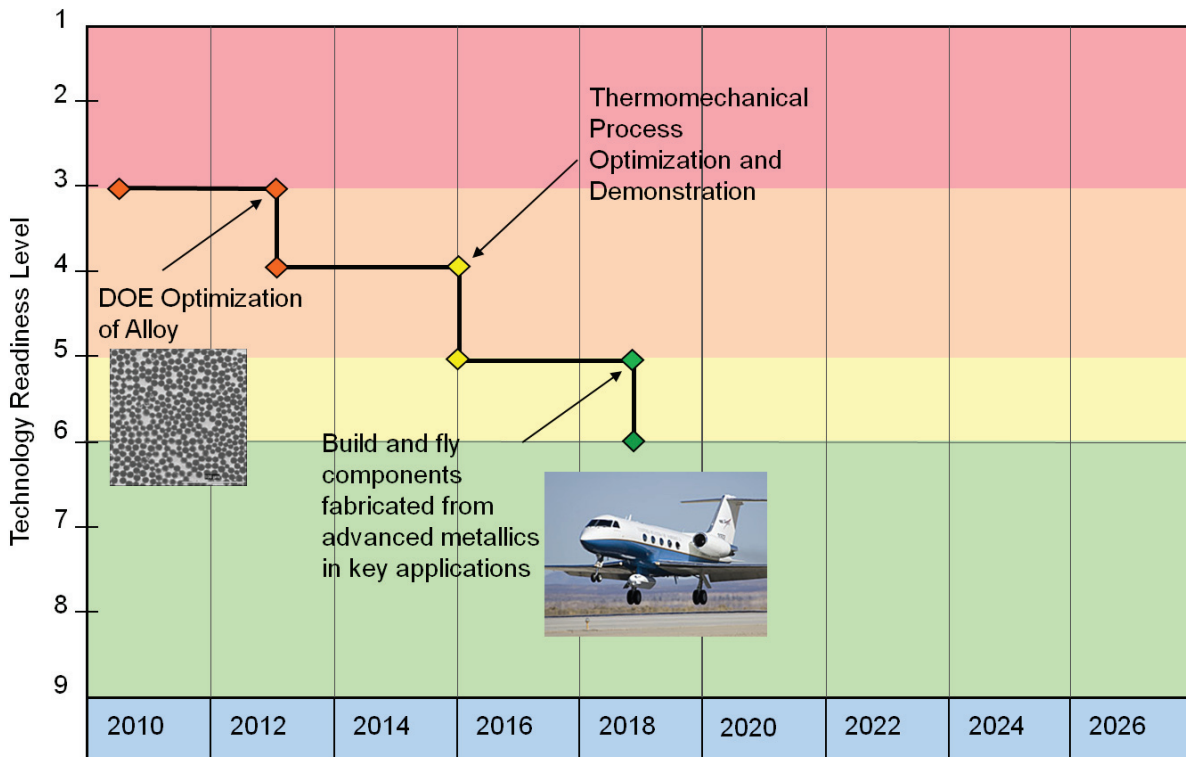


Figure 7-5. TMP for Advanced Structural and Subsystem Alloys

7.7 SMA Variable Geometry Nozzles

Variable geometry nozzles using SMA materials to actuate a high-bypass ratio fan nozzle are estimated to be at a TRL of 4 (Figure 7-6). SMA characterizations should be performed to reliably (minimizing hysteresis) actuate at least a two-position nozzle practical for takeoff and cruise operations. This should be demonstrated in a full-scale exhaust system cold-flow sector test in a highly instrumented laboratory setting to confirm nozzle performance. Investigating the tradeoff between continuously varying nozzle area, and two or multiposition fixed positions should be performed by exploring multiple configurations over a 2 to 3 year period. CFD studies should be validated across the range of test conditions. An optimized closed-loop control system to manage SMA deflections should be demonstrated at this stage. This stage should be concluded with a warm-flow sector test to confirm performance in relevant, but not full-scale exhaust flow conditions. TRL 6 achievement should be attained by demonstrating an integrated variable area nozzle concept on a demonstration engine ground test. Thrust stand performance measurements and control system operation and tuning should be the primary verification metrics. Limited acoustic measurements should be made to confirm noise reduction trends.

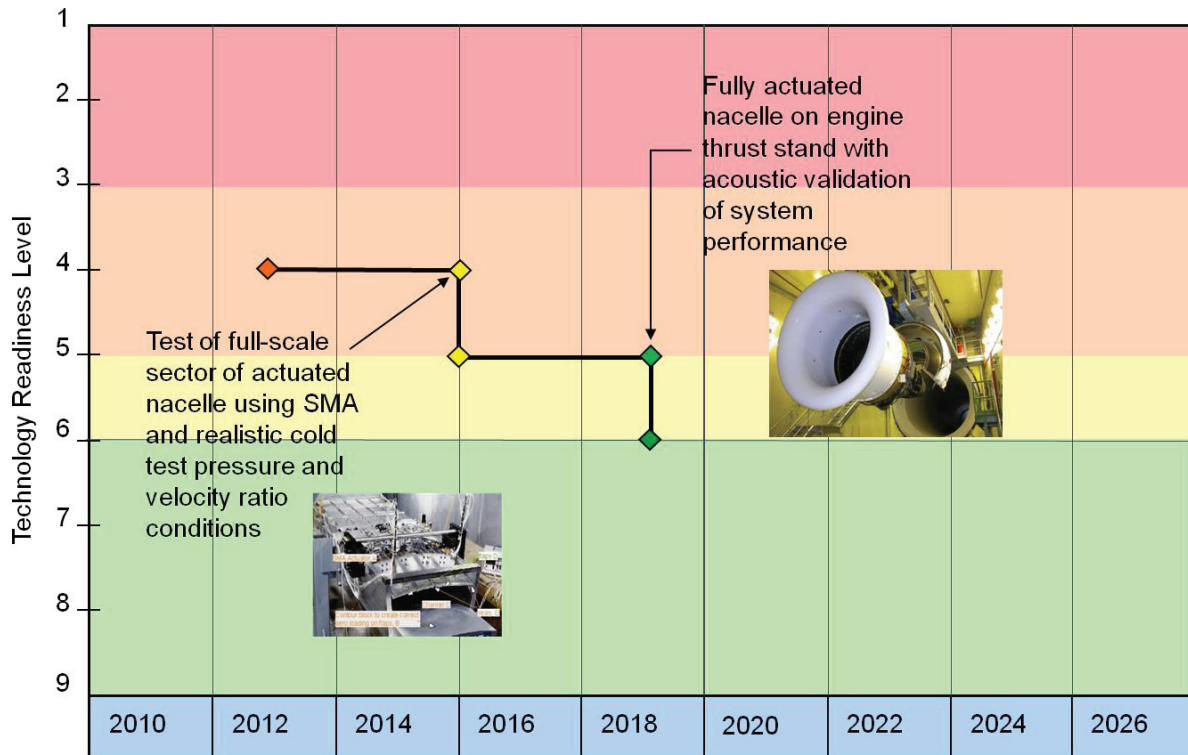


Figure 7-6. TMP for SMA Variable Geometry Nozzles

7.8 M5 Organic Fiber Composites

The fabrication of composite layup panels using the high-performance M5 organic polymer fiber is currently estimated at a TRL of 3 (Figure 7-7). Further work to verify performance for aircraft panel applications should focus on using the status M5 fibers, which have known fabrication quality limitations, to develop layup processes with appropriate resins. Due to the excellent compressive properties, composite structural components should also be investigated at this point in system benefit studies. Fiber manufacturing development must occur in parallel to improve fiber performance and manufacturability to reinforce the TRL 3 level risk. Coupon testing to examine basic composite properties through break tests and surface examination, along with basic stress/strain testing should occur at this stage. For moving to TRL 4, improved fibers must be available starting in several years following coupon testing to advance a simple composite panel structure through compression and break testing, as well as verifying layup procedures and the expected resin-fiber interface properties. Examining the resilience to moisture and solvents should be preliminarily investigated, along with further surface examinations and sample preparations to gain confidence in suitability to finish applications. Advancement to TRL 5 will require building of a moderately complex array of structural samples to mimic various layups appropriate for different aircraft applications. More extensive properties testing will occur, along with failure mode and vibration examination for basic panel geometries. Fiber properties should have essentially reached “goal” values at this point, so that the focus will be on successful integration. TRL 6 will pursue more complex panel development emulating scaled realistic implementations, alongside a structural allowables database development activity that will last at least several years.

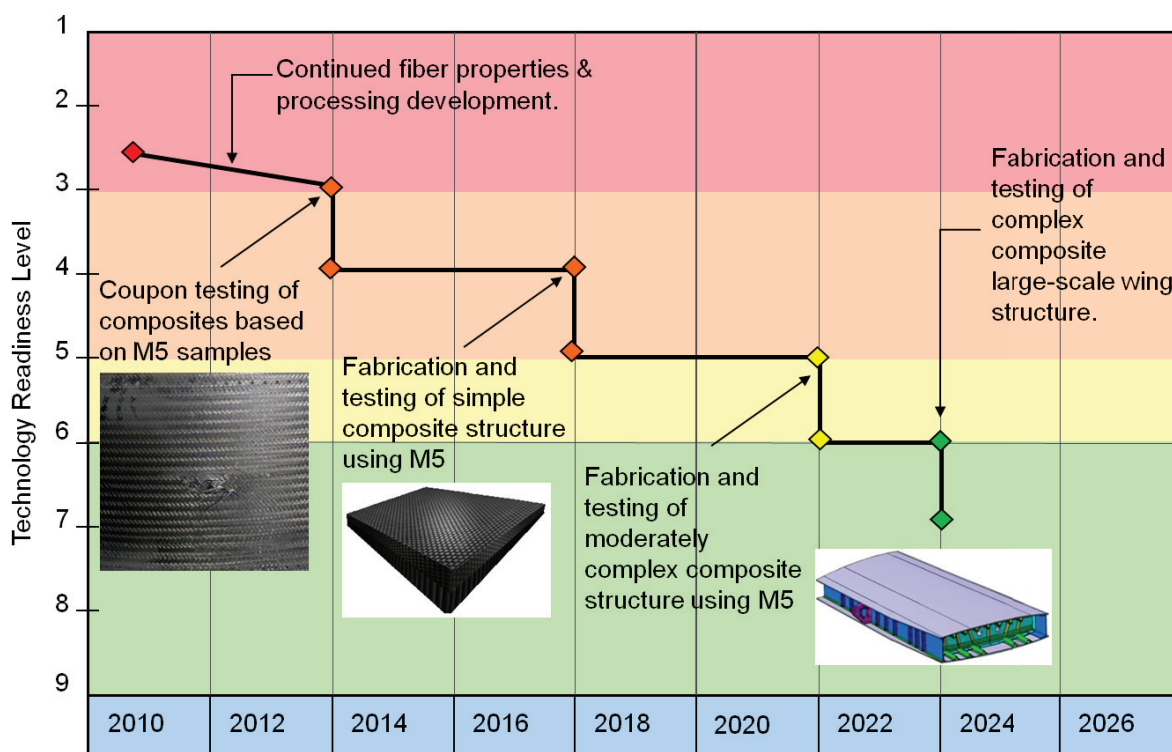


Figure 7-7. TMP for M5 Organic Fiber Composites

7.9 Carbon Nanotube Electrical Cables

Carbon nanotube cables are currently estimated at a TRL of 3, and must be pursued in terms of both core wire performance, and outer mesh conductor performance (coaxial arrangement) (Figure 7-8). To reach TRL 4 for both of these components, at least two years of development is foreseen to assess feasibility of optimized designs for combined prototypes. Separate development will occur on each to adequately lower risk levels initially, and identify and isolate technical hurdles. Close collaboration between development activities should occur, and culminate in the demonstration of at least one but possibly several candidate wire prototypes for adequate standalone evaluation of properties. For acquiring a TRL of 5, performance of a subsystem prototype installation for a moderately complex electrical system should be evaluated. Reaching TRL 6 should address any deficiencies in the properties of the TRL 5 through design and/or insulator optimization, and should culminate in the demonstration of a complete ground-based HITL subsystem.

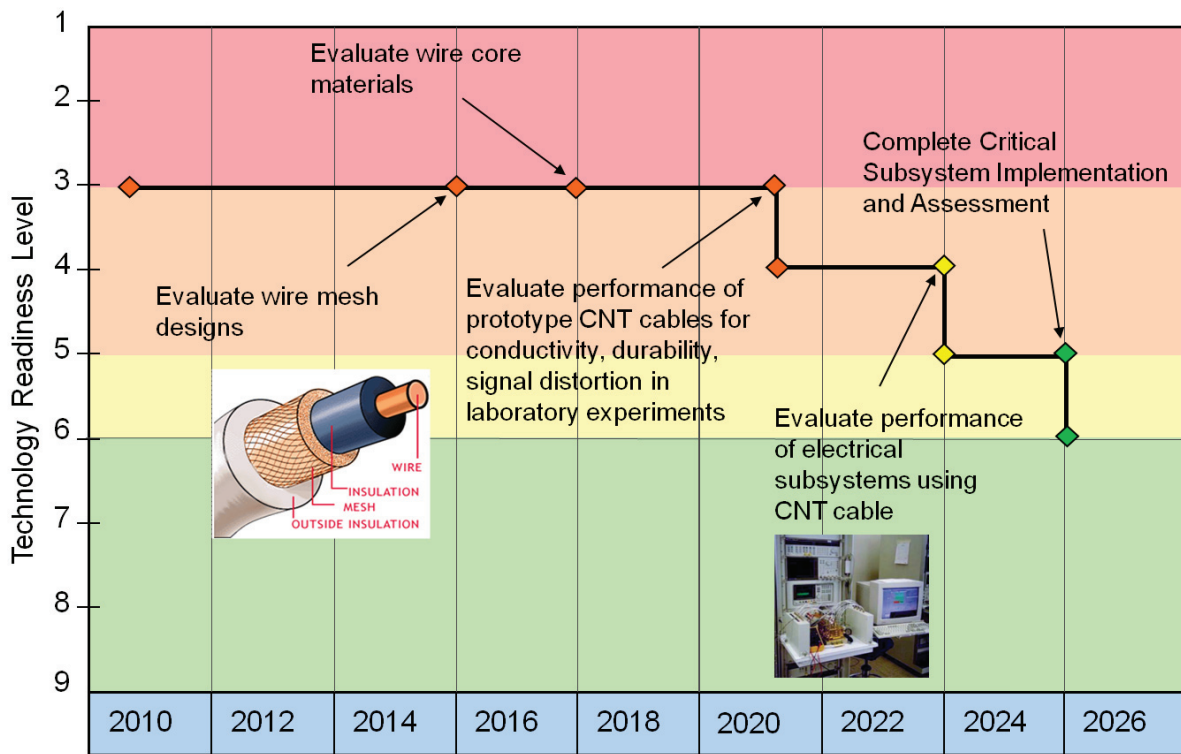


Figure 7-8. TMP for Carbon Nanotube Electrical Cables

7.10 Computational Inlet Optimization

Early-design cycle optimization of inlet installations is estimated to be at a current TRL of 3 (Figure 7-9). Researchers have demonstrated some components of low- and moderate-fidelity transport of fan-face distortion through to the bypass duct and core compressor, but this has not been in concert with other activities required to bring this capability to TRL 4. This would also require adding additional multi-fidelity models of inlet losses and integration effects to estimate performance quickly for MDO applications. Further, the handling of complex geometry requirements (to handle BLI, podded, embedded configurations) passed automatically through an application program interface (API) that must be devolved into a set of modeling constraints should be a cornerstone component. To move to TRL 5, the capability of the multifidelity tool should include tools that are essentially used currently for preliminary design, for use in the concept evaluation process. This could be enabled by adapting to new highly-parallelized GPUs and nodal numerical PDE solution methods that offer the potential for more than an order of magnitude increase in CFD solutions appropriate for this moderate level of fidelity. This matured capability, accompanied with robust geometry handling and aero effects modeling including spill drag and afterbody effects, will advance the tool to TRL 6. Integration of enabling technology models for secondary effect, including flow control for serpentine inlet applications, should be performed at this level when the tool is mature enough to have a validation background and a history of successful trade studies. This TRL 6 task is considered ongoing with continuous improvements to fidelity as computational resources improve, and as experimental databases come online for novel integration concepts.

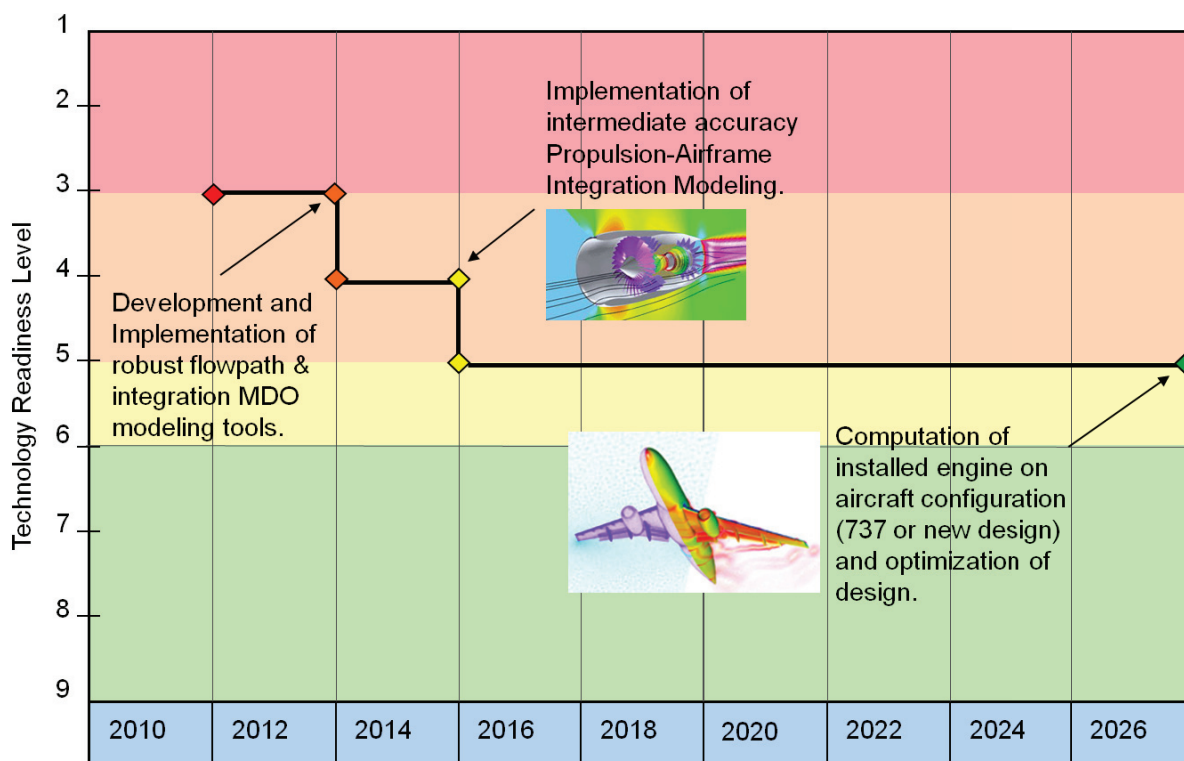


Figure 7-9. TMP for Computational Inlet Optimization

7.11 Large Integrated Structures

The current TRL of large integrated structures is estimated at 4, updated from an initial estimate used in the QFD study, which assumed TRL 3 (Figure 7-10). Continued development to further reduce risk at this level should include prototype development activities including reliability based design (RBD) methods for joint designs. Advanced structural models should be developed to predict performance at joint component and integrated structure levels. Weight models should be updated for system-level evaluations. A follow-on task for advancement to TRL 5 is the implementation of previous design and prediction tools to design/fab/test a large substructure in the NASA COLTS facility, in concert with the stitched/woven composites development activities. Validation of structural design through NDE and large-scale test results should provide adequate feedback for improving predictive analysis. Machining improvements should be pursued at this stage to meet TRL 6 requirements. A full-scale flight demonstration on a structural testbed aircraft, using improved prototype processes and performance predictions should advance this technology to TRL 6.

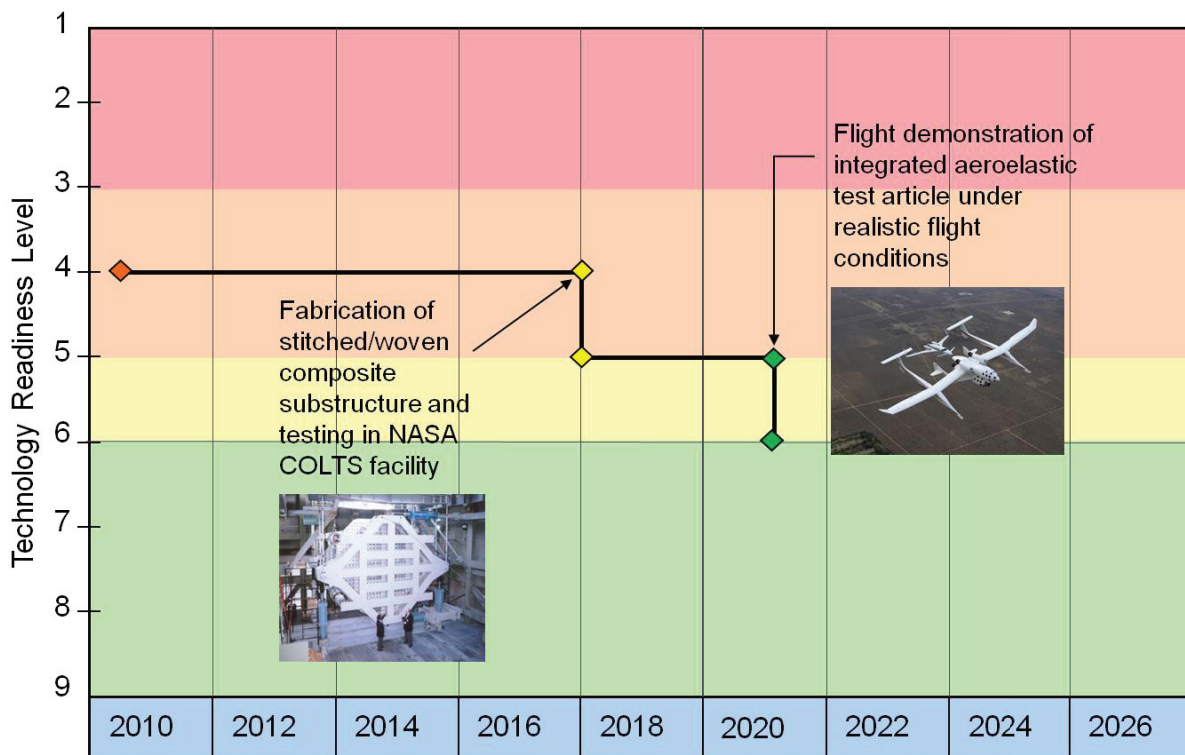


Figure 7-10. TMP for Large Integrated Structures

7.12 Aeroservoelastic Structures

The current TRL of commercially viable aeroservoelastic structures is estimated at 3 (Figure 7-11). Previous development of advanced state-space simulations, analysis methods, and flutter control law development should be leveraged to develop a simplified high aspect ratio wing design to be evaluated by testing of a cantilevered semispan wind-tunnel model. A static aeroelastic scaling of this subscale model should be sufficient for this activity. Moderate drag reduction and load control goals, with active or simulated sets of control surface deflections and twist, should be pursued. Comparison should be made to the best passive aeroelastic design candidate, in a similar lead-up testing effort, to quantify the risk and benefits of the active implementation over the passive tailored aeroelastic wing. Parallel refinement of requirements for an integrated system should be performed and incorporated into future model designs to a practical extent. By demonstrating adequate modeling and benefits, TRL 5 will be earned through a further design sophistication level, including a symmetry mounting condition with active and dynamic demonstration of load and drag effects, and integration into a status N+3 design candidate. Subsystem integration and laminar flow design integration should be demonstrated at a high level. Continued design tools development and increasing control-law study will culminate in reaching TRL 6 with a flight test article at realistic flight Reynolds numbers in a subset of the intended flight envelope.

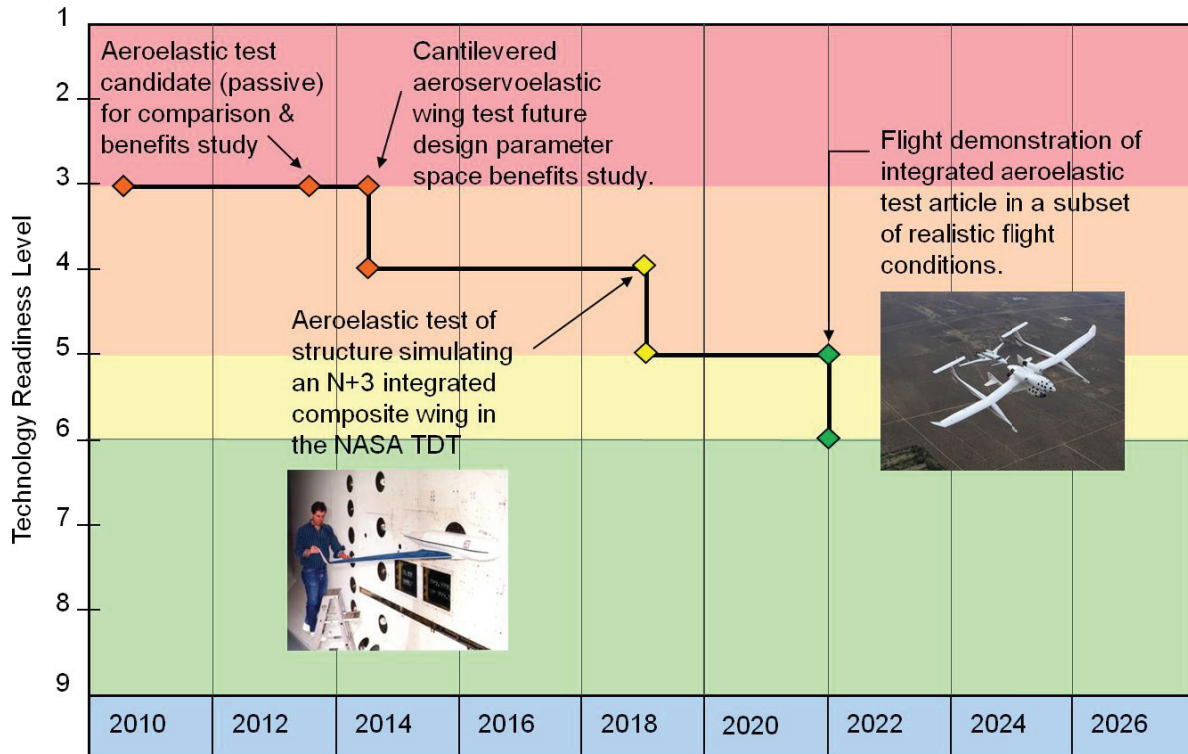


Figure 7-11. TMP for Aeroservoelastic Structures

7.13 Lightweight Fan Structure and Cowl

The design maturity of the lightweight fan structure and cowl is estimated at a current TRL of 3 (Figure 7-12). Preliminary design and analysis, including impacts on the isolated engine system in terms of weight, flowpath losses, external aerodynamic effects, and integration challenges, should be performed to raise the TRL to 4. CFD databases should confirm the design for a subset of driving parameters, and possibly include DOE to develop a response surface for interdisciplinary modeling. Some component development/modification to verify design assumptions should be performed for key elements, likely the AGB and fan cowl. TRL 5 should be reached by component demonstration on an available engine simulator with a reference nacelle design, indicating compatibility with an available gas generator, and proving predictions and limited integration challenges. Status goals should be achieved for the weights and flows at the design conditions, and at a limited set of off-design points. Advancement to TRL 6 should be made through a concerted design effort to establish the validity of an advanced prototype for performance and acoustic goals. Pylon integration should be investigated with a reference pylon, for impact on scrubbing losses, and aeroacoustics. A simulated full-scale engine test at static conditions will be the definitive ground performance assessment activity. Acoustic microphone measurements alongside plume diagnostics, along with the incorporation of a thrust stand will confirm performance predictions.

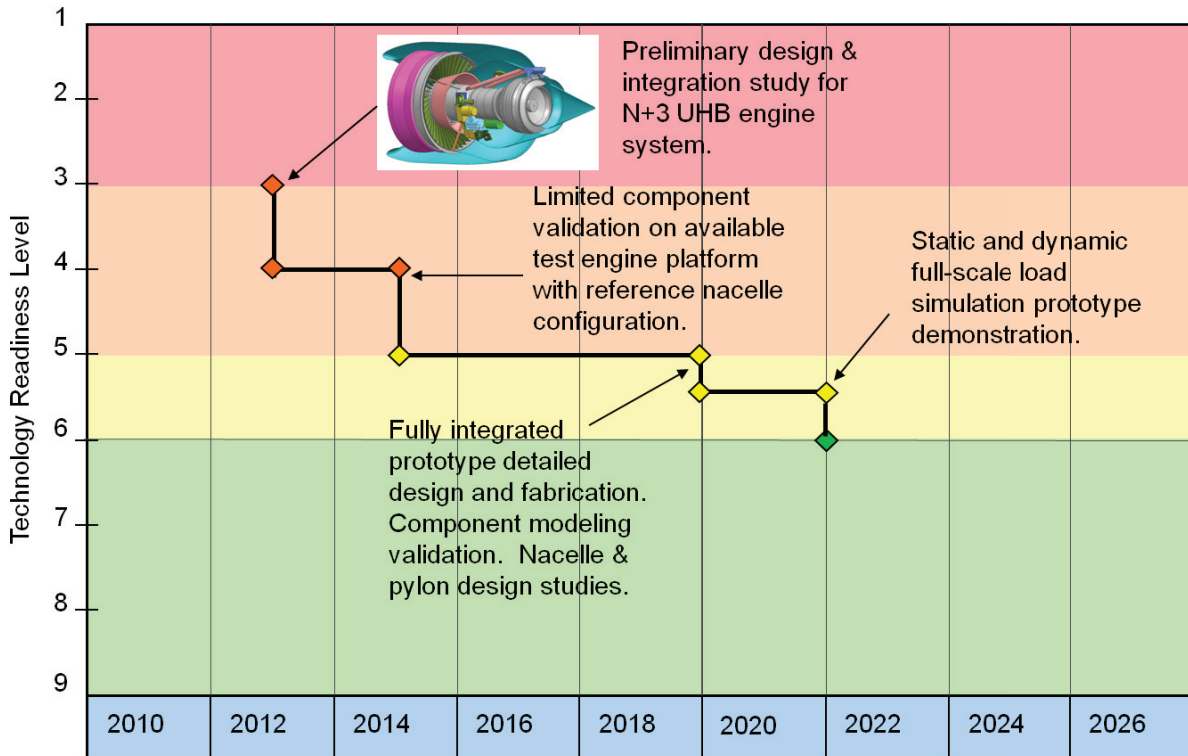


Figure 7-12. TMP for Lightweight Fan Structure and Cowl

7.14 Intercooled Compressor Stage

Compressor intercooling for high-OPR engines is estimated to be at a current TRL of 3 (Figure 7-13). Evaluation of subscale concepts to investigate pressure loss and cooling performance should be performed in the next several years. This should occur in simulated design flow (flow rates, pressure) conditions downstream of HPC installation to bring to TRL 4. CFD simulations should be carried out to understand pressure loss mechanisms and improve heat transfer rates. TRL 5 should be attained by installing a representative prototype intercooler into a temperature and pressure simulator rig, at large scale, to identify performance map across engine flow conditions of interest. Design should pursue appropriate goal weights. TRL 6 attainment should occur by a full-scale rig implementation in a high OPR (>50) core engine compressor simulator.

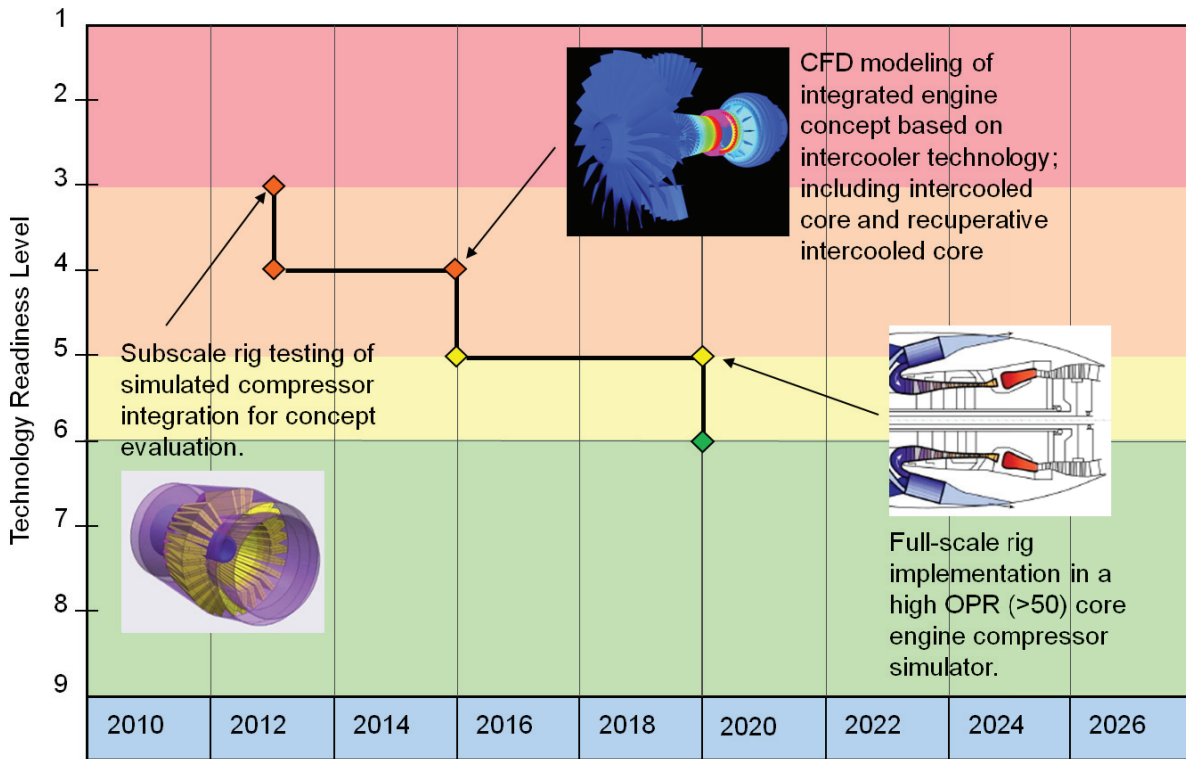


Figure 7-13. TMP for Intercooled Compressor Stage

7.15 Cooled Cooling Air

Cooled cooling air is currently estimated at a TRL of 5 (Figure 7-14). To advance to a TRL of 6, demonstration on an integrated, ground-based engine should be performed. Assessment of flow levels and heat exchanger pressure losses, with surrogate cooling fluids representative of cracked fuels (if none are available) should be performed. A low-loss, lightweight heat exchanger design should be validated as a key outcome.

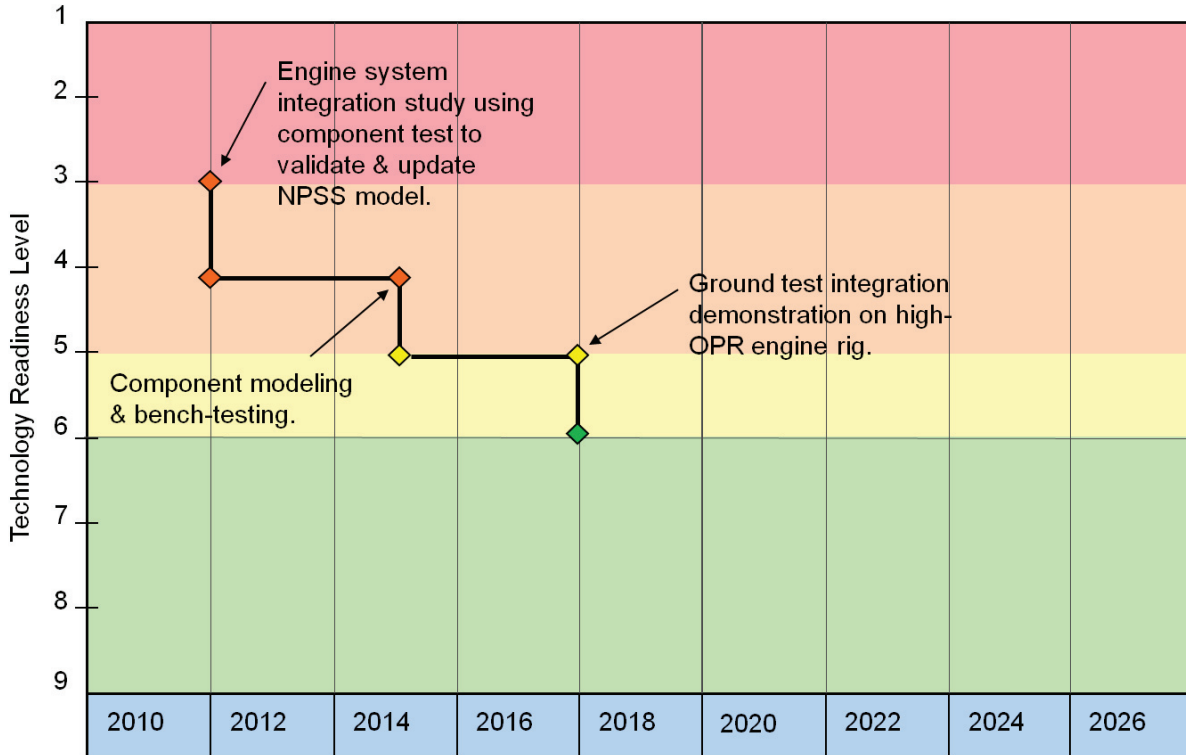


Figure 7-14. TMP for Cooled Cooling Air

7.16 Endothermic Fuel Cracking

The use of endothermic jet engine fuels as a physical heat-sink through a decomposition reaction to absorb sensible heat (“cracking”) is estimated at a current TRL of 3 (Figure 7-15). Developing an array of potential candidates of jet fuels in bench-test burners measuring heat sink capability and exothermic properties would elevate this technology to a TRL of 4. Simultaneous efforts to deoxidize the fuel and pursue other coke-mitigation strategies, although not detailed here, should be made to sufficiently reduce coke deposition due to the oxidation mechanism across the temperature range relevant to an inline turbofan fuel heat exchanger for cooled cooling air. To achieve TRL 5, demonstrating lean-burning fuels in representative conditions of critical design points (takeoff, cruise) in the laboratory setting would be required, while maintaining acceptable increases in heat-sink capabilities over conventional hydrocarbon jet fuels. Complete emission studies should be performed to characterize the reactions and provide detailed data for kinetic reaction models. To reach TRL 6, application to an advanced burner configuration, confirming both low NO_x production and high heat-sink capability must be demonstrated, while simultaneously confirming low coking.

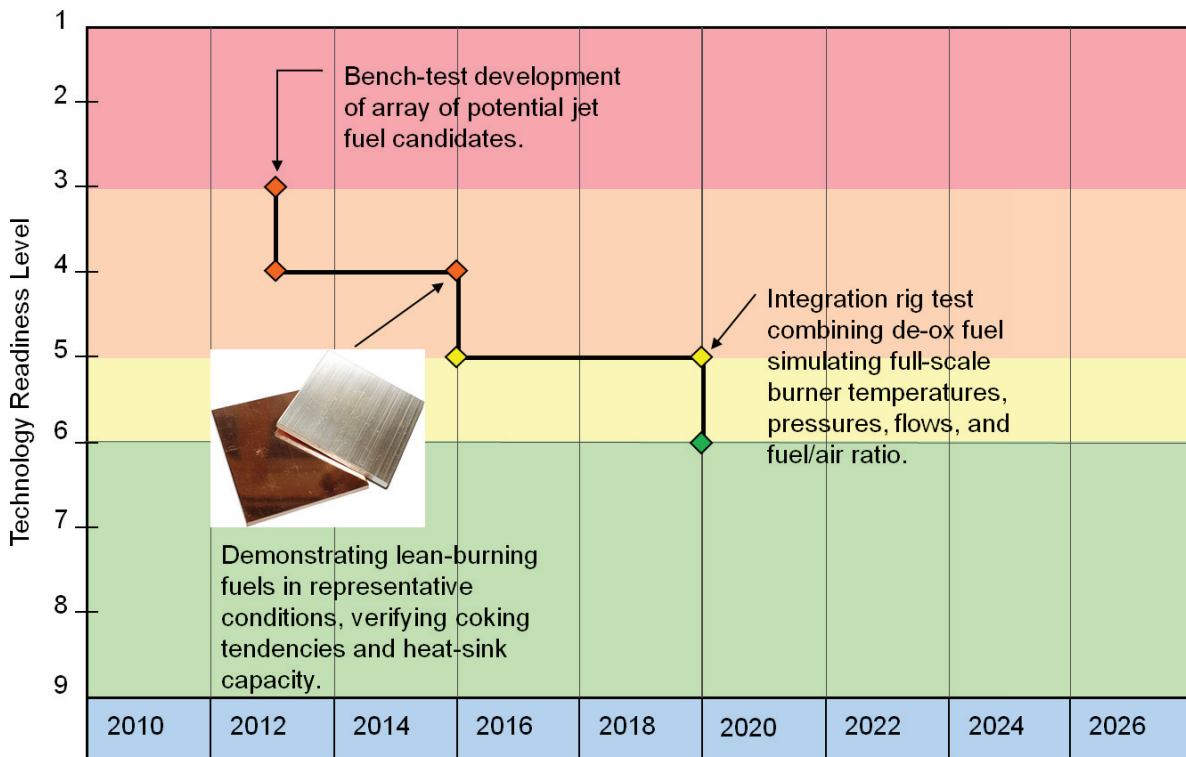


Figure 7-15. TMP for Endothermic Fuel Cracking

7.17 Lean-Burn Staged Combustion Liner

This technology item, estimated at a current TRL of 5, is a technology synthesis of staged combustion (TRL 6) as well as the CMC burner liner (TRL 5) required to allow operation of the staged combustor at cruise conditions in a well-mixed injection state to promote lower NO_x. Thus development of the CMC liner technology should occur in parallel with this activity so that the design for staged combustion, which will allow huge NO_x reductions across the power setting range, can assume CMC availability (Figure 7-16). To raise the staged combustion design to TRL 6, several steps should occur to validate the components in an increasing level of combined system complexity, eventually culminating in a demonstration involving lean direct-injection, staged combustors in an optimized geometric configuration and count, and using a CMC burner prototype. The first activity should be the design and test of injector concepts for use in staged combustion on a flame tube to validate the design and also investigate the compatibility with alternative fuels. This level of component test is deemed a higher TRL than similar N+3 TMP activities due to the extensive investigation performed under the DOE Advanced Turbine Systems program. The next development activity should use the diagnostics data from the previous study to evaluate performance on a two-cup sector test at high OPR with focus on integration, ignition, lean blowout, and sub-idle efficiency. A CMC liner should be demonstrated at this phase in a follow-on activity prior to larger-scale or subsystem evaluations. Finally, TRL 6 will be reached by demonstrating a well-integrated design in a scale engine simulator near design OPR and at off-design conditions. A CMC liner integration should be included at this stage to verify the wall-cooling flow requirements and integration with the staged injectors.

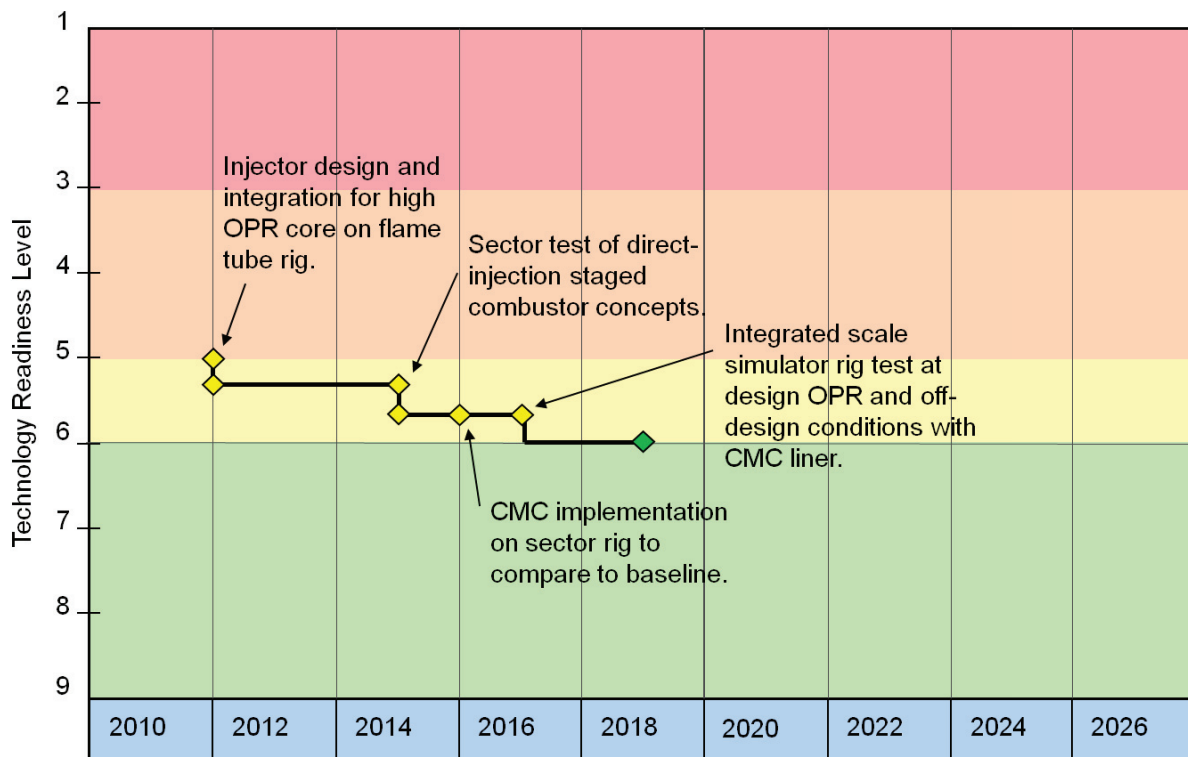


Figure 7-16. TMP for Staged Combustion

8 CONCLUSIONS AND RECOMMENDATIONS

A conceptual commercial passenger transport study was performed to define a single vehicle capable of meeting the future demands of entering into market service in the 2030-35 timeframe. The primary vehicle requirements that drove technology selection, configuration selection, and optimization were derived from the published NASA N+3 goals. These goals were further refined based on context derived from an overarching future scenario that captured likely future economic and operational factors suggesting that fuel burn and NO_x emissions would be primary market drivers in this timeframe. Simulations of the vehicle in the National Airspace with the implementation of NextGen air traffic management capabilities were used to provide additional requirements on vehicle sizing by investigating the impact of the metroplex operations model to projected traffic levels. Results of this study suggested that a 5,000 ft runway capability would be sufficient to leverage existing reliever airports and meet the demands of future air traffic. Furthermore, the inclusion of aircraft with reduced cruise speed would not hinder the predicted air traffic, while achieving better levels of specific fuel consumption. This paradigm shift towards a slower commercial transport at higher altitude is a key driver towards reaching the fuel burn objectives of the N+3 generation of aircraft.

A single design that best fills a broad, primary market need for 2030-2035 entry-into-service was developed after considering various combinations of technology suites, revolutionary and traditional configurations, and requirements trades. This design is characterized by an advanced technology tube and wing configuration with a three-shaft advanced technology turbofan. The resulting aircraft achieves a 64% reduction in fuel burn, a 70 EPNdb reduction in noise, and a 91% reduction in NO_x when compared to a reference aircraft incorporating technologies representative of aircraft in service in 2010. Field performance for this preferred concept enables operation from metroplex airports.

Technologies targeting engine performance and vehicle empty weight were most beneficial in reducing fuel consumption. Estimates for structural weight reductions in the N+3 timeframe led to configurations in which the takeoff gross weight is constrained by passenger count, equipment, and furnishings. This result suggests targets for future weight reduction strategies. While the primary scenario-weighted N+3 metrics were determined to be fuel burn and emissions, it must be noted that realistically cost is a major driver in aircraft design. While structural technologies can permit access to higher aspect ratios than have been seen in the past, the weight increases accompanying larger wings will also drive cost. Hence, the aircraft that burns the least fuel will, in all likelihood, not be the least expensive aircraft.

Noise was found to be dominated by fan sources and landing gear. To mitigate these sources, two degree-of-freedom liners were applied to address fan noise, and landing gear fairings targeted the gear source. In order to take advantage of swept-wing laminar flow, leading edge slat technology had to be excluded at the expense of takeoff aerodynamics. However, the removal of slat noise drove down airframe noise appreciably. With the preferred configuration, approach noise seems to be the dominating contributor to overall EPNL.

A large contributor to reducing fuel burn was the three-shaft advanced technology turbofan engine. Driving high propulsive efficiencies with its ultrahigh-bypass ratio and thermal efficiencies with its high overall-pressure ratio, the engine achieved specific fuel consumption levels that were fractions of those realizable in modern engine technology. This engine also employs a suite of advanced propulsion technologies, including CMC turbine blades, compressor intercooling, and active compressor clearance control.

Ever more stringent emissions requirements have been addressed by the use of staged combustion technology. Through work at Rolls-Royce Liberty Works, in conjunction with NASA Glenn Research Center, this technology has been demonstrated to lead to significantly reduced NO_x emissions. This is accomplished by optimizing the burner for lean combustion at multiple flight conditions, including low

power settings during which the bulk of LTO NO_x is formed. In addition, this configuration allows for enhanced lean blowout and ignition characteristics.

A promising technology to reduce fuel burn was the open rotor engine. However, when compared on the basis of a system effectiveness rating, it was determined that the open rotor would earn its way onto the aircraft only if it was marginally louder than the three-shaft turbofan. With limited experimental acoustic research available on the topic of open rotor noise, a conservative assumption was made that its noise characteristics will be louder than the three-shaft turbofan. However, this critical assumption requires validation, and it is recommended that further research be conducted in an attempt to quantify the noise associated with this type of propulsion system. Through computational fluid dynamic modeling and noise source quantification, acoustic propagation analysis can predict the cumulative noise associated with this type of engine. In this manner, a more definitive comparison can be made between the open rotor and three-shaft turbofan engines, and the configurations they drive.

Significant reduction in empty weight was a key contributor to reduced fuel burn. The most promising structural technology is the M5 ultrahigh-performance fiber. Because of the potential empty weight reduction of the aircraft stemming from the implementation of this material, exploratory studies are recommended with the goal of developing sizeable panels. This type of feasibility study could go far towards realizing the empty weight savings possible through the development of advanced materials. Other high impact structural technologies included aeroservoelastic structures and advanced metallic alloys, whose development is expected to involve less commercial risk than M5.

Trade studies showed that there are complications to achieving significant laminar flow. Maintaining a smooth leading edge conducive to laminar flow precludes the use of conventional leading edge devices for high lift. The removal of a leading edge slat and reshaping of the airfoil for laminar flow must be compensated with some degree of leading edge flow control or morphing structure to prevent the wing from having to be oversized to meet takeoff requirements. These complications appeared to be more challenging for a hybrid wing body configuration. Steady or unsteady leading edge stagnation point blowing has been shown in a few studies to result in improved maximum lift coefficient and stall angle. This technology is recommended for further experimental work to complement ongoing laminar flow research.

Overall, this conceptual design study shows that significant progress is achievable for designing and building aircraft to meet the needs of the 2030-2035 time frame. Technology can be applied to make a more socially and environmentally responsible air transportation system that meets the needs of the future. Technology roadmaps show a logic path forward to develop the technologies to enable this level of achievement. Northrop Grumman looks forward to being a partner with NASA in the innovation, development, and demonstration of these critical technologies.

Appendix A

Airframe Selections

Appendix A Airframe Selections

A.1 Airframe Technology Selections

Airframe Concept #1.01	Advanced Metallic Structural and Sub-System Alloys
Airframe Concept #1.02	Fiber Metal Laminates
Airframe Concept #1.03	Metallic Digital Direct Manufacturing
Airframe Concept #1.04	Structural Materials Laser Surface Treatment
Airframe Concept #1.05	3-D Woven/Stitched Composites
Airframe Concept #1.06	M5 Ultrahigh-Performance Fiber
Airframe Concept #1.07	Light-Weight Foamed Composites
Airframe Concept #1.08	Conformal Load-Bearing Antenna Structures
Airframe Concept #1.09	Integrated Aeroservoelastic Structures
Airframe Concept #1.10	Open-Celled and Stamped Composite Structures
Airframe Concept #1.11	Post-Buckled Composite Structures
Airframe Concept #1.12	Affordable Airframe Large Integrated Structures
Airframe Concept #1.13	Direct Manufacturing/Laser Sintering of Polymeric Materials
Airframe Concept #1.14	Carbon Nanotube (CNT) Electrical Cables

A.2 Aerodynamic Technology Selections

Aero Concept #2.01	Steady Fluidic Separation Control
Aero Concept #2.02	Synthetic Jet Separation Control
Aero Concept #2.03	Upper Surface Exhaust Nozzle and Flap
Aero Concept #2.04	Fluidic Thrust Vectoring for Upper Surface Exhaust Nozzle and Flap
Aero Concept #2.05	Lower Surface Exhaust Nozzle and Flap
Aero Concept #2.06	Distributed Exhaust Nozzle and Flap
Aero Concept #2.07	Steady Circulation Control
Aero Concept #2.08	Unsteady Circulation Control
Aero Concept #2.09	Swept-Wing Laminar Flow
Aero Concept #2.10	Riblets and Microvortex Generators
Aero Concept #2.11	Active Drag Reduction
Aero Concept #2.12	Modeling for Inlet Optimization
Aero Concept #2.13	Inlet Flow Control (Microvortex Generators, Jets, etc.)
Aero Concept #2.14	Channel Wing

A.3 Noise Technology Selections

Noise Concept #3.01	Distributed Exhaust Nozzle (DEN)
Noise Concept #3.02	Shielding (Fan, Jet, other Propulsive Sources)
Noise Concept #3.03	Chevrans
Noise Concept #3.04	Ejectors
Noise Concept #3.05	Fan Blade Sweep Design
Noise Concept #3.06	Fan Blade Flow Control
Noise Concept #3.07	Geared Turbine
Noise Concept #3.08	Variable Geometry Nozzles
Noise Concept #3.09	Porous Plug Designs
Noise Concept #3.10	Aerothermodynamic Concepts (Inverted Flow Nozzle, Thermal-Acoustic Shield)
Noise Concept #3.11	Ultra-High Bypass Turbofans
Noise Concept #3.12	Acoustic Excitation
Noise Concept #3.13	Curved, Scarfed Inlet Ducts
Noise Concept #3.14	Moveable Winglets
Noise Concept #3.15	Deployable Vortex Generators
Noise Concept #3.16	Brush-type Trailing Edges
Noise Concept #3.17	Trailing Edge Serrations
Noise Concept #3.18	Porous Flap Side Edges
Noise Concept #3.19	Flap Tip Fences
Noise Concept #3.20	Slat Trailing Edge Serrations
Noise Concept #3.21	Slat Cove Fillers
Noise Concept #3.22	Slat Gap Liners
Noise Concept #3.23	Porous Slat Pressure Surfaces
Noise Concept #3.24	Slat Tip Fences
Noise Concept #3.25	Continuous Mold-Line Linkages
Noise Concept #3.26	Streamlined Slat Tracks
Noise Concept #3.27	Micro-tab Features
Noise Concept #3.28	Wing Morphing (Shape Memory Alloys, Piezoelectrics)
Noise Concept #3.29	Active Noise Cancellation
Noise Concept #3.30	Landing Gear Assembly Fairings
Noise Concept #3.31	Landing Gear Assembly Component Integration
Noise Concept #3.32	Wheel Caps
Noise Concept #3.33	Wheel Gap Filler
Noise Concept #3.34	Landing Gear Assembly Plasma Fairings

Noise Concept #3.35	Linear Acoustic Liner
Noise Concept #3.36	Single Degree-of-Freedom Liner
Noise Concept #3.37	Double Degree-of-Freedom Liner
Noise Concept #3.38	Multiple Degree-of-Freedom Liner
Noise Concept #3.39	Metal Foam Liner
Noise Concept #3.40	Nanotube Liner

A.4 Propulsion Technology Selections

Prop Concept #4.01	Conformal Polymer Solar Cell Power Augmentation
Prop Concept #4.02	Constant Volume Combustion/Wave Rotors
Prop Concept #4.03	Plane Jet Combustion
Prop Concept #4.04	Swept Fan Outlet Guide Vanes
Prop Concept #4.05	Open Rotor with Counter-Rotating Fan Blade Rows
Prop Concept #4.06	Electric Subsystems
Prop Concept #4.07	Oil-Less Engine
Prop Concept #4.08	Boundary Layer-Ingesting Inlets
Prop Concept #4.09	Embedded/Conformal Inlets
Prop Concept #4.10	Thrust Vectoring Nozzles
Prop Concept #4.11	Thrust Vectoring Open Rotor
Prop Concept #4.12	Alternative Hydrocarbon Biofuels
Prop Concept #4.13	Compressor Flow Control
Prop Concept #4.14	Third Engine Stream
Prop Concept #4.15	Lightweight Fan Structure and Cowl
Prop Concept #4.16	Low Tip Speed Counter-Rotating Ducted Fan
Prop Concept #4.17	Four-Shaft Turbine
Prop Concept #4.18	Active Compressor Clearance Control
Prop Concept #4.19	Combined/Compound Cycles
Prop Concept #4.20	Turbo-Electric Distributed Fans
Prop Concept #4.21	Fuel Cell APU
Prop Concept #4.22	Hybrid All-Electric Propulsion
Prop Concept #4.23	TO/C-Assist Propulsion Unit
Prop Concept #4.24	Variable Pitch Fan Blades
Prop Concept #4.25	Cryogenic Motors
Prop Concept #4.26	Intercooled Compressor Stages
Prop Concept #4.27	Porous Ceramic Materials
Prop Concept #4.28	Low-Noise Fan Blades

Prop Concept #4.29	Combined Steam Cycle
Prop Concept #4.30	Ceramic Matrix Composite Turbine Blades
Prop Concept #4.31	Water Injection
Prop Concept #4.32	Staged Combustors
Prop Concept #4.33	NonTurbine Distributed Fans
Prop Concept #4.34	All Electric (no AGB)
Prop Concept #4.35	Turboshaft-Powered Direct-Drive Distributed Fans

Appendix B

Technology Dispositions

Appendix B Technology Dispositions

B.1 Constant Volume Combustors/Wave Rotors

Constant volume combustion (CVC) engines use the detonative mode of combustion to access higher thermal (and overall) engine efficiencies [Ref. 104]. Inherent unsteadiness in the detonation process makes it difficult to capitalize on the theoretical performance and emissions benefits associated with this type of engine. CVC engines will typically have a large number of independently controlled detonation tubes. Constant volume combustion/wave rotor engines could be incorporated as augmenters to current turbofan technologies, or as stand-alone propulsion systems. In either case, their integration into an aircraft will be extremely complex and system-dependent. Potential benefits include reduced fuel consumption, driven by increased thermal efficiency, and reduced emissions due to short residence times associated with the detonation process [Ref. 105]. Penalties include increased engine complexity, potential for increased noise due to unsteady shock waves, and structural considerations due to impulsive shock loading of the engine nozzle.

Theoretical thermodynamics show a monotonic decrease in SFC benefit as overall pressure ratio increases [Ref. 104]. As such it was determined that for the size of engine under investigation in this study, CVC technology was not applicable, and could not be utilized to its full potential. This, combined with a low TRL, currently estimated to be 2, resulted in CVC/wave rotor technology not being considered for further investigation.

B.2 Turboelectric Distributed Fans

This type of engine architecture uses the core of a gas turbine engine to supply power to a generator, which in turn supplies power to a series of motors. These motors then drive propulsors, which may be distributed in any functional configuration around the airframe. This distributed propulsion system would ideally be combined with embedded, boundary-layer ingesting inlets to minimize the acoustic signature of the aircraft. Distributed propulsion can be used to create a more uniform velocity profile behind the vehicle, reducing drag and increasing propulsive efficiency [Ref. 106]. Theoretically, the gas turbine core can be driven at its optimum cycle point to minimize fuel consumption while supplying power to the generator. Electric drive trains offer improved energy efficiency over mechanical drive trains, along with greater system flexibility and lower system stress. The electric drive train would convert the mechanical energy from the engine to electrical energy through the integration of a high-speed generator, which would supply electricity to the distributed fans and other vehicle systems through the use of superconductors and power converters. According to a NASA presentation by Brown, current power converters/inverters operate at 95% efficiency, and are targeted to reach 99.8% efficiency [Ref. 107]. However, replacing the direct shaft connection between the gas turbine core and the propulsor with a generator and motor will always lead to a heavier propulsion system. This is especially true in light of the power densities of motors and generators required to make this system practical. In the coming decades, superconducting motors and generators can be utilized with larger power densities; however, such components require cooling systems, which in turn add additional weight to the system.

Currently estimated at a TRL of 2, this technology has been deemed to be unrealistic in the N+3 timeframe due to the complexity of the propulsion architecture, and the requirement for the more advanced components that comprise it.

B.3 Turboshaft-Powered Direct-Drive Distributed Fans

Turboshaft-powered direct-drive distributed fans use a single or multiple engines to provide power for up to four propulsors per engine. The enables ultrahigh-bypass engine performance, and allows core components to operate more ideally. This would be used with a partially- or fully-integrated propulsion

system. Multiple fans increase system redundancy, improving safety. This concept has also been suggested to be integrated for boundary layer ingestion, noise reduction, and high lift systems. As mentioned previously, distributed propulsion can be used to create a more uniform velocity profile behind the vehicle, reducing drag and increasing propulsive efficiency [Ref. 108].

Turboshaft-powered direct-drive distributed fans use a mechanical drive train instead of electric. The mechanical drive train employs several driveshafts and gearboxes to transfer energy from the engine to the distributed fans. A mechanical drive train in a dual-fan gear system shows 94% efficiency between the power of the fan and the power of the engine [Ref. 107]. Disadvantages of turboshaft-powered direct-drive distributed fans include a weight penalty over conventional propulsion configurations. An electrical driveshaft configuration would have increased weight over its mechanical counterpart due to the need for generators, motors, inverters, coolers, and the rest of the superconducting system [Ref. 109]. Both systems would add increased complexity to airframe configurations, propulsion, and integration.

Currently estimated to be TRL 2, this technology was not considered for further investigation due to its being out of scope of the N+3 timeframe.

B.4 Nonturbine Distributed Fans

Nonturbine distributed fans use distributed propulsion to achieve efficiency and drag benefits discussed for Turboshaft-Powered Direct-Drive Distributed Fans. The previous distributed propulsion technologies have a central engine to supply power to an array of fans, whereas the nonturbine distributed fan configuration uses separate independent power systems for each distributed fan. This allows for flexibility in the propulsive system, and allows for the use of alternative power systems or cycles. Diesel or biodiesel fuels could be used to reduce NO_x emissions. Nonturbine distributed fans enable configuration flexibility through the use of shielding and placement. However, this propulsive configuration would add a significant amount of complexity to both the vehicle and propulsion systems, as well as require the propulsive system to be partially or fully integrated with the airframe.

Currently estimated to be TRL 2, this technology was not considered for further investigation due to being out of scope of the N+3 timeframe.

B.5 Hybrid All-Electric Propulsion

Compared to other forms of hybrid propulsion, the all-electric version replaces the power source from the turbojet core to fuel cells, chemical batteries, solar cells, or any combination of electric-power generating options. Because these types of propulsion systems depend on propeller fans to generate thrust, noise is reduced dramatically. Depending on the power source, the remaining effects on the N+3 metrics varies, as do the system penalties. Driving the system with chemical batteries, for instance, simplifies the system tremendously; however, the weight of chemical batteries becomes prohibitive. The introduction of a fuel cell bank as the power source drives down LTO NO_x emissions, but adds the complexity of additional components. For example, in order to supply the fuel cell with oxygen, a compressor and motor are needed. Furthermore, depending on the type of fuel cell, it may be necessary to include a jet fuel reformer or a supply of liquid or gaseous hydrogen. Of course, gaseous hydrogen storage is dangerous, and requires a large storage tank, and liquid hydrogen brings along with it the requirements of a refrigeration system. All forms of electric propulsion will also necessitate a power management and distribution system, with batteries to supplement the system and act as backup power supply. The benefit of all-electric propulsion is realized in the fuel reduction capability of the technology; however, the power requirements for takeoff drive the sizes of the components to infeasible proportions.

For this reason, combined with the currently estimated TRL of 2, this type of propulsion system has been set aside as an impractical technology that will not be mature enough for aircraft applications in the N+3 timeframe.

B.6 Inlet Flow Control (Microvortex Generators, Jets, etc.)

Several inlet optimization techniques exist for improving inlet flow field and conditions for inlets that are in, or near, the boundary layer. Recirculating fan bleed systems divert a portion of fan exit flow back to the inlet to increase the momentum of the boundary layer. This creates a more favorable boundary layer profile and a more uniform flow field, reducing distortion and preventing flow separation. Similarly, suction systems involve bleeding air from the inlet through the use of a porous surface in the region of a momentum-deficient boundary layer to prevent flow separation in embedded, blunt, and poorly-conditioned inlets. If the configuration allows, the inlet may be designed such that no inlet flow control is necessary. However, if the configuration is complex and volume is limited, a highly conformal inlet that is susceptible to flow separation or high levels of distortion may be necessary.

Vortex generators require no engine bleed, and can be effective in reducing face distortion and preventing flow separation. Vortex generators create turbulent flow in the boundary layer, aiding in the formation of a more favorable boundary layer and increasing pressure recovery. In a study by Jirasek, vortex generators were found to have a maximum of 1.95% increase in pressure recovery. Vortex generators would result in a very small weight penalty [Ref. 110].

The pressure recovery associated with blowing and suction systems has the potential to be significantly higher than that of vortex generators, depending on the extent of integration and the level of blowing/suction. Engine performance gains bought through increased pressure recovery must be balanced against the penalties associated with engine bleed. Both blowing and suction flow control systems would result in a weight penalty, as complex ducting would be required, as opposed to vortex generators, which would result in a negligible weight penalty and require no engine bleed. None of these technologies would be required on a subsonic podded engine configuration, as extremely high inlet pressure recoveries are already achievable.

The TRL varies per individual flow control technology. Due to the weight penalty associated with ducting, and the propulsive efficiency penalties due to engine bleeding, the flow control methodologies of recirculating fan bleed, blowing and suction, and inlet vortex generators were not investigated further. Inlet flow control was not considered for further investigation due to the vehicle operating in sub-sonic conditions which eliminates the formation of shocks in the inlet and therefore the need for a robust flow control system, such as blowing or suction.

B.7 Wing Morphing (Piezoelectrics, Shape Memory Alloys, etc.)

Wing morphing entails the ability to alter the shape of the wing, including aspect ratio, sweep, or airfoil design. Morphing allows for achievement of the optimal lift-to-drag ratio for each segment of the flight envelope by morphing the wing into the most optimized configuration. Wing morphing can be achieved through several systems, including pneumatics, shape memory alloy-based actuators, and piezoelectrics. These systems would be distributed throughout the wing surface, or in the sub-structure of the wing. Such systems would increase wing weight and complexity to the wing cavity, as well as remove wing volume that could be used for fuel storage.

Wing morphing can be achieved by autonomously varying the camber of the wing through the use of flaps and symmetric aileron deflection, while flying away from the design condition. Because commercial aircraft spend the majority of flight time in cruise, there is little benefit to optimizing the wing geometry for climb and descent when considering the weight penalties involved. This technology would be more applicable to vehicles with varying flight conditions such as military aircraft that might have dash, loiter, and air-to-air engagement as part of their mission.

The TRL varies per wing morphing technology. Due to these reasons discussed above, wing morphing was not further investigated.

B.8 All Electric (No Accessory Gear Box)

Accessory gear boxes (AGBs) are currently used to convert mechanical energy from the engine into electrical energy from generators to be used by various subsystems of the vehicle, such as an AC alternator, DC starter, generator, and various pumps. Integration of electrical generators into the engine would eliminate the requirement for an AGB. Current AGBs are attached near the bottom of the engine, driving nacelle geometry to accommodate this added volume, and causing the nacelle to be wider and asymmetric. Removal of this component would lead to a more symmetric design, and reduced nacelle size, reducing drag and weight. If takeoff gross weight, fuel load, and wave drag are held constant, removal of the AGB could lead to a 0.6% increase in range and a 0.37% reduction in gross weight [Ref. 111]. Holding range constant, this would result in reduced fuel burn. If the vehicle were resized after the AGB removal, weight and fuel burn reductions would only increase.

Currently estimated to be TRL 3, this technology was not considered for further investigation due to marginal improvements and incompatibility with the lightweight fan structure and cowl design.

B.9 Structural Materials Laser Surface Treatment

Advanced materials laser surface treatment uses a process known as laser peening, or laser shock peening. This process hardens metallic surfaces through the use of a powerful laser. Laser peening creates a highly compressible surface residual stress, which greatly improves structural properties, fatigue resistance, and life. This technology can be used to prevent stress corrosion cracking, overall corrosion, and pitting. Laser peening has demonstrated a smooth surface finish and good process control through testing and production. A laser is fired at a material that is covered with a dark coating, which absorbs the laser energy. The energy causes the coating to explode and produces a shock wave that propagates into the material, creating an array of compression indentations. This process is repeated until the entire desired area is treated. Laser peening has been, and is currently, demonstrated in industry with no known in-service problems. This technology is in full commercial production on two continents, including utilization in the F-22, P-3, and KC-10, as well as the Boeing 777, A340-500, and -600. The new Boeing 787 uses laser peening on its Rolls-Royce Trent engine line, and has shown significant lifetime enhancement against failure and stress corrosion cracking. It was found, however, that laser surface treatment is not used for structural weight savings, but only to improve fatigue resistance and material life [Ref. 112].

Currently estimated to be TRL 5, this technology was not considered for further investigation due to having no significant vehicle weight, noise, or emissions benefits.

B.10 Lightweight Foamed Composites

Lightweight foamed composites are comprised of a sandwich structure with foam filler, based off nickel crystal polymer foam. Lightweight foamed composite has promising ballistic qualities, as well as being easy to machine. The advantages of foam include increased corrosion resistance and insusceptibility to water damage, giving it advantage over honeycomb core. Isotropic properties of foam enable increased durability. Lightweight foamed composites are seen as potential replacements for secondary structures that use honeycomb sandwich structures, including luggage bins, galley lower-wall panels, and ceiling panels. Based on internal analysis, foam core composites offer a lower strength-to-weight ratio compared to metallic and nonmetallic honeycomb core structures. However, as stated previously, foam core composites offer dimensional stability and increased durability, and may potentially leading to weight savings in select secondary structures.

Currently estimated to be TRL 4, this technology was not considered for further investigation due to its small projected weight benefits.

B.11 Unsteady Circulation Control

Unsteady circulation control is a subset of circulation control wing technology using pulsed jets of air, requiring less engine bleed, and reducing drag compared to steady circulation methods. This technology can enable short takeoff and landing distances, thus allowing for the down-sizing of lifting surfaces. Pulsed pneumatics are used to cyclically blow a sheet of air over a rounded trailing edge, taking advantage of the Coanda effect to delay separation of flow on the airfoil with extended flaps. Pulsed blowing effectiveness is largely dependent on the efficiency of the actuator system, as well as the response of the internal volume of gas prior to the jet exit. Ideal pulsed blowing requires a square waveform in wave response. However, as the complexity of the actuator system increases, this ideal waveform becomes more difficult to achieve. In addition, as the frequency of pulsing increases, blowing distortion increases, limiting the mass flow through the jet exit. At a duty cycle of 20%, unsteady circulation yields a lift coefficient increment of approximately 1.0. An equal lift coefficient with steady circulation requires approximately 92% more mass flow. At a fixed mass flow rate of 25 SCFM, the unsteady circulation control configuration yielded a 35% increased lift coefficient compared to the steady circulation control configuration [Ref. 113]. Weight penalties or benefits are configuration-dependent.

Currently estimated to be TRL 2, this technology was not considered for further investigation due to its low TRL, combined with the result that traditional high-lift systems proved sufficient for this study.

B.12 Water Injection

This technology entails injecting high-pressure water into the combustor in order to decrease flame temperatures. Associated NO_x emissions decrease due to the drop in combustion temperature. However, in the limit of excessive water use, less fuel will burn, and soot may form, affecting the performance of the combustor. This has been shown in computational studies performed by Fan et al [Ref. 114]. Water injection needs to be incorporated into a combustor in the design phase; retrofitting would be extremely difficult. In the implementation of this technology, the propulsion system requires that water be transported on the aircraft, as well as the associated injection mechanisms and control systems.

Although it is currently evaluated at a TRL of 6, it has been deemed unnecessary to achieving the NO_x goals of the N+3 study, in light of the success of the lean combustor technology outlined in Section 5.3.3.18.

B.13 Variable Pitch Fan Blades

Controlling the pitch of fan blades would allow for the optimization of the fan pressure ratio at various operating conditions. This capability could remove the need for a thrust reverser and reduce windmilling drag [Ref. 115]. The incorporation of variable pitch fan blades would depend heavily on the methodology employed to generate the variable pitch. Any system that can control the geometry will add weight to the overall engine system. While experimental studies have shown that variable pitch fans can exhibit higher efficiencies than fans with variable inlet guide vanes, the mechanism to control the fan blade pitch would need to be compact enough to fit inside the fan hub [Ref. 116].

Currently estimated at TRL 5, this technology has potential to mature in the N+3 timeframe, but the necessity for the efficiency gains is outweighed by the complexity and weight of the system.

B.14 Fuel Cell Auxiliary Power Unit

A fuel cell auxiliary power unit (APU) would be used as a replacement for the current turbine-powered APU. When a vehicle is on the ground, and engines are off, vehicle power is supplied by the APU. Vehicles that spend a significant amount of time on the ground would see a significant fuel burn reduction from improvement in APU efficiency [Ref. 117]. The fuel cell APU uses hydrogen fuel in an electrochemical process to generate electricity. Due to integration constraints, hydrogen tanks are not

easily integrated or desirable, leading to the requirement of a jet fuel reformer. Historically, fuel cells have been extremely heavy, large in volume, and have demonstrated low power density. These properties have seen significant improvements in the past 30 years, and continue to improve.

The use of a fuel cell APU in flight would improve engine efficiency and reduce fuel consumption by unloading a portion of the electrical load on the engines [Ref. 118]. Current aircraft are approximately 40-45% efficient in converting fuel to electrical energy in the engine through a turbine, while fuel cell APUs can be up to 75% efficient in converting fuel to electricity during cruise. This increase in efficiency, and the relieving of portions of the electrical load from the engines, has been estimated to burn 40% less fuel in cruise for the purpose of producing electricity. However, it must be noted that the fraction of fuel used to produce electricity during cruise is minimal with respect to total aircraft fuel burn.

Currently estimated to be at a TRL of 4, the fuel cell APU was not investigated further due to its low TRL, and the relatively low impact the technology would have on fuel reduction for the given mission.

B.15 TO/C-Assist Propulsion Unit

Takeoff and climb assist propulsion units are systems designed to enable STOL capabilities. Detachable autonomous propulsion units attach to the vehicle, and assist the aircraft during takeoff and climb. Upon reaching cruise altitude, the propulsion units detach and return autonomously to the airport. High-lift systems typically add weight and increase cruise drag while greatly improving field performance. This technology would enable the high lift benefits without the cruise drag or weight penalties. However, incorporating detachable autonomous propulsion units would add complexity to vehicle design, and increase the complexity of air traffic control, as propulsion units would need to be tracked and directed appropriately. In addition, they would increase the time and complexity of ground operations for maintenance, retrieval, and attachment of propulsion units prior to takeoff. Propulsion units that are expendable, jet-fueled assisted takeoff (JATO), could be considered, as such systems exist on many missiles, rockets, and targets. However, retrieval of units must be taken into consideration, as well as their impact on the surrounding air and ground space.

Currently estimated to be TRL 1, this technology was not considered for further investigation due to traditional high-lift systems proving sufficient in this study, it's extremely low TRL, and the added complexity to air traffic control operations, ground operations, and vehicle configuration.

B.16 Microvortex Generators and Riblets

Microvortex generators and riblets use passive means to affect the basic aerodynamics of the vehicle. Advances in CFD, nano-manufacturing, and greater understanding of boundary layer physics may soon enable the complete control of the aircraft flow field. Passive techniques such as riblets and microvortex generators do not require on-board support for power and pneumatics. Combining two or more passive drag reduction technologies could provide a multiplying effect. Riblet technology has demonstrated drag reduction, and tailored porosity, combined with riblets, is forecasted to enhance drag reduction. Riblets are designed for a single point design and can theoretically reduce friction drag by 8% at that point design. At off-design points, the benefits decrease, and at some flight conditions, riblets may cause a drag penalty. A small weight penalty would be present, as well as increased maintenance on surfaces where the technology is applied.

Riblets have been integrated and demonstrated on commercial vehicles, including the A340, where they demonstrated a 1-1.5% decrease in fuel burn [Ref. 119]. A business jet equipped with riblets demonstrated a 6% reduction in parasite drag [Ref. 120]. In this report, the effects of riblet height and width were visualized. Additional correlations between shape and dimensions can be seen in Walsh [Ref. 121].

Microvortex generators have the capability to minimize uncontrollable airflow that causes boundary layer separation over the wings and flaps. Microvortex generators can be used to both increase lift and

decrease drag, enhancing vehicle performance during approach and landing. If the technology is used to reduce drag, less engine power is needed to produce equivalent lift on the aircraft, allowing for decreased landing and takeoff noise. Since microvortex generators can be easily stored in the flaps at cruise speed, there is no increase in cruise drag. Microvortex generators would have a small weight penalty associated with the technology. According to studies by NASA Langley Research Center, microvortex generators can result in a 10% increase in lift, 50% decrease in drag, and 100% increase in lift-to-drag ratio on a single flap configuration [Ref. 122].

The TRL varies per individual technology. Riblets have been flight tested and successfully demonstrated on commercial aircraft. For a short range vehicle, benefits from friction drag reduction would be less significant than a longer range mission during cruise. As mentioned previously, riblets at off-design points potentially experience an increase in drag.

Both technologies are currently estimated at a TRL 3. Due to the relatively low percentage of fuel burn reduction and conventional high-lift systems proving sufficient, riblets and passive drag reduction were not investigated further.

B.17 Conformal Polymer Solar Cell Power Augmentation

Quantum dot nanoparticles embedded in polymer can be used to capture radiation in the extended electromagnetic spectrum beyond visible to infrared. Conformal polymers would coat the outside of an aircraft, and the captured electromagnetic energy would be converted to electricity to supplement or replace that generated by the gas turbine for use in auxiliary systems. According to Nadarajah et al., thicknesses on the order of 30 nm can be achieved with the polymer [Ref. 123]. However, energy conversion efficiencies are extremely low, on the order of 1%. While the weight penalty may be minimal, the electrical conversion rate is likewise minimal. Placing this polymer across 930 ft² of an aircraft would generate less than 1.6 hp.

Although the technology is currently rated at a TRL of 3, it is believed that significant advances in energy conversion efficiency are required before it becomes practical to use as an alternate power source for commercial aircraft.

B.18 Moveable Winglets

Fixed winglets are common in modern commercial aircraft, as they reduce wing tip vortices and increase wing tip sectional lift. Both of these contribute to an increased lift-to-drag ratio and reduced fuel burn. However, fixed winglets are designed for cruise. Due to their fixed nature, they do not operate as well at off-design conditions. Moveable winglets could use shape memory alloy to reduce wing tip vortices and reduce fuel burn for all flight conditions, and produce lower bending loads than fixed winglets [Ref. 124]. In an interview with Wired, Airbus lead project engineer Askin Isikveren stated that fixed winglets optimized for cruise conditions vary from 3-5% reduction in fuel reduction. If moveable winglets were used, a 5% reduction in fuel could be maintained [Ref. 125]. Reduction in wing tip vortices and wing bending would further lead to a reduction in wing tip noise during takeoff and landing.

Currently estimated at TRL 2, this technology was not considered for further analysis due to its long road to maturity, combined with the relative insignificance of wing tip noise compared to other airframe sources.

B.19 Combined/Compound Cycles

The integration of multiple thermodynamic cycles into a single engine core can drive up thermal efficiencies, with the potential for substantial increases in overall cycle efficiency. For example, cycles such as Otto, Brayton, Humphrey, Rankine, or Sterling cycles could be combined together to drive thermal efficiency gains. The incorporation of combined/compound cycles into aircraft engines could

eventually be performed on any scale for any type of aircraft, but would require a completely new engine architecture that would be a function of the cycles involved. Substantial complexity would be involved in such an engine, and it is estimated that the development of these new designs would take far greater time than the N+3 timeframe allows.

Currently estimated at TRL 2, extensive investment is required before this technology can progress to the point of commercial application.

B.20 Curved, Scarfed Inlet Ducts

Scarfed inlet technology relies on an asymmetric inlet lip, protruding farther in the keel than in the crown of the inlet, to provide additional shielding in the direction of observers on the ground. The resultant flow field asymmetry has been shown to lead to extensive inlet distortion, which could theoretically lead to a negation of the acoustic benefits. However, modern flow control technology is more than sufficient to accommodate these levels of inlet flow distortion.

This technology cannot be applied to embedded or boundary layer ingesting inlets, though these integration methods are generally sufficient in themselves to contain noise in the direction of the observer. In addition, scarfed inlets are known to exhibit reduced foreign object ingestion. Scarfed inlets will most likely be lighter to some degree than standard inlets, but may be more sensitive to angle of attack due to their asymmetry.

Conservative weight estimates showing inlet weight reductions in the range of 5% are based on previous computational results by Abbott for scarfed inlets [Ref. 126]. Abbott has also shown that pressure recovery associated with a scarf inlet is in the range of 0.965 to 0.98 [Ref. 127]. Many acoustic studies have also sought to assess the noise benefits of scarfed inlet ducts [Ref. 128,129,130]. These studies have shown that this SPL reduction is approximately 5 dB in the direction of the observer.

Currently estimated to be TRL 8, this technology was not considered for further investigation due to the weight of required flow control devices, and incorporation of the lightweight fan structure and cowl, discussed previously.

B.21 Steady Fluidic Separation Control

Steady fluidic separation control uses blowing or suction on the wing leading edge to energize low-momentum flow in the boundary layer to delay or prevent flow separation [Ref. 131]. This enables the wing to operate at increased angles of attack, potentially shortening takeoff and landing field lengths. Steady fluidic separation control can be used as a replacement for leading-edge slats, which would reduce wing weight and noise. However, a blowing or suction system would require complex ducting, increasing weight, requiring engine bleed, and thereby decreasing engine performance.

Currently estimated to be TRL 4, this technology was not considered for further investigation due to the estimated engine performance penalty, and due to traditional high-lift systems proving sufficient.

B.22 Synthetic Jet Separation Control

Synthetic jet separation control uses a small piezoelectric pump to convert acoustic oscillations into fluid motion. The piezo-electric pump is mounted inside a cavity near an aerodynamic surface. This cavity converges near the surface to focus acoustic oscillations. The converging portion of the cavity is oriented downstream, tangent to the flow and surface. This enables the pump to generate suction of the fluid upstream of the pump during the in-stroke, and tangential blowing of the flow aft of the pump during the out-stroke.

Integration of a synthetic jet separation control system would add weight to the vehicle, in addition to requiring power to operate. While no engine bleed is required with the use of synthetic jet separation

control, power to operate the system must be generated by the engine. In a low Reynolds number experiment, McCormick found that the implementation of synthetic jet separation control could increase the stall angle approximately 37% and increase the maximum lift coefficient by 20% at a Reynolds number of 500,000 [Ref. 132]. In addition, the experiment demonstrated to be energy efficient when comparing system benefit to input power.

Currently estimated to be TRL 3, this technology was not considered for further investigation due to the weight and system power penalty.

B.23 Nanotube Liner

A nanotube liner is an inlet liner designed to reduce tonal fan noise, similar to single and multi-DOF liners. Liners use small acoustic cavities to cause resonance of acoustic waves and dissipate acoustic energy. However, current liners are limited in the number of frequencies they can target. But nanotube liners could potentially provide a sound reduction system independent of frequency. Through the utilization of a honeycomb matrix that traps acoustic waves, energy is dispersed through viscous shear instead of resonance. The friction between the compressed gas of the acoustic wave and the honeycomb material slows the wave. Super alloys are the leading technology for larger, broadband noise dissipation applications, and are estimated to reduce aircraft engine noise by up to 30% [Ref. 133]. A tradeoff exists between the absorption capacity of the liner and the drag that is generated by the face sheet. Additionally, the weight and volume penalties associated with acoustic liners increases with thickness and area.

Currently estimated to be TRL 2, this technology was not considered for further investigation due the technology being out of scope of the N+3 timeframe.

B.24 Plane Jet Combustion

The idea behind plane jet combustion is to inject fuel flow into a thin film distributed in space to form a plane of jet fuel. The aim of this method of combustion is to enhance combustion efficiency and lower NO_x emissions. These low emissions derive from better fuel atomization, stemming from the increased surface area against which shear forces can act relative to standard injection techniques, combined with lower residence time. This type of combustion is also known to form strong recirculation zones on either side of the plane jet, providing a strong anchor for flame stabilization [Ref. 134].

While the current TRL of this technology is 5, it was set aside due to the successes achieved in lowering NO_x emissions through staged combustion.

B.25 Electric Subsystems

Electric subsystems use an electrical converter, as well as other electrical components, as the main power supply for the aircraft. This power supply is able to power advanced radar, avionics, and a completely electromechanical flight control system. Aircraft dating from the F-14 to the B-2 have used power supplies connected to engines to produce a main power supply of 115 VDC, and have incorporated a hydraulic flight control system. The F-22 was the first aircraft to use 270 VDC as the main power supply, while still using a hydraulic flight control system. The F-35 and B-787 were the first two aircraft to fully integrate a 270 VDC power supply and an electromechanical flight control system. The 270 VDC power supply was originally designed to power large radar devices, but was adapted for the commercial market to power flight control system and avionics.

An electromechanical flight system would increase system weight, but increase electrical efficiency, leading to improved engine performance and a reduction of fuel burned. Based on conservative estimates by Phillips and Wood, a vehicle with partially-electric subsystems would realize a subsystem weight reduction of 634 pounds compared to a conventional vehicle [Ref. 135]. However, a vehicle with fully-electrical subsystems would see an increased subsystem weight. All vehicles in this study were sized for a

62,000 pound payload and a 2,600 nautical mile range. The vehicles with all-electric and partially electric subsystems showed an improvement in SFC of 1.41% of 0.895%, respectively. The vehicles' fully and partially electric subsystems showed 1,421 and 3,113 lb reductions in ramp weight, and 569 and 2,141 lb reductions in operating empty weight, respectively. Due to the date of this report, and conservative estimates, benefits from fully- and partially-electric subsystems could be much greater in the N+3 timeframe.

Currently estimated to be TRL 8, this technology was not considered for further investigation. Improvements in weight and performance were not predicted to be significant.

B.26 Third Engine Stream

The third stream concept involves the introduction of an additional bypass stream into a standard turbofan engine, whose flow rate can be modulated. This can be achieved in a multitude of ways, including placing the inner fan duct downstream of two separate fans and the outer fan duct behind the upstream fan, or by having the outer fan duct supplied solely by the flow passing through the fan tip. Methods of modulating the flow, or varying the geometry of the outer fan duct, can be achieved through variable pitch fan blades, fan exit guide vanes, etc. This can be used to access higher bypass ratios than standard turbofans, with corresponding reductions in jet noise by shielding the high-speed, high-temperature core flow with slower outer fan duct flow. An additional flow path with variable geometry will allow for higher thrust levels at takeoff and climb and will allow for the maintenance of higher cruise efficiency. This separate flow path can also be used as a supply of air for flow control applications or thermal protection purposes. However, this can also result in larger engine diameters and additional complexity through the control system.

While the currently estimated TRL of this engine architecture is 4, it was not chosen to be pursued for this particular mission due to the added complexity of supplying an additional fan duct with air, and the predicted system performance penalties associated with a larger engine.

B.27 Alternative Hydrocarbon Biofuels

Biofuels have the potential to replace fossil fuels, which is becoming important in light of the results of the scenario study. One of the major drivers behind biofuels is the reduced emissions over more conventional fuels. A study by the Baylor Institute for Air Science showed that the introduction of up to a 30% fraction of cooking oil, plant-, and animal matter-based biofuel in Jet-A reduced NOx emissions [Ref. 136]. For fractions below 20%, no degradation in engine performance was recorded. Biofuels may be a cheaper alternative to kerosene-based aviation fuels in the long term, but currently will be more expensive. Many biofuels have already been tested in commercial engines; however, their characteristics must be considered relative to current aviation gasoline prior to implementing them into modern engine technology. Since emissions are shown in Section 6.2.3 to be extremely low due to the use of lean combustor technology, the need for alternative hydrocarbon biofuels has been set aside for the time being.

Although the TRL is estimated to currently be around 4, the necessity for this technology is farther off in the future.

B.28 Embedded/Conformal Inlets

Embedded/conformal inlets reduce the size of the aerodynamic wake of the aircraft by ingesting a portion of the boundary layer and reducing the extent to which the inlet protrudes from the aircraft. This technology employs high area diffusion rates and large offsets which can enhance propulsion systems due to their light weight, tight and compact packaging, and low volume properties. However, due to the shortened inlet and the potential for severe duct turning, high distortion levels are common due to variation in total pressure in the incoming boundary layer. If the turning is extreme enough, boundary layer separation is possible in the inlet duct.

Embedded/conformal inlets would be utilized on embedded propulsion configurations. A decrease in inlet length and volume can potentially reduce the empty weight of a vehicle by 1.8%, and increase fuel capacity by 1.8%, from a normal shock inlet with serpentine diffuser [Ref. 137]. The inlet pressure recovery of this configuration would be approximately 9.6% lower than podded propulsion configuration. Inlet flow control such as vortex generators, bleed, or blowing could be used to reduce distortion and improve pressure recovery. However, adding such systems would add weight to the vehicle.

This technology was not considered for further investigation due to the dismissal of configurations using embedded propulsion systems.

B.29 Low-Noise Fan Blades

NASA Glenn Research Center is developing a low-noise fan blade that has reduced weight with increased propulsive efficiency, named the quiet high-speed fan (QHSP). This blade is designed to reduce takeoff EPNL by 6 EPNdB [Ref. 138]. The fan blade is designed to channel free stream air into the core spinner, main core, and through the fan blade before exiting the fan blade trailing edge. This fan blade trailing edge flow energizes the airflow, and increases engine performance, while reducing fan noise. Noise levels produced by the fan are estimated to be proportional to the velocity of the fan tip speed to the fifth power. However, with the QHSP, NASA was able to design a high speed fan that reduces noise through forward swept fan blades and a leaned stator that creates a more favorable rotor-stator interaction, reducing this passing tone. It was found that the reduction in EPNL was largely due to the reduction in the passing tone and its respective harmonics.

The current technology readiness level associated with low-noise fan blades is estimated to be TRL 2; however, due to the low TRL, combined with the added complexity of the blown fan blades, this technology was not investigated further.

B.30 Fan Blade Flow Control

As mentioned in Subsection B.29, high levels of tonal noise are caused by rotor and stator interactions at the blade passing frequency and its harmonics. The use of flow control in this region could result in reduced engine noise. Air is ducted through the fan blades and ejected through the fan blade trailing edge, thus suppressing unsteady fan blade and stator interactions by reducing viscous boundary layer losses. Blowing can be applied in the fan blades in several configurations: every-blade trailing edge blowing (TEB), alternating fan blade trailing edge blowing (ATEB 1x1) and applying trailing edge blowing to two adjacent fans, skipping the next two, and applying trailing edge blowing to the next two (ATEB 2x2). The latter two cases result in reductions of peak tones but introduce several new tones. However, this new acoustic spectrum is easier to control by acoustic liner treatment than regular TEB. Figure B-1 shows the reduction in sound power as a function of blowing rate, as a percentage of inlet flow [Ref. 139]. Using trailing edge blowing in the absence of stators, the far-field noise was found to be 94.8 dB, placing a lower bound of the achievable sound power level by removing all rotor-stator interaction noise. TEB reduces the inlet and aft duct sound power levels by 7% and 6.9% with blowing rates of 1.5% and 1.52%, respectively. ATEB 1x1 reduces the inlet and aft duct sound power levels by 4.3% and 5% with blowing rates of 0.9% and 0.9%, respectively. Reduced amounts of blowing result in increased engine performance. Additionally, it was found that using TEB, ATEB 1x1, and ATEB 2x2 increases acoustic liner sound reduction by 31%, 50.7%, and 58%, respectively, showing that fan trailing edge blowing increases acoustic liner effectiveness.

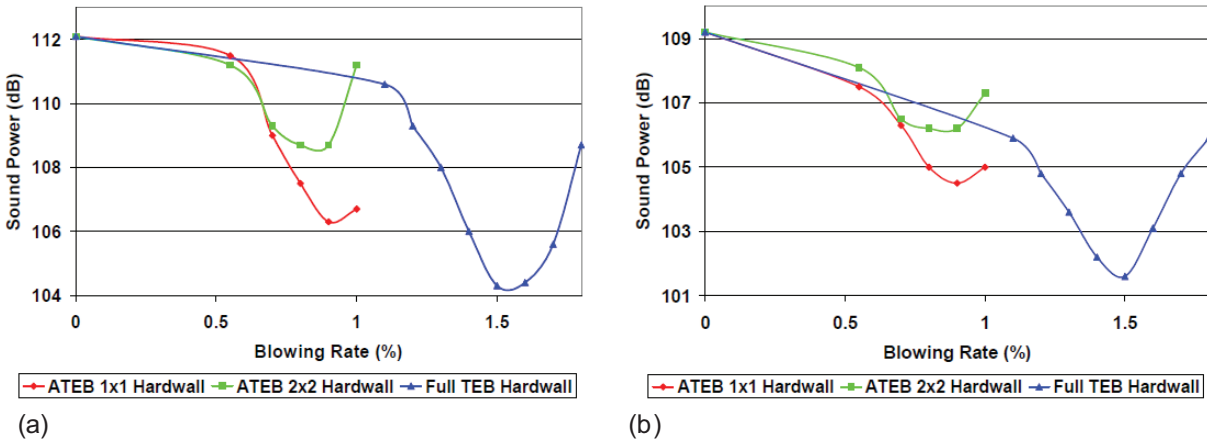


Figure B-1. Sound Power vs. Blowing Rate (% Inlet Flow Rate) for (a) Inlet Duct and (b) Aft Duct [Ref. 139]

According to Fite et al, the fan efficiency of an engine with 2% blowing is equivalent to the efficiency of a baseline fan with no trailing edge blowing [Ref. 140]. There would be a weight penalty and added complexity associated with the engine, as ducting would need to be installed. Currently estimated to be TRL 4, this technology was not considered for further investigation due the estimated degree of benefit being outweighed by the added weight and complexity.

B.31 Conformal Load-Bearing Antenna Structures

Conformal load-bearing antenna structures (CLAS) embed sensors such as antennas and avionics where traditional methods use bolt-on methods. Traditional avionic sensors are able to be replaced with active or passive sensors that allow for controllable and reconfigurable antennas. CLAS eliminates bolt-on sensors and structural cutouts associated with these methods, improving structural efficiency, and enabling the consolidation of single-function sensors into multifunction installations. This allows for potential weight reduction and volume reduction in the vehicle. CLAS offers potential drag reduction by allowing for a more continuous skin surface. Based on internal research and studies, CLAS could reduce vehicle empty weight between 200 and 1400 lbs, reduce acquisition cost between \$0.5 million and \$4.0 million, and may offer potential noise and drag improvements through a more continuous skin surface.

This technology has a varied TRL, based on configuration and extent of integration, but was not considered for further investigation due to the small magnitude of weight, drag, and noise reduction. Commercial aircraft contain significantly fewer sensors than military or surveillance vehicles. As a result, a commercial vehicle that uses CLAS would see benefits toward the lower end of the ranges discussed above.

B.32 Upper Surface Exhaust Nozzle and Flap

The upper surface exhaust nozzle and flap system uses pylon-mounted engines located on the wing. High-momentum exhaust from the engines is vectored downward which prevents flow separation during large flap deflection angles and provides super circulation [Ref. 141,142]. This increased flap deflection and super circulation would lead to an increase in lift coefficient during takeoff and landing to improve vehicle field length performance. Integrating the vectoring nozzle and ducting would increase wing weight and complexity, and decrease usable wing volume. Vehicle parasite drag would increase for all segments of mission, increasing fuel burn. Additional penalties associated with mechanical thrust vectoring can be found in the Subsection B.71. Figure B-2 illustrates a comparison between an upper surface exhaust nozzle and flap configuration and a conventional flap configuration. Upper surface exhaust nozzle with flaps shows significant ESTOL characteristics compared to the traditional flap configuration.

Currently estimated to be TRL 3, this technology was not considered for further investigation. For the mission requirements, traditional high-lift proved sufficient.

B.33 Lower Surface Exhaust Nozzle and Flap

Lower surface exhaust nozzle and flap is similar to upper surface exhaust nozzle and flap, but instead of mounting the engine on the upper surface, the engine is mounted beneath the wing. Externally blown flaps (EBF) energize flap flow with the use of engine exhaust. EBF delays or prevents flow separation on high lift systems and allows for greater flap deflection. These effects contribute to an increase in lift, reducing field length and allowing for steeper climb and descent trajectories. This, in turn, limits the time and area exposed to aircraft noise. According to two-dimensional analysis by Griffin et al, at a 0° angle of attack, lower surface EBF produced a 157% and 273% increase in lift coefficient for flap deflections of 20° and 30° , respectively, during takeoff [Ref. 143]. However, lift-to-drag ratio decreased 71.3% and 68.7%, respectively. At a 0° angle of attack, lower surface EBF produced a 220.8% and 490.6% increase in lift coefficient for flap deflections of 30° and 35° , respectively, during landing. However, lower surface EBF reduced the lift-to-drag ratios 65.4% and 52.8%, respectively. On the other hand, three-dimensional results have shown a decrease in lift performance. Based on three-dimensional analysis, at a 0° angle of attack, lower surface EBF produced a 6.9% and 37.8% increase in lift coefficient for flap deflections of 20° and 30° , respectively, during takeoff. Lift-to-drag ratio decreased 36.2% and 46.1%, respectively, as a result of lower surface EBF. At a 0° angle of attack, lower surface EBF produced a 20.8% and 128.8% increase in lift coefficient for flap deflections of 30° and 35° , respectively, during landing. However, lower surface EBF reduced the lift-to-drag ratios 24% for 30° flap deflection and increased the lift-to-drag ratio 12% for 35° flap deflection. Benefits of EBF vary per configuration, and decrease as wing span increases. Based on internal research, EBF would increase propulsion system weight approximately 6%, and increase scrub drag by 0.0001.

Figure B-2 illustrates a comparison between an lower surface exhaust nozzle and flap configuration and a conventional flap configuration. Lower surface exhaust nozzle with flaps shows significant ESTOL characteristics compared to the traditional flap configuration.

Currently estimated to be TRL 3, this technology was not considered for further investigation, as traditional high-lift devices proved sufficient to meet the field length requirements.

B.34 Fluidic Thrust Vectoring for Upper Surface Exhaust Nozzle and Flap

Fluidic thrust vectoring for upper surface exhaust nozzle and flap is similar to the upper surface exhaust nozzle and flap described above. Fluidic thrust vectoring provides a smaller weight penalty and

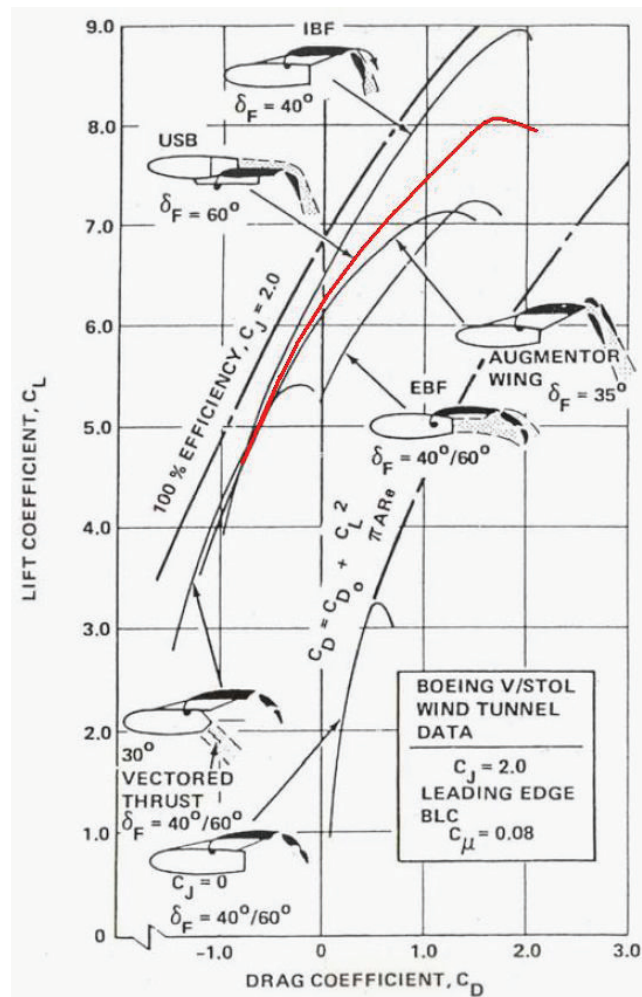


Figure B-2. Upper Surface Exhaust Nozzle and Flap Lift Comparison

an improved thrust efficiency compared to mechanical thrust vectoring as described in the Subsection B.71. Currently estimated to be TRL 3, this technology was not considered for further investigation. For the mission requirements, traditional high-lift proved sufficient.

B.35 Single DOF Liner

Single degree-of-freedom (DOF) liners are a type of inlet acoustic liner generally comprised of acoustic absorbing material covered by a perforated face sheet. The absorbing sections of the liner may be divided up into smaller cells designed to target specific tonal frequencies. In the inlet liner design process, face-sheet resistance and cavity depth are optimized to minimize noise in the inlet. Noise in the inlet is generated primarily by fan tonal noise through the interaction between rotor blades, stator blades, and the rotor pressure field. At subsonic speeds, however, inlet noise is dominated by rotor-stator interactions.

The most common type of inlet acoustic liner is a single degree-of-freedom liner, referring to the number of frequencies that can primarily be targeted. Acoustic impedance is dependent on liner resistance, cavity reactance, and face-sheet mass reactance [Ref. 144]. A tradeoff exists between the absorption capacity of the liner and the drag generated by the porous face sheet. Additionally, the weight and volume penalties associated with acoustic liners increases with the number of degrees-of-freedom. Based on analysis, it was found that a double DOF inlet liner provided increased noise reduction compared to a single DOF liner. As such, this technology, currently estimated to be TRL 9, was not considered for further investigation.

B.36 Active Drag Reduction

Active drag reduction focuses on reducing the vehicle boundary layer, leading to a reduction in skin friction drag. Transition control and laminar flow encounter problems for very large applications and regions with increased local Reynolds numbers, such as the fuselage, where as much as half of the skin friction on the vehicle occurs. For a successful active device, the energy needed to control and reduce the turbulent boundary layer must not exceed the energy saved from turbulent boundary layer reduction. While active flow control systems require energy to function, they offer potential larger reductions in drag over passive systems.

Past CFD studies have shown drag reductions of 25-30% from suction and blowing [Ref. 145], 71% from tangential blowing [Ref. 146], 40% from spanwise wall oscillation [Ref. 147], 20% from utilization of counter-rotating streamwise vortices, and 50% from utilization of colliding spanwise jets [Ref. 148]. However, CFD studies tend to overestimate system performance by allowing for control at each grid point, when this is not possible in a realistic active control environment. In terms of experimental studies, a 45% reduction in drag has been experimentally measured through spanwise oscillation [Ref. 149] and a 7% reduction in drag has been measured through the use of an array of spanwise synthetic jets [Ref. 150].

The current TRL varies per individual technology. These technologies were not considered for further investigation due to the relatively low TRLs, weight penalties, and operating energy restrictions associated with each technology. Several technologies would require large amounts of complex ducting which would further increase weight and possible engine bleed which would decrease engine performance.

B.37 Multi-DOF Liner

Multi-DOF liners are built upon the current state-of-the-art single DOF acoustic liners for reducing tonal fan noise. Multi-DOF liners contain multiple layers of absorbing material and additional perforated sheets separating it into other layers. Similar to single DOF liners, multi-DOF can have the absorbing sections divided up into smaller cells designed to target specific tonal frequencies. Multi-DOF liners allow for attenuation which targets multiple different tonal frequencies. A tradeoff exists between the absorption capacity of the liner and the drag that is generated by the porous face sheet. Additionally, the

weight and volume penalties associated with acoustic liners increases with its number of DOF. Based on analysis, it was found that a double DOF inlet liner proved superior in noise reduction and overall system performance compared to single- and multi-DOF liners. As such, this technology, although currently estimated at TRL 8, was not considered for further investigation.

B.38 Oil-less Engine

Oil-less engines use magnetic bearings instead of traditional oil-lubricated bearings. These magnetic bearings could potentially offset the weight reduction seen by the removal of conventional bearings, though a slight weight increase would likely be present at a local level [Ref. 151]. Magnetic bearings would eliminate friction inherent in gas turbine engine systems, improve shaft rotation, and reduce fuel consumption. Engine efficiency is also increased through larger clearances associated with magnetic bearings, and the elimination of engine operating temperature restrictions normally found with other forms of bearings and liquid lubricants. In addition to efficiency improvements, magnetic bearings would remove one of the main factors limiting single-mission duration and engine lifetime. Though magnetic bearings would slightly increase weight at a local level, their use would lead to the elimination of lubrication plumbing system, and simplification of the engine casing and support, leading to a potential 10% decrease in overall engine weight [Ref. 152].

Currently estimated to be TRL 2, this technology was not considered for further investigation due to its need to mature.

B.39 Low Tip Speed Counter-Rotating Ducted Fan

This engine architecture concept entails using two separate fans with reduced tip speed compared to conventional turbofans. Similar to an open rotor concept, the fans will be counter-rotating, necessitating either a gearbox system or separate shafts and turbines to drive each fan. This will unavoidably add weight to the system in either configuration. Though the ducted architecture can allow access to higher flight Mach numbers through the diffusion of inlet air, and noise reduction compared to its unducted counterpart, it cannot achieve the fuel reduction potential of unducted propfans. Furthermore, while efficiency gains and noise reduction can be bought through the dual-level compression and reduction in fan tip speed, the required lower fan diameter comes with the added penalty of reducing bypass ratio, providing a further hindrance to fuel savings. In addition, ducted propfans are reported to have fan pressure ratios lower than more conventional turbofan engines, putting the engine at risk of surge. These conflicts with high efficiency necessitate the implementation of variable pitch fan blades, discussed elsewhere in this report.

At a current TRL of 3, this technology was not considered for further pursuit due to the combined effects of reduced bypass ratio and reduced fuel consumption relative to the alternative configurations, specifically, the open rotor and three-shaft turbofan.

B.40 Wheel Caps

Wheel caps are designed to cover the hubs of landing gear wheels to reduce the separation that occurs in this cavity region while the landing gear is deployed. When present, this separation leads to low-frequency airframe noise due to cavity flow. Assuming there is a way to affix the wheel caps to the wheels, this technology could be applied to any aircraft, and should generate positive results in terms of noise reduction. However, the added weight must be taken into consideration.

As reported in Dobrzynski et al, wheel caps provide a benefit of 0.5 dB reduction in OASPL in the forward radiation direction, but are especially beneficial in the 500 Hz range [Ref. 66]. In addition, the work of Soderman et al shows a benefit of 0.6 dB due to the addition of a wheel cap [Ref. 153]. Based on a 3 foot landing gear tire, an estimated 10 pound wheel cap would be required for each tire. With two tires

on the nose gear and two on each of the main landing gears, this would add up to a total of 60 pounds of additional landing gear weight.

Currently estimated to be TRL 6, this technology was not considered for further investigation due to the small magnitude and narrowband nature of the noise attenuation benefit versus the weight penalty that would be incurred.

B.41 Wheel Gap Filler

As described by Smith and Chow, an axial gap between two landing gear generates noise due to the impingement of the turbulent wake from the leading wheel on the leading edge of the rear wheel [Ref. 154]. The majority of this noise is directed towards the ground, as described by the computational results of Lazos [Ref. 155]. A wheel gap filler consists of a solid structure designed to occupy the volume between the two axially spaced wheels, in order to prevent the turbulent wake of the leading wheel from impinging on the trailing wheel. While this structure necessitates adding weight to the landing gear, it must be weighed against the noise benefit that can be achieved in terms of EPNL. Since wheel gaps are generally associated with a broad mid-frequency peak, these are the frequencies that would be affected by the inclusion of a wheel gap filler.

Although the estimated TRL of this technology is 6, due to the relative contribution of the wheel gap source to the overall landing gear noise, this technology was not considered for further analysis on the configurations under investigation in this study.

B.42 Acoustic Excitation

Acoustic excitation is designed to promote mixing through the use of different tonal frequencies that induce turbulence in excited jets. It has been shown that significant modifications can be made on vortex formation on large scale structures through acoustic excitation. These induced vortices can lead to increased mixing, causing the noise source region to become more compact, smoothing out the jet velocity profile, and reducing the overall jet plume length, leading to reductions in far-field noise [Ref. 156]. Mixing of the jet flows is similar in effect to chevrons, without the structure required for chevrons, and the drag penalty associated with the technology.

Currently estimated to be TRL 4, this technology was not considered for further investigation due to the small magnitude and narrowband nature of the noise attenuation benefit and low TRL.

B.43 Brush-type Trailing Edges

Brush-type trailing edges employ flexible fibers emanating from the trailing edge of a lifting surface. These bristles serve to alleviate the bluntness of the trailing edge, which would otherwise result in large-scale vortex shedding. As a result, the noise associated with these shed vortices is mitigated to some degree. Furthermore, the flexibility of the fibers allows them to remain unloaded and adapt to different flow conditions. This technology can be applied to trailing edges of any lifting surface in order to mitigate vortex shedding. Its passive nature suggests that it will have a minimal weight penalty associated with it, and no added complexity in terms of electronics or control systems. Failure of this technology would consist of the detachment of the bristles on the trailing edge of the lifting surfaces. Depending on the attachment methodology, the entire brush-type trailing edge could be removed, or only certain bristles. In either case, the portion of the trailing edge that becomes detached would experience vortex shedding, leading to increased airframe noise. As reported in Herr and Dobrzynski, a properly designed trailing edge brush can show a noise reduction in excess of 10 dB (in a limited frequency range proportional to the flow velocity and trailing edge thickness), citing the ability of flexible brush fibers to adapt to the flow and be minimally affected by flow disturbances by remaining unloaded for different incidence conditions. This is in contrast to trailing edge serrations, which can only achieve noise reductions on the order of 2-3 dB [Ref. 157]. Aerodynamic effects of including brush-type trailing edges were studied computationally

by Ortmann and Wild [Ref. 158]. While the noise reduction at the target frequencies can be significant, the broadband frequency reduction potential of the technology is severely limited. Additionally, the targeted acoustic source is among the most negligible contributors to the overall EPNL of the aircraft. Research has also shown a potential to reduce drag on the wing by controlling the trailing edge flow; however, this is accompanied by a corresponding decrease in its lift coefficient.

Because only specific frequencies can theoretically be targeted with this type of trailing-edge device, even though its current TRL stands at 4, the ability of this technology to dramatically affect the noise footprint of the aircraft is minimal. For this reason the technology was set aside from further consideration for the duration of this study.

B.44 Trailing Edge Serrations

Similar to the trailing edge serrations researched for control of flap noise, serrations can also be applied to the trailing edges of flaps or the main wing element. Trailing edge serrations would involve cutting or constructing V-shaped grooves into the flap or wing material. In the presence of serrations, the periodic vortex shedding from the trailing edge of the wing element that would typically occur becomes less coherent in the spanwise direction. Instead it would be replaced by longitudinal vortices that form from the serrations. This can be seen in the oil-flow visualizations produced by Knepper and Garry to delay flow separation on the upper surface of the flap [Ref. 159]. Further wind tunnel measurements by this group showed that an optimally placed flap, with well-designed serrations on the wing trailing edge, can see an L/D benefit of up to 17% due to this effect. However, this benefit only corresponded to a change in wing lift coefficient of less than 0.1. Furthermore, the noise benefit is expected to target only the wake shedding frequency associated with the finite thickness trailing edge, replacing it instead with higher frequency noise from the serrations.

Currently estimated at TRL 4, this technology has been set aside as its projected benefits are small compared to the overall acoustic field surrounding the aircraft.

B.45 Chevrons

Chevrons are triangular serrations integrated into the exhaust nozzle trailing edges of turbofan engines. These notches are designed to induce streamwise vorticity into the shear layers. This vorticity promotes the mixing of the jet streams, reduces the overall jet plume length, and leads to reductions in far-field noise [Ref. 160]. This technology is the current state-of-the-art in medium- to high-bypass ratio turbofan engine jet noise reduction, and imposes a negligible weight penalty to the engines. However, chevrons penetrate slightly into the exhaust flow, leading to thrust penalties at cruise. For this reason, some studies are looking into deployable chevrons by means of shape memory alloys, etc., which can be deployed for take-off noise reduction and retracted during cruise. As chevrons are designed into the structure of the engine, no failure modes are associated with them. Experiments have shown that approximately 3 dB reduction can be achieved with a chevron nozzle, mostly at lower frequencies, while incurring at most a 0.55% thrust penalty at cruise [Ref. 161]. Because the frequency reduction potential is limited to lower frequencies, and the associated thrust penalty is carried through the entire cruise portion of the mission in the absence of advanced control systems, this technology was excluded from further consideration.

While the current TRL of this technology is at 9, and some aircraft have implemented them, the emphasis on fuel burn savings derived from the scenario study has led to this technology being set aside for the remainder of this study.

B.46 Combined Steam Cycle

A derivative of the combined/compound cycle technology described above, a combined steam cycle can describe a variety of different engine architectures, though in general the features remain the same.

In one example, portions of the hot jet exhaust are utilized to support a closed Rankine cycle. The hot jet exhaust is passed through a heat exchanger and used to vaporize liquid water into superheated steam. In turn, this steam is passed through a turbine which is used to drive a shaft. This shaft can then be employed to create excess power through a generator or to drive a propeller to produce additional thrust. The two-phase mixture leaving the steam turbine is then passed through a condenser, after which it becomes liquid water again. At this point it is forced through a pump and again passed through the heat exchanger. This type of system architecture introduces a variety of additional components to the engine: the water pump, heat exchanger, condenser, steam turbine, and either a generator or propulsor. Furthermore, there is a need for additional piping/tubing to transport the water between these components. In an industrial application where this has been implemented, steam tubes can be excessively large. Because of this their direct translation into an aircraft application can be prohibitive, unless smaller diameter tubing can be utilized.

For aircraft engine applications, the estimated TRL of the combined steam cycle is only 2. More complete use of the heat generated by the gas turbine cycle increases the overall efficiency of the engine; however, the addition of a steam cycle into the system would require a complete redesign of the engine architecture. Furthermore, weight penalties become excessive in light of the large number of components required to perform the cycle. While theoretical cycle analyses have shown the potential of such a cycle to reduce specific fuel consumption by up to 20% in an uninstalled engine [Ref. 162], this technology has a long road to maturity before it can be considered further as a potential propulsion system for aircraft applications.

B.47 Linear Acoustic Liner

Similar to the construction of single degree-of-freedom acoustic liners described above, linear acoustic liners consist of a cellular material, such as honeycomb, sandwiched between a solid back sheet and a perforated front sheet. However, with linear liners this perforated front sheet generally consists of a bonded woven metal wire cloth. For the liner to be considered linear, the perforations on the front face sheet must be sufficiently small to force the acoustic impedance of the cavities to be insensitive to the magnitude of the flow rate across the liner. It is reported that this critical diameter is 10 μm [Ref. 163]. For this reason, it is far more practical to develop linear liners by using woven cloth. Experimental measurements, such as those reported by Drouin et al, explain that flow through the porous holes of a linear liner is completely dominated by viscous forces [Ref. 164]. As such, this type of liner will exhibit a skin friction coefficient that is largely insensitive to sound pressure level. Liners consisting of larger perforations, on the other hand, tend to experience increases in skin friction as the sound pressure level rises due to the effect of pressure fluctuations on the flow inside the cavities. For this reason, linear liners are more capable of operating successfully over a wide range of flight conditions. A downside to this design, however, is the impracticality of using woven metal cloth in the exhaust nozzle due to the high temperature flow. This limits the use of this type of liner to inlets and fan ducts. In addition, for larger engines it is limited in its sound pressure level attenuation compared to other liner designs for community noise flight conditions.

Though the current TRL for this technology is 9, it was decided that a larger degree-of-freedom liner would be optimum for the configuration being explored in this study.

B.48 Four-Shaft Turbine

Like the three-shaft turbofan, a turbofan driven by four shafts has the added independence of rotational components with respect to one another. This allows for more of the turbomachinery to operate at ideal speeds, while stage matching increases thermal efficiency. The additional shaft can be utilized for additional fan stages, compressors, power turbines, etc.

Currently estimated at TRL 1, this technology is predicted to increase the weight of the engine for only a minor benefit in fuel consumption relative to a three-shaft turbofan. For this reason, combined with the long road to technological maturity, the technology was set aside from further consideration.

B.49 Active Noise Cancellation

Active noise cancellation is based on destructive interference of airframe noise by the introduction of an out-of-phase power source. Methods by which this can be achieved are to employ either a high-powered acoustic source in the form of a loudspeaker, or to generate an out-of-phase vibration into the noise-radiating elements of the aircraft. This methodology allows for the active control of noise generation in any portion of the aircraft into which it can be installed. Both methods require the measurement of generated noise to properly tune their destructive output. Active noise cancellation systems must be built into the elements of the aircraft that will be expected to generate noise. This will involve not only the actuation mechanism to force the vibration, but also the electrical and control systems. Power considerations must also be taken into consideration. Using an acoustic source to destructively interfere with the airframe noise will demand expensive power requirements, but may be easier to implement in existing aircraft. Weight and system complexity must be considered. Noise reduction from active noise cancellation varies per component and noise cancellation method.

Based on previous research, active noise cancellation can achieve duct noise reductions of up to 20 dB for frequencies up to 500 Hz, fuselage noise by more than 13 dB at certain frequencies, and fan noise reductions between 10-20 dB. There are several methods used in active noise control, including near source, which is desirable due to its ability to cancel noise at the source and prevents noise propagation. However, this is difficult to implement due to the location of many noise sources in extreme environments. Enclosures are another method that can be used to either prevent noise from propagating or preventing noise from entering a confined space. They allow for nonintrusive equipment placement, and allow the control of a well-defined space. However, enclosures can become large and complex. Single-point noise control aims to cancel noise at a single point. Applications are limited, but high performance results are easily achievable. Single-point uses a microphone to pick up a tone and uses a secondary source to emit an inverted signal. The last method for active noise control is free-field, which uses secondary sources to surround a primary source to prevent noise propagation or to create a region into which no noise can enter. Secondary sources must be placed no more than half a wavelength together, which is generally not possible.

Currently estimated at TRL 2, this technology was not investigated further due to the added weight and complexity, decreased energy efficiency, and low TRL.

B.50 Landing Gear Assembly Plasma Fairings

Landing gear assembly plasma fairings consist of electrodes which introduce energy into the flow field surrounding the landing gear assembly. The “fairing” typically would take the form of a single dielectric barrier discharge (SDBD) plasma actuator and a power supply. The addition of this energy into the flow field delays or prevents separated flow in the bluff body wake of the landing gear, which is a primary source of landing gear noise. This technology could be applied to any unfaired landing gear system which meets the spatial requirements associated with the implementation of the plasma generating devices. There would also be power requirements involved with the use of such technology, and a slight weight penalty. Failure of the plasma system would simply reduce the landing gear to its nominal dressed state, in which there is extensive vortex shedding noise. In addition, the baseline drag of the system would be restored. There are no expected modes of failure that would cause a significant disruption of aircraft activity. Experimental work conducted at Notre Dame, as reported in Thomas et al, shows the application of landing gear plasma fairings for landing gear noise reduction [Ref. 165]. A subsequent work by the same group shows the source SPL reduction from a vortex shedding cylinder, and it was found that up to 13.3 dB reduction in noise could be achieved by pulsing at the Strouhal number associated with the

vortex shedding [Ref. 166]. In addition, a drag coefficient reduction of 30% for the landing gear is assumed based on related work on physical landing gear fairings (e.g. Quayle et al [Ref. 65]).

While the potential of this technology to address the challenges of the N+3 metrics exists for a minimal weight penalty, it was determined that at a current estimated TRL of 2, this technology could not be made viable in the timeframe of aircraft entering service in the range of 2030-2035. However, given another decade or so to mature, this technology could prove feasible for future airframes to use in meeting stringent noise regulations.

B.51 Slat Cove Fillers

Upon deployment of leading edge slats, a slat cove is generated on the lower side of the slat where it conforms to the wing in the undeployed state. This technology seeks to fill this gap with a solid body to prevent flow separation and result in a more streamlined flow between the leading edge of the main wing and the lower surface of the slat during takeoff. At the same time, it is desired to maintain the overall aerodynamic performance for the high-lift devices in which they are to be implemented. The main purpose of this device is to minimize vortex shedding resulting from lower side flow separation, which leads to broadband noise generation.

This technology could be applied to any wing which employs slats, though in an end-product form, it would need to be deployable so that the slat and wing would still be able to conform to one another. There will be a slight weight penalty due to the additional material, and any deployment mechanism that must be added could add complexity to the system. In the experimental work by Kolb et al [Ref. 167], it is shown that a slat cove filler can achieve an average slat SPL reduction of around 4.6 dB across the frequency range. This noise reduction is greatest in the range 1-3 kHz.

The current technology readiness level associated with slat cove fillers is estimated to be TRL 4; however, due to their noise reduction spanning only a slight portion of the frequency spectrum, combined with the relative importance of the slat noise when compared to other airframe noise sources, this technology was not considered for further analysis.

B.52 Continuous Mold-Line Linkages

Continuous mold-line linkages are designed to reduce noise generated from slat and flap side edge vortices. Noise is reduced through the blending of the wing and slat leading edges, as well as the wing and flap trailing edges. This blended surface greatly diffuses the vortices caused by slat and flap linkage gaps, and significantly reduces aircraft noise. According to Berton et al, continuous mold-line linkages are estimated to reduce flap noise by 8 dB [Ref. 168]. Noise reduction is constant across all one third octave band frequencies, ranging from 0.1 to 10 kHz and across all directions and airspeeds. Continuous mold-line linkages would increase slat and flap system weight a minimal amount.

The current technology readiness level associated with continuous mold-line linkages is estimated to be TRL 3; however, due to the low TRL combined with the relative importance of flap noise compared to other airframe noise sources, this technology was not considered for further analysis.

B.53 Flap Tip Fences

Flap tip fences are flat plate obstructions employed at the inboard and/or outboard portions of wing flaps. They can be aerodynamically contoured depending on the platform on which they are used, extending below the lower surface of the flap. Their purpose is to prevent the shedding of streamwise vortices from the edges of the flap caused by the discontinuity in the wing surface upon deployment of the flap. These vortices have been associated with high levels of airframe noise during landing. This technology can be applied to any wing flap, and generally can be retrofitted to any wing flaps that do not currently implement them. However, there will be a slight weight penalty due to their implementation. In

Soderman et al [Ref. 153], source noise reduction using a flap tip fence was in the range of 1-3 dB. In Horne et al, a reported flap tip benefit of 3-4 dB was achieved [Ref. 169].

The current technology readiness level associated with flap tip fences is estimated to be TRL 8. However, due to their noise reduction spanning only a slight portion of the frequency spectrum, combined with the relative importance of flap noise when compared to other airframe noise sources, this technology was not considered for further analysis.

B.54 Ejectors

An ejector is a duct placed around the exhaust of a jet engine, circumferentially lined with passages, which allows the entrainment of ambient air into the main exhaust flow. By mixing the high-speed, high-temperature jet exhaust with the cooler, lower-speed ambient air, the resulting mixed flow velocity is decreased. As a result, the intensity of the turbulent mixing process between the primary hot stream and the secondary ambient stream is decreased, resulting in a reduction in noise generated by the exhaust jet [Ref. 170]. Depending on the ejector inlet geometry, the addition of this secondary air increases the static thrust by creating a suction on the inlet lip [Ref. 171]. It was reported by General Electric that the implementation of an ejector on the Northrop T-38 Talon resulted in a thrust improvement of 1-2% at takeoff conditions [Ref. 172]. Furthermore, flow mixing may be enhanced through the use of mixing lobes, vortex generators, etc. However, the implementation of these devices may themselves generate additional high frequency noise. This may be combated with liner technology along the interior surfaces of the ejector. In practical applications there can be a significant weight penalty associated with the implementation of an ejector. To maximize noise reduction, the length of the ejector must grow to such an extent that mixing becomes as complete as possible. However, longer ejectors add weight and frictional flow losses that contribute to an ultimate reduction in the thrust augmentation potential of the ejector. Depending on the relative diameters of the jet engine exhaust and the ejector inlet, ram drag effects could also become significant during flight conditions.

Although the current TRL of this technology is estimated at 8, it was not considered for this study due to the estimated weight penalties associated with the technology. While benefits can be achieved during takeoff, in terms of noise, the weight associated with the ejector must be carried through the entire flight.

B.55 Thrust Vectoring Open Rotor

Thrust vectoring open rotor engine configurations can be achieved in two ways. The first is to thrust vector the jet exhaust, described in the Subsection B.71. The second is to enable rotation of the engine, which would allow for STOL, or even VSTOL, capabilities. This engine configuration would be similar to that found on the V-22. As engine sizing is driven largely by takeoff performance, VSTOL and STOL could potentially allow for decreased engine sizing. However, as described by Chana and Sullivan, during takeoff and landing, the stationary wing acts as a flat plate in the downwash of the tilted rotor, causing a download [Ref. 173]. This download reduces the net lift of the vehicle, thus limiting payload and range. In addition, tilt rotor vehicles show a decrease in cruise aerodynamics compared to traditional fixed propulsion aircraft. Figure B-3 illustrates the increase in parasite drag of the V-22 compared to commercial jet transports [Ref. 174]. Due to the increase in passengers, the jet transport aircraft have increased wetted areas. If a V-22-like vehicle was sized to equivalent passenger counts, the total wetted area and parasite area would be expected to increase even more. Figure B-3 illustrates the increase in cruise efficiency of the C-130, a fixed rotor configuration, compared to the V-22. In addition, Figure B-3 shows the airspeed limitations of the V-22 tilt rotor configuration for optimum cruise performance. The current technology readiness level associated with open rotor thrust vectoring is estimated to be TRL 5; however, due to the increase in vehicle drag, and conventional high-lift systems proving sufficient, this technology was not investigated further.

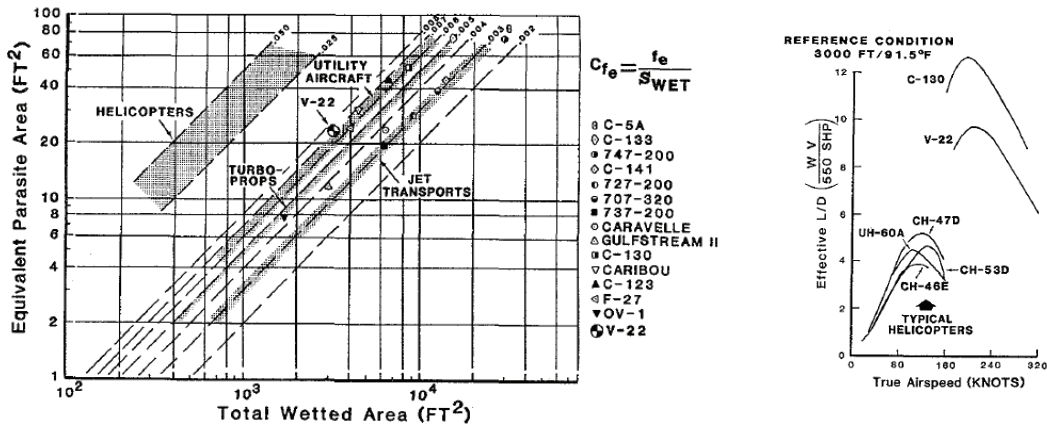


Figure B-3. Tilt Rotor Aerodynamics

B.56 Slat Tip Fences

Slat tip fences are flat plate obstructions employed at the inboard and/or outboard portions of wing slats. They can be aerodynamically contoured depending on the platform on which they are utilized, extending below the lower surface of the slat. Their purpose is to prevent the shedding of streamwise vortices from the edges of the slat caused by the discontinuity in the wing surface upon slat deployment. These vortices have been associated with high levels of airframe noise during landing. This technology can be applied to any wing slat, and generally can be retrofitted to any wing slats that do not currently implement them. There will be a slight weight penalty due to their implementation. Failure of this technology would consist of failure of the attachment of the slat tip fence, at which point it would separate from the slat and fall from the aircraft. It could potentially cause damage to the leading edge of the main wing body, leading to a loss of the acoustic reduction benefit for which it is designed. In a recent experimental study, source noise reduction using an inboard slat tip fence was in the range of 4 dB, while at the outboard tip, a reduction of 2 dB was achieved [Ref. 153]. Weights associated with these devices are minimal. Although slat tip fences are currently estimated to be at a TRL of 5, because of the limited noise reduction potential of the technology, the incompatibility of slats with laminar flow, and the relative contribution of slat noise to the overall aircraft EPNL, this technology was discarded from further examination.

B.57 Cryogenic Motors

Employing motors cooled to superconducting temperatures would allow for operation at extremely high efficiencies. However, the engine architectures that would employ this type of motor are generally more complex than the conventional gas turbine cycle. Using motors for propulsive systems requires them to be driven by other devices, such as generators or fuel cells, and requires them to drive propellers to generate thrust. State-of-the-art advanced motors have specific power densities in the range of 2 hp/lb, meaning that in order to create enough takeoff power, the motor would have to be extremely heavy. In addition, a cryogenic motor necessitates the use of a cooling system to keep its temperature substantially low. This would generally take the form of liquid gas (e.g. hydrogen), requiring additional weight, insulation, and storage requirements.

A cryogenic motor could operate with nearly no emissions, but at a current TRL estimated to be 1, it has been deemed impractical for the N+3 timeframe.

B.58 Porous Plug Designs

Porous nozzle plug designs consist of nozzle plugs which have a degree of porosity in the form of holes and a typically hollow interior. They are generally associated with the reduction of shock associated

noise in supersonic jets by controlling the formation of shocks and shock cells. However, when applied to subsonic flows, benefits are also achieved in noise reduction. This is mainly due to the reduction of shear noise. Subsonic noise suppression has been attributed to a reduction of the length of the jet potential core. It has also been proposed that the centerbody modifies the turbulent structure of the jet by inhibiting vortex pairing. This technology could be applied to any aircraft which uses a plug nozzle, by replacing the solid plug with a porous counterpart. In the case of an aircraft which does not have a plug nozzle implemented, the retrofitting of such a nozzle would be significantly more difficult. There would be a need to incorporate not only the plug nozzle, but the structure to maintain it in place. A porous plug nozzle design could suffer three modes of failure: a rupture of the structure of the plug due to its porosity (and possible weaker structural integrity), melting closed of some or all of the holes in the plug, or the detachment of the plug from the engine system. In the first case, it is likely that thrust losses will occur and noise would increase in certain frequencies, due to vortex shedding off of the rupture location. In the second case, with some or all holes melted closed, the plug would behave more like a solid plug with more noise associated with it. In the third mode of failure, the detachment of the entire plug, engine performance would suffer greatly due to the radically different geometric nozzle conditions compared to those for which it was designed. Aeroacoustic and thrust measurements were conducted by Bauer et al [Ref. 175]. In this study, eight different porous nozzle configurations were studied (mostly for supersonic applications, but at one subsonic pressure ratio) with various temperature core flows. OASPL reduction was measured at multiple directivity angles, and thrust losses were reported for each configuration. Weight penalty is assumed to be negligible, as porosity is introduced into a preexisting structure.

Currently estimated at a TRL of 4, it was determined for this study that the thrust losses associated with the use of the plug nozzle outweighed the potential acoustic benefits in the subsonic flight regime.

B.59 Porous Ceramic Materials

Porous ceramic materials are being explored due to their lightweight nature and both their capacity for acoustic absorption and tolerance to high temperatures. By varying the porosity, pore size, flow resistance, thickness, and length, specific frequencies can be targeted depending on the location of their use in the engine core. The most common projected use for this material is as a nozzle or ejector liner where it can reduce noise associated with the jet engine exhaust while withstanding the heat produced by the combustor. In fact, porous ceramic materials can withstand temperatures in excess of 1000°C [Ref. 176].

The current TRL of this technology has been estimated to be 2; however, due to the implementation of variable nozzle geometry and the exclusion of ejector technology, this technology was not pursued further in the course of this study.

B.60 Porous Flap Side Edges

Streamwise vortex shedding from flaps is a contributor to airframe noise. These vortices have the effect of entraining the wake from the main wing element, and with the pressure fluctuations from the combined flow impinging on the side edge of the flap, whereby airframe noise is generated. By incorporating a flap side edge with porosity, the turbulent stresses contained in this vortex are reduced and the vortex becomes displaced further from the flap surface. In this manner, the noise from the impingement on the flap surface is minimized. This technology can be applied to any wing flap in which there is space to include them, and generally could be retrofitted to any wing flaps that do not currently implement them. There will be a slight weight penalty due to their use. Failure of this technology would consist of failure of the attachment of the porous flap side edge, at which point it would separate from the flap and fall from the aircraft. This would lead to a loss of the acoustic reduction benefit for which it was designed. As reported in Fink and Bailery, flap side edge porous treatment led to a total flap noise reduction of up to 2 to 3 dB [Ref. 177]. In another experimental study, it is reported that the aerodynamic of porous flap side edges is negligible [Ref. 178].

With a currently estimated TRL of 4, it was decided to not pursue this technology further due to its limited capacity for noise reduction in a narrow frequency range, combined with the negligible contribution of flap noise to the overall EPNL of the system.

B.61 Slat Trailing Edge Serrations

Trailing-edge serrations on wing slats involve cutting or constructing V-shaped grooves into the slat material. In the presence of serrations, the periodic vortex shedding from the trailing edge of the slat that would typically occur becomes less coherent in the spanwise direction. In this manner, the noise radiated from the trailing edge of the slat is reduced. This technology can be used on the trailing edge of any slat. Depending on the construction of a particular slat, retrofitting the technology may be possible. Because no additional material must be introduced into the slat to implement the serrations, there will be a negligible weight penalty. This technology is built into the slat of the wing, and as such the only available mode of failure would be for serrations to break apart or bend in the flow. If this were to happen, then the aerodynamic modifications to the flow associated with the presence of the serration would be nullified or changed, and localized pockets of higher noise generation would be created. In an experimental wind tunnel study, a peak noise reduction of 3 dB was achieved by using slat trailing edge serrations [Ref. 153]. However, according to this study, the average noise reduction across the frequency range was approximately 2 dB. Weight penalties are negligible for this technology. However, due to the limited noise reduction potential of this technology, combined with the obsolescence of the technology in the presence of laminar flow (which requires complete removal of leading edge slats), this technology has been discarded for further examination.

With a currently estimated TRL of 4, it was decided to not pursue this technology further due to its limited capacity for noise reduction combined with the removal of slats associated with the integration of laminar flow.

B.62 Porous Slat Pressure Surfaces

Porous slat pressure surfaces are designed to reduce slat noise. Based on wind tunnel results performed by NASA, U.S. partners, and the University of Southampton, vortices generated from the slat trailing edge were found to be a significant portion of the slat noise. These vortices are often amplified in the region between the slat and the main element through resonant reflection. Porous slat pressure surfaces have been found effective in reducing slat trailing edge vortices strength and when placed appropriately, can be effective in reducing flap noise by weakening the vortex generated from the flap side edge. Porous pressure surfaces reduce this vortex by reducing the intensity of pressure fluctuations near the trailing edge of the slat. According to Khorrami and Choudhari, porous slat pressure surfaces can reduce slat far field noise by more than 20 dB [Ref. 179]. In addition to the SPL level reduction, this technology increases the dominant frequency approximately 25%. However, this dominant frequency on full scale applications is expected to exceed human auditory range, thus this shift in frequency would lead to a further reduction in noise. Porous slat pressure surfaces are surfaces composed of a finely woven wire mesh and could use material that is currently used for turbine blade wall cooling or acoustic treatment of engine ducts. This use of commonly used material would only be effective if designed and applied correctly. Weight penalties are negligible for this technology.

Currently estimated at TRL 4, this technology was not investigated further due to the obsolescence of the technology in the presence of laminar flow (which requires complete removal of leading edge slats).

B.63 Micro-Tab Features

Micro-tab features consist of small retractable tabs embedded inside the flap of a high-lift wing that are deployed on either the upper or lower surface of the flap perpendicular to the oncoming flow in order to increase the effective camber of the wing. The height of these tabs is on the order of boundary layer

thickness, so they do not result in excessive drag penalties. This increase in lift on the wing from the micro tabs allows for the flap and slat setting to be slight eased leading to reduction in flap and slat generated noise. If the micro-tabs are designed to be retractable, complexity would be added through wiring and controls. The weight penalty of the micro-tabs themselves is negligible. Noise in high-lift systems is extremely configuration dependant and any increase in flap angle will lead to an increase in noise as a result of increasing the load on the high-lift components and may generate stronger vortex shedding and turbulent wake downstream. In an experiment by Kuo and Sarigul-Klijn, a baseline airfoil with 30 degree slat and flap deflection at an angle of attack of 6 degrees with no noise reduction technologies was used to compare against an airfoil with a 20 degree deflected slat and flap deflection at an angle of attack of 8.8 degrees with microtab integration [Ref. 180]. Both high lift airfoils were derived from a Boeing 737 type midspan airfoil with a single flap. It was found that beyond 100 Hz, the micro tab configuration reduced wing noise levels by 2-5 dB over the entire frequency spectrum compared to the baseline configuration. When the A-weighted acoustic results are compared, it can be seen in Figure B-4 that the microtab configuration shares a noise spike at a frequency of approximately 315 Hz and a reduced noise spike at 630 Hz when compared to the baseline configuration. The noise spike of the baseline at 1260 Hz is not present in the microtab configuration. Microtabs were found to reduce the overall noise levels by 2.3 dB. In addition, the microtab configuration was found to decrease drag by 5%.

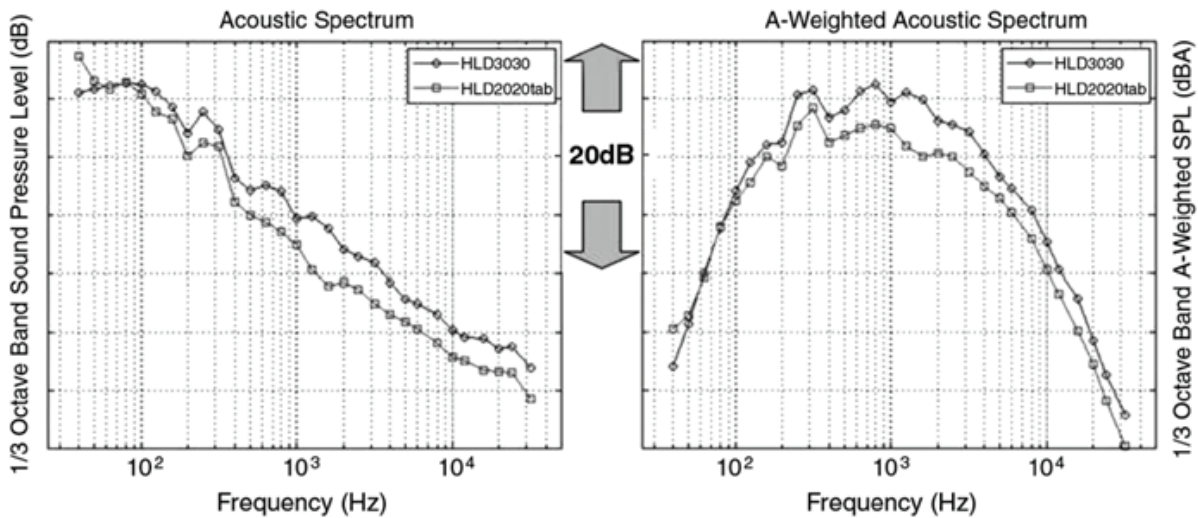


Figure B-4. Noise Attenuation With and Without Microtab Features

Currently estimated at TRL 4, this technology was not investigated for further analysis due to the relative importance of the wing noise when compared to other airframe noise sources in addition to decreased effectiveness in the presence of laminar flow (which requires complete removal of leading edge slats). Fuel burn by mission segment for preferred configuration.

B.64 Fiber Metal Laminates

Fiber metal laminate (FML) is a class of metallic materials consisting of a laminate of several thin metal layers bonded with layers of composite material, commonly glass fiber and aluminum that was designed to enhance the fatigue performance of aluminum structures. FMLs combine the high bearing strength and impact properties of metals with the high fatigue, strength, and stiffness properties of composite matrices [Ref. 181]. This allows the material to behave much as a simple structure with specifically tailored advantages regarding structural properties including crack propagation.

This increase in fatigue and other material properties, offers potential weight savings. This technology has not seen extensive military use, but has been utilized in cargo doors and fuselage skins of nonmilitary vehicles. Based on internal research, FMLs have shown weight savings for only very few applications. Composite structures would be lighter than FML for tension dominated structures. In addition,

compression strength dominated structures would gain increased weight savings from composites versus FML. FMLs have been forecasted to be not competitive for use with min-gauge structures, which are the majority of structures found in flying wing bodies. Potential acreage applications on vehicles would be impact prone areas including cargo floors, ramps, and doors.

Although positive benefits are expected due to increased fatigue and impact properties, internal analysis has revealed that FML effects with regard to the overall vehicle weight is minimal when weighed together with the relative immaturity of the technology.

Currently estimated at TRL 4, this technology was not investigated further due to having no significant weight benefits.

B.65 Metallic Digital Direct Manufacturing

Metallic Digital Direct Manufacturing (MDDM) is a manufacturing process that creates physical parts from a 3-D CAD file or data using additive fabrication techniques [Ref. 182]. Several MDDM techniques use a laser or electron beam as the main energy source. The system aims to create a 3-D part with the sequential solidification of 2-D layers. The process uses one of three methods for injecting material into the energy source, which fuses the material onto the surface, creating a layer. This process is repeated until the part is completed. This allows for the fabrication of extremely complex parts with 100% density. Manufacturing speed, preciseness, and productivity is also increased.

MDDM can be used for any metallic component in the vehicle including titanium. Through internal research, it was found that MDDM would offer potential weight savings through manufacturing of complex integrated part that would normally be comprised of fastened sub-components, reducing part count. Although positive benefits are expected due reduction in part count, internal analysis has revealed that MDDM effects with regard to the overall vehicle weight is minimal when weighed together with the relative immaturity of the technology.

Currently estimated at TRL 4, this technology was not investigated further due to having no significant weight benefits.

B.66 Open-Celled and Stamped Composite Structures

Open-celled and stamped composite structures use a composite-based trussed beaded or sinewave structure. Through the use of composites and structural layout, structural weight reduction is possible. Open-celled and beaded structures offer high volumetric efficiency, high dynamic damping, mechanical isotropy, increased shelf life and ease of manufacturing. The current baseline is composed of nonbuckled metallic and composite structures, with sandwich structures as the leading candidate. Based on internal research and testing, depending on application and on the minimum gage definition for composite sandwich, open-celled and stamped composite structures could offer a part weight savings up to 20%. Candidate applications for open-celled structures are minimum gage structures with low loading such as a trussed substructure's webs with holes. Candidate applications for stamped structures, such as beaded or sinewave structures, are structures that have some degree of loading and hence thickness. However, this application would be limited to substructural webs.

Reduced vehicle weight would reduce fuel burn and field length for landing and takeoff. When the relative system level weight reduction from this technology was compared to other airframe technologies, it was felt that an additional structural technology with similar effects was not warranted as its model would fall in line with the result of the others.

The current technology readiness level associated with open-celled and stamped composites is estimated to be TRL 5; however, due to the weight reduction being applicable to select applications and larger scale weight reduction being in line with other structural technologies, this technology was not investigated further.

B.67 Post-Buckled Composite Structures

Post-buckled composite structures deviate from the traditional design of allowing initial buckling to occur at or slightly above the ultimate load of a structure and lead to reduced weight and manufacturing costs [Ref. 183]. Post-buckled structures demonstrate that certain structures exhibit significant strength beyond that demonstrated at initial buckling [Ref. 184,185]. An increased reliance on design and model analysis is required due to the nonlinear material and geometric behavior associated with post-buckled composite structures. This structural design allows for the use of minimum gage designs in candidate components. Aggressive use of minimum gage designs would result in a major part weight reduction in structures that are not extremely heavily loaded. The current baseline is nonbuckled composed of nonbuckled metallic and composite structures with sandwich as the leading candidate. Based on internal research, depending on the minimum gage definition for composite sandwich, post-buckled composite panels could result in part weight reduction up to 20%. Candidate applications for post-buckled structures are structures that have some degree of loading and hence thickness and in both substructures and outer mold line skins. Large bulkhead subsections could potentially be post-buckled to reduce weight. Regarding outer mold line skins, many transport fuselage and deep section skins are mostly minimum gauge. Wing skins demonstrate potentially large benefits from post-buckled structures. Reduced vehicle weight would reduce fuel burn and field length for landing and takeoff. When the relative system level weight reduction from this technology was compared to other airframe technologies, it was felt that an additional structural technology with similar effects was not warranted as its model would fall in line with the result of the others.

The current technology readiness level associated with post-buckled composite structures is estimated to be TRL 5; however, due to the weight reduction being applicable to select applications and larger scale weight reduction being in line with other structural technologies, this technology was not investigated further.

B.68 Direct Manufacturing/Laser Sintering of Polymeric Materials

Direct part manufacturing/laser sintering is an additive process capability that uses net-shape and layer build technology. Components are produced from a machine without tooling with engineering data generated from a 3-D computer model. The component is produced to be dimensionally accurate and requires little to no postprocessing or sizing prior to finishing. The machine uses a laser to machine away excess ceramic material and fuses together the polymer that will be used for the part.

The parts produced with this manufacturing method are limited to non-load bearing structures within subsystem assemblies and subassemblies. This technology is primarily used to reduce part count, tooling, post processing, part weight, and is able to fabricate complex designs. Nylon 12 is currently used with this manufacturing technique in the Global Hawk and in the F-18. However, Nylon 12 is limited to temperatures less than 180 degrees Fahrenheit. Higher temperature materials are needed in order to see a more significant vehicle level weight reduction.

The TRL of direct manufacturing/laser-sintering is 9 for Nylon 12 and 3 for higher temperature materials. Due to the low weight reduction relative to other technologies on the vehicle level, this technology was not investigated further.

B.69 Slat Gap Liners

This technology entails lining the lower surface of the slat and portions of the main wing leading edge with acoustic liners to suppress noise in certain frequency ranges, particularly those associated with the convection of turbulence through the slat gap and past the sharp trailing edge of the slat. Due to the embeddable nature of acoustic liners, there is little to no effect on the aerodynamic performance of the high-lift device caused by the presence of the liner, and they are easily tunable to particular frequencies in the design phase. However, current liner technology is passive in nature, so it is possible that this

technology would not be optimized for all conditions. Depending on the attachment method, slat gap liners could be affixed to any wing that employs slats for added lift capabilities. This will adversely (though minimally) affect the aircraft weight, though due its passive nature there will be no additional requirements in terms of electrical cables or hydraulics. Failure modes of the technology depend on how the liners are affixed or embedded into the slat and main wing leading edge. If it is a retrofit situation where the attachment method could fail, then the liner sections could become projectiles in the case of a failure. However, due to their size and weight, any capacity for damage would be minimal. In Smith et al, it is shown through wind tunnel experimentation that in the range of 2-10 kHz, a fully-lined (slat cove and main wing leading edge) high-lift device averages around 1.5 dB noise reduction averaged over directivity angles [Ref. 186]. This test also confirmed that a properly attached liner has no notable effect on the aerodynamic performance of the wing through a comparison of $CL-\alpha$ curves with and without the liner installed. Weight could effectively be reduced by the use of liners since they are porous in nature, though to accommodate for attachment requirements, it will be assumed that these benefits and penalties balance out. However, due to the limited noise reduction potential of these liners, combined with the obsolescence of the technology in the presence of laminar flow (which requires complete removal of leading edge slats), this technology has been discarded for further examination.

The TRL of slat gap liners is currently estimated to be 3. Due to its limited capacity for noise reduction combined with the removal of slats associated with the integration of laminar flow, slat gap liners were not considered for further investigation.

B.70 Streamlined Slat Tracks

Current slat tracks guide the slat between its deployed and undeployed state with little consideration given to the noise and aerodynamic penalties that may exist. These components generate noise, and high-lift noise on approach is generally dominated by the slat. Streamlining the slat tracks is a potential contributor to high-lift noise reduction. Slat tracks could either be modified using add-on treatments to fill cavities and generally smooth out the surfaces, or could be redesigned at an earlier stage in the aircraft design process to give a more aerodynamic geometry. In the case of add-on treatments, a small degree of weight would be added to the system depending on the material used in the treatment. For newly designed streamlined slat tracks, the design could represent a reduced component weight.

In the case of an add-on treatment for streamlining the slat track, this treatment could become loosened or damaged with use. This may affect the retraction of the slat, leading to undesirable performance characteristics after the lift-off sequence. If the slat track were geometrically redesigned with no add-on parts, failure would be more dramatic (but less likely). In this case a possible mode of failure would be the structural weakening or breaking of the slat track, which would have serious consequences for the retraction of the slat.

According to Dobrzynski et al [Ref. 187], slat tracks constitute sources of excessive flow noise, on the order of 8 dB higher than the rest of the slat. A flight test of an add-on slat track treatment showed a reduction of 0.4 EPNdB due mainly to noise reduction at and above the 315 Hz 1/3-octave band [Ref. 188]. This work also reports that no changes in drag performance was noticed or expected as a result of the add-on treatments.

Although positive benefits are expected due to the implementation of streamlined slat tracks, experimental measurements have revealed that their effects with regard to the overall EPNL of the aircraft is minimal when weighed together with the relative immaturity of the technology. Currently estimated at TRL 3, this technology was not investigated further.

B.71 Thrust Vectoring Nozzles

Thrust vectoring is a technology that allows for the vectoring of engine thrust improving maneuverability and allowing STOL capabilities. According to Friehmelt, vehicles that were integrated

with thrust vectoring nozzles demonstrated a 38% shorter take-off distance and 60% shorter landing roll [Ref. 189]. However, Friehehl states that up to 30% of the net thrust can be lost due to undesirable deflection in portions of the flow. This decrease in thrust efficiency would increase fuel burned throughout the vehicle mission. According to other studies, mechanical thrust vectoring systems result in significant increased weight and present integration issues [Ref. 190]. Mechanical thrust vectoring systems are present on many modern military vehicles. Fluidic thrust vectoring offers improved thrust efficiency with a less significant weight penalty. However, this technology is still in early stages of development.

Figure B-2 compares the lift capabilities of thrust vectoring and flap configuration to a conventional flap configuration. Vectored thrust with flaps shows considerable improvements for STOL capabilities compared to a conventional flap configuration.

Although positive field length benefits are expected due to the implementation of thrust vectoring, the structural and fuel weight penalties associated with both fluidic and mechanical thrust vectoring outweigh the field length improvements for the given mission. As a result of integrated propulsion and advanced field length configurations being dismissed in Section 7.2.9, and low TRL level of fluidic thrust vectoring, thrust vectoring was not investigated further.

B.72 Metal Foam Liner

Traditional DOF liners are located in the inlet where metal foam liners allow for the placement closer to the engine rotor, which is closer to the noise source and can provide increased effectiveness in noise reduction. Metal foam liners would be able to reduce engine far field noise by providing a pressure relief region and altering the acoustic near field. This can reduce noise generation sources and allow improved reduction in regions further away from the rotor. Based on the work of Sutliff and Jones Ref. 191, it was found that if a foam-metal liner was installed over the rotor, a possible noise reduction of 4 dB was attainable.

A tradeoff exists between the absorption capacity of the liner and the drag that is generated. Additionally, the weight and volume penalties associated with acoustic liners increases as the thickness and area increases.

Metal foam acoustic liners are currently estimated to be TRL 6, this technology was not considered for further investigation due a two DOF liner proving to be superior for the current configuration.

Appendix C

Preferred Vehicle Aerodynamics

Appendix C Preferred Vehicle Aerodynamics

Tables C-1 through C-2 and Figures C-1 through C-3 show preferred vehicle aerodynamics

Table C-1. Preferred Vehicle High Speed Drag Polar at 45,000 feet Altitude

MACH NUMBER	CL														
	0.1	0.15	0.2	0.25	0.3	0.35	0.4	0.45	0.5	0.55	0.6	0.65	0.7	0.75	0.8
0.2	0.024	0.0241	0.0244	0.0249	0.0257	0.0267	0.0278	0.0291	0.0307	0.0326	0.0344	0.0365	0.0388	0.0414	0.0442
0.3	0.02217	0.0223	0.0226	0.0231	0.0239	0.0248	0.026	0.0272	0.0289	0.0308	0.0326	0.0347	0.037	0.0396	0.0424
0.4	0.02095	0.021	0.0213	0.0219	0.0227	0.0236	0.0248	0.026	0.0277	0.0296	0.0314	0.0334	0.0358	0.0383	0.0411
0.5	0.02004	0.0201	0.0204	0.021	0.0217	0.0227	0.0238	0.0251	0.0267	0.0287	0.0305	0.0325	0.0348	0.0374	0.0402
0.6	0.01935	0.0194	0.0197	0.0202	0.0211	0.022	0.0231	0.0244	0.026	0.0279	0.0297	0.0318	0.0341	0.0367	0.0395
0.7	0.01929	0.0193	0.0196	0.0201	0.021	0.0219	0.023	0.0242	0.0259	0.0278	0.0296	0.0317	0.034	0.0366	0.0394
0.75	0.01936	0.0193	0.0196	0.0202	0.0211	0.022	0.023	0.0242	0.0259	0.0278	0.0296	0.0317	0.034	0.0366	0.0394
0.8	0.01965	0.0196	0.0198	0.0204	0.0214	0.0222	0.0232	0.0244	0.0261	0.028	0.03	0.0326	0.0359	0.0399	0.0446
0.825	0.0201	0.02	0.0202	0.0208	0.0218	0.0227	0.0236	0.0248	0.0265	0.0284	0.0317	0.0357	0.0405	0.046	0.0522
0.85	0.02134	0.0211	0.0213	0.0219	0.023	0.0241	0.0252	0.0268	0.0291	0.0333	0.0373	0.0433	0.0514	0.0617	0.0743

Table C-2. Preferred Vehicle Reynold's Number Drag Coefficient Corrections

ALTITUDE, ft	MACH NUMBER											
	0.2	0.3	0.4	0.5	0.6	0.7	0.75	0.8	0.825	0.85	0.875	0.9
0	-0.00568	-0.00507	-0.00468	-0.0044	-0.00418	-0.00399	-0.00391	-0.00383	-0.00379	-0.00376	-0.00372	-0.00369
5000	-0.00526	-0.0047	-0.00433	-0.00407	-0.00386	-0.00369	-0.00361	-0.00354	-0.00351	-0.00347	-0.00344	-0.00341
10000	-0.00482	-0.00429	-0.00396	-0.00372	-0.00353	-0.00337	-0.0033	-0.00323	-0.0032	-0.00317	-0.00314	-0.00311
15000	-0.00434	-0.00386	-0.00356	-0.00334	-0.00317	-0.00303	-0.00296	-0.0029	-0.00288	-0.00285	-0.00282	-0.0028
20000	-0.00382	-0.0034	-0.00313	-0.00294	-0.00279	-0.00266	-0.0026	-0.00255	-0.00253	-0.0025	-0.00248	-0.00245
25000	-0.00326	-0.0029	-0.00267	-0.0025	-0.00237	-0.00226	-0.00221	-0.00217	-0.00215	-0.00213	-0.00211	-0.00209
30000	-0.00265	-0.00235	-0.00216	-0.00203	-0.00192	-0.00183	-0.00179	-0.00176	-0.00174	-0.00172	-0.00171	-0.00169
35000	-0.00198	-0.00176	-0.00161	-0.00151	-0.00143	-0.00137	-0.00134	-0.00131	-0.0013	-0.00128	-0.00127	-0.00126
40000	-0.00106	-0.00093	-0.00086	-0.0008	-0.00076	-0.00073	-0.00071	-0.00069	-0.00069	-0.00068	-0.00067	-0.00067
45000	0	0	0	0	0	0	0	0	0	0	0	0
50000	0.00113	0.001	0.00092	0.00086	0.00081	0.00077	0.00076	0.00074	0.00073	0.00073	0.00072	0.00071
55000	0.00235	0.00208	0.0019	0.00178	0.00168	0.0016	0.00156	0.00153	0.00152	0.0015	0.00149	0.00147
60000	0.00367	0.00323	0.00296	0.00276	0.00261	0.00248	0.00243	0.00238	0.00235	0.00233	0.00231	0.00228

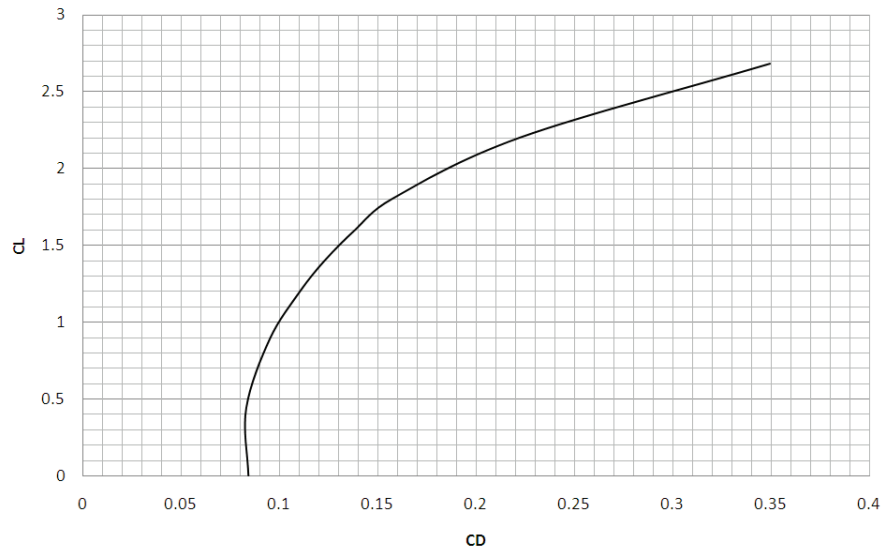


Figure C-1. Preferred Vehicle Low-Speed Drag Polar for Takeoff at 0 feet Altitude

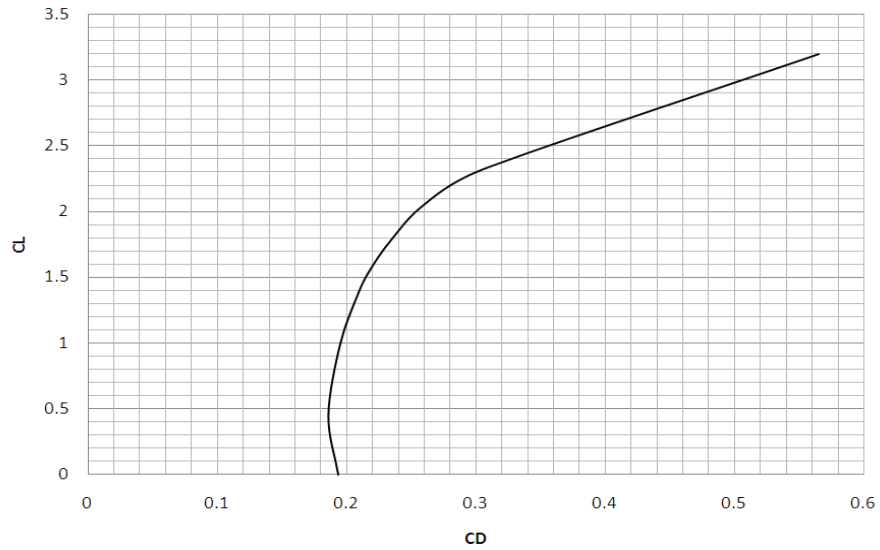


Figure C-2. Preferred Vehicle Low-Speed Drag Polar for Landing at 0 feet Altitude

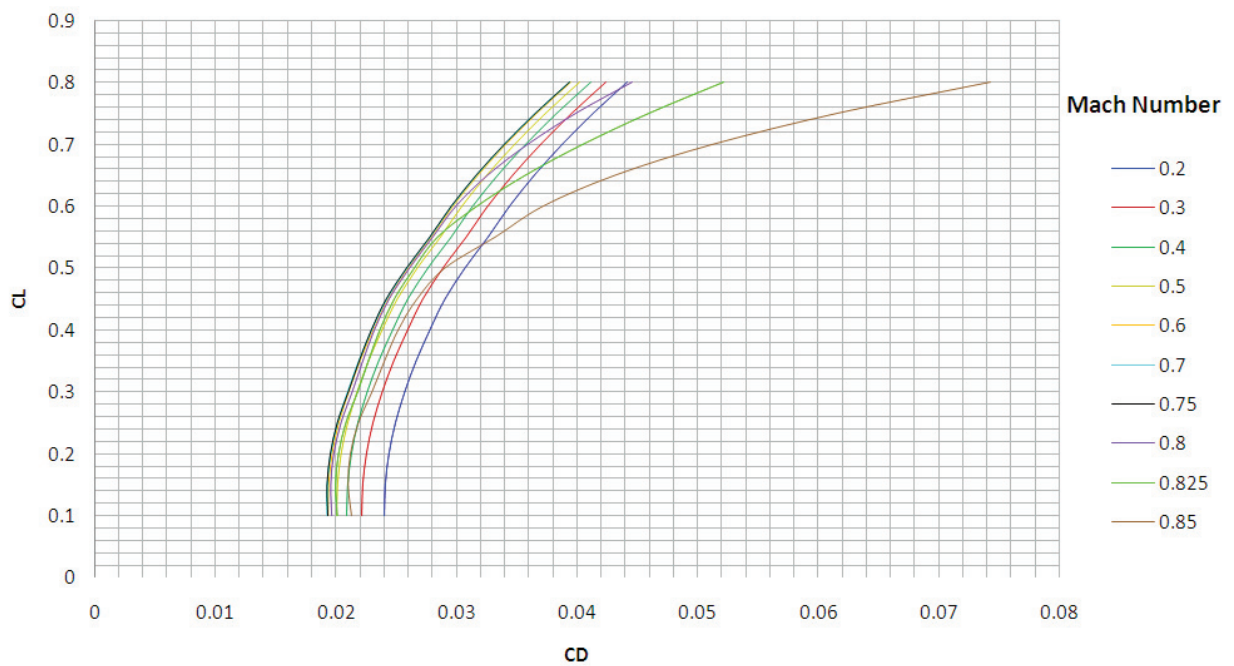


Figure C-3. Preferred Vehicle High-Speed Drag Polar, R_n associated with 45,000 feet Altitude

Appendix D

Vehicle OASPL Maps

Appendix D Vehicle OASPL Maps

Figure D-1 shows an example overall sound pressure level (OASPL) result for a random vehicle source. OASPL is plotted against polar angle, from -90 to +90 degrees, measured about the fuselage from one wing to the other, and against the azimuth angle, from 0 to 180 degrees, measured in the plane of the aircraft from the nose to its tail. Figures D-2 through D-9 use these standardized axes and scales, allowing for easy, uniform comparison.

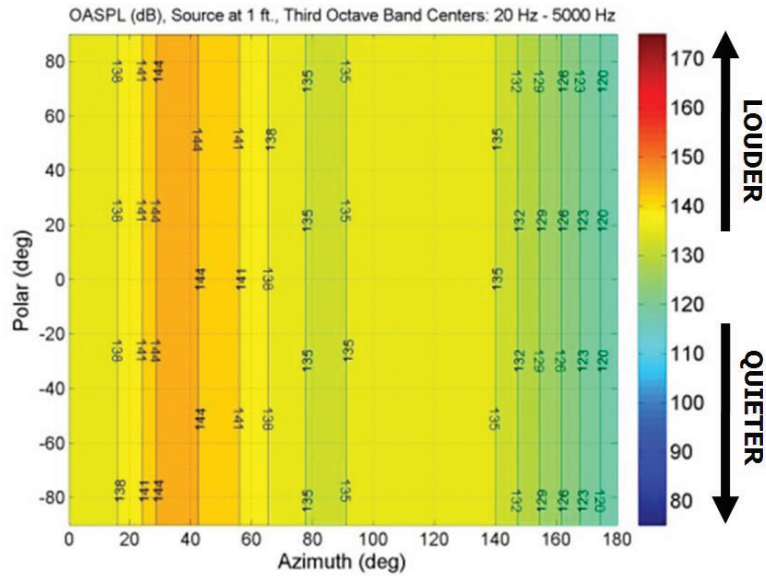


Figure D-1. OASPL Example Source Plot

D.1 Reference Vehicle – OASPL

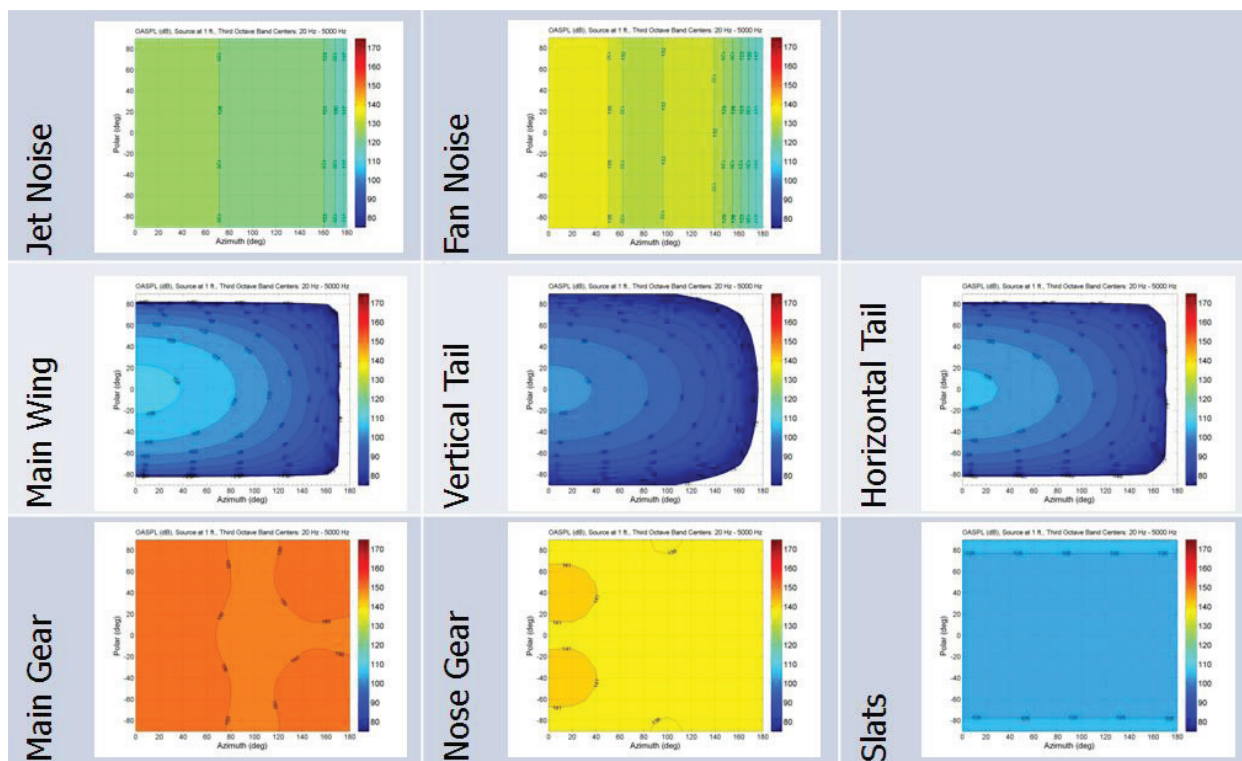


Figure D-2. Noise Source Levels Reference Vehicle at 250 feet Altitude [Descent-Landing]

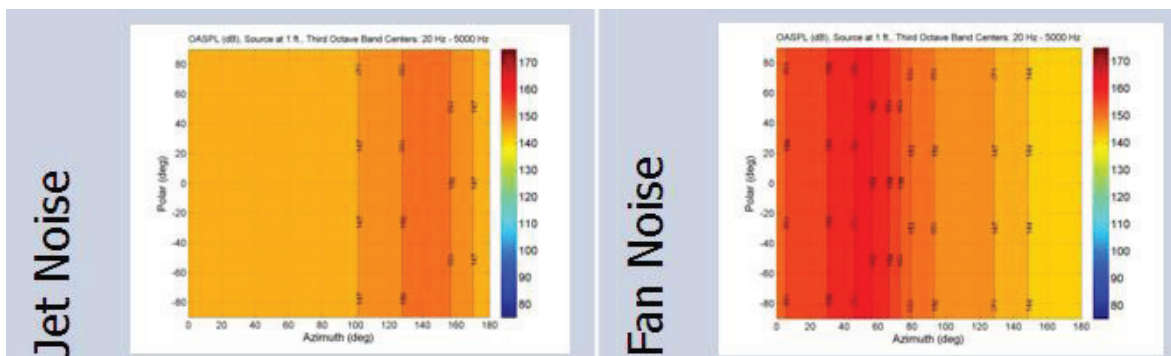


Figure D-3. Noise Source Levels Reference Vehicle at 250 feet Altitude [Takeoff-Climb]

D.2 Advanced Tube-and-Wing, Scaled CFM56-3B1, No Technologies – OASPL

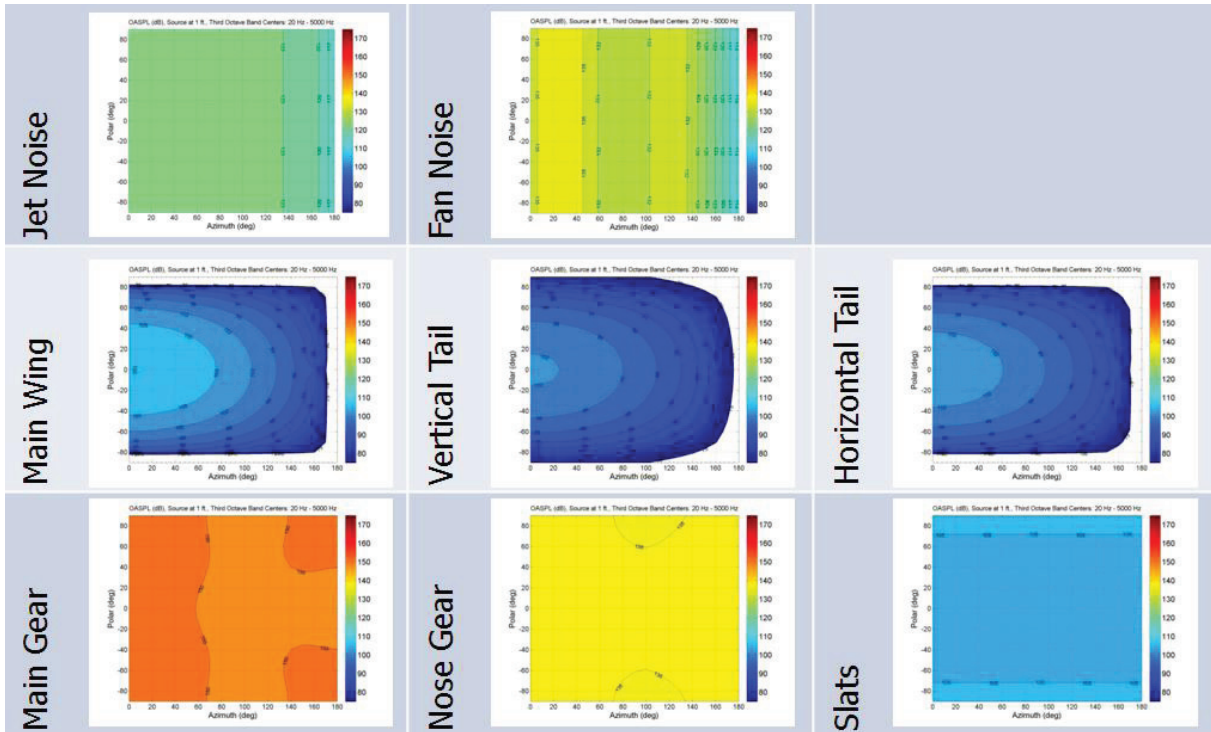


Figure D-4. Noise Source Levels ATW, Scaled CFM56-3B1, No Advanced Technologies at 250 feet Altitude [Descent-Landing]

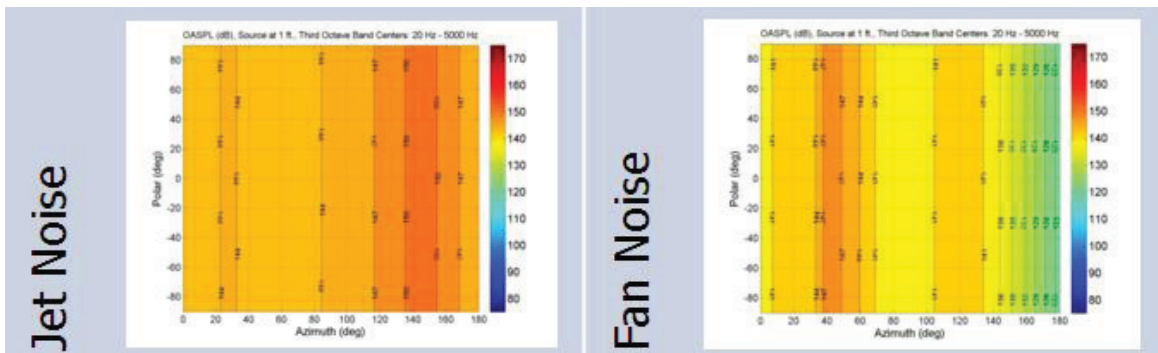


Figure D-5. Noise Source Levels ATW, Scaled CFM56-3B1, No Advanced Technologies at 250 feet Altitude [Takeoff-Climb]

D.3 Hybrid Wing-Body, Scaled CFM56-3B1, No Technologies – OASPL

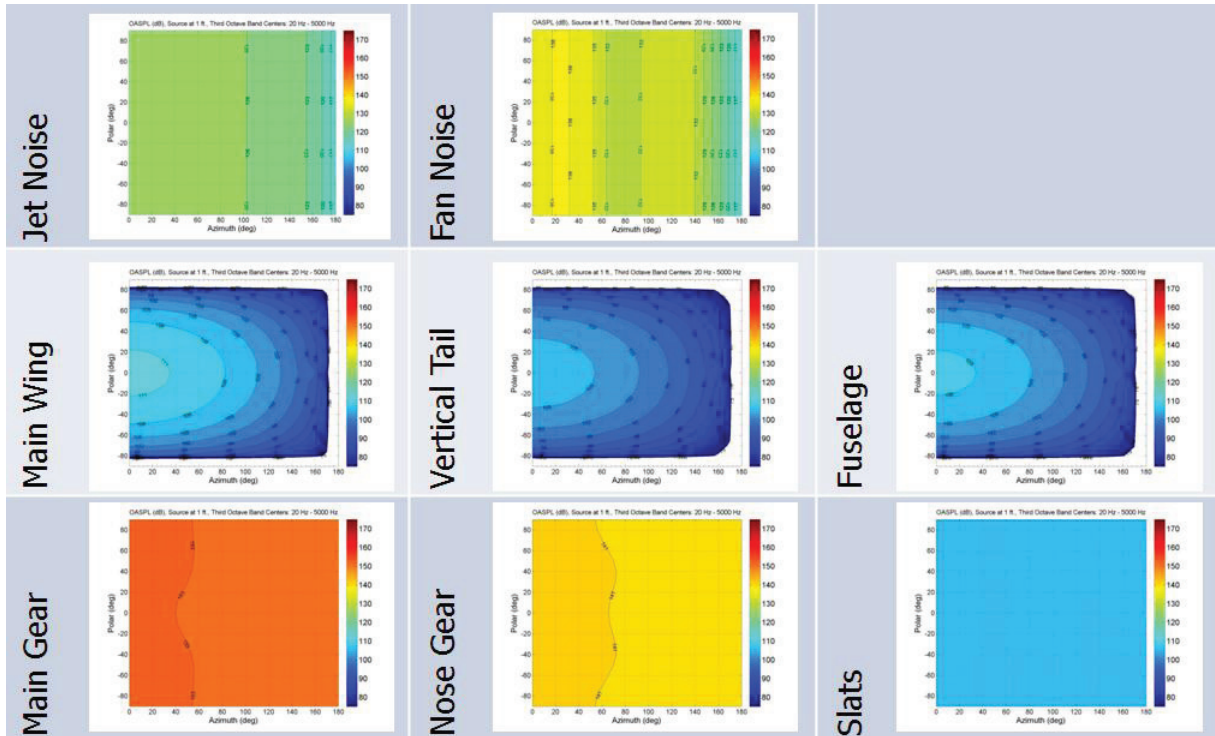


Figure D-6. Noise Source Levels HWB, Scaled CFM56-3B1, No Advanced Technologies at 250 feet Altitude [Descent-Landing]

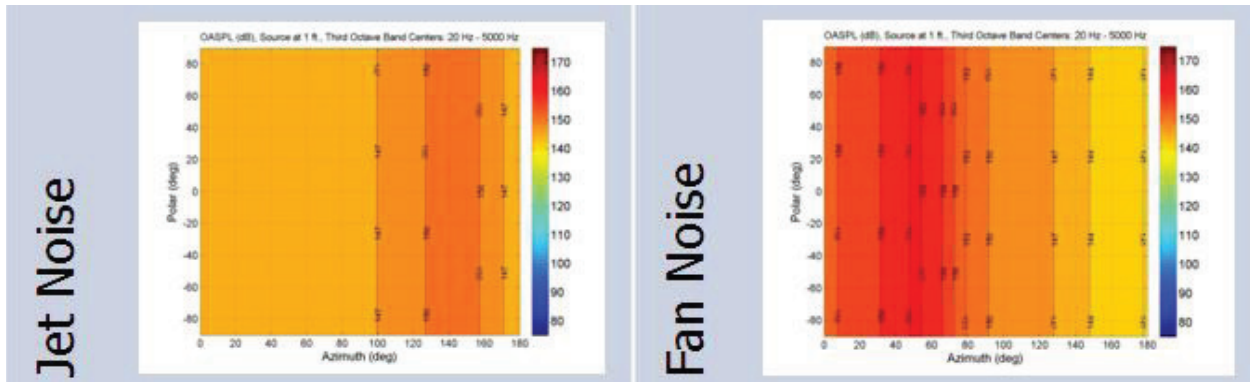


Figure D-7. Noise Source Levels HWB, Scaled CFM56-3B1, No Advanced Technologies at 250 feet Altitude [Takeoff-Climb]

D.4 Preferred Configuration – OASPL

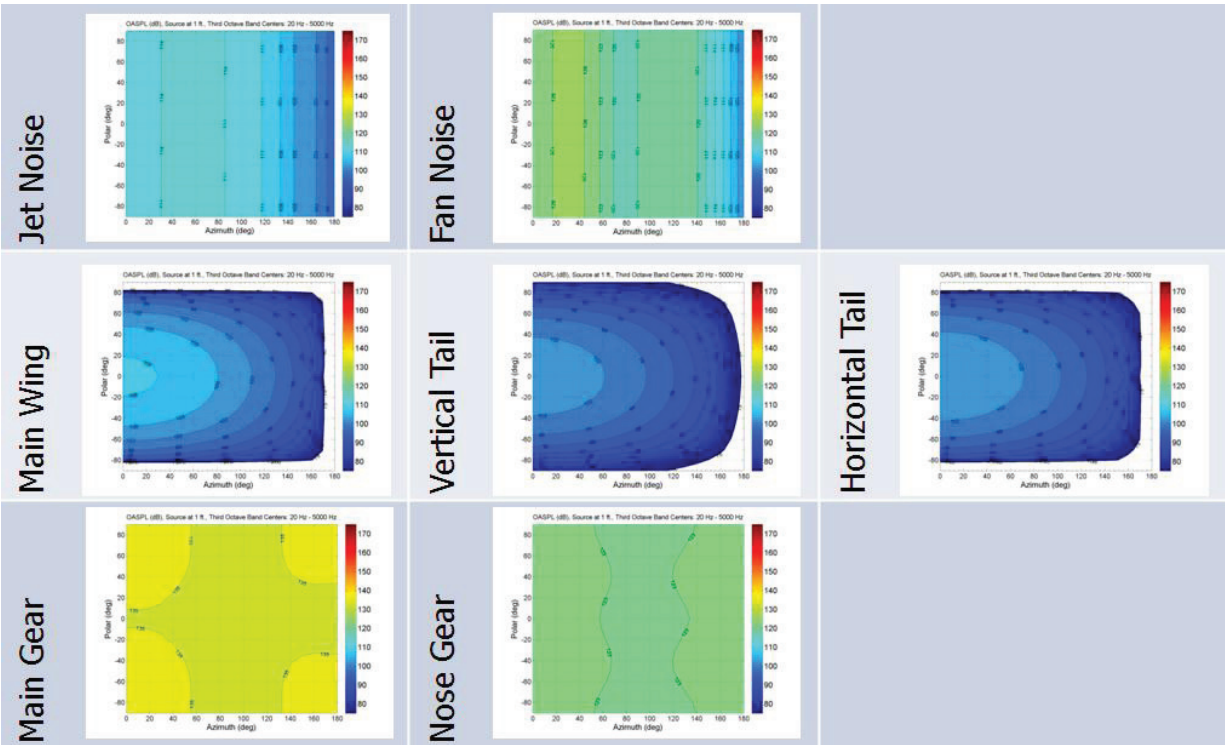


Figure D-8. Noise Source Levels Preferred Configuration at 250 feet Altitude [Descent-Landing]

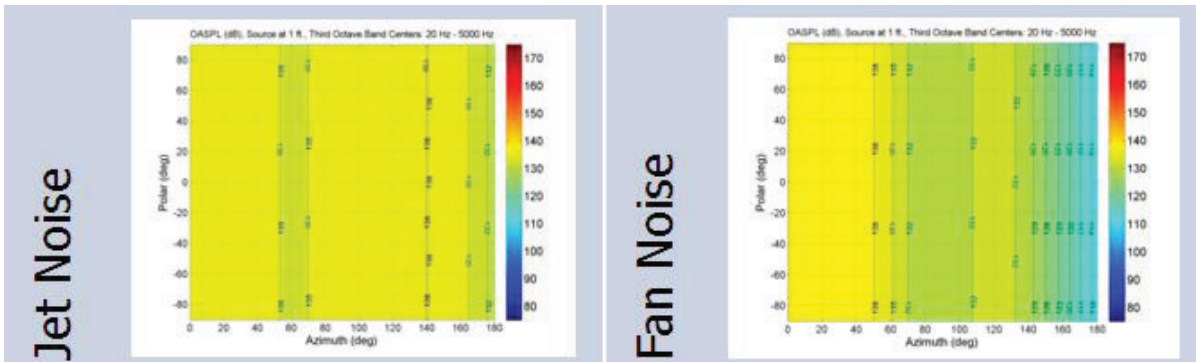


Figure D-9. Noise Source Levels Preferred Configuration at 250 feet Altitude [Takeoff-Climb]

Appendix E

QFD Spreadsheet

ID	Designation:	Description:	Fuel Burn		Field Length		LTO NOx		Noise L _{pn}		TER Sub-Total		Interaction Quotient		TER Grand Total		
			Input	IER	FL	FL	NOx	NOx	dB	dB	IER	IER	IER	IER		IER	IER
 <p>OVERALL SCENARIO APPLIED</p>			<p>SELECT Goals:</p> <p>Scale Factor (Priority) 1.00</p> <p>Normalized Scale Factor 33.33</p> <p>Units Qualitative</p> <p>Goal 3</p> <p>Threshold 3</p> <p>Fz (Threshold Value On Gaussian Curve): 3</p>		<p>13.33 9 13.33 9 33.33 9</p> <p>10.00 3 4.00 3 10.00 3</p>		<p>19.52 5 7.81 5</p> <p>3.92 9 13.33 5</p> <p>29.16 5 7.81 3</p>		<p>6.00 52.8 3 6.00 52.8</p> <p>17.50 54.3 7 17.50 54.3</p> <p>6.00 53.0 3 6.00 53.0</p>		<p>9 10 2 5 9 9 2</p> <p>100.0 100.0 1 100.0 1 100.0 1</p>		<p>0.33</p> <p>1.00</p>				
<p>Physical Principles Summary:</p> <p>Upper wing surface separation control to allow higher stall angle and CL_{max} for takeoff and descent at steeper trajectories. Offtake fan bleed flow for high lift systems via blown flap, CCW, etc. Embedded starter/generator provide mechanical efficiency over hydraulics. Several new aluminum and titanium alloys are currently in development for structural and subsystem applications. Surface treatment of metal components by LASER shock peening has shown increased residual stresses and stress depth, increasing fatigue life, and improving material properties. Advanced 3-dimensionally woven or stitched fiber composites to enable integrated bonded structures with standard and intermediate modulus carbon fibers. Single process fabrication of foamed composite core with skins. Structural weight reduction through gust/flutter/maneuver load control, potential reduction of actuation system weight through active aero-elastic wing technology. Distributed Exhaust Nozzles Integrated into Flap Provide Flow Control/Supercirculation. Pulsed Effectors Provide Similar Benefits as Steady CCW. Series of combustion chambers burn leaner so that total NOx production is lowered, and slight thermal efficiency gains realized. Reduced emissions. Vary blade pitch to optimize FPR at various conditions, eliminates need for thrust reverser, reduce windmilling drag. Decrease pressure losses especially for lower FPR designs. Reduce fan-tip noise. Reduced Skin Friction by Increasing Regions of Laminar Flow Through Shaping. Replace traditional APU with regenerative fuel cells.</p>			<p>Max Score Baseline</p> <p>This is the maximum score</p>		<p>33.33 9 13.33 9 33.33 9</p> <p>10.00 3 4.00 3 10.00 3</p>		<p>19.52 5 7.81 5</p> <p>3.92 9 13.33 5</p> <p>29.16 5 7.81 3</p>		<p>6.00 52.8 3 6.00 52.8</p> <p>17.50 54.3 7 17.50 54.3</p> <p>6.00 53.0 3 6.00 53.0</p>		<p>9 10 2 5 9 9 2</p> <p>100.0 100.0 1 100.0 1 100.0 1</p>		<p>0.33</p> <p>1.00</p>				
43	Noise Concept #3.15	Deployable Vortex Generators	5	19.52	5	7.81	5	19.52	3	6.00	52.8	5	22.2	1.040	2.3	-1	55.0
21	Aero Concept #2.07	Steady Circulation Control	1	3.92	9	13.33	5	19.52	7	17.50	54.3	3	34.2	1.000	2.34	-1	54.3
103	Prop Concept #4.35	All Electric (no AEB)	7	29.16	5	7.81	3	10.00	3	6.00	53.0	3	34.2	1.000	4	0	53.0
1	Airframe Concept #1.01	Advanced Metallic Structural and Sub-System Alloys	5	19.52	5	7.81	5	19.52	3	6.00	52.8	3	34.2	1.000	1	5	52.8
4	Airframe Concept #1.04	Structural Materials Laser Surface Treatment	5	19.52	5	7.81	5	19.52	3	6.00	52.8	3	34.2	1.000	1	3	52.8
5	Airframe Concept #1.05	3-D Woven / Stitched Composites	5	19.52	5	7.81	5	19.52	3	6.00	52.8	3	34.2	1.000	1	1	52.8
7	Airframe Concept #1.07	Light-Weight Foamed Composites	5	19.52	5	7.81	5	19.52	3	6.00	52.8	3	34.2	1.000	1	2	52.8
9	Airframe Concept #1.09	Integrated Aeroelastic (ASE) Structures	5	19.52	5	7.81	5	19.52	3	6.00	52.8	3	34.2	1.000	0	0	52.8
20	Aero Concept #2.06	Distributed Exhaust Nozzle Flap (DEN Flap)	1	3.92	9	13.33	5	19.52	7	17.50	54.3	2	46.1	0.961	2.34	13	52.1
22	Aero Concept #2.08	Offtake Engine Flow Used for Circulation Control via Blown Flap, IBF, Coanda Jet Flap, etc.)	1	3.92	9	13.33	5	19.52	7	17.50	54.3	2	46.1	0.961	2.34	0	52.1
101	Prop Concept #4.33	Staged Combustors	3	10.00	3	4.00	7	29.16	3	6.00	49.2	6	18.3	1.053	0	0	51.8
100	Prop Concept #4.32	Water Injection	3	10.00	5	7.81	5	19.52	5	11.71	49.0	6	18.3	1.053	0	0	51.6
93	Prop Concept #4.25	Variable Pitch Fan Blades	3	10.00	5	7.81	5	19.52	5	11.71	49.0	5	22.2	1.040	1.4	-1	51.0
72	Prop Concept #4.04	Swept Fan Outlet Guide Vanes	5	19.52	5	7.81	3	10.00	5	11.71	49.0	5	22.2	1.040	3.4	22	51.0
23	Aero Concept #2.09	Swept-Wing Laminar Flow	7	29.16	3	4.00	3	10.00	3	6.00	49.2	4	27.2	1.023	2.3	6	50.3
90	Prop Concept #4.22	Fuel Cell APU	5	19.52	3	4.00	5	19.52	3	6.00	49.0	4	27.2	1.023	2.4	20	50.2

Figure E-1. QFD Worksheet (Sheet 2 of 6)



OVERALL SCENARIO APPLIED

ID	Description:	Fuel Burn		Field Length		LTO NOx		Noise L _{EPN}		TER Sub-Total	TRL	Interaction Quotient		TER Grand Total		
		Input	TER	FL Input	FL TER	NOx Input	NOx TER	dB Input	dB TER			Input	Factor		Input	Factor
	SELECT Goals:															
	Scale Factor (Priority)	1.00		0.40		1.00		0.60			0.33		1.00			
	Normalized Scale Factor															
	Units	33.33		13.33		33.33		20.00								
	Goal	Qualitative		Qualitative		Qualitative		Qualitative								
	Threshold	3		3		3		3								
	Fz (Threshold Value On Gaussian Curve):	0.3		0.3		0.3		0.3								
	Max Score Baseline	33.33		13.33		33.33		20.00		100.0						
	TER Baseline	10.00		4.00		10.00		6.00		30.0						
	Physical Principles Summary:															
	PROVIDE DESCRIPTION - KYLE															
34	Noise Concept #3.06	3	10.00	3	4.00	3	10.00	7	17.50	41.5	4	27.2	1.023	1.2,4	15	42.5
68	Noise Concept #3.40	3	10.00	3	4.00	3	10.00	9	20.00	44.0	2	46.1	0.961	3,4	8	42.3
28	Aero Concept #2.14	1	3.92	7	11.66	5	19.52	3	6.00	41.1	4	27.2	1.023	2,3,4	7	42.1
71	Prop Concept #4.03	3	10.00	3	4.00	5	19.52	3	6.00	39.5	5	22.2	1.040	4	-1	41.1
74	Prop Concept #4.06	5	19.52	3	4.00	3	10.00	3	6.00	39.5	5	22.2	1.040	0	1	41.1
82	Prop Concept #4.14	5	19.52	5	7.81	3	10.00	1	2.35	39.7	4	27.2	1.023	3,4	48	40.6
80	Prop Concept #4.12	3	10.00	3	4.00	5	19.52	3	6.00	39.5	4	27.2	1.023	4	-2	40.4
77	Prop Concept #4.09	5	19.52	3	4.00	3	10.00	3	6.00	39.5	4	27.2	1.023	2,3,4	65	40.4
87	Prop Concept #4.19	5	19.52	3	4.00	3	10.00	3	6.00	39.5	4	27.2	1.023	4	9	40.4
97	Prop Concept #4.29	3	10.00	3	4.00	3	10.00	7	17.50	41.5	2	46.1	0.961	3,4	21	39.9
83	Prop Concept #4.15	5	19.52	5	7.81	3	10.00	1	2.35	39.7	3	34.2	1.000	3,4	21	39.7
8	Airframe Concept #1.08	5	19.52	3	4.00	3	10.00	3	6.00	39.5	3	34.2	1.000	0	0	39.5
12	Airframe Concept #1.12	5	19.52	3	4.00	3	10.00	3	6.00	39.5	3	34.2	1.000	1	1	39.5
99	Prop Concept #4.31	5	19.52	3	4.00	3	10.00	3	6.00	39.5	3	34.2	1.000	4	0	39.5
29	Noise Concept #3.01	3	10.00	3	4.00	1	3.92	9	20.00	37.9	5	22.2	1.040	2,3,4	5	39.4
17	Aero Concept #2.03	1	3.92	9	13.33	5	19.52	1	2.35	39.1	3	34.2	1.000	2,4	0	39.1
18	Aero Concept #2.04	1	3.92	9	13.33	5	19.52	1	2.35	39.1	3	34.2	1.000	2,4	3	39.1
64	Noise Concept #3.36	3	10.00	3	4.00	3	10.00	5	11.71	35.7	9	10.0	1.080	3,4	8	38.6
25	Aero Concept #2.11	7	29.16	3	4.00	3	10.00	3	6.00	49.2	1	100.0	0.783	1,2	8	38.5

Figure E-1. QFD Worksheet (Sheet 4 of 6)



OVERALL SCENARIO APPLIED

ID	Designation:	Description:	SELECT Goals		Fuel Burn	Field Length	LTD NOX	Noise Ltn	TER Sub-Total	TRL	Interaction Quotient		TER Grand Total	
			Scale Factor (Priority)	Normalized Scale Factor Units							Input	Factor		Input
66	Noise Concept #3.38	Multi DOF Liner	1.00	0.40	1.00	1.00	0.60	100.0	10	2	5	9	2	
75	Prop Concept #4.07	Oil-Less Engine	33.33	13.33	33.33	33.33	20.00	30.0	100	1	0	1	1	
76	Prop Concept #4.08	BLI Inlets	Qualitative	Qualitative	Qualitative	Qualitative	Qualitative	6.00	39.5	2	46.1	0.961	0	3
96	Prop Concept #4.28	Porous Ceramic Materials	3	3	3	3	3	6.00	39.5	2	46.1	0.961	1,3,4	15
84	Prop Concept #4.16	Low Tip Speed Counter-Rotating Ducted Fan	0.5	0.5	0.5	0.5	0.5	6.00	39.5	2	46.1	0.961	2,3,4	49
60	Noise Concept #3.32	Wheel Caps	1	3.92	3	4.00	3	10.00	37.9	3	34.2	1.000	3,4	0
61	Noise Concept #3.33	Wheel Gap Filler	3	10.00	3	4.00	3	10.00	37.9	6	18.3	1.053	0	0
38	Noise Concept #3.10	Aerothodynamic Concepts (Inverted Flow, Thermal-Acoustic Shield)	3	10.00	3	4.00	3	10.00	35.7	6	18.3	1.053	0	0
40	Noise Concept #3.12	Acoustic Excitation	3	10.00	3	4.00	3	10.00	35.7	4	27.2	1.023	3,4	8
44	Noise Concept #3.16	Brush-type Trailing Edges	3	10.00	3	4.00	3	10.00	35.7	4	27.2	1.023	2,3	0
45	Noise Concept #3.17	Trailing Edge Serrations	3	10.00	3	4.00	3	10.00	35.7	4	27.2	1.023	2,3	0
31	Noise Concept #3.03	Chevrons	2,22	3	4.00	3	7	17.50	33.7	9	10.0	1.080	1,3,4	9
98	Prop Concept #4.30	Combined Steam Cycle	3	10.00	1	1.57	3	19.52	37.1	2	46.1	0.961	4	0
63	Noise Concept #3.35	Linear Acoustic Liner	1	3.92	1	1.57	3	10.00	33.0	9	10.0	1.080	3,4	8
65	Noise Concept #3.37	Double DOF Liner	1	3.92	1	1.57	3	10.00	33.0	9	10.0	1.080	3,4	9
85	Prop Concept #4.17	4-Shaft Turbine	5	19.52	3	4.00	3	10.00	45.2	1	100.0	0.783	4	4
57	Noise Concept #3.29	Active Noise Cancellation	3	10.00	3	4.00	3	10.00	35.7	2	46.1	0.961	3	0
62	Noise Concept #3.34	Landing Gear Assembly "Plasma"	3	10.00	3	4.00	3	10.00	35.7	2	46.1	0.961	3	0
49	Noise Concept #3.21	Slat Cove Fillers	3	10.00	1	1.57	3	10.00	33.3	4	27.2	1.023	2,3	-3
53	Noise Concept #3.25	Continuous Mold-Line Linkages	3	10.00	1	1.57	3	10.00	33.3	3	34.2	1.000	2,3	15
47	Noise Concept #3.19	Flap Tip Fences	3	10.00	3	4.00	3	10.00	30.0	8	12.3	1.072	2,3	3
32	Noise Concept #3.04	Ejectors	1	3.92	3	4.00	3	10.00	29.6	8	12.3	1.072	1,3,4	8
79	Prop Concept #4.11	Thrust Vectoring Open Rotor	3	10.00	5	7.81	3	10.00	30.2	5	22.2	1.040	2,3,4	20
52	Noise Concept #3.24	Slat Tip Fences	3	10.00	3	4.00	3	10.00	30.0	5	22.2	1.040	2,3	3
94	Prop Concept #4.26	Cryogenic Motors	3	10.00	3	4.00	5	19.52	39.5	1	100.0	0.783	1,2,4	28
37	Noise Concept #3.09	Porous Plug Designs	3	10.00	3	4.00	3	10.00	30.0	4	27.2	1.023	1,3,4	0
46	Noise Concept #3.18	Porous Flap Side Edges	3	10.00	3	4.00	3	10.00	30.0	4	27.2	1.023	2,3	0

Physical Principles Summary:

Accelerating streamtube creating airframe drag may provide higher propulsive efficiency independent of bypass ratio. Retain bulk acoustic absorption properties with reduced weight. Lower tip speed increases efficiency, reduces weight, and will increase propulsive efficiency. Elimination of Wheel Cavities Streamlined Wheel Assembly Impedance Changes Inducing Shielding Effects Acoustically Excited Jets Go Violent When Excited by Pure Tones Which Increases Turbulence and Enhances Mixing Viscous Damping of Turbulent Flow Pressures in the Brush-Region Reduced Acoustic Scattering, Reduced Spanwise Correlation Scaloped Edges Applied Jet Exhaust Nozzles Combined gas plus steam turbine takes advantage of waste heat to produce work, improving thermal efficiency. Increasing the ability of the turbomachinery to rotate at ideal speeds and stage matching increases efficiencies. Destructive Interference Introduced by a Powered Source Electrodes Which Introduce Energy into the Flow Field Surrounding the Gear Assembly Elimination of the Slat-Gap Elimination of the Slat-Gap Reduction of Vortex Generation Enhanced Jet Mixing, Increased Turbulence Through Entrained Air Flow deflection or engine rotation may allow STOL operation. Reduction of Vortex Generation Motors cooled to superconducting temperatures would operate at extreme efficiencies. Reduced Vortex Shedding Reduced Vortex Shedding

Figure E-1. QFD Worksheet (Sheet 5 of 6)

ID	Designation:	Description:	Fuel Burn		Field Length		LTD NOx		Noise L _{EPN}		TER Sub-Total	Interaction Quotient		TER Grand Total			
			FB Input	FB TER	FL Input	FL TER	NOx Input	NOx TER	dB Input	dB TER		TRL R.I.	TRL Factor		Inter-action	IQ Input	IQ Factor
 <p>OVERALL SCENARIO APPLIED</p>			<p>SELECT Goals:</p> <p>Scale Factor (Priority) 1.00 0.40 1.00 0.60</p> <p>Normalized Scale Factor Units:</p> <p>33.33 13.33 33.33 20.00</p> <p>Qualitative 3 3 3 3</p> <p>Goal 9 9 9 9</p> <p>Threshold 3 3 3 3</p> <p>Fz (Threshold Value On Gaussian Curve): 9 33.33 9 13.33 9 33.33 9 20.00 100.0</p> <p>3 10.00 3 4.00 3 10.00 3 6.00 300.0</p>														
<p>Max Score Baseline</p> <p>This is the maximum score Baseline</p>			<p>Physical Principles Summary:</p> <p>Reduced Acoustic Scattering, Shift to High Frequencies</p> <p>Reduced Vortex Shedding</p> <p>Reduced Flap Deflections/Maintained Lift</p> <p>Glass fiber reinforcement bonded between aluminum sheet</p> <p>Fiber Metal Laminates</p> <p>Metallic Digital Direct Manufacturing</p> <p>Open-Cell and Stamped Composite Structures</p> <p>Post-Buckled Composite Structures</p> <p>Direct Manufacturing / Laser Sintering of Polymeric Materials</p> <p>Carbon Nanotube Electrical Cables</p> <p>Slat Gap Liners</p> <p>Streamlined Slat Tracks</p> <p>Thrust Vectoring Nozzles</p> <p>Metal Foam Liner</p>														
48	Noise Concept #3.20	Slat Trailing Edge Serrations	3	10.00	3	4.00	3	10.00	3	6.00	30.0	4	27.2	1.023	2.3	-3	30.7
51	Noise Concept #3.23	Porous Slat Pressure Surfaces	3	10.00	3	4.00	3	10.00	3	6.00	30.0	4	27.2	1.023	2.3	0	30.7
55	Noise Concept #3.27	Micro-tab Features	3	10.00	3	4.00	3	10.00	3	6.00	30.0	4	27.2	1.023	2.3	0	30.7
2	Airframe Concept #1.02	Fiber Metal Laminates	3	10.00	3	4.00	3	10.00	3	6.00	30.0	3	34.2	1.000	1	6	30.0
3	Airframe Concept #1.03	Metallic Digital Direct Manufacturing	3	10.00	3	4.00	3	10.00	3	6.00	30.0	3	34.2	1.000	1	2	30.0
10	Airframe Concept #1.10	Open-Cell and Stamped Composite Structures	3	10.00	3	4.00	3	10.00	3	6.00	30.0	3	34.2	1.000	1	0	30.0
11	Airframe Concept #1.11	Post-Buckled Composite Structures	3	10.00	3	4.00	3	10.00	3	6.00	30.0	3	34.2	1.000	1	0	30.0
13	Airframe Concept #1.13	Direct Manufacturing / Laser Sintering of Polymeric Materials	3	10.00	3	4.00	3	10.00	3	6.00	30.0	3	34.2	1.000	1	0	30.0
14	Airframe Concept #1.14	Carbon Nanotube Electrical Cables	3	10.00	3	4.00	3	10.00	3	6.00	30.0	3	34.2	1.000	0	0	30.0
50	Noise Concept #3.22	Slat Gap Liners	3	10.00	3	4.00	3	10.00	3	6.00	30.0	3	34.2	1.000	2.3	0	30.0
54	Noise Concept #3.26	Streamlined Slat Tracks	3	10.00	3	4.00	3	10.00	3	6.00	30.0	3	34.2	1.000	2.3	3	30.0
78	Prop Concept #4.10	Thrust Vectoring Nozzles	1	3.92	7	11.66	3	10.00	1	2.35	27.9	6	18.3	1.053	3.4	31	29.4
67	Noise Concept #3.39	Metal Foam Liner	1	3.92	1	1.57	3	10.00	5	11.71	27.2	6	18.3	1.053	3.4	8	28.6

Figure E-1. QFD Worksheet (Sheet 6 of 6)

References

References

- 1 McCullers, A., "Flight Optimization System (FLOPS) User's Guide," Release 7.40, Aug. 2008.
- 2 "737 Airplane Characteristics for Airport Planning," Boeing Commercial Airplanes, October 2005.
- 3 McCullers, A., Private Communication, Nov. 11, 2009.
- 4 Patnaik, S., Coroneos, R., Guptill, J., Hopkins, D., and Haller, W., "A Subsonic Aircraft Design Optimization with Neural Network and Regression Approximators," 10th AIAA/ISSMO Multidisciplinary Analysis and Optimization Conference, Albany, New York, AIAA 2004-4606.
- 5 Post, J., Bonn, J., Borener, S., Baart, D., Hasan, S., and Huang, A., "A Validation of Three Fast-Time Air Traffic Control Models," 5th AIAA Aviation, Technology Integration, and Operations Conference, Arlington, VA, AIAA 2005-7375.
- 6 Evans, A., Follen, G., Naiman, C., and Lopez, I., "Numerical Propulsion System Simulation's National Cycle Program," 34th AIAA/ASME/SAE/ASEE Joint Propulsion Conference and Exhibit, Cleveland, Ohio, AIAA 1998-3113.
- 7 Gallman, J. and Kunze, R., "Grazing Flow Acoustic Impedance Testing for the NASA AST Program," 8th AIAA/CEAS Aeroacoustics Conference and Exhibit, Breckenridge, Colorado, AIAA 2002-2447.
- 8 "Advanced Sound Propagation in the Atmosphere (ASOPRAT) User's Guide, Version 3.0," University of Mississippi, 1991.
- 9 Frederickson, C., Bass, H., Raspet, R., and Messer, J., "Comparison of Measured and Predicted Pure Tone Propagation Levels from JAPE-1: An Evaluation of the Performance of ASOPRAT," *Journal of the Acoustical Society of America*, Vol. 94, No. 3, p. 1875, Sept. 1993.
- 10 "Futures Working Group Final Report (Draft)," Joint Planning and Development Office Futures Working Group, May 2004.
- 11 National Research Council, Maintaining U.S. Leadership in Aeronautics: Scenario-Based Strategic Planning for NASA's Aeronautics Enterprise, Washington, D.C.: National Academy Press, 1997.
- 12 "Exploring Sustainable Development: Global Scenarios 2000-2050," World Business Council for Sustainable Development, Nov. 1997.
- 13 "Shell Energy Scenarios to 2050," Shell Corporation, URL: www.shell.com/scenarios, 2008.
- 14 TradeStats Express National Trade Data, URL: <http://tse.export.gov>, data extracted 26 Feb 2009.
- 15 Tanaka, N., "World Energy Outlook 2008: Options for a Cleaner, Smarter Energy Future," UN Climate Change Conference, Poznan, Dec. 2008.
- 16 "Annual Energy Review 2007," U.S. Energy Information Administration, DOE/EIA-0384, June 2008.
- 17 "Tomorrow's Energy: A Perspective on Energy Trends, Greenhouse Gas Emissions, and Future Energy Options," ExxonMobil Corporation, URL: <http://www.exxonmobil.com>, Feb. 2006.
- 18 "Clearing the Air: The Myth and Reality of Aviation and Climate Change," Climate Action Network Europe, T&E 06/2, 2006.
- 19 "Aviation and the Environment: A National Vision Statement, Framework for Goals and Recommended Actions," Partnership for Air Transportation Noise and Emissions Reduction, Dec. 2004.

- 20 “Discoveries: The Fill-Up That is Failing,” URL: <http://watd.wuthering-heights.co.uk/mainpages/discoveries.html>.
- 21 Marais, K., Lukachko, S., Jun, M., Mahashabde, A., and Waitz, I., “Assessing the Impact of Aviation on Climate,” *Meteorologische Zeitschrift*, Vol. 17, No. 2, pp. 157-172, April 2008.
- 22 Huang, Alex, “Futuristic US Flight Demand Generation Approach Incorporating Fleet Mix Evolution,” AIAA Modeling and Simulation Technologies, Honolulu, HI, August 2008.
- 23 Gawdiak, Y., Carr, G., and Hasan, S., “JPDO Case Study of NextGen High Density Operations,” 9th AIAA Aviation Technology, Integration, and Operations Conference, Hilton Head, South Carolina, AIAA 2009-6918.
- 24 Federal Aviation Administration, Terminal Area Forecast, URL: <http://aspm.faa.gov/main/taf.asp>.
- 25 Bureau of Transportation Statistics Aircraft Transtats Database, URL: <http://www.transtats.bts.gov/homedrillchart.asp>, March 2010
- 26 Peeters, P., Middel, J., and Hoolhorst, A., “Fuel Efficiency of Commercial Aircraft: An Overview of Historical and Future Trends,” NLR-CR-2005-669, 2005.
- 27 “Next Generation Air Transportation System: In Brief,” Joint Planning and Development Office, 2006.
- 28 Blake, M., Smith, J., Wright, K., and Mediavilla, R., “Advanced Vehicle Concepts and Implications for NextGen,” Final Project Report, NASA/CR, 2010.
- 29 Next Generation Air Transportation System (NextGen), Federal Aviation Administration (FAA), URL: <http://www.faa.gov/about/initiatives/nextgen/>, Jan 2010.
- 30 F. Wieland, J. Smith, and J. P. Clarke., “Implications of New Aircraft Technologies on the Next Generation Air Transportation System,” USA/Europe ATM conference, 2009.
- 31 Trent 900 Fact Sheet, URL: http://www.rolls-royce.com/Images/brochure_Trent900_tcm92-11346.pdf.
- 32 Seidenman, P. and Spanovich, D., “Powerplant Performance,” *Aviation Week & Space Technology*, Nov. 2, 2009.
- 33 “Pratt and Whitney PW1000G,” Jane’s Aero-Engines, URL: <http://www.janes.com>, Jan. 2010.
- 34 Morris, J., “PurePower PW1000G Engine Core Heading for Tests by Year-End,” *Aviation Week & Space Technology*, Nov. 14, 2009.
- 35 Farassat, F., Dunn, M., Tinetti, A., and Nark, D., “Open Rotor Noise Prediction Methods at NASA Langley – A Technology Review,” 15th AIAA/CEAS Aeroacoustics Conference, Miami, Florida, AIAA 2009-3133.
- 36 Norris, G., “New-Generation GE Open Rotor and Regional Jet Engine Demo Efforts Planned,” *Aviation Week & Space Technology*, May 2009.
- 37 Whitfield, C., Mani, R., and Gliebe, P., “High-Speed Turboprop Aeroacoustic Study (Counterrotation), Vol. 1 – Model Development,” NASA C/R 185241, July 1990.
- 38 Whitfield, C., Mani, R., and Gliebe, P., “High-Speed Turboprop Aeroacoustic Study (Counterrotation), Vol. 2 – Computer Programs,” NASA C/R 185242, July 1990.
- 39 Hanson, D., “Noise of Counter-Rotation Propellers,” *Journal of Aircraft*, Vol. 22, No. 7, pp. 609-617, July 1985.

- 40 Byrnes, A., Hensleigh, W., and Tolve, L., "Effect of Horizontal Stabilizer Vertical Location on the Design of Large Transport Aircraft," 2nd AIAA Annual Meeting, San Francisco, California, AIAA 1965-0331.
- 41 Roskam, J., Airplane Design, Part III: Layout Design of Cockpit, Fuselage, Wing and Empennage. Lawrence, Kansas: Design, Research, and Analysis Corporation, pp. 36-37, 2002.
- 42 Raymer, D. Aircraft Design: A Conceptual Approach. Third ed., Reston, VA: American Institute of Aeronautics and Astronautics, Ch. 10, p. 247, 1999.
- 43 Davies, R., "The World's First Commercial Jets," AIAA/ICAS International Air and Space Symposium and Exposition: The Next 100 Years, Dayton, Ohio, AIAA 2003-2882.
- 44 Sobester, A., "Tradeoffs in Jet Inlet Design: A Historical Perspective," *Journal of Aircraft*, Vol. 44, No.3, May-June 2007.
- 45 McGeer, T. and Kroo, I., "A Fundamental Comparison of Canard and Conventional Configurations," *Journal of Aircraft*, Vol. 20, No. 11, pp. 983-992, Nov. 1983.
- 46 Keith, M. and Selberg, B., "Aerodynamic Optimization, Comparison, and Trim Design of Canard and Conventional High Performance General Aviation Configurations," 21st AIAA Aerospace Sciences Meeting and Exhibit, Reno, Nevada, AIAA 1983-0058.
- 47 Raymer, D. Aircraft Design: A Conceptual Approach. Third ed., Reston, VA: American Institute of Aeronautics and Astronautics, Ch. 4, pp. 80-83, 1999.
- 48 Strohmeyer, D., Seubert, R., Heinze, W., Österheld, C., and Fornasier, L., "Three Surface Aircraft – A Concept for Future Transport Aircraft," 38th AIAA Aerospace Sciences Meeting and Exhibit, Reno, Nevada, AIAA 2000-0566.
- 49 Raymer, D. Aircraft Design: A Conceptual Approach. Third ed., Reston, VA: American Institute of Aeronautics and Astronautics, Ch. 20, p. 664, 1999.
- 50 Hange, C., "Performance Challenges of Hybrid Wing CESTOL Transports," 47th AIAA Aerospace Sciences Meeting and Exhibit, Orlando, Florida, AIAA-2009-1133.
- 51 Papamoschou, D. and Salvado, M., "Experiments on Noise Shielding of Jet Noise by Airframe Surfaces," 15th AIAA/CEAS Aeroacoustics Conference, Miami, Florida, AIAA-2009-3326.
- 52 Tindell, R., "Highly Compact Inlet Diffuser Technology," *Journal of Propulsion & Power*, Vol. 4, No. 6, pp. 557-563, Nov-Dec. 1988.
- 53 Englar, R. and Campbell, B., "Pneumatic Channel Wing Powered-Lift Advanced Super-STOL Aircraft," 1st Flow Control Conference, St. Louis, Missouri, AIAA 2002-3275.
- 54 Sellers, W., Jones, G., and Moore, M., "Flow Control Research at NASA Langley in Support of High-Lift Augmentation," 2002 Biennial International Powered Lift Conference, Williamsburg, VA, AIAA 2002-6006.
- 55 Blick, E. and Homer, V., "Power-On Channel Wing Aerodynamics," *Journal of Aircraft*, Vol. 8, No. 4, pp. 234-238, April 1971.
- 56 Wolkovitch, J., "The Joined Wing: An Overview," *Journal of Aircraft*, Vol. 23, No. 3, pp. 161-178, 1986.
- 57 Samuels, M., "Structural Weight Comparison of a Joined Wing and a Conventional Wing," *Journal of Aircraft*, Vol. 19, No. 6, pp. 485-491, June 1982.
- 58 Wolkovitch, J., "Joined-Wing Research Airplane Feasibility Study," AIAA/AHS/ASEE Aircraft Design Systems Operations Meeting, San Diego, California, AIAA 1984-2471.

- 59 Raymer, D. Aircraft Design: A Conceptual Approach. Third ed., Reston, VA: American Institute of Aeronautics and Astronautics, Ch. 20, pp. 677, 1999.
- 60 Mukhopadhyay, V., “Blended Wing Body (BWB) Fuselage Structural Design for Weight Reduction,” 46th AIAA/ASME/ASCE/AHS/ASC Structures, Structural Dynamics, and Material Conference, Austin, Texas, AIAA 2005-2349.
- 61 Crouse, G., “Conceptual Design of a Submersible Airplane,” 48th AIAA Aerospace Sciences Meeting and Exhibit, Orlando, Florida, AIAA 2010-1012.
- 62 Fuhrmann, H., “Application of Natural Laminar Flow to a Supersonic Transport Concept,” AIAA 1993-3467.
- 63 Crouch, J., “Modeling Transition Physics for Laminar Flow Control,” 38th Fluid Dynamics Conference and Exhibit, Seattle, Washington, AIAA 2008-3832.
- 64 Guo, Y., Yamamoto, K., and Stoker, R., “Experimental Study on Aircraft Landing Gear Noise,” *Journal of Aircraft*, Vol. 43, No. 2, pp. 306-317, March-April 2006.
- 65 Quayle, A., Dowling, A., Babinsky, H., Graham, W., Shin, H., and Sijtsma, P., “Landing Gear for a Silent Aircraft,” 45th AIAA Aerospace Sciences Meeting and Exhibit, Reno, Nevada, AIAA 2007-0231.
- 66 Dobrzynski, W., Chow, L., Guion, P., and Shiells, D., “Research into Landing Gear Airframe Noise Reduction,” 8th AIAA/CEAS Aeroacoustics Conference and Exhibit, AIAA 2002-2409.
- 67 Gaeta, R., Ahuja, K., Schein, D., and Solomon, W., “Large Jet-Noise Reductions Through Distributed Nozzles,” 8th AIAA/CEAS Aeroacoustics Conference and Exhibit, AIAA 2002-2456.
- 68 Plas, A., Sargeant, M., Madani, V., Crichton, D., Greitzer, E., Hynes, T., and Hall, C., “Performance of a Boundary Layer Ingesting (BLI) Propulsion System,” 45th AIAA Aerospace Sciences Meeting and Exhibit, Reno, Nevada, AIAA 2007-0450.
- 69 Rodriguez, D. “Multidisciplinary Optimization Method for Designing Boundary-Layer-Ingesting Inlets,” *Journal of Aircraft*, Vol. 46, No. 3, pp. 883-894, May-June 2009.
- 70 Osborn, R., Kota, S., Geister, D., Lee, M., and Tilmann, C., “Active Flow Control Using High Frequency Compliant Structures,” AIAA Guidance, Navigation, and Control Conference and Exhibit, Montreal, Canada, AIAA 2001-4144.
- 71 Kuo, B. and Sarigul-Klijn, N., “Numerical Investigation of Micro-Tab in Airframe Noise Reduction,” 13th AIAA/CEAS Aeroacoustics Conference and Exhibit, AIAA 2007-3452.
- 72 Osborn, R., Kota, S., Hetrick, J., Geister, D., Tilmann, C., and Joo, J., “Active Flow Control Using High-Frequency Compliant Structures,” *Journal of Aircraft*, Vol. 41, No. 3, May-June 2004.
- 73 Flexsys, Inc. URL: <http://www.flxsys.com>.
- 74 Cunniff, P., Auerbach, M., Vetter, E., and Sikkema, D., “High Performance M5 Fiber for Ballistics/Structural Composites,” 23rd Army Science Conference, Orlando, Florida, AO-04, 2004.
- 75 Shirk, M., Hertz, T., and Weisshaar, T., “Aeroelastic Tailoring – Theory, Practice, and Promise,” *Journal of Aircraft*, Vol. 23, No. 1, pp. 6-18, Jan. 1986.
- 76 Shirk, M.H., Hertz, T.J., and Weisshaar, T.A., “Aeroelastic Tailoring – Theory, Practice, and Promise,” AIAA/ASME/ASCE/AHS 25th Structures, Structural Dynamics and Materials Conference, Palm Springs, CA, AIAA 1984-0982.

- 77 Wakayama, S. and Kroo, I., "Subsonic Wing Planform Design Using Multidisciplinary Optimization," *Journal of Aircraft*, Vol. 32, No. 4, pp. 746-753, July-Aug. 1995.
- 78 Holzwarth, R., "An Overview of the Advanced Lightweight Aircraft Fuselage Structures (ALAFS) Program," 37th AIAA/ASME/ASCE/AHS/ASC Structures, Structural Dynamics and Materials Conference and Exhibit, Salt Lake City, Utah, AIAA 1996-1573.
- 79 Ascani, L, Burroughs, B., Lackman, L., and O'Brien, W., "Advanced Structures: Meeting the Challenge of Low Cost Future Aircraft Systems," AIAA Aircraft Systems Meeting, Anaheim, California, AIAA 1980-1868.
- 80 Velicki, A. and Thrash, P., "Advanced Structural Concept Development Using Stitched Composites," 49th AIAA/ASME/ASCE/AHS/ASC Structures, Structural Dynamics, and Materials Conference, Schaumburg, Illinois, AIAA 2008-2329.
- 81 Sheahan, P., Bersuch, L., Holcombe, T., and Baron, B., "Robust Composite Sandwich Structures," 39th AIAA/ASME/ASCE/AHS/ASC Structures, Structural Dynamics, and Materials Conference, Long Beach, California, AIAA-1998-1873.
- 82 Nihart, G. and Brown, J., "Supersonic Propulsion Systems and Community Noise Suppression Concepts," 24th AIAA/ASME/SAE/ASEE Joint Propulsion Conference, Boston, Massachusetts, AIAA 1988-2986.
- 83 Strout, F. and Atencio, A., "Flight Effects on Noise Generated by the JT8D Engine with Inverted Primary/Fan Flow as Measured in the NASA-Ames 40 by 80 Foot Wind Tunnel," 5th AIAA Aeroacoustics Conference, Seattle, Washington, AIAA 1979-0614.
- 84 Miller, A., "Ideas on How AMTAS Can Support the Aviation Industry (and More)," Advanced Materials in Transport Aircraft Structures (AMTAS) Spring 2005 Meeting, 2005.
- 85 Kohlman, D., Introduction to V/STOL Airplanes, Ames, Iowa: The Iowa State University Press, First ed., p. 163, 1981.
- 86 Bloomer, H., "Investigation of Wing Shielding Effects on CTOL Engine Noise," 5th AIAA Aeroacoustics Conference, Seattle, Washington, AIAA 1979-0669.
- 87 Goodmanson, L. and Gratzler, L., "Recent Advances in Aerodynamics for Transport Aircraft," 9th Annual Meeting and Technology Display, Washington D.C., AIAA 1973-0009.
- 88 LaChapelle, D., Noe, M., Edmonson, W., Stegemiller, H., Steibel, J., and Chang, D., "CMC Materials Applications to Gas Turbine Hot Section Components," 34th AIAA/ASME/SAE/ASEE Joint Propulsion Conference and Exhibit, Cleveland, Ohio, 1998, AIAA 1998-3266.
- 89 Lohmann, R. and Fear, J., "NASA Broad Specification Fuels Combustion Technology Program – Pratt and Whitney Phase I Results and Status," 18th AIAA/SAE/ASME Joint Propulsion Conference, Cleveland, Ohio, AIAA 1982-1088.
- 90 General Electric Power LMS100 Brochure. URL:
http://www.gepower.com/prod_serv/products/aero_turbines/en/downloads/lms100_brochure.pdf.
- 91 Schulten, J., "Vane Sweep Effects on Rotor/Stator Interaction Noise," *AIAA Journal*, Vol. 35, No. 6, pp. 945-951, June 1997.
- 92 Thomson, D., Watson, K., Norden, C., Gorell, S., Braisted, W., and Brockman, R., "Assessment of Organic Matrix Composites for a Forward Swept Fan Stage," 35th AIAA/ASME/ASCE/AHS/ASC Structures, Structural Dynamics, and Materials Conference, Hilton Head, South Carolina, AIAA 1994-1353.

- 93 Neubert, R., Hobbs, D., and Weingold, H., "Application of Sweep to Improve the Efficiency of a Transonic Fan, Part I – Design," *Journal of Propulsion & Power*, Vol. 11, No. 1, pp. 49-54, Jan-Feb 1995.
- 94 Mercer, C.R., Haller, W.J., Tong, M.T., "Adaptive Engine Technologies for Aviation CO2 Emissions Reduction," 42nd AIAA/ASME/SAE/ASEE Joint Propulsion Conference and Exhibit, Sacramento, California, AIAA 2006-5105.
- 95 Weimer, M., "Design and Test of an Active Tip Clearance System for Centrifugal Compressors," 28th Joint Propulsion Conference and Exhibit, Nashville, TN, 1992, AIAA 1992-3189.
- 96 Gaeta, R., Lee, W., and Flick, A., "Over-the-Wing, Powered Lift, Engine –Airframe Integration Effects on Acoustic Shielding," 47th AIAA Aerospace Sciences Meeting and Exhibit, Orlando, Florida, AIAA 2009-0282.
- 97 Fujino, M., Oyama, H., and Omotani, H., "Flutter Characteristics of an Over-the-Wing Engine Mount Business-Jet Configuration" 44th AIAA/ASME/ASCE/AHS Structures, Structural Dynamics, and Materials Conference, Norfolk, Virginia, AIAA 2003-1942.
- 98 Fujino, M. and Kawamura, Y., "Wave-Drag Characteristics of an Over-the-Wing Nacelle Business-Jet Configuration," *Journal of Aircraft*, Vol. 40, No. 6, Nov.-Dec. 2003.
- 99 Mason, W., *Configuration Aerodynamics*, Ch. 7, URL: http://www.aoe.vt.edu/~mason/Mason_f/ConfigAero.html.
- 100 ICAO Annex 16, Vol. II, *Aircraft Engine Emissions*.
- 101 ICAO Engine Exhaust Emissions Databank, ID #1CM004, CFM56-3B1. URL: http://www.caa.co.uk/docs/702/1CM004_01102004.pdf.
- 102 Electronic Code of Federal Regulations, URL: <http://ecfr.gpoaccess.gov/cgi/t/text/text-idx?c=ecfr&rgn=div5&view=text&node=14:1.0.1.3.19&idno=14>.
- 103 Macri, F., "Advanced Turbine System Federal Assistance Program, Final Program Technical Report", Information Bridge: DOE Scientific and Technical Information, October, 2003
- 104 Heiser, W. and Pratt, D., "Thermodynamic Cycle Analysis of Pulse Detonation Engines," *Journal of Propulsion & Power*, Vol. 18, No. 1, Jan-Feb 2002.
- 105 Yungster, S., Radhakrishnan, K., and Breisacher, K., "Computational and Experimental Study of NOx Formation in Hydrogen-Fueled Pulse Detonation Engines," 40th AIAA/ASME/SAE/ASEE Joint Propulsion Conference and Exhibit, Fort Lauderdale, Florida, AIAA 2004-3307.
- 106 Ko, A., Leifsson, L., Schetz, J., Mason, W., Grossman, B., Haftka, R., "MDO of a Blended-Wing-Body Transport Aircraft with Distributed Propulsion," 3rd AIAA Aviation Technology, Integration and Operations Forum, Denver, Colorado, AIAA 2003-6732.
- 107 Brown, G.V., "Turboelectric System for Aircraft Propulsion," NASA presentation, Turboelectric Distributed Propulsion Planning Meeting, Feb. 10-11, 2009.
- 108 Ko, A., Leifsson, L., Schetz, J., Mason, W., Grossman, B., and Haftka, R., "MDO of a Blended-Wing-Body Transport Aircraft with Distributed Propulsion," 3rd AIAA Aviation Technology, Integration and Operations Forum, Denver, Colorado, AIAA 2003-6732.
- 109 "Felder, J, Kim, H., Brown, G., "Turboelectric Distributed Propulsion Engine Cycle Analysis for Hybrid-Wing-Body Aircraft," AIAA 2009-1132.
- 110 Jirasek, A., "Evaluation of the vortex generator flow control in the FOI-EIC-01 Inlet at Different Flight Conditions" 43rd AIAA/ASME/SAE/ASEE Joint Propulsion Conference and Exhibit, Cincinnati, Ohio, AIAA 2007-5065.

- 111 Ensign, T., "Performance and Weight Impact of Electric Environment Control System and More Electric Engine on Citation CJ2," 45th AIAA Aerospace Sciences Meeting and Exhibit, AIAA 2007-1395.
- 112 Metal Improvement Company presentation to the US Air Force and Navy/NAVAIR, "Laser Peening Technology of Integrated Bladed Rotors Background on laser peening," October 29, 2008.
- 113 Jones, G., Viken, S., Washburn, A., Jenkins, L., and Cagle, C., "An Active Flow Circulation Controlled Flap Concept for General Aviation Aircraft Applications," 1st AIAA Flow Control Conference, St. Louis, Missouri, AIAA 2002-3157.
- 114 Fan, L., Yang, S., and Kundu, K., "Evaluation of Water Injection Effect on NO_x Formation for a Staged Gas Turbine Combustor," 34th AIAA Aerospace Sciences Meeting and Exhibit, Reno, Nevada, AIAA 1996-0706.
- 115 Zimbrick, R. and Colehour, J., "Investigation of Very High Bypass Ratio Engines for Subsonic Transports," *Journal of Propulsion & Power*, Vol. 6, No. 4, pp. 490-496, 1990.
- 116 Healy, H., "V/STOL Performance Comparisons with Variable Pitch and Variable Inlet Guide Vane Fans: A Report on Experimental Data," 15th AIAA/ASME/SAE/ASEE Joint Propulsion Conference and Exhibit, Las Vegas, NV, 1979, AIAA 1979-1286.
- 117 Breit, J., and Szydlo-Moore, J., "Fuel Cells for Commercial Transport Airplanes Needs and Opportunities," 45th AIAA Aerospace Sciences Meeting and Exhibit, Reno, NV, AIAA 2007-1390.
- 118 Daggett, D., Eelman, S., and Kristiansson, G., "Fuel Cell APU for Commercial Aircraft," AIAA International Air and Space Symposium and Exposition: The Next 100 Years, Dayton, Ohio, AIAA 2003-2660.
- 119 Sellers, W., Singer, B., Leavitt, L. "Aerodynamics for Revolutionary Air Vehicles," 21st AIAA Applied Aerodynamics Conference, Orlando, Florida, AIAA 2003-3785.
- 120 Walsh, M., Sellers, W., and McGinley, C., "Riblet Drag Reduction at Flight Conditions," 6th AIAA Applied Aerodynamics Conference, Williamsburg, Virginia, AIAA 1988-2554.
- 121 Walsh, M., "Turbulent Boundary Layer Drag Reduction Using Riblets" 20th Aerospace Sciences Meeting, Orlando, Florida, AIAA 1982-0169.
- 122 "Micro-Vortex Generators Enhance Aircraft Performance," NASA Fact Sheet, FS-2000-06-52-LaRC, 2000.
- 123 Nadarajah, A., Word, R., VanSant, K., and Könenkamp, R., "Nanowire-Quantum-Dot-Polymer Solar Cell," *Physica Status Solidi (b)*, Vol. 245, No. 9, pp. 1834-1837, 2008.
- 124 Sankrithi, M. and Frommer, J., inventors, 18 Dec. 2008, Controllable Winglets, U.S. Patent No. 0308683A1.
- 125 Demerjian, D., "Morphing Wing Tips Will Cut Drag and Save Fuel," *Wired.com*, URL: <http://www.wired.com/autopia/2009/02/new-wing-tips-w/>.
- 126 Abbott, J., "Computational Study of the Aerodynamic Performance of Subsonic Scarf Inlets," 40th AIAA/ASME/SAE/ASEE Joint Propulsion Conference and Exhibit, Fort Lauderdale, Florida, AIAA 2004-3406.
- 127 Abbott, J., "Aerodynamic Performance of Scarf Inlet," 17th AIAA Aerospace Sciences Meeting, New Orleans, Louisiana, AIAA 1979-0380.

- 128 Weir, D., Bouldin, B., and Mendoza, J., "Static and Flight Aeroacoustic Evaluations of a Scarf Inlet," 12th AIAA/CEAS Aeroacoustics Conference, Cambridge, Massachusetts, AIAA 2006-2462.
- 129 Li, X., Schoenwald, N., Yan, J., and Thiele, F., "A Numerical Study on the Acoustic Radiation from a Scarfed Intake," 9th AIAA/CEAS Aeroacoustics Conference, Hilton Head, South Carolina, AIAA 2003-3245.
- 130 Montetagaud, F. and Montoux, S., "Negatively Scarfed Intake: Design and Acoustic Performance," 11th AIAA/CEAS Aeroacoustics Conference and Exhibit, Monterey, California, AIAA 2005-2944.
- 131 McCormick, B., Aerodynamics of V/STOL Flight, Mineola, New York: Dover Publications, Inc., p. 201, 1967.
- 132 McCormick, D., "Boundary Layer Separation Control with Directed Synthetic Jets," 38th AIAA Aerospace Sciences Meeting and Exhibit, Reno, Nevada, AIAA 2000-0519.
- 133 Robinson, R., "Micro Honeycombs Aim to Muffle Aircraft Noise," *DesignFax e-Magazine*, URL: <http://www.designfax.net>, November 4, 2008.
- 134 Jing-Bin, W., "On Combustion with Bi-Flat Jets Attached to the Walls," IUTAM Symposium on Aerothermodynamics in Combustors, Taipei, 1991.
- 135 Phillips, J. and Wood, N., "All Electric Subsystems for Next Generation Transport Aircraft," AIAA Aircraft Systems and Technology Meeting, Washington, D.C., AIAA 1979-1832.
- 136 "Development of Bio-Based Fuels for Aircraft Turbine Engines—Final Report 1998," Baylor Institute for Air Science, Renewable Aviation Fuels Development Center, 1998.
- 137 Gridley, M. and Cahill, M., "ACIS Air Induction System Trade Study," 32nd AIAA/ASME/SAE/ASEE Joint Propulsion Conference and Exhibit, Lake Buena Vista, Florida, AIAA 1996-2646.
- 138 Weir, D. and Podboy, G., "Flow Measurements and Multiple Pure Tone Noise from a Forward Swept Fan," 43rd AIAA Aerospace Sciences Meeting and Exhibit, Reno, Nevada, AIAA 2005-1200.
- 139 Halasz, C., Arntz, D., Burdisso, R., and Ng, W., "Fan Flow Control for Noise Reduction Part 1: Advanced Trailing Edge Blowing Concepts," 11th AIAA/CEAS Aeroacoustics Conference, Monterey, California, AIAA 2005-3025.
- 140 Fite, E., Woodward, R., and Podboy, G., "Effect of Trailing Edge Flow Injection on Fan Noise and Aerodynamic Performance," 3rd AIAA Flow Control Conference, San Francisco, California, AIAA 2006-2844.
- 141 Doonan, J. and Davis, W., "Advanced Exhaust Nozzle Concepts Using Spanwise Blowing for Aerodynamic Lift Enhancement," 18th AIAA/SAE/ASME Joint Propulsion Conference, Cleveland, Ohio, AIAA 1982-1132.
- 142 Bowers, D. and Buchan, F., "An Investigation of the Induced Aerodynamic Effects of a Vektored Non-Axisymmetric Exhaust Nozzle," 14th AIAA/SAE Joint Propulsion Conference, Las Vegas, Nevada, AIAA 1978-1082.
- 143 Griffin, H., Gonzalez, L., and Shrinivas, K., "Computational Fluid Dynamics Analysis of Externally Blown Flap Configuration for Transport Aircraft," *Journal of Aircraft*, Vol. 45, No. 1, pp. 172-184, Jan.-Feb. 2008.

- 144 Lafronza, L., McAlpine, A., Keane, A., and Astley, J., "Response Surface Method Optimization of Uniform Segmented Duct Acoustics Liners," *Journal of Aircraft*, Vol. 43, No. 4, pp. 1089-1102, July-Aug. 2006.
- 145 Choi, H., Moin, P., and Kim, J., "Active Turbulence Control for Drag Reduction in Wall Bounded Flows," *Journal of Fluid Mechanics*, Vol. 262, pp. 75-110, 1994.
- 146 Balogh, A., Liu, W., and Krstic, M., "Stability Enhancement by Boundary Control in 2D Channel Flow, I. Regularity of Solutions," in Proceedings of the 38th IEEE Conference on Decision and Control, Vol. 3, pp. 2869-2874, 1999.
- 147 Jung, W., Mangiavacchi, N., and Akhavan, R., "Suppression of Turbulence in Wall-Bounded Flows by High-Frequency Spanwise Oscillations," *Physics of Fluids*, Vol. 4, No. 8, pp. 1605-1607, 1992.
- 148 Schoppa, W. and Hussain, F., "A Large Scale Control Strategy for Drag Reduction in Turbulent Boundary Layers," *Physics of Fluids*, Vol. 10, No. 5, pp. 1049-1051, 1998.
- 149 Choi, K., DeBisschop, J., and Clayton, B., "Turbulent Boundary Layer Control by Means of Spanwise Wall Oscillation," *AIAA Journal*, Vol. 36, No. 7, pp. 1157-1163, July 1998.
- 150 Rathnasingham, R. and Breuer, K., "Active Control of Turbulent Boundary Layers," *Journal of Fluid Mechanics*, Vol. 495, pp. 209-233, 2003.
- 151 Meeks, C., DiRusso, E., Brown, G., "Development of a Compact, Light Weight Magnetic Bearing," AIAA/SAE/ASME/ASEE 26th Joint Propulsion Conference, Orlando, FL, AIAA 1990-2483.
- 152 Chamis, C.C., "Technology Insertion Benefits Assessment in Engines and Aircraft," AIAA 1997-1191.
- 153 Soderman, P., Kafyeke, F., Burnside, N., Chandrasekharan, R., Jaeger, S., and Boudreau, J., "Airframe Noise Study of a CRJ-700 Aircraft Model in the NASA Ames 7- by 10- Foot Wind Tunnel No. 1," 8th AIAA/CEAS Aeroacoustics Conference and Exhibit, AIAA 2002-2406.
- 154 Smith, M. and Chow, L., "Prediction Method for Aerodynamic Noise from Aircraft Landing Gear," 4th AIAA/CEAS Aeroacoustics Conference, Toulouse, France, AIAA 1998-2228.
- 155 Lazos, B., "Reynolds Stresses Around the Wheels of a Simplified Four-Wheel Landing Gear," *AIAA Journal*, Vol. 42, No. 1, pp. 196-198, Jan. 2004.
- 156 Gopala, Y., Kochar, Y., Shareef, A., Chakravarthy, S., "Experimental Investigation of 2-D Confined Laminar Jet Subjected to Downstream Acoustic Excitation" 45th AIAA Aerospace Sciences Meeting and Exhibit, Reno, Nevada, AIAA 2007-1321.
- 157 Herr, M. and Dobrzynski, W., "Experimental Investigations in Low Noise Trailing Edge Design," *AIAA Journal*, Vol. 43, No. 6, pp. 1167-1175, June 2005.
- 158 Ortmann, J. and Wild, J., "Effect of Acoustic Slat Modifications on Aerodynamic Properties of High-Lift Systems," *Journal of Aircraft*, Vol. 44, No. 4, pp. 1258-1263, July-August 2007.
- 159 Knepper, A. and Garry, K., "A Preliminary Investigation of Trailing Edge Serrations in High Lift Systems," 35th AIAA Fluid Dynamics Conference and Exhibit, Toronto, Canada, AIAA 2005-5261.
- 160 Callender, B., Gutmark, E., and Martens, S., "Near-Field Investigation of Chevron Nozzle Mechanisms," *AIAA Journal*, Vol. 46, No. 1, pp. 36-45, Jan. 2008.
- 161 Saiyed, N., Mikkelsen, K., and Bridges, J., "Acoustics and Thrust of Quiet Separate-Flow High-Bypass-Ratio Nozzles," *AIAA Journal*, Vol. 41, No. 3, pp. 372-378, Mar. 2003.

- 162 Droujinin, L. and Molchanova, M., “Combined Cycle Aircraft Engines,” 27th AIAA/ASME/SAE/ASEE Joint Propulsion Conference and Exhibit, Sacramento, CA, AIAA 1991-2377.
- 163 Emborg, U. and Sarin, S., inventors, 2004 Nov. 2, Device at an Acoustic Liner, U.S. Patent No. 6811372 B1.
- 164 Drouin, M., Gallman, J., and Olsen, R., “Sound Level Effect on Perforated Panel Boundary Layer Growth,” 12th AIAA/CEAS Aeroacoustics Conference, Cambridge, Massachusetts, AIAA 2006-2411.
- 165 Thomas, F., Kozlov, A., and Corke, T., “Plasma Actuators for Landing Gear Noise Reduction,” 11th AIAA/CEAS Aeroacoustics Conference, Monterey, California, AIAA 2005-3010.
- 166 Thomas, F., Kozlov, A., and Corke, T., “Plasma Actuators for Bluff Body Flow Control,” 3rd AIAA Flow Control Conference, San Francisco, California, AIAA 2006-2845.
- 167 Kolb, A., Faulhaber, P., Drobietz, R., and Grunewald, M., “Aeroacoustic Wind Tunnel Measurements on a 2D High-Lift Configuration,” 13th AIAA/CEAS Aeroacoustics Conference, AIAA 2007-3447.
- 168 Berton, J., Envia, E., Burley, C., “An Analytical Assessment of NASA’s N+1 Subsonic Fixed Wing Project Noise Goal,” 15th AIAA/CEAS Aeroacoustics Conference, Miami, Florida, AIAA 2009-3144.
- 169 Horne, W., Hayes, J., Ross, J., and Storms, B., “Measurements of Unsteady Pressure Fluctuations on the Surface of an Unswept, Multi-Element Airfoil,” 3rd AIAA/CEAS Aeroacoustics Conference, Atlanta, Georgia, AIAA 1997-1645.
- 170 Tew, D., Teeple, B., and Waitz, I., “Mixer-Ejector Noise-Suppressor Model,” *Journal of Propulsion & Power*, Vol. 14, No. 6, pp. 941-950, Nov-Dec 1998.
- 171 Presz, W., Reynolds, G., and Hunter, C., “Thrust Augmentation with Mixer/Ejector Systems,” 40th AIAA Aerospace Sciences Meeting and Exhibit, Reno, Nevada, AIAA 2002-0230.
- 172 Brisken, T., Howell, P., and Ewing, A., “J85 Rejuvenation Through Technology Insertion,” presented at the NATO Research and Technology Organization Applied Vehicle Technology Lecture Series on “Aging Engines, Avionics, Subsystems, and Helicopters,” Madrid, Spain, 2000.
- 173 Chana, W. and Sullivan, T., “Download - the Open Rotor’s Downfall,” AIAA International Powered Lift Conference, Santa Clara, California, AIAA 1993-4814.
- 174 Rosenstein, H. and Clark, R., “Aerodynamic Development of the V-22 Tilt Rotor,” AIAA/AHS/ASEE Aircraft Systems, Design and Technology Meeting, Dayton, Ohio, AIAA 1986-2678.
- 175 Bauer, A., Kibens, V., and Wlezien, R., “Jet Noise Suppression by Porous Plug Nozzles,” NASA C/R 3613, Contract NAS1-16284, October 1982.
- 176 Nakamura, Y. and Oishi, T., “Development of Mixer-Ejector with Ceramic Acoustic Liner,” 5th AIAA/CEAS Aeroacoustics Conference, Bellevue, Washington, AIAA 1999-1928.
- 177 Fink, M. and Bailery, D., “Model Tests of Airframe Noise Reduction Concepts,” 6th AIAA/CEAS Aeroacoustics Conference and Exhibit, AIAA 1980-0979.
- 178 Angland, D., Zhang, X., and Molin, N., “Measurements of Flow Around a Flap Side Edge with Porous Edge Treatment,” *AIAA Journal*, Vol. 47, No. 7, pp. 1660-1671, July 2009.
- 179 Khorrami, M. and Choudhari, M., “Application of Passive Porous Treatment to Slat Trailing Edge Noise,” NASA/TM-2003-212416, May 2003.

- 180 Kuo, B. and Sarigul-Klijn, N., "Effect of Microtab on Reduction of Noise Due to Aircraft High-Lift Devices," *Journal of Aircraft*, Vol. 46, No. 5, pp. 1812-1815, Sept-Oct 2009.
- 181 Alderliesten, R. and Benedictus, R., "Fiber/Metal Composite Technology for Future Primary Aircraft Structures," *Journal of Aircraft*, Vol. 45, No. 4, pp. 1182-1189, July-Aug 2008.
- 182 Arcella, F., Abbott, D., House, M., "Titanium Alloy Structures for Airframe Application by the Laser Forming Process," 41st Structures, Structural Dynamics, and Materials Conference, Atlanta, GA, AIAA 2000-1465.
- 183 Collier, C., Yarrington, P., and Van West, B., "Composite, Grid-Stiffened Panel Design for Post Buckling Using Hypersizer®," 43rd AIAA/ASME/ASCE/AHS/ASC Structures, Structural Dynamics, and Materials Convention, Denver, CO, AIAA 2002-1222.
- 184 Williamson, C. and Lord, S., "Damage Prediction and its Effect on Post-Buckled Wing Design," 2nd International Conference on Buckling and Postbuckling Behaviour of Composite Laminated Shell Structures, Braunschweig, Germany, 2008.
- 185 Seresta, O., Abdalla, M., and Gurdal, Z., "Optimal Design of Laminated Composite Plates for Maximum Post Buckling Strength," 46th AIAA/ASME/ASCE/AHS/ASC Structures, Structural Dynamics and Materials Conference, Austin, TX, AIAA 2005-2128.
- 186 Smith, M., Chow, L., and Molin, N., "Attenuation of Slat Trailing Edge Noise Using Slat Gap Acoustic Liners," 12th AIAA/CEAS Aeroacoustics Conference, AIAA 2006-2666.
- 187 Dobrzynski, W., Nagakura, K., Gehlhar, B., and Buschbaum, A., "Airframe Noise Studies on Wings with Deployed High-Lift Devices," 4th AIAA/CEAS Aeroacoustics Conference, AIAA 1998-2337.
- 188 Piet, J., Davy, R., Elias, G., Siller, H., Chow, L., Seror, C., and Laporte, F., "Flight Test Investigation of Add-On Treatments to Reduce Aircraft Airframe Noise," 11th AIAA/CEAS Aeroacoustics Conference, AIAA 2005-3007.
- 189 Friehmelt, H., "Thrust Vectoring and Tailless Aircraft Design – Review and Outlook," AIAA Atmospheric Flight Mechanics Conference, San Diego, California, AIAA 1996-3412.
- 190 Mason, M. and Crowther, W., "Fluidic Thrust Vectoring for Low Observable Air Vehicles," 2nd AIAA Flow Control Conference, Portland, Oregon, AIAA 2004-2210.
- 191 Sutliff, D. and Jones, M., "Foam-Metal Liner Attenuation of Low-Speed Fan Noise," 14th AIAA/CEAS Aeroacoustics Conference, Vancouver, British Columbia, AIAA 2008-2897

REPORT DOCUMENTATION PAGE			Form Approved OMB No. 0704-0188		
<p>The public reporting burden for this collection of information is estimated to average 1 hour per response, including the time for reviewing instructions, searching existing data sources, gathering and maintaining the data needed, and completing and reviewing the collection of information. Send comments regarding this burden estimate or any other aspect of this collection of information, including suggestions for reducing this burden, to Department of Defense, Washington Headquarters Services, Directorate for Information Operations and Reports (0704-0188), 1215 Jefferson Davis Highway, Suite 1204, Arlington, VA 22202-4302. Respondents should be aware that notwithstanding any other provision of law, no person shall be subject to any penalty for failing to comply with a collection of information if it does not display a currently valid OMB control number.</p> <p>PLEASE DO NOT RETURN YOUR FORM TO THE ABOVE ADDRESS.</p>					
1. REPORT DATE (DD-MM-YYYY) 01-11-2010		2. REPORT TYPE Final Contractor Report		3. DATES COVERED (From - To)	
4. TITLE AND SUBTITLE NASA N+3 Subsonic Fixed Wing Silent Efficient Low-Emissions Commercial Transport (SELECT) Vehicle Study Revision A			5a. CONTRACT NUMBER NNC08CA86C		
			5b. GRANT NUMBER		
			5c. PROGRAM ELEMENT NUMBER		
6. AUTHOR(S) Bruner, Sam; Baber, Scott; Harris, Chris; Caldwell, Nicholas; Keding, Peter; Rahrig, Kyle; Pho, Luck; Wlezian, Richard			5d. PROJECT NUMBER		
			5e. TASK NUMBER		
			5f. WORK UNIT NUMBER WBS 561581.02.08.03.13.66		
7. PERFORMING ORGANIZATION NAME(S) AND ADDRESS(ES) Northrop Grumman Corporation			8. PERFORMING ORGANIZATION REPORT NUMBER E-17429		
9. SPONSORING/MONITORING AGENCY NAME(S) AND ADDRESS(ES) National Aeronautics and Space Administration Washington, DC 20546-0001			10. SPONSORING/MONITOR'S ACRONYM(S) NASA		
			11. SPONSORING/MONITORING REPORT NUMBER NASA/CR-2010-216798		
12. DISTRIBUTION/AVAILABILITY STATEMENT Unclassified-Unlimited Subject Category: 05 Available electronically at http://gltrs.grc.nasa.gov This publication is available from the NASA Center for AeroSpace Information, 443-757-5802					
13. SUPPLEMENTARY NOTES					
14. ABSTRACT A conceptual commercial passenger transport study was performed to define a single vehicle for entry into service in the 2030 to 2035 timeframe, meeting customer demands as well as NASA goals for improved fuel economy, NOx emissions, noise, and operability into smaller airports. A study of future market and operational scenarios was used to guide the design of an advanced tube-and-wing configuration that utilized advanced material and structural concepts, an advanced three-shaft high-bypass turbofan engine, natural laminar flow technology, and a suite of other advanced technologies. This configuration was found to meet the goals for NOx emissions, noise, and field length. A 64 percent improvement in fuel economy compared to a current state-of-the-art airliner was achieved, which fell slightly short of the desired 70 percent goal. Technology maturation plans for the technologies used in the design were developed to help guide future research and development activities.					
15. SUBJECT TERMS Passenger aircraft; Subsonic aircraft; Turbofan aircraft					
16. SECURITY CLASSIFICATION OF:			17. LIMITATION OF ABSTRACT UU	18. NUMBER OF PAGES 185	19a. NAME OF RESPONSIBLE PERSON STI Help Desk (email:help@sti.nasa.gov)
a. REPORT U	b. ABSTRACT U	c. THIS PAGE U			19b. TELEPHONE NUMBER (include area code) 443-757-5802

